2-1-2020

The effect of pruning treatments on the vibration properties and wind-induced bending moments of Senegal mahogany (*Khaya senegalensis*) and rain tree (*Samanea saman*) in Singapore

Daniel Burcham

The effect of pruning treatments on the vibration properties and wind-induced bending moments of Senegal mahogany (*Khaya senegalensis*) and rain tree (*Samanea saman*) in Singapore

A Dissertation Presented

by

DANIEL C. BURCHAM

Submitted to the Graduate School of the
University of Massachusetts Amherst in partial fulfillment
of the requirements for the degree of

DOCTOR OF PHILOSOPHY

FEBRUARY 2020

Environmental Conservation

The effect of pruning treatments on the vibration properties and wind-induced bending moments of Senegal mahogany (*Khaya senegalensis*) and rain tree (*Samanea saman*) in Singapore

A Dissertation Presented

by

DANIEL C. BURCHAM

Approved as to style and content by:

Brian C. P. Kane, Chair

H. Dennis P. Ryan III, Member

Wesley R. Autio, Outside Member

Yahya Modarres-Sadeghi, Outside Member

Curt Griffin, Department Head
Environmental Conservation

Timothy Randhir, Graduate Program Director
Environmental Conservation

DEDICATION

To my grandmother, Ms. Diane K. Miller, who showed me love and loyalty.

ACKNOWLEDGMENTS

I thank my advisor, Dr. Brian Kane, for confidently supporting this project at its inception and maintaining that support over many years. I am thankful for his extraordinary insight on how to think about the science and practice of arboriculture, for his useful guidance on productive work habits, and for constantly guiding my efforts toward useful outcomes. He gave me a long lead, allowing me to pursue and explore my own interests, and gave instruction when I needed it. I am also grateful for the advice, instruction, and insight offered by my committee members, Dr. Wesley Autio, Dr. Kenneth James, Dr. Yahya Modarres-Sadeghi, and Dr. Dennis Ryan.

This project could not have happened without support from the National Parks Board, Singapore, whose shared vision of a city in a garden lends significance to these efforts. The extraordinary foresight of Singapore's first Prime Minister, Mr. Lee Kuan Yew and others inspired to advance his greening policies deserve much credit. I hope the insight offered by this project contributes positively to these ongoing efforts.

I am also grateful for the practical contributions of many hardworking people. Field research in the equatorial tropics is hard work and progress is continuously opposed by rain, heat, and humidity. This project could not have succeeded without help from Rick Thomas, Lee Sheehan, Boo Ghim Yew, Martin Tay, Lau Lai Hock, Leonard Tan, Thomas Chua, Rajesh Singh Gill, and Joseph Oh from the Singapore Arboriculture Society; Nelson Abarrientos, Clayton Lee, Shirley Lim, Chia Choong Soon, and Daniel Heng from the National Parks Board; Lynette Sim, Syuhaidah Bte Mohamed Gapor, Joey Lim, Yeo Yong Ping, Chong Yan Huan, and Mohd Qurshairy Relferi Bin Mohd Hisham from Republic Polytechnic; Tan Eng Hwa, Samarth Kapoor, Jahnavi Mekala, Derrick Poh, Vincent Wei, Sven Yeo, and Kelvin Yong from BioMachines Pte. Ltd.; and Habib Mohd Ahasan, Mofazzel Jomadder, Ahamed Mohd Elroz, S. Sukan, A.

Velmurugan, Neaiveli Muthy, and Thongsai Phiraphon from Toh Kim Bock C-E Contractor Pte. Ltd.

ABSTRACT

THE EFFECT OF PRUNING TREATMENTS ON THE VIBRATION PROPERTIES AND WIND-INDUCED BENDING MOMENTS OF SENEGAL MAHOGANY (*KHAYA SENEGALENSIS*) AND RAIN TREE (*SAMANEA SAMAN*) IN SINGAPORE

FEBRUARY 2020

DANIEL C. BURCHAM, B.S., OHIO STATE UNIVERSITY

M.S., UNIVERSITY OF DELAWARE

Ph.D., UNIVERSITY OF MASSACHUSETTS

Directed by: Professor Brian Kane

During pruning, arborists often intend to increase a tree's resistance to wind loading by selectively removing branches, but there are few studies examining the efficacy of these interventions, especially for large, open-grown trees. In this study, the mass and vibration properties of Senegal mahogany (*Khaya senegalensis*) and rain tree (*Samanea saman*) were measured before and after the crowns of trees were incrementally raised or reduced between 0 and 80%. In addition, the wind-induced vibration and bending moments of Senegal mahoganies were monitored before and after the same pruning treatments. For both species, total mass and leaf mass both decreased faster on reduced than raised trees. The frequency and damping ratio of trees varied with the severity of pruning for reduced, but not raised, trees. The frequency of reduced trees generally increased with pruning severity. In contrast, damping ratio of reduced trees generally decreased with the severity of pruning, except for the unique increase in damping ratio on Senegal mahoganies reduced by 10 to 20%. Post-pruning vibration properties were significantly related to the post-pruning morphometric attributes of reduced, but not raised, trees. For reduced trees, most of the examined tree and branch attributes better explained variability in post-pruning frequency than damping ratio.

At each pruning severity, Fourier energy spectra showed that raised trees continued to vibrate primarily at their fundamental mode. As the severity of pruning increased, however, reduced trees vibrated progressively less than raised trees at all analyzed frequencies. Similarly, the average 30-minute maximum bending moment associated with a given 30-minute maximum wind speed decreased more for reduced than raised trees at low pruning severities. For those seeking to decrease the likelihood of tree failure, the results suggest that arborists should reduce trees to change their vibration properties and wind loads, but trees should be reduced by small amounts to avoid the undesirable decrease in damping ratio. Although the observed changes on reduced trees contributed favorably to risk mitigation, there are many adverse biological consequences of some pruning methods, especially topping, that shorten tree parts without considering the anatomy of trees or remove an excessive amount of branches and leaves, and arborists should use good judgment when pruning trees to reduce their size without unnecessarily disturbing tree growth and development. Moreover, these mechanical properties will inevitably change as trees grow after pruning, and more work is needed to understand both the long-term biological and mechanical consequences of pruning treatments.

TABLE OF CONTENTS

Page

LIST OF TABLES

Table **Page**

LIST OF FIGURES

Figure **Page**

Figure 115: Scatter plot and best-fit lines of the 30-minute maximum bending moment, M_B (kN·m), against 30-minute maximum wind speed, U (m·s^{-1}), measured 18.3 m above ground (z/H_{TREE} = 0.69) for Senegal mahogany (*Khaya senegalensis*) tree number 24 raised by 0% (black empty circle marker, solid line), 10% (dark gray empty circle marker, long dash line), and 20% (light gray empty circle marker, short dash line). At 0%, 10%, and 20% severity, least squares regression equations are $y = 0.92\ x^2 + 2.14\ x + 11.3$ (n = 177; R^2 = 0.34), $y = 0.17\ x^2 + 5.12\ x + 11.4$ (n = 620; R^2 = 0.31), and $y = 0.62\ x^2 + 2.32\ x + 11.3$ (n = 244; R^2 = 0.33), respectively. ... 263

LIST OF FREQUENTLY USED SYMBOLS

Symbols

A	Amplitude
α	Scaling exponent
β	Scaling coefficient
c	Coefficient of viscous damping
C_D	Drag coefficient
D	Basal diameter
DBH	Trunk diameter at breast height
d	Apical diameter
δ	Logarithmic decrement
E	Modulus of elasticity
ε	Strain
F	Force
f	Frequency
g	Gravitational constant
γ	Branch rotation angle
H	Height above ground
I	Second moment of area
k	Spring constant
ξ	Height of branch apex
ς	Spread of branch apex
ψ	Stockiness ($D \cdot H^{-2}$)
L	Length
λ	Slenderness ($L \cdot D^{-1}$)
ln	Natural (base e) logarithm
log	Common (base 10) logarithm
m	Mass
M_B	Bending moment
M_C	Critical moment
μ	Dynamic viscosity
ω	Circular frequency
ϕ	Phase angle
φ	Branch attachment angle
r	Correlation coefficient
r^2	Coefficient of determination
R	Flexural stiffness
R^2	Coefficient of multiple determination
$\mathfrak{R}_\mathbf{B}$	Branch aspect ratio
P	Drag
ρ	Density
S	Surface area
$S(f)$	Spectral energy
σ	Stress
T	Period
t	Time
θ	Polar angle (Inclination)
U	Wind speed
u, v, w	Wind velocity components
V	Volume
W	Width
x, y, z	Cartesian coordinates
χ	Wind direction
z	Vertical distance
ζ	Damping ratio

Subscripts

$_{BRANCH}$	Branch
$_{CROWN}$	Crown
$_{LEAF}$	Leaf
$_{TREE}$	Tree
$_{u}$	Streamwise
$_{WOOD}$	Wood

Vector quantities

$\boldsymbol{a}$	Branch acceleration
$\boldsymbol{u}$	Wind velocity
$\boldsymbol{x}$	Trunk displacement

CHAPTER 1

INTRODUCTION

Trees have been a prominent feature of communities in Western civilization after dense, walled settlements gave way to new urban forms in the 16th Century (Lawrence 2006). Historically, trees were used to reinforce the sovereign authority, aesthetic beauty, and cultural traditions of a place; but they are now increasingly appreciated for their contributions to ecosystems (Roy et al. 2012), economies (Netusil et al. 2010; Pandit and Laband 2010; Sander et al. 2010; Pandit et al. 2013), psychological well-being (Kuo 2001; Taylor et al. 2002; Gidlof-Gunnarsson and Ohrstrom 2007), and human health (Lovasi et al. 2008; Donovan et al. 2013). For example, trees render valuable environmental services, including air pollution reduction (Cavanagh et al. 2009), storm water runoff attenuation (Hunt et al. 2008), carbon sequestration (Johnson and Gerhold 2003), and microclimate amelioration (Hamada and Takeshi 2010). In many places, urban expansion has paralleled a growing interest in urban forests. While economic opportunities have attracted a global majority of people to live in urban areas, many cities now consider trees and green spaces an important priority in their efforts to improve the sustainability, livability, and resilience of urban landscapes (McPherson et al. 2011).

Trees are living organisms that continuously grow and respond to their environment. Trees regularly shed organs (i.e., branches, leaves, fruit) no longer serving a useful physiological purpose, and they can fail when applied external forces generate internal stresses that exceed their material strength. Most trees easily tolerate a variety of physical disturbances caused by the environment, and many experience great longevity despite occasional damage sustained during their life. However, tree failures can have severe consequences when they occur around valuable property, infrastructure, and people. Between 1995 and 2007, at least 407 deaths were caused by tree failure events in the United States (Schmidlin 2008), and reports suggest that 20% to 50% of power outages in North America were associated with tree failures (Poulos and Camp 2010).

Costs arising from legal liability are a concern for many tree owners (Mortimer and Kane 2004). Although these events are rare, many seek to avoid unfortunate outcomes by carefully managing their trees to reduce the inherent risk.

Risk is generally understood to be a combination of the likelihood of an event and the severity of potential outcomes; and, in the context of trees, the likelihood of an event is the combination of the likelihood of failure and likelihood of impact (Smiley et al. 2017). Arborists commonly assess risk using industry standards (TCIA 2017a), and, depending on the circumstances, one might perform a limited visual, basic, or advanced assessment through general observation, close inspection, or diagnostic testing, respectively (Dunster et al. 2017). Although it is relatively straightforward to determine the likelihood and consequences of impact using basic information about a site's occupancy rates and potential targets, it remains practically challenging to confidently estimate the likelihood of failure in a given timeframe. In conducting these assessments, most have chosen to use a qualitative approach that avoids the precision implied by quantitative probabilities. The inherent uncertainty and complexity that confound tree risk assessment are widely acknowledged; in practice, risk assessment relies heavily on professional experience and judgment (Matheny and Clark 1994; Dunster et al. 2017).

Tree failure occurs when an externally applied force exceeds the load-bearing capacity of the structure. During failure, the entire tree or its parts may fail by uprooting or fracture. It can occur under a variety of conditions by trunk or branch fracture or by the loss of mechanical support in the root system. Many have investigated the causes of tree failure using phenomenological observations, controlled experiments, and theoretical modeling. Several field surveys of tree failures after severe wind events showed that large trees and those more exposed to the wind failed most often, but the studies differed on whether other attributes affected the likelihood of failure (Gibbs and Greig 1990; Duryea et al. 2007a, b; Kane 2008). Controlled experiments have

demonstrated that the load-bearing capacity of different tree parts can be reduced by cracks or decay (Farquhar and Yong 2006; Ciftci et al. 2014; Kane 2014), weak wood (Ennos and van Casteren 2010; van Casteren et al. 2012), poorly attached branches (Gilman 2003; Kane 2007; Kane et al. 2008a), and saturated soil (Dupuy et al. 2005). Numerous studies conducted in a variety of settings have revealed the importance of crown architecture on drag (Vollsinger et al. 2005) and dissipation of wind energy (Sellier and Fourcaud 2005; Sellier et al. 2006; Rodriguez et al. 2008). This growing body of knowledge has improved our understanding of tree failure, but arborists still face practical challenges when assessing the likelihood of failure.

If a tree presents unacceptable risk, pruning is frequently used to (presumably) reduce the likelihood of failure by improving branch structure, reducing leaf area, or increasing crown porosity (Gilman and Lilly 2008). Tree pruning is a ubiquitous maintenance activity that is guided by industry standards, cultural practice, and aesthetic norms. A few studies have demonstrated that, consistent with work on conifers (Mayhead et al. 1975), pruning significantly reduces wind-induced bending moment (Smiley and Kane 2006; Pavlis et al. 2008) and stem deflection (Gilman et al. 2008a, b, 2015) roughly in proportion with the mass of branches and foliage removed. These studies evaluated a range of pruning treatments, but the relative decrease in overall movement among reduced, raised, thinned, and lion tailed trees was not consistent.

Pruning modifies the vibration properties of trees (Kane 2018), and this may affect their ability to resist applied forces. Studies generally demonstrate that pruning treatments increase a tree's natural frequency of vibration, f_n (Hz), and decrease its ability to dissipate kinetic energy, assessed as a damping ratio, ζ (dimensionless), but pruning type and severity often interact uniquely with different species to produce distinct outcomes (Moore and Maguire 2005; Kane and James 2011). In particular, several studies demonstrated that removing higher-order branches

near the top of the crown had a significant effect on tree vibration properties (Moore and Maguire 2005; Sellier and Fourcaud 2005) and wind loads (Pavlis et al. 2008).

However, many studies examining the mechanical consequences of pruning were conducted on relatively small, young trees, and more work is needed to evaluate the effects of pruning on large, mature trees (Gilman et al. 2008a). There are many distinctions between a tree's juvenile and mature characteristics; trees are long-lived sessile organisms whose longevity is partly attributed to their ability to change over time. They exhibit systematic anatomical, morphological, and chemical changes in many organs during ontogeny (Anten et al. 2011). For example, wood produced at the trunk periphery during maturity is generally stiffer and stronger than that produced during juvenile growth stages (Bruchert et al. 2000; Lundstrom et al. 2007, 2008; Gardiner et al. 2011; Auty et al. 2014), and these spatial gradients in wood material properties parallel changes to the size and mass of vegetative organs that contribute meaningfully to a tree's ability to withstand external forces. Most of these changes are uniquely influenced by the interaction between the environment and internal growth processes, and the distinctions between small and large trees have important mechanical implications that make it less appropriate to extrapolate results from small to large trees. Therefore, the proposed study will seek to determine:

1. the effect, if any, of pruning treatments on the mechanical properties of mature tropical trees,
2. the relationship, if any, between mechanical properties and morphometric attributes of pruned trees, and
3. the effect, if any, of pruning treatments on wind loads of mature tropical trees.

CHAPTER 2

LITERATURE REVIEW

The likelihood that any structure will fail can be understood in terms of the applied loads and load-bearing capacity of the structure. This conceptually simple statement belies the challenges associated with assessing the factors that it describes. During tree risk assessment, arborists must contend with meteorological conditions, local topography, site layout, soil attributes, and tree characteristics (Mayer et al. 1989; Quine and Gardiner 2007). For example, some records indicate that trees growing in forests and urban landscapes undergo branch, trunk, or root failure with different regularity (Harris et al. 2004). The following sections will review the state of knowledge about these varied considerations necessary to determine the likelihood of tree failure. In this study, SI measurement units will be used; Table 1 gives conversion factors for several common U.S. customary units.

Tree Mechanics

Tree risk assessment requires a detailed visual inspection of a tree's biological condition, physical integrity, and obvious defects that, alone or in combination, may increase or decrease the likelihood of failure (Smiley et al. 2017). This process requires specialized knowledge about trees, whose adaptive flexibility contrasts starkly against the rigid strength of most built structures. Their flexibility, controlled by material properties and geometry (Denny 1987), permits slender trees to react slowly to an applied load. As a result, an interdisciplinary perspective is often necessary to fully appreciate these varied biological and mechanical considerations.

Wood Material Properties

In large trees, wood (secondary xylem) provides the mechanical support necessary to maintain an upright posture and tolerate environmental disturbances. The wood of living trees must endure a

variety of external forces, including gravitational self-loading, wind-induced bending, and twisting from an unbalanced, asymmetrical posture (Speck et al. 1990; Speck and Burgert 2011). These external forces create an internally distributed stress, σ (Pa), throughout a structure, the magnitude of which is defined as the force per unit area over which it operates (Niklas 1992). Depending on loading conditions, the wood in different parts of standing trees endures a variety of stresses, including tensile, compressive, shear, or torsional stress. Although some forces, like self-weight, slowly change over longer periods of time, others, like wind, are highly variable in magnitude and direction, even over short time periods. The deformation resulting from these stresses is called a strain, ε, represented as the dimensionless ratio of a deformed to undeformed dimension:

$$\varepsilon = \Delta l / l, \qquad \text{Eq. 1}$$

where Δl is the change in length of the object after loading and l is the length before loading. A material's stiffness or modulus of elasticity, *MOE* or, simply, E (MPa), is the linear proportionality between σ and ε exhibited by most materials during small displacements:

$$MOE = \sigma / \varepsilon. \qquad \text{Eq. 2}$$

In general, this linear proportionality holds in wood for strains not exceeding 1% to 2% (Speck et al. 1990). This relationship often becomes nonlinear after continued loading, and the transition between linear and nonlinear $\sigma(\varepsilon)$ proportionality is called the proportional limit. Stress at the proportional limit is called the yield stress, σ_{YIELD}, (MPa). Strains that do not exceed the proportional limit are elastic, or recoverable: the material returns to its original dimensions after the load is released. Strains that exceed the proportional limit induce plastic or unrecoverable material deformations (Niklas 1992). At failure, $\sigma(\varepsilon)$ truncates and the corresponding stress is called the critical stress, σ_{CRIT} (MPa). In general, brittle materials fail abruptly without considerable deformation and tough materials absorb substantial energy in plastic deformation before breaking (Ennos 2012).

Wood is a hierarchically organized composite material whose anatomy reflects its multiple functionality (Lachenbruch and McCulloh 2014). The cellular tissue consists of vessel elements, fibers, and parenchyma that chiefly perform hydraulic conduction, mechanical support, and physiological functions, respectively (Evert 2006). Its mechanical behavior is mostly affected by its density and the alignment of reinforcing elements. Wood has one of the highest density-specific strengths among all natural materials, and its exceptional toughness can be partially explained by the helical arrangement of cellulose microfibrils in the S_2 layer of the secondary cell wall (Jeronimidis 1980). The angle at which this helix is declined from the longitudinal cell axis, denoted as the microfibril angle (MFA), influences the mechanical behavior of wood. Tests conducted on individual wood fibers (Page et al. 1971; Page and El-Hosseiny 1983) and microtome sections (Reiterer et al. 1999, 2001), for example, revealed that wood with larger MFA had lower *MOE* and higher strain at breaking stress, or extensibility, ε_{MAX}.

Wood's construction results in unique strength characteristics depending on the direction of loading (Kretschmann 2010), and this anisotropic behavior requires different material property values to describe three major orthogonal axes: the longitudinal axis oriented parallel to vascular elements; the radial axis parallel to a cross sectional radius between the pith and the bark; and the tangential axis normal to a cross sectional radius between the pith and the bark. For example, *MOE* of hybrid poplar [*Populus tremula* × *alba* L. (Salicaceae)] wood held under tension along each of these axes was reported as follows: 18,200 MPa longitudinally, 1,501 MPa radially, and 527 MPa tangentially (Perre et al. 2013).

There are also important differences between the directions of loading along each of these axes. For example, most woods are stronger in longitudinal tension than compression; ultimate breaking stress of European beech [*Fagus sylvatica* L. (Fabaceae)] wood at 14.3% moisture held in longitudinal tension was reported as 83.6 MPa while similar samples subjected to longitudinal

compression failed at 36.4 MPa (Ozyhar et al. 2013). Reports describing wood material properties along the radial and tangential axes are scarce; most available information describes these properties exclusively along the longitudinal axis.

Wood density, ρ ($g \cdot cm^{-3}$), is a useful surrogate measure that positively correlates with several wood material properties, including *MOE* and *MOR* (Niklas 1997; Niklas and Spatz 2010, 2012). As a result, it is often used as an indicator of mechanical behavior. Basic density is calculated as the ratio of dry mass to fresh volume (ASTM 2014).

Wood material properties affect the fracture behavior of trees (Farquhar and Yong 2006). Given the larger longitudinal tensile strength of most woods, failure often occurs first during bending by buckling under axial compression (Lundstrom et al. 2007, 2008; Ennos and van Casteren 2010; van Casteren et al. 2012). Thereafter, however, the transverse stresses operating radially in bending can increase rapidly, and the ensuing mode of failure depends on a species' unique anatomical characteristics (Ennos and van Casteren 2010).

For example, van Casteren et al. (2012) demonstrated that wood material properties and anatomy interacted to affect the failure modes of European hazel [*Corylus avellana* L. (Betulaceae)], European ash [*Fraxinus excelsior* L. (Oleaceae)], and white willow [*Salix alba* L. (Salicaceae)] branches subjected to three-point bending. Among these species, the density of European hazel ($0.51\ g \cdot cm^{-3}$) and European ash ($0.49\ g \cdot cm^{-3}$) wood was significantly greater than white willow ($0.44\ g \cdot cm^{-3}$). As a result, the proportional decrease in white willow transverse compressive strength led to its complete failure in transverse buckling; European hazel and European ash, meanwhile, failed in tensile fracture with cracks propagating differently through their diffuse and ring porous wood, respectively (van Casteren et al. 2012). In particular, European ash exhibited clean (greenstick) fracture, possibly facilitated by the mechanically weak interface between late

and early wood cells at ring boundaries, and the European hazel splintered irregularly in diffuse fracture (van Casteren et al. 2012).

Considerable work exists on the interspecific variability, anatomical characteristics, and material properties of wood harvested for use as a building material (Kennedy 1965; Kretschmann 2010), and there is a growing body of knowledge about the mechanical behavior of wood in living trees (Speck and Burgert 2011). Shah et al. (2017) provide a critical summary of test protocols used for measuring the mechanical properties of plant stems. Crucially, these wood material properties describe how much a tree should deform and when it should break during loading, but the test procedures used to determine these properties occasionally yield different estimates for standing trees, logs, and milled specimens (Raymond et al. 2008). For example, Kane (2014) reported that stiffness and breaking stress determined on standing red oak [*Quercus rubra* L. (Fagaceae)] trees were 69% and 43% less than *MOE* and *MOR*, respectively, determined by testing wood specimens extracted from the same trees. In a meta-analysis of Canadian studies involving four conifer species, Ruel et al. (2010) similarly reported that intraspecific *MOR* estimates determined on standing trees and milled specimens were significantly different. This variation is an important subject for arborists concerned with the mechanical integrity of living trees and the likelihood that their parts may fail; it is necessary to establish a critical stress limit after which the likelihood of failure can be considered imminent.

This disparity likely arises from sources associated with each of the testing methods. In most tests, specimens are subjected to a bending moment, M_B (N·m), tending to cause rotation about some axis, and the resulting deformation is systematically recorded. Large trunks, for example, are often tested by pulling trees to induce a maximum M_B near the ground (Milne and Blackburn 1989; Bruchert et al. 2000; Kane 2014). Although tree pulling handily allows for testing large specimens, it is not always straightforward to account for the applied loads and associated

deformations (Lundstrom et al. 2008; Ruel et al. 2010; Kane 2014). For example, many authors have not included the rotational stiffness of the root-soil system, and this omission contributes to an underestimate by neglecting a portion of horizontal displacement caused by the basal rotation (Neild and Wood 1999; Jonsson et al. 2006). During these tests, it is also practically challenging to account for trunk stress distributions (Wood 1995) and the forces caused by the weight of the overhanging crown (Peltola et al. 2000). In relative terms, most accept that the latter contributes minimally to total M_B (Mayer 1987; Ancelin et al. 2004; Kane and Clouston 2008); depending on tree size, the weight of the overhanging crown increases total M_B by 7% to 22% (Peltola 1995). Ultimately, the error associated with material properties determined by tree pulling remains unclear, and these estimates should be regarded with some caution.

Bucked logs and milled lumber, on the other hand, are often tested using three- or four-point bending machines that provide accurate force-displacement records (Cannell and Morgan 1987; Bruchert et al. 2000; Lundstrom et al. 2007, 2008). In many cases, authors reported that *MOE* and *MOR* determined for logs and milled specimens in three- or four-point bending were not significantly different from one another, especially after carefully accounting for under bark diameters (Cannell and Morgan 1987) and taper (Lundstrom et al. 2008). Still, authors note that these tests are limited by the absence of longitudinal growth stresses released during felling (Huang et al. 2005) and the relative scarcity of defects on small test specimens (Gardiner et al. 2000). Still, Ruel et al. (2010) reported that *MOR* estimates obtained from logs containing moderate decay were not different from those obtained on clear milled wood specimens. Some arborists have used a tree's measured response to controlled loading to determine the likelihood of failure (Sinn and Wessolly 1989), but this persistent variability in *MOR* contributes uncertainty to these estimates.

Moreover, there is considerable variation in material properties throughout tree parts (Anten et al. 2011), reflecting a mechanical acclimation of mature trees over time whose stiff basal parts resist deformation and compliant distal parts bend to reduce wind resistance (Speck et al. 1990). During bending, tensile and compressive stresses attain a maximum at the periphery of the trunk near its base (Speck et al. 1990), and a radial increase in material properties ensures that stiffer and stronger wood accommodates these large stresses. For example, Lundstrom et al. (2007) reported an increasing trend among material properties along a radial gradient from pith to bark in Norway spruce [*Picea abies* (L.) Karst (Pinaceae)]. Specifically, *MOE* increased by a factor of 3.2 from 5.7 to 18.1 GPa, *MOR* by a factor of 3.9 from 23 to 90 MPa, density by a factor of 1.7 from 0.37 to 0.63 $g \cdot cm^{-3}$, and work of fracture by a factor of 6.4 from 20 to 128 kPa (Lundstrom et al. 2007). Analogously, most authors have reported a longitudinal decrease in material properties (Bruchert et al. 2000; Lundstrom et al. 2007, 2008).

In addition to material stiffness, the resistance to bending of beam-like plant organs depends on their geometry; the contribution of a material element to a total bending moment is proportional to the square of its distance from the neutral axis (Ennos 2012). Mathematically, their flexural rigidity, R ($N \cdot m^2$), is given by:

$$R = E_{STRUCT} \cdot I, \quad \text{Eq. 3}$$

where E_{STRUCT} is the structural modulus depicting the stiffness of a heterogeneous, composite material (Bruchert et al. 2000) and I is the second moment of area (m^4) that can be determined by summing many, infinitesimally small moments distributed over a cross section:

$$I = \int y^2 dA. \quad \text{Eq. 4}$$

For a circle of radius r, the solution by integration is:

$$I = \pi/4 \cdot r^4. \quad \text{Eq. 5}$$

Similarly, the solution for an ellipse is:

$$I = \pi/4 \cdot ab^3, \quad \text{Eq. 6}$$

where *a* and *b* are the ellipse radii situated normal and parallel to the direction of bending, respectively. Many authors emphasize that E_{STRUCT}, synonymously called apparent stiffness, E_{APP} (Cannell and Morgan 1987), or tree stiffness, E_{TREE} (Kane 2014), is not necessarily equivalent to *MOE* determined using small, uniform milled specimens (Cannell and Morgan 1987; Bruchert et al. 2000; Kane 2014). Given the increasing contribution of material situated farther from the neutral axis (Ennos 2012), differences in the stiffness of these test specimens should mostly reflect the material situated at the periphery of their respective cross sections.

Using composite theory refined by Speck et al. (1990), Bruchert et al. (2000) combined hierarchically-organized empirical data describing the abundance and distribution of tissue in a Norway spruce trunk to reconstruct its flexural rigidity, *R*. In this study, the authors measured *R* at several heights by subjecting a tree to static pull tests in the field, and they subsequently dissected trunk sections to obtain milled specimens from the inner heartwood, outer heartwood, and sapwood for material properties determination in three-point bending (Bruchert et al. 2000). Finally, the authors re-calculated the trunk *R* based on the dimensions, tissue composition, and test specimen *MOE* determined for each cross section, and they reported reasonable agreement between measured and estimated *R* (Bruchert et al. 2000). These results uniquely demonstrate how material properties determined for small specimens can be used, in combination with trunk geometry and anatomy, to predict the bending mechanics of standing trees.

In trees, wood is arranged during primary and secondary growth to construct a large structure whose design reflects the multiple competing requirements exerted by an environment, including light interception, hydraulic transport, mechanical support, reproduction, and wind resistance (Farnsworth and Niklas 1995). While most material properties are expressed independent of geometry by normalization, the mechanical behavior of trees is clearly influenced by the size, shape, and arrangement of their component parts (Ennos 2012). In terms of structural

characteristics, researchers have considered the mechanical behavior of trees subjected to static (Peltola 2006) and dynamic loads (Mayer 1987; Moore and Maguire 2004; Spatz and Theckes 2013). Static loads do not appreciably change in direction or magnitude for longer periods of time (e.g., ice accreting to branches over a period of hours), while dynamic loads quickly change in direction or magnitude (e.g., a gusty wind blowing on a tree).

Response to Static Loads

Many investigators have winched trees to assess the critical overturning moment, M_C (N·m), required to cause failure, and numerous studies describe the relationship between M_C and various tree attributes, stand characteristics, and management practices (Peltola 2006). Fraser (1962) and Fraser and Gardiner (1967) first conducted tree pulling tests on Sitka spruce [*Picea sitchensis* (Bong.) Carriere (Pinaceae)]; Nicoll et al. (2006) provide a comparative methodological summary of tree pulling techniques (Figure 1) commonly used in these studies. In one notable descriptive study, Coutts (1986) rendered valuable insight about the components of Sitka spruce root anchorage in England. By selectively cutting roots and removing soil, the author determined the resistive contributions of various root system components. Specifically, he found that the soil offered considerable resistance at the onset of winching but failed soon thereafter in shear. At ultimate failure, he reported that the resistive contributions made by all components could be ordered in decreasing magnitude as follows: windward roots >> root plate mass >> hinge resistance > soil strength (Coutts 1986).

Not surprisingly, many authors have reported that root plate width and depth are positively related to M_C (Papesch 1997; Ray and Nicoll 1998; Moore 2000; Peltola et al. 2000). Consistently, similar reports described the reductions in M_C caused by features limiting root system development, including shallow water tables (Ray and Nicoll 1998), root system fungal infections (Fraser 1962), and poor soils (Nicoll et al. 2006). However, there is some evidence of

an adaptive response by trees growing in unfavorable soil conditions; Nicoll and Ray (1996) reported that shallow Sitka spruce root systems adapted with altered secondary root growth resulting in stiffened I- or T-shaped cross sections. Pragmatically, some reported that certain forest management techniques, such as drainage (Fraser 1962) and soil ripping treatments (Somerville 1979), address these subterranean limitations and increase M_C or alter the mode of failure.

Results of tree-pulling studies converge on the positive, significant relationship between tree mass and M_C for a variety of defect-free trees, including plantation-grown coniferous trees of excurrent form (Fraser 1962; Fraser and Gardiner 1967; Smith et al. 1987; Fredericksen et al. 1993; Nicoll et al. 2006), i.e., monopodial plagiotropic *sensu* Halle et al. (1978), subsequently referred to as "plantation-grown trees," and open-grown broadleaf trees of decurrent form (Peterson and Claassen 2013), i.e., sympodial orthotropic or plagiotropic *sensu* Halle et al. (1978), subsequently referred to as "open-grown trees." Comparable measures of tree size, including tree height, trunk volume, and trunk diameter, similarly predicted but did not explain as much of the variance of M_C (Smith et al. 1987; Fredericksen et al. 1993; Papesch 1997; Peterson and Claassen 2013). Other factors, including trunk slenderness (Papesch 1997; Moore 2000; Peltola et al. 2000) and climatic season (Peltola et al. 2000; Bergeron et al. 2009), affect the mode of failure by influencing the relative stiffness of aboveground and belowground components. For example, Peltola et al. (2000) reported that all tested Scots pine [*Pinus sylvestris* L. (Pinaceae)] trees (100%) failed by trunk fracture during freezing temperatures compared with 18% that failed similarly during warm temperatures. During these tests, most authors reported that plantation-grown trees predominantly failed by uprooting in above-freezing temperatures (Smith et al. 1987; Papesch 1997; Ray and Nicoll 1998; Peltola et al. 2000; Achim et al. 2005a; Nicoll et al. 2006; Bergeron et al. 2009). Very few pulling tests have been conducted on open-grown trees. On such

trees, trunk or branch failure is more frequent (Kane and Clouston 2008; Peterson and Claassen 2013; Kane 2014).

Response to Dynamic Loads

However, some authors have suggested that resistive moments determined by pulling tests tend to overestimate the critical wind speed at which failure occurs (Oliver and Mayhead 1974; Blackburn et al. 1988). Trees sway in response to dynamic wind loads, and the amplitude of this motion is affected by the mechanical characteristics of the moving wind and the tree structure (Theckes et al. 2011). The interval over which a periodic process, such as a swaying tree or gusting wind, repeats itself is especially important; the inverse of this interval length is called a frequency and will be reviewed in detail later. Theoretically, sway amplitudes should increase greatly if the frequency of the external wind force approaches the tree's natural frequency of vibration, often called the resonant frequency. As a result, trees deform during wind events in a frequency-dependent manner, but the displacement gain contributed by dynamic wind loading, called the dynamic response factor (R_D), during resonance is attenuated by many complex resistive forces that act to dissipate motion energy (Chopra 2012).

Several authors offered early evidence that the failure criteria predicted by static analyses greatly exceeded the wind speeds at which damage actually occurred to commercial Scots pine and Sitka spruce stands in the United Kingdom, and the larger deformations caused by dynamic loading were assumed to be responsible for this disparity (Fraser and Gardiner 1967; Oliver and Mayhead 1974; Blackburn et al. 1988). Static analyses largely ignore the important inertial effects (de Langre 2008) arising from the momentum created by swaying branch and trunk mass to interact with applied external forces. In addition, the absorption (Vogel 1984, 2009; Rudnicki et al. 2004; Vollsinger et al. 2005; Kane and Smiley 2006) and dissipation (Jonsson et al. 2007; Theckes et al. 2011) of wind energy by leaves are velocity dependent, and a tree's response to wind depends on

these time-varying loading conditions. As a result, many authors have adopted investigative approaches reflecting the dynamic interaction between trees and wind (Mayer 1987; Gardiner 1991; Moore and Maguire 2004; de Langre 2008; Schindler et al. 2013b).

Natural Frequency and Damping Ratio

There have been numerous investigations of two dynamic mechanical properties: natural frequency, f_n, and damping ratio, ζ. A tree's natural frequency is represented as the reciprocal of the time required to undergo one complete sway cycle by:

$$f_n = 1/T, \quad \text{Eq. 7}$$

where f_n is the natural frequency (Hz) and T is the natural period of vibration (sec). If the vibrating motion is represented by a rotating vector projected onto a circle's horizontal axis, its angular velocity is the natural circular frequency (ω_n) obtained by multiplying f_n by 2π. Damping ratio is a dimensionless representation of the efficiency with which kinetic energy is dissipated (Chopra 2012) in a swaying tree by:

$$\zeta = c/c_c, \quad \text{Eq. 8}$$

where c is the coefficient of viscous damping ($N \cdot s \cdot m^{-1}$) and c_c is critical damping ($N \cdot s \cdot m^{-1}$), the point of transition from an underdamped to a critically damped system:

$$c_c = 2m\omega_n, \quad \text{Eq. 9}$$

where m is the structure's mass (kg). These properties are often measured during free vibration using pull-and-release, or "pluck", tests where a tree is deflected from its resting position and instantaneously released under calm wind conditions. After release, the tree vibrates and interacts with the surrounding air, and its response time history is recorded for vibration analysis. The equation of motion for a freely vibrating single-degree-of-freedom (SDOF) mass-spring-damper system (Kreyszig 2011), derived from Newton's second law of motion, is:

$$0 = kx + c\dot{x} + m\ddot{x}, \quad \text{Eq. 10}$$

where k is the spring constant (i.e., stiffness) ($N \cdot m$) and whose auxiliary equation has two roots

that give rise to three categories of damped vibration, including overdamped ($\zeta > 1$), critically damped ($\zeta = 1$), or underdamped ($\zeta < 1$). A mechanical system has one degree of freedom if its position can be expressed at any time by one number (Den Hartog 1985). Most trees are underdamped structures (Moore and Maguire 2004; James et al. 2006) whose damping ratios are well below unity, and the resulting equation can be rewritten as:

$$x(t) = Ae^{-\zeta\omega_n t} sin\,(\omega_d t + \phi), \qquad \text{Eq. 11}$$

where A is the initial amplitude, ϕ is the phase angle, and ω_d is the damped circular frequency:

$$\omega_d = \omega_n\sqrt{1-\zeta^2}. \qquad \text{Eq. 12}$$

According to Eq. 12, ω_d decreases with ζ between zero and one along a 90° circular arc, and the slope of the tangent line at $\zeta(0) = 0$ indicates that the damped and undamped circular frequencies are approximately equal for ζ near zero ($\zeta < 0.2$).

Researchers have used a variety of measurement devices to record plant motion during free vibration tests. Sugden (1962) and Mayhead (1973a) recorded sway periods using handheld stopwatches, and van Casteren et al. (2013) similarly measured the sway periods of individual branches by recording the elapsed time during a fixed number of cycles. Others have used accelerometers (Mayhead et al. 1975; Mayer 1987; Peltola et al. 1993; Peltola 1996; Jonsson et al. 2007; Reiland et al. 2015), strain gauges (Moore and Maguire 2005; Moore et al. 2005; Bruchert and Gardiner 2006), displacement probes (James et al. 2006; James and Kane 2008; Kane and James 2011; James 2014; Kane et al. 2014), linear potentiometers (Holbo 1980; Milne 1991; Baker and Bell 1992; Roodbaraky et al. 1994), clinometers (Rudnicki et al. 2001, 2008; Sellier and Fourcaud 2005; Granucci et al. 2013; James et al. 2013), and electromagnetic or optical tracking methods (Baker 1997; Hassinen et al. 1998; Rodriguez et al. 2012; Barbacci et al. 2014) to record this multi-dimensional, time-varying motion.

Importantly, these devices must offer measurement resolution suitable for the magnitude of excitation for a given position on a tree. In general, displacements at distal organs far exceed those proximal to the base of the tree, and measurement resolution is especially important when recording movement on the lower trunk where displacements are small (James and Kane 2008). Several authors have reported that the minimum sampling frequency for recording the dynamic response of trees to wind loads is 20 Hz (James and Kane 2008; Schindler et al. 2013b). In general, the Nyquist sampling theorem requires that vibrations are recorded at a sampling frequency at least twice the highest frequency contained in the signal; insufficient sampling frequencies below this limit risk aliasing signals towards false estimates (Den Hartog 1985). Equally important, the devices must not alter the mechanical properties of plant organs being measured by contributing disproportionately to their mass or stiffness (Sellier and Fourcaud 2005).

The natural frequency of a tree can be determined using Eq. 7 by identifying the location of amplitude maxima in a free vibration response time history (Sellier and Fourcaud 2005; Kane and James 2011; Miesbauer et al. 2014). This approach works well for sway responses best approximated by a simple harmonic function whose amplitude peaks can be detected using a variety of methods, including first derivative root-finding techniques. Some authors have determined f_n by fitting Eq. 11 to a free vibration time history (Sellier and Fourcaud 2005; James 2014). In addition, spectral transformations, especially the Fourier transform, have been used to evaluate the distribution of spectral energy across a range of frequencies in both simple harmonic and complex periodic signals (Jonsson et al. 2007; Granucci et al. 2013; Schindler et al. 2013b; Kane et al. 2014). The Fourier transformation is a generalization of the Fourier series expansion of complex periodic signals as an infinite sum of harmonic sine and cosine waves:

$$F(x) = a_0 + \sum_{n=1}^{\infty} a_n \cos(n\omega_0 x) + \sum_{n=1}^{\infty} b_n \sin(n\omega_0 x), \qquad \text{Eq. 13}$$

where a_n and b_n are the amplitudes of the nth harmonics of frequency $n\omega_0$ (Chopra 2012).

Mathematically, it is expressed as a definite, improper integral transformation by:

$$F(\omega) = \int_{-\infty}^{\infty} e^{-i\omega t} f(t)\, dt \qquad \text{Eq. 14}$$

that converts a function from its original *t*-space (i.e., time domain) to a new ω-space (i.e., frequency domain) (Mallard 2009). The transformation decomposes a complex periodic signal into its constituent periodic components, allowing a determination of spectral energy associated with each analyzed frequency (Den Hartog 1985). Spectral analysis is useful for determining the frequency of complicated tree motion recorded during free vibration (Roodbaraky et al. 1994; Moore and Maguire 2005; Sellier and Fourcaud 2005; Jonsson et al. 2007; Reiland et al. 2015) or wind loading (Holbo 1980; Roodbaraky et al. 1994; Hassinen et al. 1998; Rudnicki et al. 2008; Schindler 2008; Schindler et al. 2010, 2012b; Granucci et al. 2013; Schindler et al. 2013b), especially for large, open-grown trees (Kane et al. 2014).

Much work has addressed the global (whole-tree) f_n of plantation-grown trees (Sugden 1962; Mayhead 1973a; Mayhead et al. 1975; Milne 1991; Roodbaraky et al. 1994; Hassinen et al. 1998; Flesch and Wilson 1999; Bruchert et al. 2003; Moore and Maguire 2005; Sellier and Fourcaud 2005; Bruchert and Gardiner 2006; Jonsson et al. 2007), whose vibrations can be reasonably approximated by a SDOF simple physical system. For example, a lumped mass attached to a spring will vibrate according to:

$$f_n = 1/2\pi\sqrt{k/m} \qquad \text{Eq. 15}$$

(Niklas 1992). This equation indicates that f_n should vary directly proportional to the system's stiffness and inversely proportional to its mass, and several studies demonstrate that plantation-grown trees broadly conform to the basic physical laws described by this equation. For example, four-year-old maritime pine [*Pinus pinaster* Aiton (Pinaceae)] f_n increased 87% from 0.6 to 1.12 Hz after the needles were removed, and this observed change can be attributed, in part, to a 45% reduction in mass following needle removal (Sellier and Fourcaud 2005). Bruchert and Gardiner

(2006) similarly reported that f_n among 60 Sitka spruce trees was inversely proportional to crown mass. Comparably, Granucci et al. (2013) reported that 18 different plantation-grown trees exhibited a 27.9% increase in f_n from 0.35 to 0.44 Hz during extended periods of freezing air temperatures (< -5°C), and this change was likely caused by the tree's increased *R* after trunk water experienced a phase change from liquid to solid.

The trunk of a plantation-grown tree, however, is arguably better approximated as an elastic beam than a simple spring-mass system, and several authors have used dynamic beam theory (Blevins 1979; Niklas 1992) to model such trees' vibration. Initially, Sugden (1962) and Mayhead (1973a) measured the sway periods of several plantation-grown tree species, and they reported broad agreement between their measurements and values obtained from theoretical formulas appropriate for a beam with negligible mass and a concentrated apical load:

$$T = \beta \sqrt{mL^3}/_{D^2}, \quad \text{Eq. 16}$$

where β is a regression coefficient, *m* is mass, *L* is beam length, and *D* is beam diameter. Subsequently, Mayhead et al. (1975) demonstrated that the theoretical equation for a cylindrical beam in flexural vibration could be simplified to reliably predict the period of several plantation-grown tree species using:

$$T = \beta L^2/D, \quad \text{Eq. 17}$$

where *D* is the trunk diameter (m) at breast height, approximately 1.37 m, and *L* is the tree height. Gardiner (1991) later used an energy-based approach to produce an equivalent theoretical predictive equation:

$$f_n = \beta\, DBH/H^2, \quad \text{Eq. 18}$$

where *DBH* is trunk diameter at breast height and *H* is tree height. Many studies subsequently provided corroborating evidence of the reliability of this predictive equation among diverse locations and tree species (Bruchert and Gardiner 2006; Jonsson et al. 2007; Schindler et al.

2010). Moore and Maguire (2004) compiled 602 f_n measurements for eight plantation-grown tree species reported by several authors and found broad interspecific conformity to this metric, despite some important differences among tree morphologies.

These equations notably reveal the importance of slenderness, often represented by the ratio of a beam's length to diameter ($L \cdot D^{-1}$) or the maximum to minimum cross-sectional dimension (de Langre 2008), towards the f_n of beamlike plant organs. Slenderness characterizes a beam's compliance, or deformability, and f_n should decrease as this ratio increases. Several authors describe the comparatively low f_n of slender plantation-grown trees (Sugden 1962; Bruchert and Gardiner 2006; Rudnicki et al. 2008) experiencing increased competition from neighboring trees for light and other resources in forests. However, Rudnicki et al. (2003) provided evidence that slender lodgepole pine [*Pinus contorta* Douglas ex Loudon var. *latifolia* Engelm. ex S. Watson (Pinaceae)] trees swayed at higher speeds over greater distances to collide more frequently with the crowns of neighboring trees compared to their stockier counterparts; and the progressive reductions in f_n alongside more frequent crown collisions during periods of high wind speed showed that these partly inelastic crown collisions dissipated some kinetic energy (Rudnicki et al. 2008).

Fewer studies have measured f_n of open-grown trees under equivalent conditions (Roodbaraky et al. 1994; Baker 1997; Kane and James 2011; Rodriguez et al. 2012; Ciftci et al. 2013; Kane et al. 2014; Miesbauer et al. 2014), but the available reports demonstrate the similar broad contributions of mass and stiffness towards whole-tree f_n. Leaf condition, for example, affected f_n of open-grown decurrent trees with comparatively greater f_n during leafless periods (Baker 1997; Kane and James 2011; Miesbauer et al. 2014; Reiland et al. 2015). Analogously, Baker (1997) reported that diseased common limes [(*Tilia* ×*europea* L. (Malvaceae)] had a higher f_n than their healthy counterparts, and this difference was most likely caused by the reduced mass of trees

whose comparatively poor physiological condition resulted in leaf loss and reduced wood moisture. Scannell (1983) likewise reported that the senescing, leafless lower branches of a Scots pine, whose wood stiffness increased after drying, vibrated at a higher f_n than the live, green upper branches in the same tree. Baker (1997) affirmed existing observations that trees vibrate at lower frequencies as they grow in size (Sugden 1962) by reporting an inverse relationship between *DBH* and f_n for healthy limes.

Parallel evidence that f_n increases in direct proportion to stiffness can also be found in studies addressing open-grown trees. Sugden (1962), for example, reported that cottonwood [(*Populus deltoides* W. Bartram ex Marshall (Salicaceae)] f_n increased during periods of freezing temperatures, although measurements were not presented. Interestingly, steel cables installed between co-dominant red oak stems increased f_n, but only during leafless periods (Reiland et al. 2015). This arboricultural treatment, commonly used to reduce the likelihood of failure of weakly attached branches, selectively reduces compliance, but its interaction with seasonal leaf condition demonstrates the important contribution of leaves towards vibration behavior of trees (Reiland et al. 2015). An obvious question that arises is whether leaf condition might similarly supersede the stiffness contributed by freezing temperatures, but leaf senescence notably prohibits an evaluation of the effect of freezing temperatures during both leaf conditions.

Although several authors have adequately modeled the vibration of plantation-grown trees as a lumped parameter system (Kerzenmacher and Gardiner 1998; Flesch and Wilson 1999) or elastic cantilever beam (Mayer 1987; Gardiner 1991), these modeling approaches are arguably poor phenotypic approximations of open-grown trees (Mayer 1987). Several studies have demonstrated the important contribution of complex sympodial branching (James et al. 2006; Kane et al. 2014) and large individual branches (Ciftci et al. 2013) towards the vibration behavior of open-grown trees. Kane et al. (2014), for example, reported that f_n of eight large, open-grown

sugar maples [(*Acer saccharum* Marshall (Sapindaceae)] was better predicted by the cumulative sum of branch diameters than $DBH \cdot H^{-2}$, and this suggests that both the quantity and size of primary branches affect the sway response of open-grown trees. In these trees, crown architecture arises largely by the development of axillary buds and shoots, while this process occurs mostly by the growth of one apical meristem in plantation-grown trees (Halle et al. 1978); and the ontogenetic differences between these two types of trees offer insight about the relative contributions of trunk and branch vibration to the overall tree response. Miesbauer et al. (2014) further evaluated the influence of branch architecture on f_n by pruning vegetatively propagated red maple [(*Acer rubrum* L. 'Florida Flame' (Sapindaceae)] trees to exhibit an excurrent or decurrent form, and reported that trees pruned to exhibit an excurrent form had significantly higher average f_n than others pruned to encourage a decurrent form.

Despite one report that f_n did not vary among six measurement positions distributed throughout a sycamore maple [(*Acer pseudoplatanus* L. (Sapindaceae)] (Baker 1997), there is considerable evidence that the vegetative organs (i.e., branches, leaves) comprising a tree vibrate at multiple, distinct frequencies (Sellier and Fourcaud 2005; Rodriguez et al. 2012; Der Loughian et al. 2014). In addition to their fundamental frequency, beams and beam-like plant organs can oscillate at higher frequencies (i.e., modes) with distinct forms (i.e., mode shapes) of vibration (Blevins 1979; Niklas 1992). Der Loughian et al. (2014), for example, subjected an unbranched hybrid poplar seedling to a range of frequencies with a stem shaker and identified the presence of vibratory modes by their resonant response. They discovered one global (i.e., whole plant) mode type at low frequencies involving stem bending, one local mode type at mid-range frequencies involving stem apex deformation, and a second local mode type at higher frequencies involving leaf deformation (Der Loughian et al. 2014). Sellier and Fourcaud (2005) similarly observed a second vibration mode exclusively on the branches of one young maritime pine, but this mode

was only observed, in addition to the fundamental mode shared by the trunk and branches, after its needles were removed.

Likewise, Castro-Garcia et al. (2008) estimated the modal parameters of olive trees [*Olea europea* L. (Oleaceae)] by using a mechanical shaker to excite the lower trunk at a range of forcing frequencies between 12 and 140 Hz. The authors observed three modes involving the entire tree structure vibrating at 20, 38, and 73 Hz (Castro-Garcia et al. 2008). These frequencies were noticeably greater than fundamental modes reported for other trees, and it was likely an artefact of the excitation methods used to simulate fruit harvesting practices.

Rodriguez et al. (2008) similarly modeled the distribution of modal frequencies among vegetative axes in four trees, including two idealized fractal trees, one maritime pine, and one English walnut [(*Juglans regia* L. (Juglandaceae)]. In their study, fractal trees were constructed using allometric constants appropriate for monopodial or sympodial branching patterns, and the relationship between branch allometry and modal frequencies was evaluated using dimensional analysis. In the case of the idealized sympodial tree, it was determined that a modal frequency could be determined simply by using:

$$f_N = f_1 \cdot \lambda^{\frac{(N-1)(\beta-2)}{2\beta}}, \qquad \text{Eq. 19}$$

where f_N is the frequency for mode group N; f_1 is the tree's first, or fundamental, frequency; β is the exponent by which branch length scales with diameter; and λ is the ratio of branch cross sectional area to that of its subtending member, referred to as a branch aspect ratio, $\Re_B$ (dimensionless), among arboriculture researchers (Gilman 2003; Kane 2007; Kane et al. 2008a). A similar equation was developed for the idealized monopodial tree that included an additional parameter, μ, for the vertical reduction in trunk cross sectional area. The modal frequencies determined from these scaling laws were then compared to those determined from an eigenvalue problem whose stiffness and mass matrices were derived from finite element (FE) models of the

plantation-grown maritime pine and open-grown English walnut branch architecture, and the authors reported that the scaling laws better predicted modal frequencies for the black walnut than maritime pine, despite broad agreement in the grouping of vibration modes among vegetative axes (Rodriguez et al. 2008). In the walnut tree, the first 25 modes between 1.4 and 2.6 Hz were arranged hierarchically according to their position and mode shape; three mode groups were associated with deformations on the trunk, first-order branches, and second-order branches, respectively, with superior axes mostly undergoing rigid-body displacements (Rodriguez et al. 2008).

Subsequently, Rodriguez et al. (2012) attempted to experimentally validate the prediction of modal frequencies using these allometric laws by conducting free vibration tests on a different 10-year-old English walnut. The scaling estimates consistently over predicted measured f_n but correctly portrayed the increasing modal frequencies in higher-order branches (Rodriguez et al. 2012). These reports offer insightful evidence about the distribution of vibratory modes among branches, but a few notable limitations preclude widespread application of the results. First, the theoretical equations, models, and experiments did not consider the resistive forces created by leaves or needles during free vibration. The important contribution of leaves towards vibration has been widely reported by several authors (Baker 1997; Kane and James 2011; Schindler et al. 2013b; Miesbauer et al. 2014; Reiland et al. 2015), and the exclusive observation of higher modal frequencies on leafless maritime pines by Sellier and Fourcaud (2005) suggests these results may be limited to leafless trees. Second, the FE model and modal analysis assumed that all vegetal axes were perfectly clamped at their base, but numerous studies demonstrate that root systems and branch attachments are not perfectly rigid connections and, under continuous loading, will undergo elastic or plastic deformation and, eventually, ductile fracture (Jonsson et al. 2006; Kane et al. 2008a; Yang et al. 2014). The exaggerated stiffness associated with flexible connections may have contributed additional error to the f_n estimates. Third, the authors assumed uniform

wood material properties within the trunk and branches, but age-related changes to these material properties have been extensively documented (Anten et al. 2011).

In large, mature trees, there is some evidence that gradients in wood material properties affect branch vibration. While studying Sumatran orangutan locomotive strategies in the Indonesian rainforest, for example, van Casteren et al. (2013) reported contrasting evidence that branch f_n should, in fact, decrease at the distal crown positions occupied by higher-order branches because of marked increase in branch compliance. In fact, they reported that branch size interacted with crown position to influence f_n. In large branches, stiffness remained constant and then declined rapidly at locations near the branch tip, but stiffness decreased continuously from locations near the attachment in small branches (van Casteren et al. 2013). Ultimately, these poorly understood site and species differences impede broad generalizations about the distribution of vibration modes among branches.

In addition to free vibration tests, many authors have measured f_n by recording wind-induced tree motion. As with free vibration tests, many more of these studies have addressed plantation-grown trees (Holbo 1980; Mayer 1987; Gardiner 1994; Peltola 1996; Kerzenmacher and Gardiner 1998; Rudnicki et al. 2001, 2008; Schindler 2008; Schindler et al. 2010, 2012b; Granucci et al. 2013; Schindler et al. 2013a) than open-grown trees (Baker and Bell 1992; Roodbaraky et al. 1994; Baker 1997; James et al. 2006; Schindler et al. 2013b). Many authors reported that the fundamental mode of vibration associated with trunk bending dominated the response of plantation-grown trees to wind loads (Holbo 1980; Mayer 1987; Gardiner 1994; Peltola 1996; Flesch and Wilson 1999; Schindler 2008; Schindler et al. 2010, 2012b) and that more wind energy is absorbed by these trees at frequencies near their primary mode (Mayer et al. 1989). Schindler et al. (2010) measured the wind-induced motion of plantation-grown Scots pine and reported that spectral energy became increasingly concentrated at the fundamental trunk vibration

mode at increasing wind speeds with very little (< 3%) energy occupying frequencies associated with higher order trunk vibration. In contrast, Schindler et al. (2013b) found that leaf condition interacted with wind speed to affect the location and mode of vibration on an open-grown Norway maple [*Acer platanoides* L. (Sapindaceae)]. During leafless periods, low wind speeds activated higher-order, localized vibration modes by deforming mostly small branches, and high wind speeds led to a concentration of spectral energy at lower fundamental modes by displacing the trunk and branches. During in-leaf periods, spectral energy was distributed across all analyzed frequencies with small peaks occurring in the range of expected vibration modes, but there was no obvious concentration of spectral energy at any of these frequencies (Schindler et al. 2013b).

This research has contributed to our fundamental understanding of tree vibration. Many of these studies demonstrate that branch architecture and leaf condition affect a tree's vibration characteristics. Plantation-grown trees predominantly vibrate at their fundamental mode. Although the vibration of plantation-grown trees is often reasonably approximated by an elastic cantilever beam, many reports suggest that the complex branch architecture of open-grown trees is unsuitably represented by a simple physical system. Open-grown trees may have a complex distribution of vibratory modes among branches, but it is not immediately clear how wind loads or leaf condition mediate the activation of these modes.

According to Eq. 8, ζ represents the resistive forces opposing motion as the dimensionless ratio of the coefficient of viscous damping to critical damping. However, energy loss mechanisms are poorly understood for many structures, including trees (Moore and Maguire 2004), and mathematical descriptions of the dissipative forces limiting vibration are prohibitively complicated (Meriam and Kraige 2012). As a result, this property is often determined experimentally using free vibration tests.

Some have determined ζ by fitting Eq. 11 to the exponentially decaying amplitudes of the recorded motion (Sellier and Fourcaud 2005; Bruchert and Gardiner 2006; James 2014). Others have used the analogous logarithmic decrement (Mayhead et al. 1975; Milne 1991; Moore and Maguire 2005; Kane and James 2011; Miesbauer et al. 2014) that represents the natural-logarithm-transformed amplitude peaks of an exponentially-decaying harmonic function as:

$$\delta = ln\left({u_i}/{u_{i+j}}\right), \quad \text{Eq. 20}$$

where δ is the logarithmic decrement (dimensionless) and u is the amplitude maximum at peak i after j cycles of motion. Some have fit an ordinary least squares regression line, whose slope approximated δ, to successive natural-logarithm-transformed amplitude maxima in the time history of displacements (Kane et al. 2014) or acceleration (Reiland et al. 2015). The dimensionless damping ratio ζ can be determined from

$$\zeta = \delta/\sqrt{4\pi^2 + \delta^2} \quad \text{Eq. 21}$$

(Meriam and Kraige 2012). Others have determined relative damping as the ratio of the loss modulus (E'') to storage modulus (E') of elasticity (Bruchert et al. 2003; Speck and Spatz 2004; Spatz et al. 2007) using:

$${E''}/{E'} = \delta/\pi. \quad \text{Eq. 22}$$

In this case, E'' and E' represent the two constituent parts of the dynamic elastic modulus (Vincent 1990). Uniquely, Jonsson et al. (2007) obtained the instantaneous amplitude (i.e., "envelope") of a time-varying signal using the Hilbert transform (Feldman 2011) that represents the exponentially decaying term in Eq. 11. In this case, ζ can be determined from the slope, α, of an ordinary least-squares linear regression line fit to the natural logarithm transformed envelope using:

$$\zeta = \alpha/\omega_n. \quad \text{Eq. 23}$$

It is important to note that all of these procedures assume viscous damping whose magnitude is proportional to velocity (Meriam and Kraige 2012). Jonsson et al. (2007) validated this

assumption for Norway spruce; and many other authors reported that ζ is amplitude dependent with observations increasing in direct proportion to the magnitude of initial displacement (Mayhead et al. 1975; Kane and James 2011; James 2014). Notably, these approaches will yield equivalent results for simple harmonic functions, but more elaborate methods are required to estimate modal ζ for complex periodic signals (Lee and Park 1992; Staszewski 1997). Equally, all techniques used to estimate ζ are sensitive to noise, measurement error, and inadequate excitation (Staszewski 1997).

In addition, Moore and Maguire (2004) noted the potential suitability of the half-power bandwidth method for estimating ζ from a frequency response curve. This response curve depicts the ratio of dynamic vibratory to static deformation, i.e., the dynamic response factor (R_D), encountered as the forcing frequency approaches and exceeds the structure's natural frequency, generally represented as a frequency ratio (ω/ω_n). The resonant frequency is the forcing frequency at which maximum deformation occurs ($\omega \approx \omega_n$) with an amplitude u_0. If ω_a and ω_b are forcing frequencies above and below, respectively, the resonant frequency at which the response amplitude equals $2^{-1/2} \cdot u_0$, then for small damping ($\zeta < 0.2$):

$$\zeta = (\omega_b - \omega_a)/2\omega_n \qquad \text{Eq. 24}$$

(Chopra 2012). In order to experimentally determine ζ using this technique, trees would need to be subjected to a range of forcing frequencies from a controlled external source, such as a rotating eccentric mass or shaking table (Moore and Maguire 2004). Although Der Loughian et al. (2014) used an external stem shaker to evaluate the response of unbranched hybrid poplar seedlings to a range of frequencies, the logistical challenges associated with manually exciting large, mature trees have restricted broader application of half-power bandwidth damping estimates (O'Sullivan and Ritchie 1992; Rodgers et al. 1995). Castro et al. (2008) used a similar approach to estimate modal damping on olive trees.

There is broad agreement on the major sources of damping in trees, despite some uncertainty about the magnitude of their respective contributions (Spatz and Theckes 2013). In general, the resistive forces acting to dissipate motion energy in trees include aerodynamic drag (Vollsinger et al. 2005; Vogel 2009), collisions (Milne 1991; Rudnicki et al. 2008), wood material viscoelasticity (Niklas 1992), root-soil friction (Mayer 1987), and structural damping by the disharmonious vibration behavior of coupled branches (Spatz and Theckes 2013). Milne (1991) estimated that internal wood friction, aerodynamic drag, and crown collisions accounted for 10%, 40%, and 50% of total damping in plantation-grown Sitka spruce. However, Speck and Spatz (2004) reported that aerodynamic (37%), material (37%), and structural (26%) damping contributed more equitably to overall damping of the giant reed [(*Arundo donax* L. (Poaceae)]. More recently, Spatz et al. (2007) observed that damping decreased 84% after removing all primary branches on one Douglas-fir [*Pseudotsuga menziesii* (Mirb.) Franco (Pinaceae)]; the authors calculated, based on frontal area estimates, that only 19% of the difference could be attributed to aerodynamic drag and suggested that structural damping accounted for the considerable remainder (Spatz et al. 2007). However, differences in the contribution of these processes towards damping across species and sites similarly impedes generalization.

Morphometric predictions of ζ are generally inhibited by the complexity of energy dissipation mechanisms in trees (Moore and Maguire 2004). Jonsson et al. (2007), for example, reported that ζ was not associated with any morphological traits on Norway spruce. However, a few authors reported evidence that ζ is related to tree size on both plantation-grown and open-grown trees. Milne (1991) reported that ζ was inversely related to trunk diameter on Sitka spruce. Subsequently, Moore and Maguire (2004) confirmed this relationship with additional observations of Sitka spruce, but other Douglas-fir ζ measurements did not conform to these observations. Bruchert and Gardiner (2006) used stepwise regression to identify site, stand, and tree characteristics accounting for the greatest variability in Sitka spruce ζ, and they determined

that ζ was inversely proportional to tree exposure and the absolute height of the first branch and proportional to the relative height of the first branch. The authors interpreted the significance of these variables mostly in the context of crown collisions with neighboring trees (Bruchert and Gardiner 2006). Kane et al. (2014) reported that ζ was proportional to crown width for large sugar maples.

Leaves provide an important boundary at which wind energy is absorbed and dissipated in trees. Their comparatively large surface area to mass ratio is more effective for aerodynamic damping, in part because of the greater inertial forces generated by the air being displaced during leaf movement (de Langre 2008). Numerous studies have shown that leaves contribute significantly towards damping through aerodynamic drag by measuring decreased ζ on leafless trees (Hoag et al. 1971; Mayhead et al. 1975; Milne 1991; Roodbaraky et al. 1994; Moore and Maguire 2005; Sellier and Fourcaud 2005; Spatz et al. 2007; Kane and James 2011; James 2014; Miesbauer et al. 2014; Reiland et al. 2015). For open-grown trees, authors have reported that ζ decreased during leafless winter periods by 58% on mature red oaks (Reiland et al. 2015), 70% on young red maples (Miesbauer et al. 2014), 88% on one semi-mature London plane [*Platanus* ×*acerifolia* (Aiton) Willd. (Platanaceae)] (Roodbaraky et al. 1994), and 75% on young Bradford pears [*Pyrus calleryana* Decne. (Rosaceae)] (Kane and James 2011).

Collisions between neighboring crowns also contribute significantly towards damping through friction and interdigitating branches (Milne 1991; Rudnicki et al. 2008). For example, Milne (1991) measured a 47.5% decrease in ζ during free vibration tests on six Sitka spruce after preventing crown collisions by restraining neighboring trees. Rudnicki et al. (2001, 2003, 2008) demonstrated that lodgepole pine f_n decreased with increasing crown collisions during wind-induced movement, and the authors attributed this reduction to the dissipation of kinetic energy by crown abrasion and deformation. Although damping was not estimated for these trees, the

reduction in the damped frequency can be attributed to the increase in ζ according to Eq. 12. Moore and Maguire (2005), however, offered contrasting evidence that Douglas-fir f_n did not change appreciably after limiting interference by neighboring branches.

Milne (1991) reported that internal wood friction accounted for the smallest component of tree damping. Hoag et al. (1971) offered supporting evidence of the comparatively low material damping by observing green wood extracted from almond [*Prunus dulcis* (Mill.) D. A. Webb (Rosaceae)] branches during free vibration tests. In this study, the authors reported ζ values between 1 and 1.6% at moisture contents above the fiber saturation point. Kretschmann (2010) indicates that internal wood friction is a complex function of temperature and moisture content that varies between 10% for hot, moist wood to 2% for hot, dry wood with other variable combinations occupying intermediate values. Material damping arises mainly from the viscoelastic properties of wood where semi-permanent plastic deformations can be partially recovered over time (Niklas 1992). Comparative wood anatomy suggests that plastic shearing deformations between stiff (i.e., tracheary elements and libriform fibers) and compliant (i.e., parenchyma) xylem tissues facilitate the dissipation of mechanical energy (Bruchert et al. 2003).

Although Mayhead et al. (1975) discussed the mechanisms by which energy might be dissipated in the root-soil system, few have experimentally investigated the root system's contributions towards damping in trees. In one comparison, Mayer (1987) reported that ζ decreased 10% on a Norway spruce in very moist soil conditions compared to the same tree in dry soil, and he attributed this decrease to the reduced friction resistance in the root system. Interestingly, Speck and Spatz (2004) reported that very little energy was dissipated by the rhizomes, adventitious roots, and soil supporting one giant reed; but the effect of soil moisture content was not determined in their experiment.

Among the sources of damping in trees, structural damping has been a source of great interest among many researchers in recent years (Spatz and Theckes 2013). Authors use several terms, including mass damping (James et al. 2006) and multiple resonance damping (Spatz et al. 2007), to describe the dissipation of energy across a system of coupled branches. James et al. (2006) observed decreased spectral energy associated with the fundamental mode of vibration among four types of trees, including the Mexican fan palm [*Washingtonia robusta* H. Wendl. (Arecaceae)], Italian cypress [*Cupressus sempervirens* L. (Cupressaceae)], hoop pine [(*Araucaria cunninghamii* Aiton ex A. Cunn. (Araucariaceae)], and two eucalypts [*Eucalyptus grandis* W. Hill ex Maiden and *E. tereticornis* Sm. (Myrtaceae)]; the authors attributed this reduced spectral energy to the damping associated with the increasing size and number of branches among these trees. Especially in open-grown trees, these authors suggested that branch vibration significantly affects the dynamic response of the entire tree, but they avoided speculation about the mechanisms by which the energy dissipation occurred (James et al. 2006).

Several authors similarly observed greater damping on plants with increasingly complex branching (Bruchert et al. 2003; Speck and Spatz 2004; Spatz et al. 2007). For example, the reduced ζ of leafless umbrella papyrus [(*Cyperus alternifolius* L. (Cyperaceae)] could be entirely attributed to aerodynamic drag associated with the surface area of the removed leaves, but the aerodynamic drag associated with leaves removed from one giant reed did not entirely account for its reduced ζ (Bruchert et al. 2003). In the case of the giant reed, the authors suggested that morphological differences between these plants offered insight about the dissipation of additional energy through structural damping; the giant reed's relatively complex morphology, with oppositely arranged leaves attached to a rigid hollow stem by flexible sheathes, allowed energy to be transferred between organs whose flexible coupling allowed independent motion of one body relative to another. In addition, Spatz et al. (2007) reported that the vibration modes for the trunk and large branches (longer than 0.5 m) of one Douglas-fir tree were densely distributed across a

narrow range of frequencies, and the authors suggested that the overlap in frequencies allowed energy to be distributed among organs. As a result, kinetic energy can be transferred from the trunk to the branches where it is dissipated more effectively (Spatz et al. 2007).

In a series of simple models, Theckes et al. (2011) sought to determine the basic mechanism by which modal energy transfer and damping occur during large-amplitude motion in trees. The authors conducted numerical and analytical simulations of a two-degree-of-freedom Y-shaped structure representing a trunk with two branches, and they found that total damping for the entire structure could be maximized by adjusting the morphological and mechanical properties of the two branches. Specifically, total kinetic energy dissipation was greatest with branches declined between 90 and 120° from upright positions, branch modal frequency approximately twice that of the trunk, branch modal damping ratio near 0.2, and a greater portion of total mass concentrated in the branches. Under ideal conditions, approximately 30% of the total energy could be dissipated in one cycle during free vibration (Theckes et al. 2011). Although untested experimentally, the analysis provides some theoretical guidance about the morphometric attributes associated with damping in trees. However, the various proposed mechanisms are not necessarily mutually exclusive and may occur simultaneously in a tree (Spatz and Theckes 2013).

Damping is an important process by which trees dissipate kinetic energy, and the efficiency of the associated processes has clear implications for the likelihood of failure. The sources of damping in trees are broadly understood (Spatz and Theckes 2013), and many reports suggest that crown architecture affects this important process. However, it remains practically difficult to predict ζ using simple morphological or mechanical tree attributes.

Defects

During inspections, arborists judge the significance of defects, including wood decay, weakly attached branches, cracks, trunk lean, and root damage (Dunster et al. 2017; Smiley et al. 2017). In practice, these conditions are often encountered by arborists, and they may increase the likelihood of failure under some loading conditions. Although trees are vulnerable to a range of problems in a growing environment, most arboricultural research describes the implications of two common defects: wood decay and weakly attached branches.

There are numerous reports about the etiology of many wood decay fungi affecting landscape trees (Deflorio et al. 2008b). After infection, trees resist the spread of wood decay using preexisting and induced physical and chemical barriers (Shigo and Marx 1977; Pearce 1996; Deflorio et al. 2009, 2011). Although some aggressive wood decay fungi circumvent this defensive response with altered growth strategies (Schwarze and Ferner 2003), not all infections are problematic. The prognosis often depends on the site-specific host-fungus interaction (Schwarze and Fink 1998; Schwarze and Baum 2000; Baum and Schwarze 2002).

After discovering a serious infection, arborists can use devices that detect or estimate the amount of internal decay in standing trees (Johnstone et al. 2010). Considerable testing has shown the suitability and limitations of devices used for this purpose (Gilbert and Smiley 2004; Rabe et al. 2004; Johnstone et al. 2007; Deflorio et al. 2008a; Wang et al. 2009; Brazee et al. 2011; Ostrovsky et al. 2017). Comparatively, however, research has yielded more insight about methods used to detect decay than others used to estimate the resulting strength loss (Ciftci et al. 2014). I accounts for the inertial forces resisting a body's external loading (Den Hartog 1948), and a tree's likelihood of failure increases with its inertial loss (Ciftci et al. 2014; Kane 2014). However, the adaptation of these calculations for practical use by arborists considering decayed trees has proven difficult (Kane and Ryan 2004). A variety of strength loss formulas exist, but the peculiar assumptions made by these formulas, including concentric decayed areas, uniform material

properties, and regular cross-sectional geometries, contribute uncertainty to their estimates (Kane et al. 2001; Kane 2002, 2014; Kane and Ryan 2004; Ruel et al. 2010). Recent methodological advancements address some of these limitations (Ciftci et al. 2014; Burcham et al. 2019).

Similarly, arborists evaluate the arrangement and condition of branch attachments during inspections, and branches that have a relatively large diameter compared to their parent often receive scrutiny. Branch attachment strength has been investigated using static pulling tests, and many authors have independently confirmed that breaking stress is inversely proportional to aspect ratio, $\Re_B$ (Gilman 2003; Kane 2007; Kane et al. 2008a). Other morphological characteristics, including branch attachment angle and diameter, are comparatively poor predictors of these branch failures (Lilly and Sydnor 1995; Gilman 2003; Pfisterer 2003; Kane 2007; Kane et al. 2008a). However, the likelihood of failure at a co-dominant attachment depends on the direction of the applied force. Kane (2014) reported that the governing failure criterion was tensile stress perpendicular to the plane of bifurcation; attachments did not fail when subjected to a compressive stress while being pulled together in the same direction.

All branch attachments exhibit features that reflect an optimization of biological, hydraulic, and mechanical pressures exerted by their environment, but the increased experimental susceptibility of co-dominant branches ($\Re_B \approx 1$) to failure can be partly understood by considering the opposite limiting case: small branches that are attached to much larger subordinates ($0 < \Re_B < 0.2$). In these attachments, the temporal variation in trunk and branch secondary growth creates conic-shaped embedded joints with overlapping trunk and branch tissue (Shigo 1985). Collectively, these features increase the load transfer area and decrease local stress (Burns et al. 2012). Several authors have suggested that a lack of embeddedness explains the relative weakness of co-dominant attachments (Gilman 2003; Kane et al. 2008a).

Interestingly, Muller et al. (2006) offered evidence of the exceptional mechanical performance of one Norway spruce branch attachment by making strain field observations of a medial longitudinal section subjected to bending. Specifically, the authors reported that strain fields were distributed homogeneously on the branch attachment, but they observed increasing strain concentrations near the branch insertion on a geometrically similar polyester cast and simplified cylindrical polyester model. However, material heterogeneity and anisotropy prohibit an equivalence between homogenous strain and stress; rather, the authors suggested that shape optimization and three-dimensional variation in material properties resulted in local areas experiencing a constant fraction of their breaking stress (Muller et al. 2006). Other studies have supported this idea by showing that large cellulose micro-fibril angles (MFA) interacted with variable density near the attachment to increase lateral toughness and abaxial flexibility (Farber et al. 2001; Jungnikl et al. 2009). The authors posited that these features limited the transmission of forces from the branch to the trunk during loading (Farber et al. 2001; Jungnikl et al. 2009). Clearly, the connections are not perfectly rigid.

In addition, three-dimensional realignment of cellular constituents near the branch attachments accommodates the direction of applied stress by orienting cells to experience longitudinal loading (Burns et al. 2012). Importantly, this means that wood is more likely to experience stress along its strongest axis, and this feature offers an explanation for the relatively low strength of co-dominant branch attachments with included bark (Smiley 2003). In these cases, the wood comprising the attachment experiences considerable transverse loads along its comparatively weak radial and tangential axes.

However, other reports caution that not all co-dominant branch attachments should necessarily be considered weak. In a series of manipulations on European hazel, Slater and Ennos (2013) removed the central 20% and peripheral 80% of the co-dominant attachment diameter at its apex

by drilling and sawing, respectively, before determining their strength under tensile loading. Compared to unaltered attachments, the maximum bending stress of drilled and sawn attachments was reduced by 32% and 49%, respectively (Slater and Ennos 2013). These results demonstrate the marked contribution of xylem tissue located centrally about the apex of co-dominant branch attachments to their strength. On average, the breaking stress of co-dominant branch attachments subjected to tensile stress was 26% less than their axillary branch wood, but there was considerably more variability in the strength of attachments with their relative strength ranging between 47% and 97% of axillary branches (Slater and Ennos 2013).

Subsequently, Slater et al. (2014) reported that European hazel xylem tissue located centrally about the apex of these co-dominant branch attachments was more tortuous and declined. At this location, they observed that vessels deviated from a straight line 14.6 times more than others in surrounding wood and were declined 74° to 89° from the orientation of the subtending member; the surrounding xylem tissue had 28.1% greater cell wall volume, 37% fewer vessels, and 100% more vessel termination (Slater et al. 2014). Mechanical tests performed on European hazel wood samples extracted from the apex of co-dominant attachments and surrounding tissue revealed changes in wood anisotropy caused by the realignment of individual cellular elements. At the attachment apex, wood had significantly higher radial and tangential compressive and tensile strength compared to surrounding wood, and this change in anisotropy caused by cellular realignment effectively reinforced the attachment along the direction where it is most likely to fail (Kane 2014).

Defect identification and evaluation is an important part of tree risk assessment. Despite some existing research, our understanding of these defects remains somewhat limited. Many arborists appreciate the significance of certain defects, but their effect on the likelihood of failure cannot be considered in isolation from site-specific loading conditions the tree must endure. Moreover,

although many structural defects increase the likelihood of failure by altering breaking loads, it is useful to remember that undamaged trees can still fail when loaded by an external force exceeding the strength of their component parts.

Wind Mechanics

Most studies addressing tree failure implicitly accept that wind is the most pervasive and severe natural disturbance (Schindler et al. 2012a), despite some work addressing other disturbances, including snow accumulation (Paatalo et al. 1999; Peltola et al. 1999), ice accretion (Proulx and Greene 2001), and the impact of falling rocks (Lundstrom et al. 2009). A historical review of natural disturbances to European forests between 1850 and 2000 supports this investigative emphasis; storm-related wind caused 53% of the total forest damage while fire, snow, and other abiotic disturbances accounted for a combined 24% of damage (Schelhaas et al. 2003). Even at low wind speeds ($< 5\ m \cdot s^{-1}$), Speck et al. (1990) estimated that wind-induced stress in the trunk periphery dominated those caused by gravitational self-loading. This review will similarly emphasize wind loads.

In general, turbulent wind flow can be described by the streamwise, lateral, and vertical components of instantaneous velocity, $\boldsymbol{u}$, which are designated u, v, and w, respectively (Raupach et al. 1996). Based on standard meteorological notation (Finnigan and Brunet 1995), overbars indicate period means and primes denote instantaneous departures from a period mean ($u' = u - \bar{u}$). The Cartesian coordinate frame is usually rotated to align the positive x-axis with the mean wind direction, aligning the mean lateral and vertical components of velocity with the y- and z-axes, respectively. This orientation results in a mean velocity vector $<u(z), 0, 0>$ and $\bar{u} = \bar{v} = 0$ (Baldocchi and Hutchinson 1987). Heights, z, measured from the ground are normalized using canopy height, H; velocity components are normalized by their corresponding value at the crown apex ($z = H$).

At the boundary between any moving fluid and solid, flow velocity is always zero with respect to the solid (Vogel 1996). As a result, velocity gradients arise between a solid surface and a fluid's free-stream velocity, and these gradients are governed in part by the fluid's dynamic viscosity, μ (Pa·s). This property affects many important phenomena arising in wind flow near solid surfaces and trees. It is expressed as a proportionality constant relating shear stress, τ (Pa), to the rate of shear:

$$\tau = \mu \cdot du/dz, \qquad \text{Eq. 25}$$

where *du/dz* is the rate of change in flow velocity with respect to height above ground. The atmospheric boundary layer near the earth's surface largely conforms to theoretical expectations for shear flow regions with mean horizontal velocity increasing logarithmically with height above ground (Cionco 1965). In this region, flow is often highly turbulent with irregular fluctuations in pressure and velocity overlying average trends (Raupach and Thom 1981; Vogel 1996).

The presence of trees disturbs airflow and extracts momentum from the moving fluid, resulting in a local decrease in velocity (Reifsnyder 1955; Allen 1968; Oliver 1971, 1975; Baldocchi and Hutchinson 1987; Amiro 1990; Gardiner 1994). The attenuation of streamwise wind speed near plant canopies, reflecting an exchange of momentum, is affected by the local leaf area density, *LAD* (m^{-1}), and roughness density, λ (dimensionless), defined as the total one-sided leaf surface area per unit crown volume and total projected crown frontal area per unit ground area, respectively. Amiro (1990), for example, reported that reductions in *u* near black spruce [*Picea mariana* (Mill.) Britton et al. (Pinaceae)], trembling aspen [*Populus treumuloides* Michx. (Salicaceae)], and jack pine [*Pinus banksiana* Lamb. (Pinaceae)] stands could be ranked by their average leaf area index, *LAI* (dimensionless), with greater decreases occurring near dense crowns. Similarly, wind measurements in a variety of forests showed that *u* decreased more in moderately stocked (Fons 1940) than sparsely stocked stands (Reifsnyder 1955).

For many tree species, a secondary streamwise wind speed maximum is often observed in the trunk space below the crown where flow is less restricted (Reifsnyder 1955; Allen 1968; Landsberg and James 1971; Oliver 1971, 1975; Baldocchi and Hutchinson 1987; Baldocchi and Meyers 1988; Amiro 1990; Launiainen et al. 2007; Dupont et al. 2011, 2012). In contrast, horizontal wind speed decreases monotonically in forests with understory vegetation (Reifsnyder 1955) and agricultural crops with a uniform distribution of foliage (Landsberg and James 1971). Considering these distinctive features, the flow region extending from the ground ($z = 0$) to maximum tree height ($z = H$) is called the canopy layer (Raupach et al. 1996).

Immediately above the canopy, there is often a rapid increase in flow velocity with maximum shear occurring at an inflection point near the canopy top where $d^2u/dz^2 = 0$. At this location, shear increases with free-stream velocity, λ, and $LAD(z)$ profiles with leaves concentrated near branch tips (Baldocchi and Meyers 1988; Amiro 1990; Gardiner 1994). Turbulence statistics are often highly correlated above tree crowns, suggesting an increased organization of turbulence (Finnigan and Brunet 1995; Raupach et al. 1996). This region, extending from $z = H$ to approximately $z = 2H$, is often called the roughness sublayer; at heights above ~$2H$, the flow assumes typical characteristics of an atmospheric boundary layer with a logarithmic mean velocity profile (Raupach et al. 1996).

Numerous investigations of agricultural crops (Finnigan 1979a, b; Brunet et al. 1994) and forests (Baldocchi and Hutchinson 1987; Amiro and Davis 1988; Baldocchi and Meyers 1988; Amiro 1990; Dupont and Patton 2012a; Mohr and Schindler 2016) have shown that large, intermittent organized structures dominate momentum exchange between the turbulent wind and plant canopies. For example, turbulence statistics reported from a range of forest types consistently showed that u and w were positively and negatively skewed, respectively, indicating that samples contained intermittent, large horizontal and vertical excursions from the mean (Shaw and

McCartney 1985; Baldocchi and Hutchinson 1987; Amiro and Davis 1988; Baldocchi and Meyers 1988; Amiro 1990; Gardiner 1994). In contrast, skewness is generally close to zero in the boundary layer above the canopy (Finnigan 2000).

Comparably, others have used conditional analyses in which instantaneous wind observations were sorted into four quadrants according to the sign of the fluctuating u (x-axis) and w (z-axis) components; the four quadrants are defined, in increasing order, as outward interaction for $u' > 0$ and $w' > 0$, ejection for $u' < 0$ and $w' > 0$, inward interaction for $u' < 0$ and $w' < 0$, or sweep for $u' > 0$ and $w' < 0$ (Baldocchi and Hutchinson 1987). Many reports indicated that vertical and horizontal gusts frequently combined into sweep events (i.e., rapid, downward incursions of air) that dominated momentum transfer inside (Baldocchi and Hutchinson 1987; Baldocchi and Meyers 1988; Gao et al. 1989; Gardiner 1994) and immediately above (Bergstrom and Hogstrom 1989) forest canopies. Among several studies, sweeps exceeded ejections by a factor ranging between one and four (Finnigan 1979a; Shaw et al. 1983; Baldocchi and Hutchinson 1987), and these events consistently transferred more momentum with greater efficiency during the passage of organized structures (Gao et al. 1989; Raupach 1989; Finnigan and Brunet 1995; Finnigan 2007).

Uniquely, Gao et al. (1989) investigated the spatiotemporal evolution of coherent structure velocity and scalar quantities using an ensemble average of 20 discrete events. Temperature, relative humidity, and wind velocity fields show the manifestation of a typical coherent structure across a vertical gradient; the plots show a sharp thermal microfront over which temperatures decrease by 1° to 2° C that is preceded by weak, upward ejection and succeeded by a strong, downward sweep (Gao et al. 1989). In general, the steeply inclined temperature microfront extends from inside the crown up to ~2.5h. In this study, the authors noted the greatest

acceleration of downward flow occurred above the crown apexes in the region of maximum shear, suggesting its contribution to the creation of these structures (Gao et al. 1989).

Ramps in scalar quantities, such as temperature, CO_2, and humidity, provide a unique identifying signature of these coherent structures; the ramps can be viewed as a slow increase (or decrease) in a scalar quantity followed by a sudden reversal (Paw U et al. 1992). Over time, the ramps appear in series as a saw tooth pattern. Paw U et al. (1992) identified such ramps for a variety of scalar quantities and meteorological conditions using observations made near corn [*Zea mays* L. (Poaceae)], almond, and English walnut plantings. The frequency of ramps was proportional to a canopy shear scale defined as $\bar{u}(z = H)/H$, indicating they occurred with greater frequency as wind shear at this location increased (Paw U et al. 1992). Interestingly, the ramps were not detected after the corn was harvested, further implicating the role of wind shear caused by crop drag in the generation of the ramp-inducing coherent structures (Paw U et al. 1992).

Collectively, these studies offered substantial evidence that aperiodic, highly turbulent coherent structures were primarily responsible for momentum transfer in forests (Finnigan 2000) and that these events originated in a region of aerodynamic instability created by an inflected horizontal wind flow profile immediately above forest stands (Gao et al. 1989; Raupach et al. 1996). Based on existing evidence, Raupach et al. (1996) postulated that coherent structures developed in a flow pattern more closely resembling a plane (co-flowing) mixing layer than a boundary layer; and subsequent comparisons of these two systems showed reasonable agreement between their turbulent features. Consequently, a detailed picture emerged of the development of aerodynamic instabilities leading to coherent structures: Kelvin-Helmholtz waves (Rogers and Moser 1992) initially develop and undergo a series of stochastic transformations caused by turbulent perturbation resulting in complex three-dimensional vortical structures (Figure 2) whose instability eventually leads to their breakup (Knio and Ghoniem 1992; Finnigan and Brunet

1995). Finnigan et al. (2009) reported that a characteristic eddy is formed by the superposition of a pair of hairpin vortices: one oriented upstream, head-down (sweep-generating) and another downstream, head-up (ejection-generating).

Coherent structures develop at streamwise intervals depending on a shear length scale, L_s:

$$L_s = \bar{\boldsymbol{u}}(h) \cdot \left\{ {d\boldsymbol{u}}/{dz} \right\}^{-1}, \quad \text{Eq. 26}$$

where $\bar{\boldsymbol{u}}$ is the mean velocity (Raupach et al. 1996). As verified for a variety of meteorological conditions and plant canopies (Brunet and Irvine 2000), their streamwise spacing, Λ_w, scaled according to canopy height can be reliably predicted by:

$${\Lambda_w}/{h} = 8.1\,{L_s}/{h}. \quad \text{Eq. 27}$$

Experimental observations made in a variety of forest types indicate that the range of temporal durations and separations for coherent structures was 4 – 40 sec and 29 – 124 sec, respectively (Bergstrom and Hogstrom 1989; Gao et al. 1989; Collineau and Brunet 1993a, b; Serafimovich et al. 2011; Mohr and Schindler 2016).

Momentum exchange, however, varies significantly with atmospheric stability, a measure of the extent to which conditions deter vertical fluid motion. The Obukhov length, L (m), represents a height of transition above and below which turbulence is mainly produced by buoyancy and shear processes, respectively; and it is given by:

$$L = -{\overline{\theta_v}(u_*)^3}\Big/{kg(\overline{w'\theta'_v})_s}, \quad \text{Eq. 28}$$

where θ_v is the mean vertical potential temperature, u_* is the friction velocity ($u'w'$), k is the von Karman constant (0.4), g is gravitational acceleration (9.81 m·s^{-2}), and $(\overline{w'\theta'_v})_s$ is the surface virtual potential temperature flux (Stull 1988). L is often used to classify five stability regimes, including, in order of decreasing stability, stable (S), transition to stable (TS), near-neutral (NN), forced convection (FoC), and free convection (FrC) (Mahrt et al. 1998; Launiainen et al. 2007;

Dupont and Patton 2012a). Specifically, Dupont and Patton (2012a) proposed the following classification limits based on canopy height, H, normalized by L (H/L), using interval notation: S [0.6 20), TS [0.02 0.6), NN [-0.01 0.02), FoC [-0.02 -0.01), and FrC [-20 -0.02). Typically, these regimes occur during similar periods of the day: TS conditions mostly occur overnight, especially after sunset; S conditions often occur just before sunrise; NN conditions mostly occur during sunset and, to a lesser extent, sunrise; FrC occurs during the day, especially in the morning; FoC occurs during the day, especially in the afternoon (Dupont and Patton 2012a).

In general, momentum flux from atmosphere to canopy attains a negative minimum during NN conditions, increases asymptotically towards zero during intermediate TS and FoC conditions, and remains approximately zero during S and FrC conditions (Dupont and Patton 2012b). During NN conditions, turbulence statistics (Dupont and Patton 2012a) and conditional analysis (Dupont and Patton 2012b) indicate that flow near the canopy resembles a plane-mixing layer, especially near the canopy apex, with momentum exchange occurring primarily by the penetration of the canopy by fast, downward-moving gusts. In heavily foliated canopies, a majority of their momentum is often absorbed by leaves, and the remaining canopy region is affected by pressure diffusion associated with the disturbance (Dupont et al. 2012). Although these coherent structures are still present during intermediate TS and FoC conditions, they are increasingly sporadic and weaker for momentum transport.

During periods of decreasing atmospheric stability (NN → FrC), "shear-driven" coherent eddies are progressively replaced by convective thermal plumes, with a possible gradual superposition of the two processes (Hommema and Adrian 2003; Dupont and Patton 2012b). These changes can be observed by a decrease in mean wind shear above the canopy (Launiainen et al. 2007) and an increase in the positive skewness of the vertical wind velocity component (Sk_w) (Dupont and Patton 2012a). In fully unstable conditions (FrC), low mean wind speeds mostly prevent the

development of coherent structures for momentum transport. During these periods, narrow, warm and humid thermal plumes originate in the canopy and move upward before coalescing into larger structures; and these are periodically replaced by large, cool and dry downward-moving parcels that undergo an attenuation of momentum as they penetrate the canopy (Dupont and Patton 2012b).

During periods of increasing atmospheric stability (NN → S), the development of coherent structures is attenuated by a lack of disturbance from background turbulence. As a result, they are weaker and more intermittent, often resembling Kelvin-Helmholtz structures (Dupont and Patton 2012b). In fully stable conditions (S), thermal stratification damps turbulence, limiting the development of shear instabilities (Thomas et al. 2006). In some cases, a distinct region may develop in a sparse lower canopy trunk space with thermal plumes driven by the radiative cooling of canopy and surface elements (Dupont and Patton 2012b).

Coherent structures have been detected from recorded observations using visual (Paw U et al. 1992) and algorithmic (Bogard and Tiederman 1986; Bisset et al. 1990) identification of sudden jumps demarcating ramp events. In addition, many authors have used wavelet transforms to investigate trends and periodicities in wind speed (Collineau and Brunet 1993a, b). These localized, zero-averaged waveforms have been used to decompose a signal into its spatial and temporal (i.e., scale) components by comparing systematic dilations of a wavelet translated along observations. As a result, the wavelet transform better detects localized, transient vibration than traditional Fourier analysis, where indefinitely oscillating trigonometric functions implicitly assume stationary processes (Grinsted et al. 2004). One frequently used wavelet, the Morlet, is defined as:

$$\psi_0(\eta) = \pi^{-1/4} e^{i\omega_0 \eta} e^{-1/2\eta^2}, \qquad \text{Eq. 29}$$

where ω_0 and η are dimensionless frequency and time, respectively (Grinsted et al. 2004). For this

wavelet, Grinsted et al. (2004) recommend $\omega_0 = 6$ provides a reasonable balance between time and frequency localization. The continuous wavelet transform (CWT) of a time history $y(t)$ with respect to the wavelet ψ is defined as:

$$W_{y,\psi}(s,t) = (y(t) * \psi_s(t)), \quad \text{Eq. 30}$$

where $\psi_s(t)$ is the wavelet at scale s and time t (Jevrejeva et al. 2003). The power of the wavelet variance spectrum is given by the squared magnitude of the wavelet transform (Jevrejeva et al. 2003).

Among wavelet-based methods to detect coherent structures, many authors have used the Ricker wavelet (Krusche and Oliveira 2004; Feigenwinter and Vogt 2005; Serafimovich et al. 2011; Mohr and Schindler 2016), defined as the second derivative of a Gaussian function $e^{-t^2/2}$ (Collineau and Brunet 1993a). Using this method, wind speed ramps are identified as positive slope zero-crossings of the Ricker wavelet coefficients corresponding to scales associated with a peak in the wavelet variance spectrum (Collineau and Brunet 1993a). Torrence and Compo (1998) offer a practical introduction to wavelet analysis, and Farge (1992) provides a comprehensive review of their application to turbulence analysis.

At short time scales, coherent structures drive most turbulent momentum exchange between the wind and trees. However, many other meteorological phenomena, such as weather systems and seasonal variation (Pinto et al. 2009), produce extreme wind speeds at different time scales, and these wind mechanisms may equally affect tree stability. Bonnesoeur et al. (2016) showed that secondary growth in European beech was most affected by large artificially-induced strains similar to those generated during extreme storm events, but the trees were less mechanically sensitive to smaller loads similar to those caused by thermal plumes. The authors suggested that the selective acclimation of trees to strong winds was primarily driven by strains experienced during synoptic-scale low pressure events (Bonnesoeur et al. 2016). Many authors have simply

described the magnitude and frequency of wind events using extreme value distributions (Shaw et al. 1979; Shaw and McCartney 1985; Reynolds 2012). Given these events' intermittency and large magnitude, their sampling can be considered as a selection of maxima from a set of extended time periods (Reynolds 2012). Specifically, many authors fit extreme value distributions to historical records of maximum wind speeds and used the associated parameters to estimate the probability of a given wind speed. Analogously, many mechanistic wind risk models use extreme value distributions to estimate the probability of a critical wind speed in a given location (Gardiner et al. 2008).

In Singapore, Georgiou (1990) used historical meteorological records collected at four locations, including Tengah Air Base, Paya Leybar Air Base, Changi Airport, and the Fullerton building, to model maximum annual gust wind speeds; their model described three-second gust speeds, U_{GUST} ($m \cdot s^{-1}$) for a given return period, r (years) as:

$$U_{GUST} = 21.0 + 2.8 \cdot \ln(r). \quad \text{Eq. 31}$$

Based on this model, the return periods associated with 20, 25, and 30 $m \cdot s^{-1}$ three-second gusts are 0.7, 4.2, and 24.9 years, respectively. Interestingly, the authors reported that many of the annual gust maxima were recorded at similar times on two or more stations, indicating events associated with brief thunderstorm activity, not long-term meteorological processes (Nathan and Goh 1981; Georgiou 1990).

Wind-Tree Interaction

Drag, P (N), is the interception of momentum from a moving fluid by a structure (Vogel 1996). Wind movement exerts pressure and generates skin friction on a tree in the direction of flow, and the conservation of momentum during turbulent conditions can be expressed using:

$$P = \rho S U^2, \quad \text{Eq. 32}$$

where ρ is the fluid density (air $\approx$ 1.21 $kg \cdot m^{-3}$ at 20°C), S is the exposed surface area (m^2), and U

is wind velocity ($m \cdot s^{-1}$). In addition to size, drag is also affected by the shape of a structure immersed in fluid, and this effect is commonly represented by the drag coefficient, C_D:

$$C_D = {}^{2P}/_{\rho S U^2}, \quad \text{Eq. 33}$$

that relates the drag per unit area experienced by a structure under different wind conditions created by the fluid's dynamic pressure (Vogel 1989). The relationship between these two variables is commonly expressed as:

$$P = \frac{1}{2}\rho S C_D U^{2+V} \quad \text{Eq. 34}$$

where V is the Vogel exponent (de Langre 2008) that describes the reduction of drag experienced by organisms through adaptive, elastic reconfiguration. During periods of high wind, tree branches and leaves often bend leeward and reconfigure in a way that streamlines shape and reduces exposed area (Harder et al. 2004). A rigid object subjected to turbulent flow experiences drag proportional to the square of velocity ($P \propto U^2$) and V is approximately zero; the increasing benefits of reconfiguration are represented by an increasingly negative V. It is important to note, however, that Eq. 34 is merely definitional and not necessarily appropriate for prediction (Vogel 1996).

Drag measurements of small trees and leaves in wind tunnels clearly demonstrate adaptive reconfiguration by trees to minimize wind loads (Mayhead 1973b; Vogel 1984, 1989; Rudnicki et al. 2004; Vollsinger et al. 2005). Similar observations of trees in natural wind flow (Koizumi et al. 2010) and vehicle-mounted tree parts accelerated through a weak or stationary wind field (Kane and Smiley 2006; Butler et al. 2012) provided corroborating evidence. In terms of V, authors report a wide range of values among tree species and vegetative organs, from -1.3 (Vogel 1984) on a 1 m tall American holly [*Ilex opaca* Aiton (Aquifoliaceae)] shoot to +0.97 (Vogel 1989) on an individual white oak [*Quercus alba* L. (Fagaceae)] leaf. Kane and Smiley (2006) reported that drag was proportional to the 1.4 power of wind velocity (V = -0.6) for in-leaf red

maples; Butler et al. (2012) reported V = -0.6, on average, for branches sampled from 39 tropical species; and Harder et al. (2004) summarized that V = -0.8, on average, for the leaves and branches of 11 temperate species. Theoretical interpretations of drag reduction in flexible bodies have consistently demonstrated V = -2/3 when bending results in the loss of one characteristic length in the structure during reconfiguration (Alben et al. 2002; Gosselin et al. 2010; de Langre 2012). Comparably, several authors have accommodated the decreased drag per unit area at higher wind velocity by modeling changes to C_D (Mayhead 1973b; Rudnicki et al. 2004; Vollsinger et al. 2005; Kane and Smiley 2006; Kane et al. 2008b; Koizumi et al. 2010) and S (Rudnicki et al. 2004; Vollsinger et al. 2005).

Many studies report a strong correlation between drag and tree or crown mass (Mayhead 1973b; Mayhead et al. 1975; Rudnicki et al. 2004; Vollsinger et al. 2005; Kane and Smiley 2006; Kane et al. 2008b). The relationship between drag and branch mass has been observed among several coniferous and broadleaf species, despite one report that drag was better correlated with crown size for swamp white oak [*Quercus bicolor* Willd. (Fagaceae)] (Kane et al. 2008b). Still, it is widely understood that leaves contribute significantly to drag; Lai (1955), for example, reported that defoliated American beech [*Fagus grandifoliola* Ehrh. (Fagaceae)] and scarlet oak [*Quercus coccinea* Munchh. (Fabaceae)] experienced a two- to ten-fold drag reduction compared to their in-leaf counterparts.

Despite these broad similarities, there are important differences among the ability of trees to reconfigure and minimize drag during wind movement. In a series of wind tunnel tests, Rudnicki et al. (2004) reported that branch compliance and foliage density interacted to affect each species' ability to reconfigure. For example, dense needles whorled along flexible lodgepole pine branches converged downstream to reduce total crown porosity, but individual scale leaves borne on horizontal Western redcedar [*Thuja plicata* Donn Ex. D. Don (Cupressaceae)] branches discretely

realigned downstream to increase crown porosity. In this instance, drag decreased comparatively more on the Western redcedar (Rudnicki et al. 2004). Somewhat counterintuitively, several authors have observed an increase in drag during low wind velocity on trees (Vogel 1984; Rudnicki et al. 2004; Kane et al. 2008b) and model structures (Gosselin and de Langre 2011) caused by the deflection of upstream-oriented parts broadside to flow before reconfiguring downstream. Based on Eq. 32, this increase is caused by a temporary increase in frontal area. After normalizing by the exposed frontal area, Vollsinger et al. (2005) reported that drag increased monotonically among five broadleaf tree species. Overall, crown architecture and morphological traits contribute in complicated ways to a tree's interception of momentum from the moving wind.

The white oak leaf whose drag increased with velocity at a rate exceeding a theoretical bluff body was an insightful outlier (Vogel 1989). Its comparatively stiff leaf blades and petioles afforded physical stability at low wind velocity conferring superior posture control for light interception, but the leaves fluttered with increasing severity during greater wind velocity (Vogel 1989). As a result, these leaves suffered physical damage at the lowest wind velocity among five tested species. In contrast, white poplar [*Populus alba* L. (Salicaceae)] leaves exhibited the greatest stability during high wind velocity to evade obvious physical damage. Poplar leaves, in contrast, are noteworthy for fluttering under relatively calm wind conditions. Vogel (1989) attributed these differences to an apparent tradeoff for physical stability under specific wind conditions, and he presumed the adaptive reconfiguration exhibited by various tree species reflected the typical wind conditions in their native range. Puijalon et al. (2011) reported similar evidence of a trade-off between morphological traits engendering drag avoidance or tolerance in 28 aquatic plant species. In terms of fitness (Arnold 1983), mechanical disturbances limiting photosynthesis or reproduction are equally problematic as those causing failure.

Butler et al. (2012), however, offered contrasting evidence that variable morphological traits among 39 species yielded a relatively narrow range of drag measurements. The authors reported that shoot *I* was the best determinant of wind performance measurements, including drag and streamlining. Although shoots with larger *I* experienced greater drag, they surprisingly exhibited more effective streamlining. As one possible explanation, the authors considered whether the increased stiffness afforded by a larger *I* contributed to enhanced stability and reduced flutter at higher wind velocities (Butler et al. 2012). The inverse relationship between *I* and *V* evinces the complex interaction among naturally variable morphological traits and is possible evidence of their functional convergence on adaptive reconfiguration.

The divergent consequences of leaf and shoot stiffness towards reconfiguration suggest that drag cannot easily be partitioned into separate components (Vogel 1984). Kane and Smiley (2006), for example, reported that C_D for 3.5 m tall red maple trees was larger than previously reported values for individual red maple leaves and leaf clusters (Vogel 1989). Leafless red maples, meanwhile, exhibited a reduced ability to reconfigure and experienced drag proportional to the 1.9 power of velocity (V = -0.1) (Kane and Smiley 2006). One would expect a similar inequality between small and large tree C_D as branches grow increasingly stiff over time (Kane et al. 2008b; Anten et al. 2011). Although observations were made in more turbulent flow conditions, C_D obtained from drag measurements on ~3.5 m tall red maple, Freeman maple [*Acer* ×*freemanii* A.E. Murray (Sapindaceae)], swamp white oak, and shingle oak [*Quercus imbricaria* Michx. (Fagaceae)] occupied a higher range of values (Kane and Smiley 2006; Kane et al. 2008b) than similar observations of smaller (< 2 m tall) coniferous and broadleaf trees tested in wind tunnels (Mayhead 1973b; Mayhead et al. 1975; Rudnicki et al. 2004; Vollsinger et al. 2005).

In addition to elastic reconfiguration, branch fracture can also be considered as a process by which drag is minimized in trees during periods of extreme fluid motion. Mayhead (1973b)

reported that one Scots pine tree broke while being subjected to 38.3 $m \cdot s^{-1}$ flow in a wind tunnel, but the risk of structural damage has prevented other wind tunnel tests of tree performance during extreme wind conditions. Lopez et al. (2011, 2014), however, considered the theoretical drag reductions afforded by flow-induced brittle fracture using analytical and numerical simulations. In these models, the location of maximum stress leading to flow-induced failure was governed mostly by branch slenderness, β, and diameter ratio, λ, as previously defined by Rodriguez et al. (2008). For most trees, where $\beta > 1$, fracture occurs in the branching system at a specific location determined by the material properties, fluid motion, and λ; each branch failure event decreased total drag and increased the tree's ability to sustain additional fluid loading (Lopez et al. 2011). However, sound wood is not a brittle material and rarely fails instantaneously.

Although experiments offer valuable insight about the response of trees to relatively uniform flow, field measurements reveal an increasingly complex, non-linear sway response by trees to stochastic, turbulent wind loads. Several authors reported that trees sway in complex downstream elliptical orbits whose magnitude generally increased in proportion to wind velocity (Holbo 1980; Mayer 1987; Peltola et al. 1993; Gardiner 1994; Peltola 1996; Hassinen et al. 1998; Rudnicki et al. 2001; James et al. 2006; Schindler 2008; Schindler et al. 2012b). Still, the individual responses of adjacent trees to wind are often markedly dissimilar. Schindler et al. (2012b) reported mutually incongruous instantaneous sway responses among four adjacent Scots pine trees during a two-minute wind event; the trees mostly displayed small-scale orbits about their neutral position and a few larger, downstream orbits with inconsistent trajectories.

A few reports indicate weak correlations between instantaneous tree displacement and u (Peltola et al. 1993) or u' (Schindler 2008). At small time scales, tree displacement is affected by short-lived gusts, elastic restoring and damping resistive forces, as well as the phase of vibration relative to neighboring trees and the applied wind force (Schindler 2008). Unsatisfactory

predictions of tree displacement in the time domain have motivated some to pursue alternative approaches in the frequency domain or time-frequency space (Schindler 2008; Schindler et al. 2010, 2012b, 2013b).

For example, the energy spectra of a wind load and tree displacement can be related mathematically by a mechanical transfer function, $H_m(f)$, (Holbo 1980; Mayer et al. 1989; Flesch and Wilson 1999; Schindler 2008):

$$H_m = \sqrt{S_x(f) \Big/ S_k(f)}, \quad \text{Eq. 35}$$

where $S_x(f)$ is the tree displacement spectrum and $S_k(f)$ is the wind load spectrum. Mayer et al. (1989) recommended that the wind load spectrum be determined using instantaneous Reynolds stress, τ (Pa):

$$\tau = \rho\overline{u'w'}. \quad \text{Eq. 36}$$

$H_m(f)$ represents the transfer of energy from the wind to a tree over the range of analyzed frequencies, and most studies have reported that wind energy is most efficiently transferred to a vibrating tree at frequencies near its f_n (Holbo 1980; Mayer 1987; Mayer et al. 1989; Peltola 1996; Hassinen et al. 1998; Flesch and Wilson 1999; Schindler 2008).

Fewer researchers have attempted to measure the magnitude of physical loads on large trees experiencing dynamic wind loading. In limited available reports, wind loads were estimated using a moment-displacement coefficient obtained by calibrating instrumented trees with a static pull test. Specifically, trees were subjected to a series of known loads, and the anticipated linear proportionality between force and displacement was estimated with a least-squares regression coefficient (Milne and Blackburn 1989; Bruchert et al. 2000; Silins et al. 2000; James and Kane 2008; Angelou et al. 2019). Using this method, James et al. (2006) recorded a 230 kN·m maximum instantaneous M_B among observations of five different tree species during a 22 $m \cdot s^{-1}$ gust. Gardiner et al. (1997) developed a predictive equation to determine maximum M_B for a

given wind speed among 12 m tall Sitka spruce:

$$M_B(\max) = (6.78s + 2.7) \cdot \bar{u}^2, \qquad \text{Eq. 37}$$

where *s* is tree spacing (m). Under similar wind conditions, this equation reasonably predicts that these small Sitka spruce would experience a much lower (7.2 kN·m) maximum instantaneous M_B. Similarly, Hale et al. (2012) reported strong correlations between the maximum hourly M_B and average hourly wind speed, with coefficients of determination between 0.77 and 0.97.

Thigmomorphogenesis

In addition to short-term responses to fluid motion, many studies demonstrate that trees acclimate over longer periods to mechanical stimuli with compensatory growth (Telewski 1986). Tree pulling studies have demonstrated the increased resistance to overturning by large trees, represented numerically by tree mass, height, diameter, or volume (Fraser 1962; Somerville 1979; Coutts 1986; Smith et al. 1987; Fredericksen et al. 1993; Papesch 1997; Ray and Nicoll 1998; Moore 2000; Peltola et al. 2000; Achim et al. 2005a, b; Jonsson et al. 2006), that indicates an acclimation of trees to environmental forces as they grow (Nicoll et al. 2008). The ontogenetic acclimation to physical disturbance occurs by alterations to morphological and anatomical characteristics that confer increased mechanical resistance; shoots experiencing physical perturbation, for example, often exhibit decreased vertical growth and increased thickness (Coutand and Moulia 2000).

Plants experiencing frequent flow-induced disturbance decrease shoot growth and increase root growth, resulting in more numerous and longer windward and leeward roots (Stokes et al. 1995; Tamasi et al. 2005) and shorter branches with fewer leaves (Telewski and Pruyn 1998; Puijalon et al. 2005). In addition to enhanced tolerance of flow-induced stress, Vogel (1984) suggested these adaptations might also reflect the tree's need to maintain physiological function during wind events. The sensitivity and responsiveness of plants to mechanical stimuli during ontogeny,

termed mechanoperception and thigmomorphogenesis, respectively, have been studied extensively (Coutand 2010).

Risk Mitigation Strategies

After conducting a tree risk assessment, an arborist may recommend appropriate risk mitigation measures that address a defect or other structural problem to diminish the likelihood of failure for a specific tree, but it is generally the responsibility of the tree owner or controlling authority to pursue any of the recommendations (TCIA 2017a). In addition to tree removal, the most common risk mitigation measures addressing physical aspects of tree condition include site modification, support systems, and pruning treatments (Dunster et al. 2017). Site modification measures may include moving a stationary target or restricting pedestrian site access, but these are often used as a temporary measure in advance of a more permanent treatment. Tree support systems and pruning treatments affect the likelihood of failure over a longer period.

Support Systems

Support systems are often used to reinforce weak parts of a tree, and these systems may include cables, guy wires, props, and brace rods (Smiley and Lilly 2014). A few existing studies have addressed hardware performance (Jeffers and Abbott 1979; Smiley et al. 2000, 2003; Kane 2011; Smiley 2011) and induced decay associated with tree support systems (Smiley 1998; Kane and Ryan 2002). There is limited rigorous evidence to describe the effect of support systems on the likelihood of failure. It is important to note that support systems are not usually intended to entirely restrict tree movement but rather supplement weak parts of the tree by selectively restricting certain modes of deformation. Reiland et al. (2015) reported that cables installed between co-dominant stems on red oak interacted with leaf condition to affect f_n with comparatively greater values during out of leaf periods.

Several studies have demonstrated that tree parts held rigid against external forces grow differently than unrestricted parts of the same tree (Burton and Smith 1972; Meng et al. 2006). Burton and Smith (1972), for example, reported that guyed loblolly pines [*Pinus taeda* L. (Pinaceae)] exhibited decreased secondary growth in the restrained trunk portion and increased secondary growth in the free swaying trunk portion compared to other trees without guy wires, and wood extracted from the restrained trunk portion had lower density and less compression wood fiber-tracheids. These observations demonstrate the inhibition of thigmotropic growth response by the guy wires, and most would regard the lost natural mechanical acclimation as detrimental to the tree's resistive capacity. Kane and Autio (2014), however, demonstrated that properly installed support systems did not affect secondary growth of the supported stems except for woundwood formation near the point of hardware installation.

Pruning

Trees are often pruned for many reasons, including to improve aesthetics, manage plant health, increase spatial clearance, and preserve unobstructed sightlines; but mitigating the likelihood of failure is often a primary goal of this common maintenance activity (Gilman and Lilly 2008; TCIA 2017b). The most common pruning methods are to clean, thin, raise, or reduce the tree crown, and any combination of these methods could be used in pursuit of the desired objectives (TCIA 2017b). Three types of pruning cuts are commonly used by arborists, including removal, reduction, and heading cuts. Removal cuts are used to remove an entire branch at its attachment, reduction cuts shorten a branch to a node containing a subordinate branch, and heading cuts shorten branches to internodal positions or small axillary buds (Gilman and Lilly 2008).

Inevitably, pruning cuts create wounds that are vulnerable to wood decay infections (Barry et al. 2000; Deflorio et al. 2007). Among all types, branch removal cuts minimize the susceptibility of wounds to decay by simulating the natural branch shedding process. Shigo (1985, 1990) first

observed that damaging the trunk tissue while removing branches resulted in greater decay, and cuts made outside the trunk tissue surrounding branches preserve important host defensive features. Subsequently, considerable work has addressed decay (White and Kile 1993; Wardlaw and Neilsen 1999; Eisner et al. 2002; Pinkard et al. 2004; Gilman and Grabosky 2006; Wiseman et al. 2006; Deflorio et al. 2007; Grabosky and Gilman 2007; Sandi et al. 2012) and wound occlusion (Neely 1979; Smith et al. 2006; Hein and Spiecker 2007; Nicolescu et al. 2012; Ow et al. 2013) associated with individual pruning cuts. In general, despite notable interspecific differences, pruning wound size is positively related to decay and negatively proportional to occlusion rates (Danescu et al. 2015). These insights into the execution of various pruning cuts allow arborists to make cuts that inflict the least amount of damage to living trees.

Pruning immediately changes tree size and shape by removing specific branches, and there is some evidence that it similarly affects crown architecture over longer periods by altering ontogeny. Many trees growing in non-limiting conditions experience a short-term net increase in photosynthetic CO_2 assimilation, driven by increased sink demand, after light to moderate pruning (Pinkard and Beadle 1998a). In shining gum [*Eucalyptus nitens* (Deane and Maiden) Maiden (Myrtaceae)], for example, de-branching resulted in a net increase in biomass production corresponding to pruning severity (Pinkard et al. 1998). After light pruning, the compensatory photosynthetic response often preserves relative height and diameter growth rates, but evidence suggests that large (> 50%) pruning severities may significantly decrease these growth rates for some tree species (Pinkard and Beadle 1998a). However, the amount of pruning at which growth is affected is considerably less for slow-growing trees (Dakin 1982).

There is some concern that excessive pruning to raise might cause an undesirable increase in trunk or branch slenderness (Gilman and Lilly 2008). Generally, trees with more branches distributed along their trunk (i.e., greater crown length) will be more tapered than trees with fewer

branches (Muhairwe 1994; Pinkard and Beadle 1998b). Tapered stems better resist applied external loads (Papesch 1997; Moore 2000; Peltola et al. 2000; Bergeron et al. 2009), and there is mixed evidence that removing secondary branches decreases (Larson 1965) or does not affect (Sutton and Crowe 1975; Bredenkamp et al. 1980) taper. The mechanical implications of increased slenderness are especially important for arborists considering the likelihood of failure (Petty and Swain 1985).

A few studies suggest that pruning interventions may improve the strength of co-dominant branch attachments by altering $\Re_B$ (Downer et al. 1994; Grabosky and Gilman 2007; Gilman 2015a, b). In these studies, shortening a branch with reduction pruning decreased that branch's secondary growth rates and reduced $\Re_B$ for the co-dominant attachment, and the decrease in $\Re_B$ was proportional to pruning severity, elapsed time after pruning, and relative height in the crown (Gilman 2015b). Consequently, arborists can identify these weak branch attachments and may be able to intervene to improve their strength with targeted reduction pruning treatments.

In terms of vibration properties, studies generally demonstrate that pruning increases f_n and decreases ζ, but pruning type and severity often interact uniquely with different species to produce distinct outcomes (Sugden 1962; Mayhead et al. 1975; Milne 1991; Moore and Maguire 2005; Kane and James 2011; James 2014). Several reports indicate that f_n did not increase until nearly all branches were removed from plantation-grown (Moore and Maguire 2005) and open-grown trees (James 2014). Moore and Maguire (2005), specifically, reported that f_n increased exponentially after ~80% of crown mass had been removed from raised Douglas-firs. In contrast, f_n increased after the height of chestnut oak and Bradford pear was reduced by 25 and 12%, respectively (Kane and James 2011).

Most trees exhibit marked reductions in ζ following increasingly severe pruning treatments, but some have observed a slight increase in ζ after lower pruning severity (Moore and Maguire 2005; Sellier and Fourcaud 2005; James 2014). Sellier and Fourcaud (2005), for example, reported a modest increase in ζ after removing all tertiary axes on small maritime pine trees resulted in their defoliation. These results suggest that pruning leafy higher-order branches, normalized by mass, may have an outsized influence on damping processes. Other studies reported that pruning did not independently affect ζ of small open-grown decurrent trees (Kane and James 2011; Miesbauer et al. 2014).

In terms of wind loads, several studies addressing open-grown trees showed that pruning reduced P (Pavlis et al. 2008), M_B (Smiley and Kane 2006), ε (Gilman et al. 2015), and trunk movement (Gilman et al. 2008a, b). Consistent with other drag measurements, several studies demonstrated that pruned trees experienced a decrease in wind disturbance proportional to the mass of branches and foliage removed, but there is little consensus about the most effective pruning type for reducing the likelihood of failure (Smiley and Kane 2006; Gilman et al. 2008a, b; Pavlis et al. 2008; Miesbauer et al. 2014). Gilman (2008a) reported that trunk movement decreased more on reduced, raised, lion's tailed, and structurally pruned than thinned trees. Subsequently, Gilman et al. (2008b) reported that trunk movement decreased more on thinned and reduced than raised trees. Although not statistically significant, Smiley and Kane (2006) reported that M_B was lower for reduced than thinned trees, and this effect became increasingly pronounced at higher wind speeds.

Mayhead et al. (1975) suggested that drag decreased more efficiently on raised than thinned trees because of the larger decrease in frontal area. Complementary wind tunnel investigations of several coniferous and broadleaf species, however, reported that crown raising had divergent consequences on drag per unit mass with some trees experiencing greater crown reconfiguration

or wind exposure and decreased or increased drag per unit mass, respectively (Rudnicki et al. 2004; Vollsinger et al. 2005); these results demonstrate the subtle ways in which pruning treatments, crown geometry, and wood material properties interact to produce unique species-specific wind performance outcomes.

This literature review illustrates the complex and varied considerations needed to assess the likelihood and mitigate the risk of tree failure. Despite a generous body of knowledge, additional study is needed to understand the mechanical properties and wind performance of large, mature trees–especially open-grown, decurrent specimens. Especially for these increasingly complex branched systems, the literature demonstrates the important contributions of crown architecture and branch morphology to mechanical performance. There is also a need to quantify changes in mechanical properties and wind loads of these trees after pruning; observations of pruning-induced changes to mechanical stability under dynamic wind loads are currently nonexistent. Therefore, an investigation is proposed to address the following three hypotheses using large, mature rain tree [*Samanea saman* (Jacq.) Merr. (Fabaceae)] and Senegal mahogany [*Khaya senegalensis* (Desr.) A. Juss. (Meliaceae] in Singapore:

1. Pruning type and severity affect the mass and vibration properties (i.e., f_n and ζ) of tree parts;
2. Morphometric attributes of pruned trees explain pruning induced changes in vibration properties; and
3. Pruning type and severity affect wind-induced vibration and bending moments.

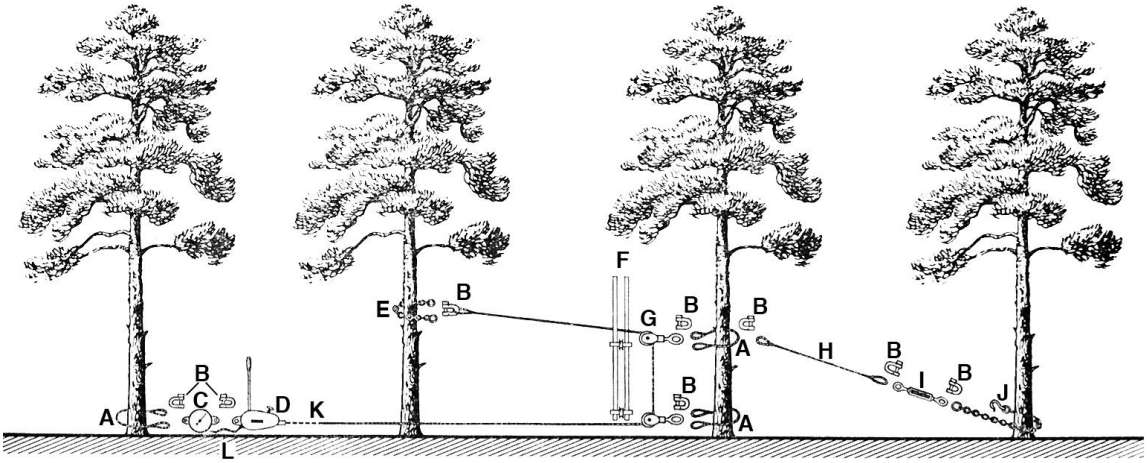

Figure 1 Schematic layout of tree pulling system, including slings (A, E, J), shackles (B), dynamometer (C), cable winch (D), block spacer (F), shingle sheave snatch blocks (G), backstay wire rope (H), adjustable rigging screw (I), painted marks approximating 1° trunk deflection increments (K), and wire rope running end (L). Figure adapted from Fraser and Gardiner (1967).

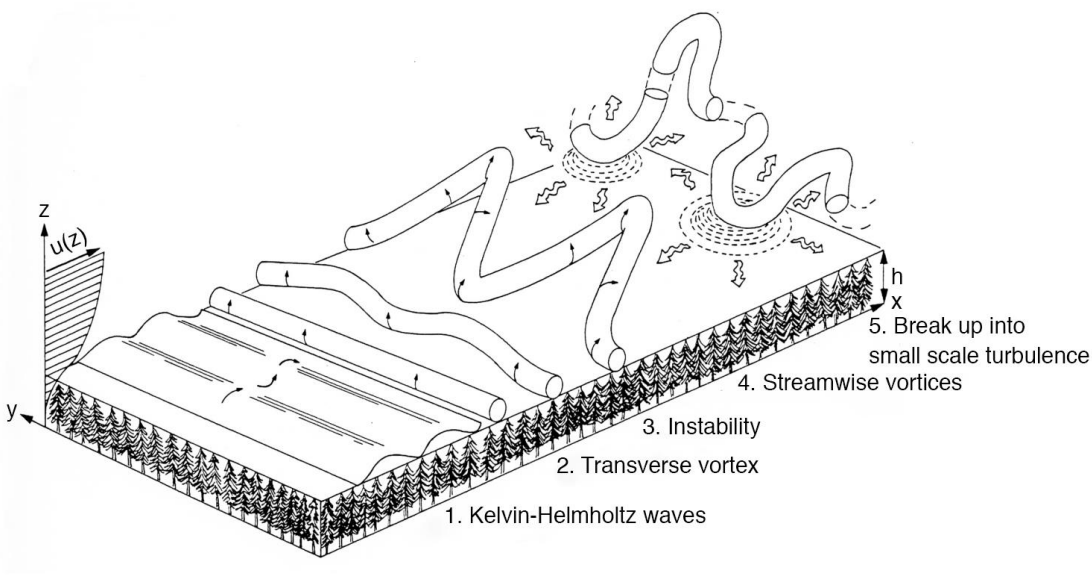

Figure 2 Three-dimensional evolution of coherent structures above a forest canopy. Figure adapted from Sellier (2004).

Table 1: Conversion factors for common units of measurement (Pennycuick 1988)

Quantity	**SI Unit** *To convert*	**U.S. Customary Unit** *Into*	**Conversion Factor** *Multiply by*
Length	meter	foot	3.2808
Mass	kilogram	pound	2.2046
Density	kilogram per cubic meter	pound per cubic foot	6.2428×10^{-2}
Speed	meter per second	miles per hour	2.2369
Force	Newton	pound-force	2.2481×10^{-1}
Pressure	Pascal	pound-force per square inch	1.4504×10^{-4}
Torque	Joule (= 1 Newton meter)	foot pound-force	7.3756×10^{-1}

CHAPTER 3

MATERIALS AND METHODS

Experimental site and tree species

Twelve Senegal mahoganies and 10 rain trees were selected for study from a managed urban woodland near Choa Chu Kang, Singapore (latitude 1° 23' N, longitude 103° 45' E, elevation 10 m). The trees were growing in a 5.5 ha even-aged, homogenous stand among 173 other large, mature trees (≈ 31 trees·ha^{-1}). The stand was composed almost entirely of Senegal mahogany and rain tree: 103 (59.5%) Senegal mahoganies had a mean trunk diameter of 0.69 m (range: 0.24 – 1.16 m) and 65 (37.6%) rain trees had a mean diameter of 0.63 m (range: 0.36 – 1.1 m). The trees were not maintained after planting on an unknown date. The understory was mechanically cut bi-monthly and consisted mainly of cow grass [*Axonopus compressus* (Sw.) P. Beauv. (Poaceae)], wild pepper [*Piper sarmentosum* Roxb. (Piperaceae)], wild sugarcane [*Saccharum spontaneum* L. (Poaceae)], and giant taro [*Alocasia macrorrhizos* (L.) G. Don (Araceae)]. Trees with similar size and shape were selected for the study. Prior to any measurements, crowns were pruned to remove epiphytes and dead, dying, diseased, damaged, or broken branches.

At this location, the climate is typical of the equatorial tropics with stable temperatures ranging daily between 24° and 32° C, abundant rainfall approaching 250 cm annually, and elevated humidity. The prevailing winds are generally mild, and their direction varies seasonally according to monsoonal periods (Nathan and Goh 1981). In Singapore, monsoons occur during winter in the Northern (December – March) and Southern (June – September) hemispheres with winds arising from the Northeast and Southwest, respectively, during these seasons (Georgiou 1990); the strongest winds occur during the Northeast monsoon with monthly mean wind speeds ranging between 2 and 5 m·s^{-1} (Nathan and Goh 1981). During inter-monsoonal periods, light and variable winds are mostly governed by thermal conditions and weather systems; and thunderstorms frequently couple with higher wind gusts and turbulence intensities throughout the

year (Choi 2000). Although rare, wind gusts can approach 20 $m \cdot s^{-1}$ during thunderstorm downdrafts in Singapore (Choi 2004).

Senegal mahogany and rain tree occur naturally throughout humid, tropical Africa and South America, respectively, reaching mature heights between 15 and 25 m. The growth dynamics and crown architecture of each species are distinct. Senegal mahogany displays subtly rhythmic meristematic growth that produces sympodial, orthotropic, and radially symmetric branches; and rain tree grows near continuously and indeterminately into a crown composed almost entirely of sympodial, plagiotropic, and dorsiventrally symmetric branches (Halle et al. 1978). Green wood of Senegal mahogany has a reported average density of 0.63 $g \cdot cm^{-3}$, stiffness of 7.9 GPa, and modulus of rupture of 5.1 MPa; green wood of rain tree has a reported average density of 0.50 $g \cdot cm^{-3}$, but little information is available to describe its mechanical properties (Chave et al. 2009; Kretschmann 2010).

Tree and branch attributes

Detailed morphological measurements were made, including trunk diameter 1.37 m above the highest root, DBH (m); tree height, H_{TREE} (m), the vertical distance between the highest root and crown apex; crown width, W_{CROWN} (m), the mean of width measured in the North-South and East-West directions; and crown length, L_{CROWN} (m), the distance between the lowest branch and crown apex. Detailed measurements of the topology and geometry of primary branches were also recorded broadly according to Godin et al. (1999). These measurements were converted into several complementary parameters that described branch-pairs as outlined by Niklas and Kerchner (1984), including, branch inclination relative to the horizontal plane, θ (°); attachment angle between a bifurcated pair, φ (°); branch rotation, γ (°); branch diameter proximal to the attachment point, D_{BRANCH} (m); branch length, L_{BRANCH} (m); and branch attachment height above ground, H_{BRANCH} (m). The inclination and attachment angle of curved branches was approximated

by that of a line segment connecting the branch base to its tip. In addition, aspect ratio, $\mathfrak{R}_B$ (dimensionless), was computed to describe the relative size of branch pairs by dividing the branch diameter of the larger member into the subordinate. All diameters were measured outside of the bark. Length measurements were recorded using a steel tape measure (Fisco Satellite, Essex, England) and angles were recorded using a handheld compass and inclinometer (Suunto MC-2, Vantaa, Finland).

Instrumentation

To record axial trunk displacement, $\boldsymbol{x}$ (mm), two LVDT displacement probes (Solartron Metrology, VS/20/U, West Sussex, UK) were installed orthogonally on the trunk of each tree 1.37 m on-center above the highest root. Mounted on top of the bark using universal joints secured with hanger bolts, the probes measured up to 20 mm displacement over a linear distance of 226.9 mm with a measurement resolution of 10 μm and accuracy equivalent to 0.20% of output, yielding a strain resolution of 43 $\mu m \cdot m^{-1}$. They were oriented axially (i.e., parallel to wood grain) and positioned on the North (0°) and East (90°) aspects of the trunk (Figure 4).

To record branch acceleration, $\boldsymbol{a}$ ($m \cdot s^{-2}$), two triaxial accelerometers (Freescale Semiconductor, MMA8452Q, Austin, Texas) were installed on a pair of large, similar-sized branches using mounting blocks secured with wood screws. They were positioned on the adaxial branch surface along the medial longitudinal plane bisecting the branch pair 1.50 m distal to the branch attachment (Figure 4). Accelerometers measured acceleration within a range of ±2 *g* with accuracy equivalent to 2.5% of output. After installation, the position and orientation of each accelerometer was recorded by measuring their height above ground, branch diameter at attachment, and compass orientation and inclination of all three measurement axes. Each accelerometer's *z*-axis was positioned parallel to the local longitudinal axis of the branch to which it was attached (Figure 4). As a result, the *x*-*y* plane in which accelerations were measured was

oriented perpendicular to the longitudinal axis of each branch. One pair of accelerometers was installed as indicated on each Senegal mahogany included in the study, and three pairs of accelerometers were installed on one Senegal mahogany and three rain trees.

To measure wind velocity, $\boldsymbol{u}$ ($m \cdot s^{-1}$), along a vertical gradient in the center of the experimental site (Figure 3), four ultrasonic anemometers (R.M. Young, Model 85106, Traverse City, MI, USA) were installed at 4.57 m intervals on an 18.3 m tall aluminum guyed mast (South Midlands Communications, PA2, Hampshire, England). The height, z (m), of anemometers normalized by the average height of experimental trees, H_{TREE} = 26.9, was 0.17, 0.34, 0.52, and 0.69. The anemometers measured wind speed within a range of 0 to 70 $m \cdot s^{-1}$ with a resolution of 0.1 $m \cdot s^{-1}$ and accuracy equivalent to 3% of output; and they recorded wind direction within a range of 0 to 360° with a resolution of 1° and ± 2° accuracy.

On each tree, the displacement probes and accelerometers recorded data continuously and delivered measurements to a local data logger (Raspberry Pi Foundation, Raspberry Pi Model B, Cambridge, England) over single strand copper wire and USB cable, respectively. The analog displacement probe output in volts was immediately converted to digital displacement values (μm). Data stored locally was transferred over Ethernet cable via HTTP protocol to a central data logger (Technologic Systems, TS-7800, Fountain Hills, AZ, USA). At the guyed mast, digital wind speed and direction measurements were sent directly to the central data logger by RS232 cables. All instruments recorded observations at irregular time intervals near 0.04 sec (27 Hz). The measurements aggregated on the central data logger were periodically transmitted wirelessly to a remote server made accessible by a web-based interface. Four solar panels and batteries (Global & Yuasa Battery Co., Rocket ESC 200-12, Seoul, Korea) provided power to the entire sensor network and data acquisition system.

Measurement of mechanical properties

Mechanical properties of each tree were determined by measuring its response to controlled loading conditions. Specifically, the structural Young's modulus, E_{STRUCT} (MPa), was measured during static deflection, and trunk and branch natural frequencies, f_n (Hz), and damping ratios, ζ (dimensionless), were measured during free vibration tests. To measure E_{STRUCT}, a series of three to four loads was applied incrementally to each tree using a rope attached to the trunk. The measured compressive displacement (mm) induced by the static pull tests was converted to ε according to Eq. 1, and this measured strain was compared to the sum of induced bending and axial stress, σ, calculated as (Kane 2014):

$$\sigma = {F \sin\theta}/{\pi ab} + {F \cos\theta \, Lb}/{I}, \quad \text{Eq. 38}$$

where F is the force (N) applied by the rope; θ is the angle (°) between the rope attachment point and a horizontal plane parallel to the ground; a and b are the trunk radii normal and parallel to the direction of bending, respectively; L is the distance (m) between the rope attachment point and the midpoint of the displacement probe; and I is the second moment of area (m^4) determined by considering each trunk cross section as approximately elliptical using Eq. 6 (Figure 4). E_{STRUCT} was determined as the slope of an ordinary least squares regression line fit to model σ as a function of ε; a linear relationship was assumed for $\sigma(\varepsilon)$ since measured ε was far below the elastic limit, i.e., 1 – 2% (Kollmann and Cote 1968). On a subsample of seven trees, E_{STRUCT} was determined by pulling Senegal mahoganies from two orthogonal directions (i.e., North and East). To estimate wind-induced bending moments, M_B (kN·m), the static pull tests were also used to determine a calibration constant, C_1 (kN·m), relating trunk ε to an applied M_B for individual trees (Wellpott 2008). The incremental M_B generated at the height of measurement was calculated as:

$$M_B = F \cos\theta \, l, \quad \text{Eq. 39}$$

with variables identical to those indicated for Eq. 38.

Pull-and-release free vibration tests were performed on days without precipitation and when ambient winds were < 3 $m \cdot s^{-1}$. Each tree was displaced from its resting position using a rope attached to the trunk incident to one of the displacement probes. The load was instantaneously released, allowing the tree to sway freely as it returned to its resting position. Crown collisions between experimental trees and their neighbors were prevented by selectively removing those branches from nearby trees that would have inhibited free sway.

Trees were displaced using a rope attached to the trunk and aligned incident to one of the displacement probes. A rope (16 mm Stable Braid or 13 mm Amsteel Blue, Samson Rope Technologies, Ferndale, WA, USA) extended from an anchor tree and through an arborist block (RP055, International Safety Components, Gwynned, United Kingdom) attached to the trunk with a round sling (Super Techlon, Technotex Industrial Supply, Coevorden, Netherlands) and returned parallel to itself. The working end of the rope was pulled using either a cable winch (WRP16, Toyo, Tianjin, China) or a capstan winch (GRCS, Good Rigging Control LLC, Hartland, WI, USA) to generate tension. The other end of the rope was connected to a digital dynamometer (EDXtreme-5T, Dillon, Fairmont, MN, USA) with 5,000 kg capacity, 1 kg resolution, and ±5 kg accuracy. This configuration made it easy to monitor rope tension during pull testing. Measurements recorded by the dynamometer were doubled because running the rope through a block approximately doubles the force applied to the tree. The dynamometer was secured with another round sling to the same anchor tree. During free vibration tests, the applied load was instantaneously released by cutting a sacrificial piece of rope with a pole saw. A continuous loop was formed by tying a double fisherman's knot with arborist's climbing rope, and this was inserted into the rigging system between the winch and running end of the rope with two D shackles. Rotation of the root-soil system was not monitored during pull testing.

Time histories of $\boldsymbol{x}$ and $\boldsymbol{a}$ from the free vibration tests were used to determine f_n and ζ. A scalar projection of each observation of $\boldsymbol{x}$ or $\boldsymbol{a}$ was made onto the corresponding resultant vector for each time history, decomposing recorded two- or three-dimensional movement into that along its primary axis. For a vector quantity $\boldsymbol{v}$, measurements were considered as a series of observations in $\mathbb{R}^n$ with components $\boldsymbol{v} = \langle v_1, v_2, \ldots v_n \rangle$, where $v_1, v_2, \ldots v_n$ are measured along orthogonal axes. The scalar projection of each observation of $\boldsymbol{v}$ onto its resultant vector $\boldsymbol{r}$ was determined using:

$$proj_{\boldsymbol{r}}\boldsymbol{v} = \boldsymbol{v} \cdot \boldsymbol{r} / |\boldsymbol{r}|. \quad \text{Eq. 40}$$

Initial displacements and accelerations recorded during free vibration tests, artefacts of the test method, were removed from time histories before analysis. Time histories were limited to 1024 observations, approximately 38 sec. Spectral analysis was used to determine the frequencies of tree parts undergoing free vibration. Since the data were sampled at uneven intervals, power spectral density (PSD) was computed using the Lomb-Scargle periodogram (Press and Rybicki 1989), and the absolute peak in PSD was used to identify the damped frequency, f_d (Hz) of the measured tree part.

ζ was determined by fitting Eq. 11 to each free vibration time history according to Bruchert and Gardiner (2006), with the constants initial displacement, A (mm), and phase angle, ϕ (rad), set equal to $A = x(t_0)$ and $\phi = \pi/2$, respectively and $\omega_d = f_d \cdot 2\pi$. In all tests, the phase angle was held constant at $\phi = \pi/2$ to allow the first observation to exactly equal a local minimum corresponding to the start of the second full cycle of periodic motion, i.e., $\sin(\pi/2) = 1$. Subsequently, the damped frequency identified in the PSD plot was converted to f_n using Eq. 12. Only the vibration properties associated with the fundamental mode were used in statistical analyses.

Measurement of wind-induced vibration and bending moments

For Senegal mahoganies, $\boldsymbol{u}$, $\boldsymbol{x}$, and $\boldsymbol{a}$ were measured continuously over extended periods of time. Two coordinate systems were used to analyze wind-tree interaction in this study. First, a standard three-dimensional Cartesian coordinate system (i.e., the "observational coordinate system") was used to record wind velocity, $\boldsymbol{u}$; trunk displacement, $\boldsymbol{x}$; and branch acceleration, $\boldsymbol{a}$, with the positive *x*-, *y*-, and *z*-axes oriented North, West, and normal to the Earth's surface, respectively. Two-dimensional $\boldsymbol{u}$ and $\boldsymbol{x}$ observations were recorded directly in this Cartesian space, but the unique alignment of accelerometers on each branch resulted in observations of $\boldsymbol{a}$ being made in different coordinate systems. As a result, each coordinate system used to record $\boldsymbol{a}$ was rotated about the three-dimensional vector observations so that all measurements existed in the same Cartesian space. A coordinate system rotation in $\mathbb{R}^3$ about the *x*-, *y*-, or *z*-axis is achieved by multiplying a vector by the corresponding 3 × 3 rotation matrix:

$$R_x(\xi_1) = \begin{bmatrix} 1 & 0 & 0 \\ 0 & \cos(\xi_1) & \sin(\xi_1) \\ 0 & -\sin(\xi_1) & \cos(\xi_1) \end{bmatrix} \quad \text{Eq. 41}$$

$$R_y(\xi_2) = \begin{bmatrix} \cos(\xi_2) & 0 & -\sin(\xi_2) \\ 0 & 1 & 0 \\ \sin(\xi_2) & 0 & \cos(\xi_2) \end{bmatrix} \quad \text{Eq. 42}$$

$$R_z(\xi_3) = \begin{bmatrix} \cos(\xi_3) & \sin(\xi_3) & 0 \\ -\sin(\xi_3) & \cos(\xi_3) & 0 \\ 0 & 0 & 1 \end{bmatrix}, \quad \text{Eq. 43}$$

where the rotation angles ξ_1, ξ_2, and ξ_3 describe the rotation of the *y*-*z* plane about the *x*-axis, the *x*-*z* plane about the *y*-axis, and the *x*-*y* plane about the *z*-axis, respectively (Arfken and Weber 2005). Total rotation is given as a combination of these three basic rotations:

$$\boldsymbol{a}' = R_x(\xi_1)R_y(\xi_2)R_z(\xi_3)\boldsymbol{a}. \quad \text{Eq. 44}$$

Second, tree movement was also analyzed with respect to the streamwise component of the mean wind vector (i.e., the "mean vector coordinate system"). Based on the assumption that drag primarily acts along the resultant wind vector, $\bar{\boldsymbol{u}}$ (Mayer 1987; Schindler 2008), scalar projections

were made of $\boldsymbol{u}$, $\boldsymbol{x}$, and $\boldsymbol{a}$ onto $\bar{\boldsymbol{u}}$ to obtain a scalar streamwise wind speed, u; trunk displacement, x_u, and branch acceleration, a_u.

Signal processing

To examine processes occurring at a range of time scales, 30-minute time histories of $\boldsymbol{u}$, $\boldsymbol{x}$, and $\boldsymbol{a}$ were used consistently for all analyses of wind-tree interaction. For all recorded signals, missing values, and those outside the measurement range of a given sensor, were replaced using nearest neighbor linear interpolation. Subsequently, the mean was removed from each signal to obtain fluctuations about this value. Remaining spikes were identified as values greater than three standard deviations from the mean and replaced with the nearest non-outlier value.

Spectral analysis

For spectral analysis, all signals were down sampled to uniform 0.05 sec intervals (20 Hz) using nearest neighbor linear interpolation and converted to the mean vector coordinate system. There was noticeable baseline drift in many signals, possibly caused by (1) solar heating of instruments or (2) hydroelastic swelling and shrinking of the tree parts during the day (Bonnesoeur et al. 2016). To remove these long-term variations as well as short-term fluctuations associated with instrument noise, signals were then filtered using a 6^{th} order infinite impulse response (IIR) Butterworth bandpass filter. Cutoff frequencies were selected based on a representative minimum time separating coherent structures, i.e., ~ 20 sec (Mohr and Schindler 2016), and a value exceeding the maximum f_n measured on trees during free vibration tests. This preserved all possible frequency components expected for both wind and trees and removed unwanted trends associated with other processes.

The following exclusionary criteria were used to reject time periods from consideration for spectral analysis (Serafimovich et al. 2011):

1. the presence of precipitation recorded by a tipping bucket rain gauge with 0.2 mm resolution and ±1.0% accuracy (S-RGB-M002, Onset Computer Corporation, Bourne, MA, USA) located approximately 1.3 km away from the experimental site, including subsequent 60-minute periods to allow for drying;
2. the occurrence of excessively calm wind conditions ($\overline{U}$ < 0.3 m·s^{-1}) with sensors operating close to their limits of detection; and
3. high variability in the direction of wind flow, χ (rad), assessed using the standard deviation of wind direction, ($\sigma_\chi \geq 0.7$ rad):

$$\sigma_\chi = \left[n^{-1}\sum_{i=1}^{n}\Delta_i{}^2 - (n^{-1}\sum_{i=1}^{n}\Delta_i)^2\right]^{0.5}, \quad \text{Eq. 45}$$

where Δ_i is the smaller of $|\chi_i - \bar{\chi}|$ and $2\pi - |\chi_i - \bar{\chi}|$ (Yamartino 1984).

In total, 20 separate 30-minute intervals were selected for spectral analysis, with four intervals chosen from each pruning severity. For each pruning severity, the set of qualifying 30-minute intervals were ranked according to their mean wind speed, $\overline{U}$ (m·s^{-1}), and the four separate intervals with the highest mean wind speed were selected for spectral analysis.

Fourier transform

To identify frequencies associated with wind-induced tree vibration, the Fourier energy spectrum S(f) was computed using 30-minute time histories of a_u and x_u. The fast Fourier transform was applied to 16 sequential, non-overlapping segments of 2048 observations using a Hanning window, and the amplitude spectrum was determined as the scaled magnitude of the single-sided Fourier transform. To obtain a smoothed amplitude spectrum, these 16 sequential spectra were ensemble averaged, and the resulting spectral estimate was smoothed using a three-sample moving average. Spectra were presented in semi-logarithmic format with f·S(f) plotted against log(f) to preserve the proportionality between the area under the curve and signal variance (Stull 1988). Since peaks are better associated with the correct scales using this spectral transformation

(Zangvil 1981), dominant frequencies were identified as those associated with the most prominent peaks in the Fourier energy spectra $f \cdot S_{au}(f)$ and $f \cdot S_{xu}(f)$ plotted against 1024 logarithmically-spaced frequencies.

Wind-induced bending moments

30-minute time histories of $\boldsymbol{u}$ and $\boldsymbol{x}$ recorded in the observational coordinate system were used to analyze the maximum wind-induced forces exerted on trees. Bending moments, M_B (kN·m), caused by wind events were estimated from measurements of trunk ε using C_1 determined during static pull tests. The maximum resultant wind-induced M_B and wind speed were selected from a series of 30-minute intervals during separate 45-day periods preceding and following all pruning treatments, to be described in detail later. All signal processing was performed in MATLAB (R2018b, MathWorks, Natick, MA).

Pruning treatments

Trees were pruned using methods commonly employed by practitioners in Singapore, broadly according to the American National Standard for Tree Care Operations ANSI A300 (Part 1) (TCIA 2017b). The crowns of one group of trees were raised to increase vertical space below the crown by progressively removing branches from the bottom of the crown upwards. The crowns of a second group of trees were reduced to decrease the overall height of each tree by shortening the length of the trunk and branches. During pruning, branches were progressively removed from horizontal slices of the crown (Figure 5). For raised and reduced trees, the slices originated from the bottom and top of the crown, respectively. As pruning severity increased, the thickness of horizontal slices increased by a distance equal to pruning severity multiplied by L_{CROWN}. On reduced trees, all tree parts were removed from each horizontal slice, and pruning cuts were made near the intersection of each tree part with the lower limit of each slice. Most tree parts were shortened using a heading cut, but some were shortened using a reduction cut – TCIA (2017b)

describes pruning cuts. On raised trees, all branches originating in each horizontal slice with a diameter less than 60% of its subtending member were removed to preserve crown structure. This simplistic approach to pruning did not represent aboricultural practice where the removal of branches depends on specific objectives, but it was needed for experimental consistency to induce similar changes to the crown dimensions of trees with different branch architecture.

Free vibration tests were conducted before pruning (i.e., 0% pruning severity), and the trees were then subjected to pruning severities between 10 and 80%. Senegal mahoganies were pruned to remove the specified tree parts from horizontal crown slices with thickness equal to 10, 20, 40, and 80% of L_{CROWN}. Rain trees were similarly pruned, except the 10% pruning severity was excluded. Pruning treatments were applied under the supervision of a single person to maintain consistency.

For Senegal mahoganies, free vibration tests were conducted immediately after each pruning treatment, but the severity of pruning was progressively increased at 45-day intervals to measure wind-induced tree movement between pruning treatments. In contrast, the severity of pruning was increased immediately after free vibration tests for rain trees without the 45-day interval. The iterative process of pruning and testing was repeated on pairs of rain trees (one of each pruning type) until 80% severity. As a result, wind-tree interaction was not examined for rain trees. The post-pruning growth response of Senegal mahogany was not measured, but it was possible to qualitatively assess whether post-pruning growth of Senegal mahoganies confounded the pruning treatments, since rain trees were pruned immediately after free vibration tests.

The basal diameter, D (m); total length, L (m); and total fresh mass (kg) of all tree parts removed during pruning were recorded in the field using a steel tape measure and the EDXtreme-5T dynamometer. Leaves were removed from each pruned tree part to determine the fresh mass of

wood, m_{WOOD} (kg), and leaves, m_{LEAF} (kg). After the final pruning treatment, the trees were felled to determine the mass of the remaining tree parts, and m_{TREE} was recorded as the total mass of each tree. The percent decrease in m_{TREE} and m_{LEAF} at each pruning severity was determined as the cumulative proportion of excised mass.

Experimental design and data analysis

Data were collected in two separate experiments independently addressing each tree species. The Senegal mahogany experiment was designed as one-way repeated measures analysis of variance (ANOVA) with one between-subject factor with two levels (pruning type: raise, reduce) and one within-subject factor with five levels (pruning severity: 0, 10, 20, 40, 80%). To minimize initial variability, trees were randomly assigned to pruning type after accounting for morphology. The rain tree experiment, conducted separately, was designed similarly to the Senegal mahogany experiment, except without the (i) 10% pruning severity and (ii) 45-day interval between pruning severities.

Scaling analysis and comparison of tree and branch attributes

First, data from both experiments were used to investigate size-dependent relationships between branch and leaf attributes, including the scaling of branch length, L_{BRANCH} (m), branch mass, m_{BRANCH} (kg), and leaf mass, m_{LEAF} (kg) with branch diameter, D_{BRANCH} (m). The basic procedure for bivariate linear regression was used consistently during analysis. Several candidate analytical functions were considered for modeling functional relationships, including linear ($y = \beta + \alpha x$), logarithmic ($y = \beta + \alpha \log x$) power ($y = \beta x^{\alpha}$), polynomial ($y = \beta + \alpha_1 x + \alpha_2 x^2 + \ldots + \alpha_n x^n$), and exponential ($y = \beta e^{\alpha x}$) functions. Despite the ubiquity of power-law relationships in biology (Xiao et al. 2011; Niklas and Hammond 2014), the mathematical form yielding the highest coefficient of determination was selected in each case to emphasize prediction (Prothero 1986).

Traditionally, power and exponential functions have been fit using linear regression of log-transformed observations of both the independent and dependent variable or only the dependent variable, respectively (Packard et al. 2011), but the additive, normal homoscedastic error associated with linear regression becomes multiplicative, lognormal heteroscedastic error after back transformation to the arithmetic scale (Packard 2014). Alternatively, nonlinear regression of untransformed observations results in a model with normally distributed, additive error (Packard 2009). As a result, the appropriate error structure was selected based on the recommendations of Xiao et al. (2011), as the model with the smallest AIC. Log-transformed parameter estimates were converted, as necessary, to their original linear scale for reporting and corrected for the mean difference between the log normal and normal distributions (Baskerville 1972; Sprugel 1983).

In all cases, the validity of statistical assumptions for linear regression was checked by (1) visually inspecting plots of residuals for uniformity, (2) testing homoscedasticity by computing the Spearman rank correlation between absolute studentized residuals and observations of the dependent variable, and (3) testing normality by computing the Kolmogorov-Smirnov statistic (Kutner et al. 2004). In addition, Cook's Distance statistic was computed to examine the influence of individual observations on the model, with cases exerting influence greater than $4/n$ inspected more closely (Marasinghe et al. 2008). Goodness of fit was examined by inspecting a graphical display of the model with its underlying data and tested using the *F*-test for lack of fit obtained from regression ANOVA (Kutner et al. 2004). The equality of scaling exponents between models fit to different species was tested using analysis of covariance (ANCOVA).

For the subset of Senegal mahoganies pulled from two orthogonal directions to estimate E_{STRUCT}, a paired t-test was used to test for differences in E_{STRUCT} between the two directions of pulling. A two-sample *t*-test was used to compare differences in E_{STRUCT} and R between species. All

statistical analyses were conducted using proc reg, proc glm, and proc ttest in SAS 9.4 (SAS Institute, Inc., Cary, NC, USA).

Effect of pruning treatments on mass and vibration properties

Second, data from both experiments were used to examine the effect of pruning treatments on mass and vibration properties determined from free vibration tests at each pruning severity. Linear mixed effects models for repeated measures ANOVA were fit to percent decrease in m_{TREE}, percent decrease in m_{LEAF}, f_n, and ζ using proc mixed in SAS 9.4. For each combination of pruning type and severity, the mean of three f_n or ζ observations was analyzed. Fixed effects for the model included pruning type, pruning severity, and their interaction. The random effect of tree, nested within pruning type, was also included in the model. For the rain tree experiment, an additional random replication effect was included to account for the iterative application of experimental treatments to pairs of trees. Model variance-covariance matrix structures were evaluated using visualization techniques (Dawson et al. 1997) and information criteria (Wang and Goonewardene 2004). The covariance structure with the algebraically lowest corrected Schwarz's Bayesian Information Criteria (BIC) was selected to preserve test power (Wang and Goonewardene 2004). The Kenward-Roger (Kenward and Roger 1997) correction was used to limit Type I error (Guerin and Stroup 2000) by obtaining error degrees of freedom adjusted for the selected covariance structure. Significant interactions were separated to determine the effect of pruning severity within each pruning type. Regression was used to separate means associated with specific levels of pruning severity (a continuous variable); total sums of squares were partitioned into single-degree-of-freedom orthogonal polynomial comparisons (OPC) to assess the significance of individual polynomial terms. Based on these results, least squares regression was used to determine the associated polynomial coefficients. An *F*-test was used to evaluate the mean difference between pruning types at 0% severity (i.e. before pruning).

Relationship between vibration properties and morphometric attributes of trees at all pruning severities

Third, data from both experiments were used to examine correlations between vibration properties (i.e., f_n and ζ) and 11 morphometric attributes of trees at all pruning severities. Morphometric attributes included apical diameter, d (m); basal diameter, D (m); total mass, m; leaf mass, m_{LEAF} (kg); length, L (m); slenderness, λ (dimensionless), computed as $L \cdot D^{-1}$; stockiness, ψ (m^{-1}), computed as $D \cdot L^{-2}$; height of branch apex, ξ (m), spread of branch apex, ς (m); branch inclination, θ (rad); and branch aspect ratio, $\mathfrak{R}_B$. At each pruning severity, ξ was determined as the vertical distance between the ground and terminus of a primary branch axis, and ς was determined as the horizontal distance between the trunk and terminus of a primary branch axis. Analyses were conducted separately for vibration properties determined from trunk displacement and branch acceleration. For branch-level correlations, d was determined as the diameter of the largest reduction cut on the branch under consideration, and it was assumed to be equal to 0.01 m – a representative thickness of twigs subtending apical meristems – at 0% severity. For tree-level correlations, d was determined as the diameter of the largest reduction cut on the tree; D and L were set equal to DBH and H_{TREE}, respectively; and branch attributes (i.e., ξ, ς, θ, and $\mathfrak{R}_B$) were determined as the mean of all primary branches on a tree.

Initially, bivariate scatter plots of vibration properties and each explanatory variable were inspected for patterns. Bivariate regression analysis was performed identically to that previously described for scaling analysis, and explanatory variables were transformed, if necessary, to linearize their relationship with vibration properties. After linearization, variables not significantly correlated with vibration properties were excluded from further consideration. The relative importance of remaining explanatory variables was investigated by computing the average squared semipartial correlation associated with each variable in all possible subsets of the full model (Kruskal 1987). Best subset selection was used to explore the suitability of various

linear combinations of explanatory variables for prediction by examining models with the lowest BIC. For these comparisons, models including and excluding an intercept term were fit. The possible existence of degrading collinearity among explanatory variables was investigated according to Belsley et al. (2004). Separately, the relationship between the two vibration properties (i.e., f_n and ζ) at all pruning severities was also examined using bivariate regression; and ζ was modeled as a function of f_n, since the former is more difficult to predict (Moore and Maguire 2004). All statistical analyses were performed using SAS 9.4. Regression models were fit using proc reg, and the relative importance of variables was computed using the dominance analysis macro (Azen and Budescu 2003).

Agreement between frequency determined from free and wind-induced vibration of trees

Three coefficients were computed to examine agreement between f_n determined using time histories of free vibration and wind-induced vibration of tree parts. Pearson's product-moment correlation (r) and Spearman's rank-order correlation (ρ) were computed to measure the strength of a linear relationship of the form $y = \beta + \alpha x$ between f_n determined from the two different measurements. Lin's concordance coefficient (p_c) was computed to measure the strength of a linear relationship of the form $y = x$ (i.e., 1:1 similarity) between the same datasets. Cook's D, measured during regression, was used to identify potential outliers in each comparison, with cases exerting influence greater than $4/n$ inspected more closely. Statistical analyses were performed using SAS 9.4; both r and ρ were computed using proc corr, and p_c was computed using the CCC macro v9 (Crawford et al. 2007).

Effect of pruning treatments on wind-induced bending moments

Fourth, data exclusively from the first experiment were used to examine the effect of pruning treatments on wind-induced bending moments, M_B (kN·m), experienced by Senegal mahogany at 0%, 10%, and 20% pruning severity. Linear mixed effects models for repeated measures analysis

of covariance (ANCOVA) were fit to 30-minute maximum M_B using proc mixed in SAS 9.4. Fixed effects for the model included pruning type, pruning severity, and their interaction. The random effect of tree, nested within pruning type, was also included in the model. A covariate was used in the model to account for the relationship between 30-minute maximum M_B and 30-minute maximum wind speed. First, the functional form of the relationship between these variables was determined using the same bivariate regression procedures employed for scaling analysis. In all cases, the validity of statistical assumptions for linear regression was checked. After determining the form of the covariate, the relationship between 30-minute maximum M_B and 30-minute maximum wind speed was examined separately for wind measurements from different anemometers, and the anemometer with measurements yielding the highest coefficient of determination was used consistently for the analysis of wind-induced M_B. Model variance-covariance matrix structures were examined using information criteria, and the covariance structure with the algebraically lowest BIC was selected. The Kenward-Roger correction was used to adjust the error degrees of freedom for the selected covariance structure. Subsequently, the homogeneity of slopes among fixed effects was tested and, if rejected, an unequal slopes model was fit to observations. Fixed effects were tested with the covariate set equal to 5 $m \cdot s^{-1}$. For significant fixed effects, LS means were computed at three values of the covariate distributed over the upper range of 30-minute maximum wind speeds: 4, 5, and 6 $m \cdot s^{-1}$. Significant interactions were separated to determine the effect of pruning severity within each pruning type. Regression was used to separate means associated with specific levels of pruning severity. Single-degree-of-freedom OPC were made to assess the significance of individual polynomial terms, and least squares regression was used to determine the associated polynomial coefficients. An *F*-test was used to evaluate the mean difference between pruning types at 0% severity (i.e., before pruning).

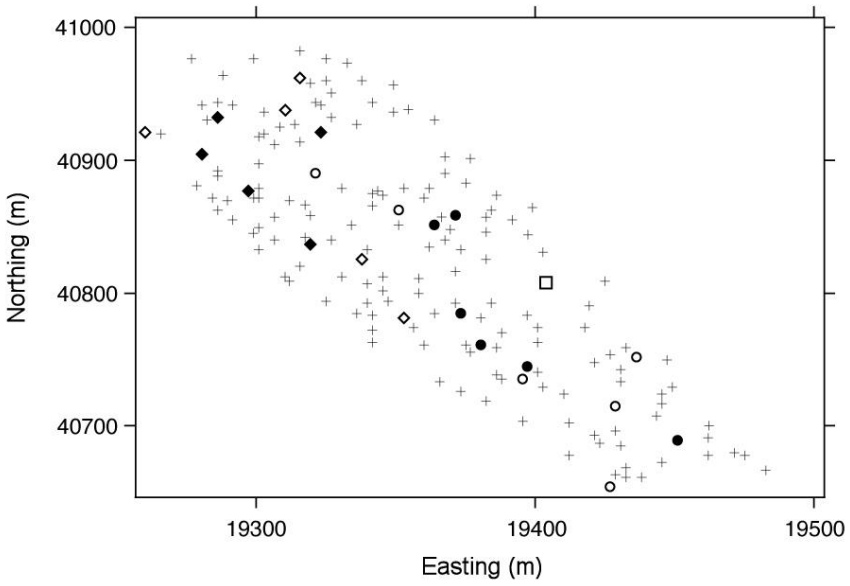

Figure 3: Site plan showing the location of experimental rain trees (*Samanea saman*, diamond marker) and Senegal mahoganies (*Khaya senegalensis*, circle marker), among other trees not involved in the study (plus marker) and the guyed mast supporting anemometers (square marker). Raised and reduced trees are identified using empty and filled symbols, respectively. Northing and easting units (m) represent distance from artificial origin at 103° 50’ 00’’ E 1° 22’ 00’’ N.

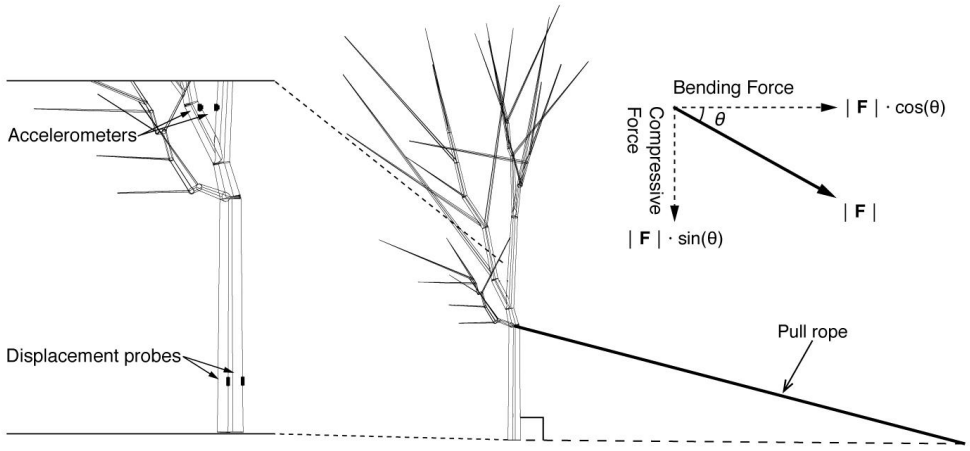

Figure 4: Schematic illustration of instrumentation (detail, left) and tree pulling layout.

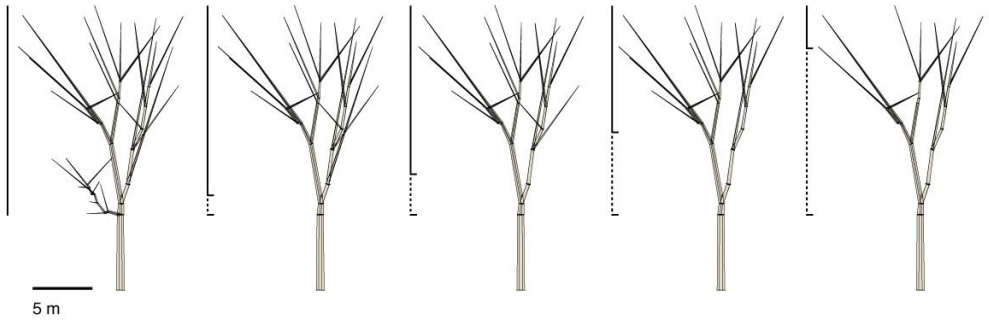

A

B

Figure 5: Crown architecture models of (**A**) raised and (**B**) reduced Senegal mahoganies (*Khaya senegalensis*) at (L – R) 0, 10, 20, 40, and 80% pruning severity. Consisting of a series of joined truncated cones, digital models were reconstructed from manual measurements of the dimension, position, and topological order of branches. During pruning, branches were progressively removed from horizontal slices of the crown. For raised and reduced trees, slices originated from the bottom and top of the crown, respectively. At each severity, the thickness of horizontal slices increased by a distance equal to pruning severity multiplied by crown length, L_{CROWN} (m). For reference, vertical lines show the thickness of crown slices (dashed line segment) relative to L_{CROWN} (combined dashed and solid segments).

CHAPTER 4

RESULTS

Tree and branch attributes

Since trees were selected to minimize initial variability in size, there was only modest variation in tree attributes of unpruned Senegal mahoganies and rain trees (Table 2). Among the trees used in the experiment, rain trees were, on average, shorter and had a larger *DBH* than Senegal mahogany. As a result, tree slenderness, λ_{TREE}, was greater, on average, for Senegal mahogany than rain tree. Moreover, rain trees had, on average, a much broader and marginally shorter crown than Senegal mahoganies. However, Senegal mahoganies had a longer branchless trunk with the height of the first branch occurring, on average, at 5.2 m (SD 2.0), nearly twice the average height of first branch on rain trees: 2.8 m (SD 0.3). The largest individual of each species had a total mass, m_{TREE}, of nearly 16 metric tons, but the range of Senegal mahogany m_{TREE} extended to include lower values, resulting in the species having a lower average m_{TREE}. Although rain trees had a higher m_{TREE}, on average than Senegal mahogany, leaves on the latter comprised 3.8% of m_{TREE}; on the former, leaves contributed only 1.0% of m_{TREE}.

Primary branches on rain tree were longer and had a larger basal diameter, on average, than their counterparts on Senegal mahogany, but Senegal mahogany branches were, on average, only 13% more slender than rain tree branches (Table 2). Concomitantly, primary branches on rain trees had a greater average total mass, m_{BRANCH}, than those on Senegal mahogany. On average, rain tree branches had larger branch attachment angles, φ, than Senegal mahogany. Similarly, rain tree branches had larger aspect ratios, $\mathfrak{R}_B$, on average, than Senegal mahogany, with the diameter of branch pairs more often nearly equal. In general, branch rotations, γ, were widely distributed among compass directions for both species.

Branch allometry

Branch allometry was examined using all branches removed from raised trees, but many branches removed from trees reduced by greater than 10% were excluded because they were shortened with reduction pruning cuts. In total, 458 Senegal mahogany and 313 rain tree branches removed during pruning were used to examine scaling relationships between branch attributes. Among these observations, D_{BRANCH} accounted for more of the variance in L_{BRANCH}, m_{BRANCH}, and m_{LEAF} using a linear function in the first case and a power function in the latter two cases. Among the power functions fit to observations using regression, the AIC for nonlinear regression (NLR) of untransformed observations exceeded AIC for linear regression (LR) of log-transformed observations; their absolute difference was consistently greater than the limit proposed by Xiao et al. (2011) to favor a model ($|AIC_{NLR} - AIC_{LR}| >> 2$). For these models, regression parameters were determined by linear regression of log-transformed observations of the independent and dependent variables. Unless stated otherwise, residuals in the regression models that follow were distributed normally with homogenous variance.

Following necessary transformation, linear regression indicated highly significant, positive relationships between all pairs of variables for both species. L_{BRANCH} increased linearly with D_{BRANCH} at a numerically similar rate for both species, but m_{BRANCH} and m_{LEAF} increased with D_{BRANCH} raised to scaling exponents greater and less than 2, respectively, for both species (Table 3). Analysis of covariance consistently indicated an inequality of slopes between the regression equations relating D_{BRANCH} to L_{BRANCH} (F = 15.19; df = 1, 767; p = < 0.001), m_{BRANCH} (F = 8.59; df = 1, 767; p = 0.004), and m_{LEAF} (F = 11.03; df = 1,767; p = 0.001) for each species. Accordingly, regression models were fit to species-specific observations. The F test for lack of fit was highly significant ($p < 0.001$) for all regression models (data not shown), and graphical inspection of the models in their original, linear scale indicated good agreement between the regression models and untransformed observations (Figures 6 – 8).

Structural Young's modulus

When subjected to a static bending moment, mean E_{STRUCT} was 6.26 GPa (SD 2.20) for Senegal mahogany and 6.14 GPa (SD 2.22) for rain tree. Three Senegal mahoganies and two rain trees had comparably large E_{STRUCT} values, which skewed observations and resulted in mean exceeding median values by approximately 18% for Senegal mahogany and 12% for rain tree. A paired *t*-test revealed that Senegal mahogany E_{STRUCT} did not vary by the direction (i.e. North, East) from which trees were pulled ($t = 0.01$, df = 6, $p = 0.993$). Although there was not a significant difference between the average E_{STRUCT} of the two species ($t = 0.13$, df = 20, $p = 0.901$), the larger average *DBH* for rain tree caused a significant difference between the average flexural rigidity, *R* ($N \cdot m^2$), of each species ($t = -3.45$, df = 20, $p = 0.003$). Mean *R* was 79.6 $GN \cdot m^2$ (SD 37.9) for Senegal mahogany and 141 $GN \cdot m^2$ (SD 45.2) for rain tree. For Senegal mahogany, mean C_1 was 989 MN (SD 383; range: 607 – 1,870).

Post-pruning changes in tree and branch attributes

Pruning treatments changed the size of residual tree parts according to the deliberate removal of branches from raised and reduced trees (Table 4). For raised rain trees, mean crown length, L_{CROWN}, did not change because the lowest branch was not removed from any of the trees, since $\mathfrak{R}_B$ consistently exceeded 0.6 (see Methods). Mean tree height, H_{TREE}, and tree slenderness, λ_{TREE}, did not change on raised Senegal mahoganies or rain trees, but the two attributes decreased on reduced trees according to the planned changes in L_{CROWN}. Crown architecture models and photographs of all pruned trees are contained in Appendix A.

Effect of pruning treatments on mass and vibration properties

Unintentional root damage to one Senegal mahogany during pull testing caused the tree's removal from the experiment, and one rain tree was similarly removed because its exceptionally short (3.7 m *L*) and stout (1.0 m *DBH*) trunk resisted the deflection necessary for free vibration

testing. As a result, the total number of trees in each experiment was decreased by one to 11 Senegal mahoganies and nine rain trees. Except for the excluded Senegal mahogany, there were no obvious indications of root system movement, such as audible cracking or visible discontinuities in the soil around the trunk, during pull testing.

Mass

An even spread of observations at each pruning severity was obvious for the percent decrease in m_{TREE} plotted against pruning severity for individual Senegal mahoganies and rain trees (Figure 9), indicating the probable existence of homogeneous variances. The AICC and BIC fit indices offered similar evidence. Homogeneous covariance structures, including first-order autoregressive [AR(1)] and compound symmetry (CS), best fit the Senegal mahogany and rain tree percent decrease in m_{TREE} datasets, respectively (Table 5). In contrast, there was a narrowing in the spread of observations across pruning severities for the percent decrease in m_{LEAF} plotted against pruning severity for individual trees of both species, especially rain trees (Figure 10). However, AICC and BIC fit indices showed that the homogeneous AR(1) and heterogenous Huynh-Feldt (HF) covariances structures best fit the percent decrease in m_{LEAF} datasets for Senegal mahogany and rain tree, respectively (Table 5).

For both species, the percent decrease in m_{TREE} and m_{LEAF} was significantly greater for reduced than raised trees (Tables 6 – 9). Although the percent decrease in m_{TREE} and m_{LEAF} increased significantly with pruning severity, pruning type and severity interacted significantly because the rate of change in the percent decrease in m_{TREE} and m_{LEAF} was greater for reduced than raised trees. While the percent decrease in m_{TREE} increased linearly up to 24% and 22% for raised Senegal mahoganies and rain trees, respectively, the percent decrease in m_{TREE} increased curvilinearly and linearly up to 61% and 65% for reduced Senegal mahoganies and rain trees, respectively (Figure 11A). For reduced rain trees, the percent decrease in m_{LEAF} was exceptionally

large at 20% severity, indicating the thorough removal of leaves concentrated near branch tips (Table 9). For most pruning treatments, the percent decrease in m_{LEAF} was greater for rain trees than Senegal mahoganies. For raised Senegal mahoganies and rain trees, the percent decrease in m_{LEAF} increased linearly up to 55% and 82%, respectively; and the percent decrease in m_{LEAF} increased curvilinearly up to 96% and 100% for reduced Senegal mahoganies and rain trees, respectively (Figure 11B). At 80% severity, pruning treatments caused total defoliation to two and five reduced Senegal mahoganies and rain trees, respectively; none of the raised trees was completely defoliated for either species.

Vibration properties

The average height at which a pull rope could be installed on Senegal mahoganies and rain trees was 9.1 m (SD 1.7) and 4.2 m (SD 0.6), respectively. The choice was mostly governed by the height of the first large branch, and the comparatively low pull height on rain trees reduced the applied M_B and initial displacement during free vibration tests. Consequently, there was insufficient excitation of accelerometers during some of these tests. In particular, it was not possible to determine f_n and ζ from time histories of 12 accelerometers installed on branches of two raised rain trees. Excluding these observations from the analysis of branch accelerations reduced the sample size to one reduced tree, precluding a comparison of the effect of pruning type on branch f_n and ζ.

In total, estimates of trunk and branch f_n and ζ were obtained from 712 free vibration tests. A single peak in power spectral density was observed in 94% of free vibration tests with trunk (Figure 12) and branch (Figure 13) motion reasonably approximated by a simple harmonic function. The remaining tests displayed more than one prominent peak in power spectral density. Using the continuous wavelet transform, time-frequency plots were used to explore the time-varying frequency components of the multi-modal vibration (Figure 14).

Multi-modal, complex periodic vibration was observed on one Senegal mahogany before pruning, and the time-frequency plots revealed transient vibration with alternate distribution of power between two separate modes and a single, intermediate mode (Figure 14). Although a similar response was observed on the same tree after being raised by 10%, only one mode was observed at pruning severities greater than 10%. Multi-modal vibration was also observed on reduced trees. It was observed in two time histories of trunk displacement and branch acceleration obtained from rain trees reduced by 20%. It was also observed in three time histories of trunk displacement and five time histories of branch acceleration obtained from rain tree and Senegal mahogany, respectively, reduced by 40%. In these tests, time-frequency plots revealed a temporal decay in power associated with two or more distinct modal frequencies (Figure 15). These tests were not excluded from analyses, but only the parameters associated with the fundamental mode were used in statistical models.

Natural frequency

Plotting f_n against pruning severity for individual Senegal mahogany trees revealed that variability increased with pruning severity among reduced trees, suggesting the probable existence of heterogeneous variances (Figure 16). This fanning of f_n at higher pruning severities was apparent for both tree species, especially with observations made on the trunk. The AICC and BIC fit indices offered similar, often mutually-corroborating, evidence (Table 10). Heterogeneous covariance structures, including heterogeneous first-order autoregressive ARH(1) and first-order banded diagonal unstructured [UN(1)], best fit the trunk and branch f_n datasets displaying unequal variances, respectively.

Senegal mahogany

On Senegal mahoganies, trunk and branch f_n varied between pruning types and severities, but pruning type interacted significantly with severity to affect both trunk and branch f_n (Table 11).

Mean trunk and branch f_n for the reduced trees was significantly greater than the raised trees. The interaction of pruning type and severity was significant because trunk and branch f_n increased curvilinearly as severity increased for reduced, but not raised, trees.

For reduced Senegal mahoganies, OPC revealed a quadratic response of trunk and branch f_n to pruning severity (Table 11). Least squares regression revealed a highly significant, positive relationship between trunk and branch f_n and the severity of reduction pruning (Figure 17). At 0% severity, the mean f_n of trunks (F = 0.01; df = 1, 36; p = 0.930) and branches (F = 0.70; df = 1, 24; p = 0.410) did not differ between pruning types. Although statistical comparisons were not made, branch f_n was approximately one-half trunk f_n at all treatment combinations, roughly consistent with the average ratio of branch to trunk diameter (0.56) for all instrumented branches. Regressed against the percent decrease in m_{TREE}, trunk and branch f_n of reduced trees revealed similar positive, highly significant quadratic relationships (Figure 18). For raised trees, pruning severity did not affect trunk or branch f_n.

Rain tree

There were highly significant differences in rain tree trunk f_n between pruning types and severities, but pruning type and severity interacted significantly to affect trunk f_n (Table 12). Mean trunk f_n for reduced trees was significantly greater than raised trees. The interaction between pruning type and severity was significant because trunk f_n increased curvilinearly with pruning severity on reduced, but not raised, trees. Similarly, the mean branch f_n of reduced trees increased curvilinearly with pruning severity.

For reduced rain trees, OPC revealed a cubic response of trunk and branch f_n to pruning severity (Table 12). Least squares regression revealed a significant, positive relationship between trunk and branch f_n and reduction pruning severity (Figure 19). At 0% severity, the mean trunk f_n of

trees in each pruning type was not significantly different (F = 0.06; df = 1, 3.42; p = 0.823). Although statistical comparisons were not made, branch f_n was approximately two-fifths of trunk f_n on trees reduced by 0, 20, and 40%; and branch f_n subsequently increased, on a relative basis, to approximately three-fifths of trunk f_n on trees reduced by 80% (Table 12). Regressed against the percent decrease in m_{TREE}, trunk and branch f_n of reduced trees revealed similar positive, highly significant cubic relationships (Figure 20). For raised trees, pruning severity did not affect trunk f_n (Table 12).

Damping ratio

Plotting ζ against pruning severity for individual Senegal mahogany trees revealed that variability in ζ decreased with pruning severity, especially among reduced trees, suggesting the probable existence of heterogeneous variances (Figure 21). This contraction of ζ after increasingly severe pruning was apparent for both tree species, especially with observations made on the trunk. The AICC and BIC fit indices mostly supported these observations (Table 13). Heterogeneous covariance structures, including UN(1), ARH(1), and heterogeneous compound symmetry (CSH), best fit the trunk and branch ζ datasets displaying unequal variances. However, the default variance components covariance structure best fit the Senegal mahogany branch ζ dataset, indicating that repeated observations on subjects did not covary over the range of tested pruning severities and the presence of uniform variances across levels of pruning severity.

Senegal mahogany

At 0% pruning severity, the mean difference in trunk (F = 2.10; df = 1, 36; p = 0.156) and branch (F = 0.92; df = 1, 110; p = 0.339) ζ between pruning types was not significant. Mean Senegal mahogany trunk ζ did not vary between the two pruning types, but there were significant differences in mean branch ζ between pruning types (Table 14). Mean branch ζ for reduced trees was significantly less than raised trees. Both trunk and branch ζ varied significantly among levels

of pruning severity, but pruning type and severity interacted significantly to affect trunk and branch ζ. Mean trunk and branch ζ decreased as pruning severity increased for reduced, but not raised, trees.

On reduced Senegal mahoganies, cubic functions described the response of trunk and branch ζ to pruning severity (Table 14). Least squares regression confirmed a highly significant, negative curvilinear relationship between pruning severity and ζ measured on the trunks and branches of reduced trees (Figure 22). Although statistical comparisons were not made, mean branch ζ was higher than mean trunk ζ at 10% and 20% pruning severity before converging to similar values at 40% and 80% pruning severity. Regressed against the percent decrease in m_{LEAF}, trunk and branch ζ of reduced trees revealed similar highly significant cubic relationships; ζ generally increased on trunks and branches until a 63% and 52% decrease in m_{LEAF}, respectively, before subsequently declining as more leaves were removed (Figure 23).

Rain tree

For rain trees, the mean difference in trunk ζ between pruning types at 0% severity was not significant (F = 2.77; df = 1, 6.71; p = 0.142). Mean trunk ζ did not vary between pruning types, but it varied significantly among pruning severities. However, pruning type and severity interacted significantly to affect trunk ζ, which varied among pruning severities only for reduced trees (Table 15). OPC revealed a quadratic response of trunk ζ to the severity of reduction. Least-squares regression confirmed the highly significant quadratic relationship between trunk ζ and reduction pruning severity (Figure 24). Regressed against the percent decrease in m_{LEAF}, however, the significant decrease in trunk ζ was linear, not quadratic, for reduced rain trees (Figure 25).

Although statistical comparisons were not made, branch and trunk ζ were similar at 0% pruning severity. On reduced rain trees, mean branch ζ also varied significantly among pruning severities

(Table 15). However, OPC indicated a linear rather than a quadratic response of branch ζ to pruning severity. Least squares regression confirmed a highly significant, negative relationship between branch ζ and pruning severity on the single reduced rain tree to which accelerometers were affixed (Figure 24). Regressed against the percent decrease in m_{LEAF}, there was a similar, highly significant linear decrease in branch ζ for the single reduced rain tree (Figure 25).

Relationship between vibration properties and morphometric attributes of trees at all pruning severities

For raised trees of both species, there was no obvious pattern to paired observations of vibration properties and morphometric attributes at all pruning severities. The *F*-test for lack of fit confirmed that there was not a significant linear relationship between vibration properties and any of the morphometric attributes for raised trees (data not shown). Consequently, the raised trees were excluded from further consideration, and the following text refers exclusively to reduced trees.

For reduced Senegal mahogany and rain tree, visual inspection of scatter plots showed obvious patterns indicating a relationship between vibration properties and most morphometric attributes, except D, θ, and $\mathfrak{R}_B$ (Figures 26 – 27). Collectively, these patterns illustrated the increased post-pruning f_n and decreased post-pruning ζ of reduced trees or branches made lighter, shorter, and stockier after pruning.

Bivariate regression

Visual inspection of paired observations at all pruning severities showed obvious nonlinearity between vibration properties and many tree and branch attributes (Figures 28 – 43). For each species, among the trunk and branch observations at all pruning severities, there was at least one instance of a nonlinear relationship between vibration properties and eight morphometric

attributes: m, m_{LEAF}, L, d, ξ, ς, λ, and ψ. Although most observations at all pruning severities showed a nonlinear relationship between f_n and ς, the relationship was linear for f_n measured on the trunk of Senegal mahogany. In contrast, most observations at all pruning severities showed a linear relationship between f_n and ψ, but the relationship was nonlinear for f_n measured on the branches of Senegal mahogany. In addition, the relationship between between ζ and m and m_{LEAF} was mostly nonlinear, except for ζ measured on the trunk of rain tree.

For observations at all pruning severities, most nonlinear relationships between vibration properties and morphometric attributes were best described by a power function (Tables 16 – 17). For a few relationships, however, an exponential, logarithmic, or polynomial function provided a better fit. For many relationships, the form of functions differed between species. Differences mostly indicated a greater change in vibration properties, especially post-pruning f_n, for rain tree over a given change in morphometric attributes. An exponential function best described the relationship between f_n and morphometric attributes more often for rain tree than Senegal mahogany, indicating the sensitivity of rain tree f_n to morphometric changes during pruning.

For observations at all pruning severities, morphometric attributes accounted for greater variance in f_n than ζ (Tables 16 – 19). Among all explanatory variables, ς consistently accounted for the least variance in f_n and ζ. Using Cook's d, some outliers were identified in most bivariate regressions, but none was removed after inspection, since the values were determined accurately. Although morphometric attributes accounted for less variability in ζ than f_n, fewer outliers were identified among functions fit to ζ. Among the functions fit to f_n, most of the outliers were associated with higher pruning severities, reflecting the increased variability observed among these observations. Although most outliers were mild, several extreme outliers, with Cook's d greater than five times the limit $4/n$, were identified in the models relating f_n to d and ψ measured on the trunk and branches of both species.

Second-order polynomials fit to ζ and some morphometric attributes showed local extrema in ζ over the range of observations. For branch observations of Senegal mahogany, the relationship between ζ and m_{LEAF} at all pruning severities showed a local maximum, demonstrating that ζ initially increased at low severity and decreased after most leaves were removed (Figure 37). For trunk observations of rain tree, the second-order polynomials fit to ζ and L, ξ, ς, and λ each showed a local minimum that preceded a modest increase in ζ at higher severities (Figures 38, 40 – 42).

For vibration properties measured on the trunk and branches of both species at all pruning severities, the functions fit to f_n increased asymptotically as m_{LEAF} approached zero, indicating a large change in f_n occurred over a small change in m_{LEAF} for the range of observations (Figure 28). Similarly, over the observed range of m_{LEAF}, ζ measured at all pruning severties on the trunk of Senegal mahogany and branches of rain tree approached and intercepted zero with an increasingly large instantaneous rate of change, indicating a precipitous decline in ζ for trees at or near complete defoliation (Figure 37).

For observations at all pruning severities, there was an obvious nonlinear relationship between ζ and f_n measured on the trunks and branches of both species (Figure 44). Although a power function best described the relationship between ζ and f_n for most observations, a logarithmic function best described this relationship uniquely for ζ and f_n measured on the trunk of rain tree. Despite this difference, however, all observations consistently showed a large decrease in ζ as f_n increased at lower pruning severities, but the rate of decrease in post-pruning ζ eventually diminished as f_n further increased at higher pruning severities. For branch observations at all pruning severities, f_n accounted for greater variability in ζ than any other examined morphometric attribute, but the same was not true for trunk observations of either species (Table 19).

Among the power and exponential functions fit to observations using regression, the AIC for nonlinear regression (NLR) of untransformed observations exceeded AIC for linear regression (LR) of log-transformed observations; their absolute difference was consistently greater than the limit proposed by Xiao et al. (2011) to favor a model ($|AIC_{NLR} - AIC_{LR}| >> 2$). For these models, regression parameters were determined by linear regression of logarithmically-transformed observations of the independent, dependent, or both variables. Graphical inspection of all models fit to vibration properties and morphometric attributes at all pruning severities in their original, linear scale indicated good agreement between the regression models and untransformed observations (Figures 28 – 44); the *F*-test for lack of fit was highly significant ($p < 0.001$) in all cases (data not shown).

Multiple regression

For all pruning severities, after transformation to linearize individual relationships, there was a significant negative correlation between f_n and m, m_{LEAF}, L, ξ, ς, and λ; and there was a significant positive correlation between f_n and d and ψ (data not shown). Conversely, there was a significant positive correlation between ζ and m, m_{LEAF}, L, ξ, ς, and λ; and there was a significant negative correlation between ζ and d and ψ (data not shown). These observations were consistent for vibration properties measured on the trunk and branches of both species. Since D, θ, and $\mathfrak{R}_B$ were not correlated with vibration properties, these variables were removed from the pool of explanatory variables.

Among all possible combinations of variables in multiple parameter models, most morphometric attributes were comparably important, in terms of the average additional variance explained by each variable across all subset models, for predicting f_n on the trunks and branches of both species (Table 20). The proportion of additional variance explained by most of the attributes ranged slightly between 10% and 18%, except post-pruning m_{LEAF} and ς contributed noticeably less to

prediction, on average, in all subset models. Among all morphometric attributes, *d* uniquely accounted for the greatest amount of additional variance in f_n for more than one dataset. Although only slightly greater than other variables, *d* accounted for the most additional variance in f_n measured on the trunks and branches of Senegal mahogany, but it accounted for less than the average additional variance explained by all morphometric attributes for trunk and branch observations of rain tree. In contrast, *m* and ξ contributed most to the prediction of f_n measured on the trunk and branches, respectively, of rain tree.

In contrast to models pertaining to f_n, there was greater disparity in the contribution of morphometric attributes to the prediction of ζ measured on the trunk and branches of both species (Table 20). In most cases, some variables accounted for three to eight times as much additional variance, on average, in ζ than others in all subset models. Except for ζ measured on the trunks of Senegal mahogany, m_{LEAF} accounted for the most, or nearly so, additional variance in ζ across all subset models. Although m_{LEAF} accounted for the second largest amount of additional variance in ζ measured on the branches of rain tree, it explained only slightly less, on average, than ς across all subset models. Among the morphometric attributes of both species, none consistently contributed least to the prediction of ζ, but all variables accounted for markedly less additional variance, on average, in all subset models fit to ζ measured on the trunk of Senegal mahogany.

Among 510 possible combinations of explanatory variables, there were numerous candidate subsets accounting for similar, often large amounts of variance in the vibration properties of both species (Tables 21 – 22). The average adjusted R^2 of all models fit to f_n exceeded 90% for the morphometric attributes of both species (Table 21), and the adjusted R^2 of all models fit to ζ, on average, exceeded 65% for most measurements. One exception was the uniquely low average adjusted R^2 (34%) for all models fit to ζ measured on the trunk of Senegal mahogany (Table 22).

For Senegal mahogany trunk measurements, only one-third of all models fit to ζ had an adjusted R^2 that exceeded 60%, indicating especially poor model fit.

Except for the multiple parameter models fit to ζ measured on the trunks of Senegal mahogany, the models with the lowest BIC fit index contained between two and five parameters (Tables 21 – 22). However, the best subset selection process did not provide compelling evidence, in terms of the BIC for individual models, of the superior prediction offered by a unique combination of variables. For vibration properties measured on the trunk and branches of both species, the BIC values for many candidate subset models were narrowly distributed near the minimum value, indicating a similar equivalence among many multiple parameter models. Among the multiple parameter models fit to f_n measured on the trunks and branches of both species, the models with the eight lowest BIC values often contained the variables d and ξ, and m_{LEAF} was often contained in the best subset of models fit to f_n measured on the branches of both species (Table 21). Among the multiple parameter models fit to ζ measured on the Senegal mahogany branches and rain tree trunks, the models with the eight lowest BIC values repeatedly contained m_{LEAF}, and d and ς were often contained in the best subset of models fit to ζ measured on the branches of rain tree (Table 22).

Among the best subset of multiple regression models with the lowest BIC, many models suffered from degrading collinearity arising from strong dependencies among morphometric attributes at all pruning severities. In many cases, collinearity diagnostics (data not shown) showed that variables involving length (i.e., L, λ, ψ) and branch extent (i.e., ξ and ς) were highly correlated with one another and contributed to these dependencies.

Effect of pruning treatments on wind-induced vibration and bending moments

Due to instrumentation failures and data acquisition errors, trunk displacement and wind observations were missing for short, discrete periods distributed widely among all measuring intervals. Likely as a result of weathering, these failures increased considerably during the 40% and 80% pruning severity treatment periods to cause greater than 80% of all expected records to be missing. As a result, the analysis of wind-induced M_B was limited to the 0, 10, and 20% pruning severities. From these remaining periods, trunk displacement and wind observations were recorded for 30% to 60% of all possible 30-minute intervals, but trunk displacement records with corresponding wind observations only existed for 13% to 15% of all possible 30-minute intervals. As a result, the total number of 30-minute intervals used to analyze wind-induced M_B was 10,390. Among the available records, four 30-minute intervals with the highest resultant wind speeds were selected from each experimental period for Fourier analysis.

Wind conditions

Although differences existed among experimental periods, wind conditions were generally mild during the entire experiment. Among all observations, approximately 12% of 30-minute mean wind speeds measured at $z/H_{TREE} = 0.69$ exceeded 1 $m \cdot s^{-1}$. The maximum 30-minute mean and instantaneous wind speed measured at the same height was 2.0 $m \cdot s^{-1}$ and 7.3 $m \cdot s^{-1}$, respectively. During the entire experiment, the modal prevailing 30-minute direction of wind flow was south (S).

Mean wind speeds increased slightly over the course of the experiment (Figures 45 – 47). During the first 45 days of the experiment before trees were pruned, wind speeds and directions were relatively low and variable, respectively (Figure 45). Among all 30-minute intervals, the resultant direction of wind flow was mostly distributed between south-southeast (SSE) and northwest (NW) during this period, although most of the highest wind speeds were recorded in wind flow moving towards the east (E). During the 45-day period after trees were pruned 10%, the mean

winds increased slightly and blew more consistently towards SSE compared to the preceding 45-day period (Figure 46). Although the resultant direction of wind flow was increasingly concentrated towards SSE, some of the highest wind speeds were recorded in wind flow moving towards S. During the 45-day period after trees were pruned 20%, mean winds increased considerably compared to the preceding experimental periods and blew near consistently towards S, with one-third of all observations occurring between 185° and 195° (Figure 47).

Over the course of the experiment, there were obvious changes in the vertical profile of the 30-minute average streamwise wind speeds, $\bar{u}$ ($m \cdot s^{-1}$), normalized by $\bar{u}$ measured at $z/H_{TREE} = 0.69$ (Figure 48). At 0% severity, there was a local increase in normalized $\bar{u}$ at lower positions near the sparse trunk space, but the local increase in normalized $\bar{u}$ progressively diminished at 10% and, especially, 20% severity. At 0% and 10% severity, $\bar{u}$ measured on the lowest three anemometers was, on average, greater than the highest anemometer (i.e., normalized $\bar{u}$ exceeded one), but the reverse was true for observations at 20% severity: normalized $\bar{u}$ measured on the lowest three anemometers was, on average, less than one.

Fourier transform

Due to instrument failures, measurements of all trees were not consistently available for spectral analysis, but all data in each 30-minute interval were used to analyze measurements for as many trees as possible. For unpruned Senegal mahoganies, Fourier energy spectra computed from 30-minute time histories of x_u showed prominent peaks between 0.11 and 0.25 Hz (mean: 0.16 Hz) (

Figure 49). In most cases, there was a single characteristic peak near the trunk frequency measured in free vibration, suggesting that the trees mostly vibrated near their fundamental mode during these wind events. For several trees, there was a second, less prominent peak at lower frequencies between 0.02 and 0.04 Hz. During a given wind event, Fourier energy associated with

the most prominent peak varied among all trees, reflecting differences in the amplitude of trunk vibration at this frequency over the entire 30-minute interval. For unpruned trees, the measured differences in Fourier energy showed that, on average, trees assigned to be reduced experienced greater wind excitation at all frequencies, including the tree's fundamental frequency, than trees assigned to be raised. On average, Fourier energy associated with the most prominent peak was 13% greater for unpruned trees to be reduced than for trees to be raised. On average, total Fourier energy for trees to be reduced was 14% greater than trees to be raised.

For Senegal mahoganies raised by 10%, prominent peaks in Fourier energy existed at frequencies similar to those observed before pruning (Figure 50). By comparison, less prominent peaks existed at slightly higher frequencies for trees reduced by the same amount, despite a broad concentration of Fourier energy in the range of analyzed frequencies. Consistent with free vibration tests, spectral estimates showed that the dominant frequency of wind-induced trunk vibration for trees raised and reduced by 10%, respectively, was similar to (mean: 0.16 Hz; range: 0.13 – 0.23 Hz) and greater than (mean: 0.19 Hz; range: 0.13 – 0.25 Hz) those measured before pruning. For reduced trees, Fourier energy associated with the most prominent peak was, on average, 10% less than raised trees, indicating that reduced trees mostly vibrated at slightly higher frequencies with a smaller amplitude during these wind events. On average, total Fourier energy for reduced trees was 1% less than raised trees, reflecting a smaller amplitude of vibration across all frequencies.

For Senegal mahoganies reduced by 20%, there were no obvious, prominent peaks in Fourier energy computed from 30-minute x_u time histories, especially compared to the energy spectra associated with trees raised by 20% (Figure 51). Fourier energy spectra computed from 30-minute x_u time histories of Senegal mahoganies raised by 20% mostly showed peak frequencies (mean: 0.17 Hz; range: 0.12 – 0.23 Hz) similar to those observed during free vibration tests and wind-

induced vibration during preceding experimental periods. For a given wind event, variability in power associated with the most prominent peak among raised trees was commensurate with other experimental periods and indicated uneven wind-induced excitation of these trees near their fundamental mode during the 30-minute interval. On average, total Fourier energy was 63% less for reduced than raised trees, indicating a considerable decrease in wind-induced vibration for reduced trees at all analyzed frequencies.

At 40% and 80% pruning severities, Fourier energy spectra computed from 30-minute time histories of x_u showed a similar decreasing trend in wind-induced vibration for reduced compared to raised trees (Figures 52 – 53). For trees raised by 40% and 80%, Fourier energy spectra showed prominent peaks between 0.14 and 0.25 Hz (mean: 0.18 Hz) and between 0.13 and 0.23 Hz (mean: 0.17 Hz), respectively, similar to frequencies measured on these trees during free vibration and wind-induced vibration during preceding experimental periods. During both periods, there was consistently less Fourier energy computed from x_u for reduced compared to raised trees. On average, total Fourier energy for trees reduced by 40% and 80%, respectively, was 72% and 70% less than trees raised by the same amount, indicating a persistent decrease in wind-induced vibration for reduced trees at all analyzed frequencies.

In agreement with free vibration tests, unpruned branches vibrated at frequencies similar to one another but noticeably less than measured on trunks before pruning (Figure 54). Among all trees, Fourier energy spectra computed from 30-minute time histories of a_u showed prominent peaks between 0.05 and 0.11 Hz (mean: 0.08 Hz), indicating that unmodified branches mostly vibrated near their fundamental mode during wind events. Energy associated with prominent peaks varied considerably, for a given wind event, reflecting differences in the excitation of branches by a heterogeneous wind field. Although branches in trees assigned to the two treatment groups experienced similar wind excitation across all analyzed frequencies, measured differences in

Fourier energy spectra showed that, on average, branches in trees to be raised vibrated with a larger amplitude near their fundamental mode compared to branches in trees to be reduced. Fourier energy associated with prominent peaks was, on average among all wind events, 17% greater for branches in trees subsequently raised than for others in trees eventually reduced. On average among all wind events, total Fourier energy associated with branches in trees assigned to be raised was 12% greater than others in trees eventually reduced.

For branches in Senegal mahoganies raised by 10%, prominent peaks in Fourier energy remained at frequencies (mean: 0.09 Hz; range: 0.07 – 0.12 Hz) similar to those observed before pruning (Figure 55). By comparison, broader and less prominent peaks existed at slightly higher frequencies (mean: 0.10 Hz; range: 0.08 – 0.12 Hz) for branches in trees reduced by the same amount. Fourier energy associated with prominent peaks was, on average among all wind events, 24% less for branches in trees reduced by 10% than branches in trees raised by 10%, indicating a smaller amplitude of vibration near the fundamental mode for branches in reduced trees. Total Fourier energy was, on average among all wind events, 18% less for branches in trees reduced by 10% than others in trees raised by 10%, reflecting a smaller amplitude of vibration for branches in reduced trees across all analyzed frequencies.

Among branches in trees raised by 20%, prominent peaks remained at frequencies (mean: 0.09 Hz; range: 0.07 – 0.12 Hz) similar to those measured in free vibration and wind-induced vibration during preceding experimental periods (Figure 56). By comparison, broad and less prominent peaks in Fourier energy existed at slightly higher frequencies (mean: 0.10 Hz; range: 0.08 – 0.13 Hz) for branches in trees reduced by 20%, indicating a decreased amplitude of vibration at higher frequencies. Among all wind events, energy associated with prominent peaks was, on average, 66% less for branches in trees reduced by 20% than branches in trees raised by 20%. Similarly, total Fourier energy measured on branches in trees reduced by 20% was 60% less than branches

in trees raised by 20%, indicating a smaller amplitude of vibration across all analyzed frequencies for branches in reduced trees.

At 40% and 80% pruning severity, a visibly obvious difference between Fourier energy spectra persisted across wind events for branches in reduced and raised trees (Figures 57 – 58). For branches in trees raised by 40% and 80%, respectively, prominent peaks in Fourier energy existed, on average, at 0.09 Hz (range: 0.07 – 0.12 Hz) and 0.09 Hz (0.07 – 0.11 Hz), commensurate with measurements in free vibration and wind-induced vibration during preceding experimental periods. In contrast, there were no obvious, prominent peaks in Fourier energy for branches in trees reduced by 40% and 80%, especially compared to the Fourier spectra associated with branches in trees raised by 40% and 80%. Overall, spectral estimates showed that branches in trees reduced by 40% and 80% experienced considerably less wind excitation than others in trees raised by 40% and 80%. On average among all wind events, total Fourier energy for branches in trees reduced by 40% and 80% trees was 77% and 74%, respectively, less than branches in trees raised by 40% and 80%.

Overall, f_n measured in free vibration was similar to that measured during wind-induced movement, indicating that free vibration tests offered reasonable estimates of tree parts vibrating mainly at their fundamental mode during wind events. The following comparisons were made using f_n estimated at all severities for raised trees, but the same comparisons were only made at 0% and 10% severity for reduced trees, since the Fourier spectra computed from wind-induced movement of trees reduced by greater than 10% lacked prominent peaks associated with a dominant frequency. On average, branch and trunk f_n measured in free vibration differed from the same measured during wind-induced movement by 10% and 15%, respectively. Significant correlations between f_n measured in free vibration and wind-induced movement indicated that estimates obtained from free vibration tests were proportional to those obtained from wind-

induced movement (Figure 59). Comparatively, these two measurements were more highly correlated for trunks (r = 0.63, ρ = 0.64, p_c = 0.59) than branches (r = 0.58, ρ = 0.49, p_c = 0.51), and correlation between the two measurements increased after combining trunk and branch observations into a single data set (r = 0.91, ρ = 0.86, p_c = 0.90), since f_n measured on branches was consistently lower than measured on trunks. For one Senegal mahogany (KS8), wind-induced f_n was underpredicted by 28% to 42% using free vibration tests on five separate occasions, and close inspection of these distinct outliers (D = 0.27 – 0.42) revealed that wind and controlled loading primarily excited the higher and lower modal frequencies, respectively, uniquely observed on this tree. Excluding the outliers, regression indicated significant linear relationships between f_n measured during wind-induced movement and free vibration for branches (F = 119.49; df = 1, 233; p < 0.001), trunks (F = 94.28; df = 1, 140; p < 0.001), and combined tree parts (F = 1926.65; df = 1, 375; p < 0.001). Coefficients of variation showed that wind-induced f_n of branches (r^2 = 0.34), trunks (r^2 = 0.40), and combined tree parts (r^2 = 0.84) could be reasonably predicted by free vibration tests.

Wind-induced bending moments

The measurement resolution of wind-induced M_B varied according to C_1 for each Senegal mahogany between 6 and 18.5 kN·m. During the entire experiment, wind-induced M_B varied between 0 and 278 kN·m, reflecting the relatively mild wind conditions encountered at the site. At 0% severity, visual inspection of scatter plots revealed a curvilinear relationship between 30-minute maximum M_B and 30-minute maximum wind speed, U (m·s^{-1}). In broad agreement with theory, a positive quadratic function best described the relationship between these two variables for individual unpruned Senegal mahoganies (Figure 60), and the greatest proportion of variance in 30-minute maximum M_B was accounted for by 30-minute maximum U measured on the anemometer positioned closest to the canopy apex at z/H_{TREE} = 0.69 (Figure 61). As a result, only

wind measurements recorded by this anemometer positioned nearest to the canopy apex were used to analyze wind-induced M_B.

Although the relationship between 30-minute maximum M_B and 30-minute maximum U was quadratic for all trees at 0% severity, visual inspection of scatter plots indicated that the form of this relationship was affected by pruning severity, especially on reduced trees. Scatter plots of 30-minute maximum M_B and 30-minute maximum U showed different patterns for individual raised and reduced trees at 10% and 20% severity. A second-order polynomial with a positive quadratic term best described the relationship between these two variables for individual raised trees at all severities, but the quadratic term approached zero and became negative at 10% and 20%, respectively, for most reduced trees (Figures 62 – 63). Scatter plots of 30-minute maximum M_B against 30-minute maximum U for all individual trees are contained in Appendix B.

In total, 12,455 observations of 30-minute maximum M_B and 30-minute maximum U were obtained from 3,623 separate 30-minute intervals between 0 and 20% pruning severity. Only four covariance structures with limited parameters were examined, since it was computationally expensive to fit covariance structures with a large number of parameters to this dataset. Among these, the AICC and BIC fit indices indicated that first-order autoregressive moving average [ARMA(1,1)] best fit the Senegal mahogany 30-minute maximum M_B dataset (Table 23).

As expected, there was a highly significant linear relationship between 30-minute maximum M_B and 30-minute maximum U^2 ($F = 407$; df = 6, 8539; $p < 0.001$), and the slopes describing the 30-minute maximum M_B as a function of 30-minute maximum U^2 varied significantly among combinations of pruning type and severity ($F = 78.7$; df = 2, 8600; $p < 0.001$). As a result, unequal slopes were fit to describe the relationship between 30-minute maximum M_B and U^2 for each combination of pruning type and severity separately (Table 24). For raised trees, the slopes

fit to describe 30-minute maximum M_B as a function of 30-minute maximum U^2 decreased by 9% and 30%, respectively, at 10% and 20% severity relative to the same at 0% severity, reflecting a moderate decrease in the maximum wind-induced M_B across all observed wind speeds. For reduced trees, these slopes decreased by 46% and 94%, respectively, at 10% and 20% severity, reflecting a substantial decrease in the maximum wind-induced M_B across all measured wind speeds.

Statistical inferences about fixed effects were made with the covariate set equal to 5 $m \cdot s^{-1}$ (U^2 = 25 $m \cdot s^{-1}$), a value near the upper limit of observed wind speeds (Table 25). For trees exposed to a 30-minute maximum wind speed of 5 $m \cdot s^{-1}$, analysis of covariance indicated that the average 30-minute maximum M_B did not vary significantly between pruning types, but the average 30-minute maximum M_B varied significantly among pruning severities, reflecting a decrease in wind loads with increasing severity of pruning. However, pruning type and severity interacted significantly to affect the average 30-minute maximum M_B of trees exposed to a 30-minute maximum wind speed of 5 $m \cdot s^{-1}$. Although the average 30-minute maximum M_B decreased significantly with the severity of pruning for both raised and reduced trees, there was a greater decrease in the average 30-minute maximum M_B on reduced than raised trees across all severities.

Mean separation was performed at three wind speeds chosen to represent the upper range of 30-minute maximum U observed in this study: 4, 5, and 6 $m \cdot s^{-1}$. For raised trees, OPC revealed a quadratic decrease in the average 30-minute maximum M_B with pruning severity for all wind speeds (Table 25), reflecting a negligible and moderate decrease, respectively, in the average 30-minute maximum M_B at 10% and 20% severity. For reduced trees, OPC revealed a linear decrease in the average 30-minute maximum M_B with pruning severity for all wind speeds, reflecting a continuous decrease in the maximum wind-induced M_B across all severities. Overall, means showed that the magnitude of 30-minute maximum M_B on raised trees decreased moderately at

20% severity, but the 30-minute maximum M_B continued to vary in proportion to 30-minute maximum U across all severities on these trees. In contrast, the magnitude of wind loads on reduced trees decreased considerably at both 10% and 20% severity, and the proportionality between 30-minute maximum M_B and 30-minute maximum U diminished with pruning severity on these trees, reflecting a more pronounced change in wind-tree interaction on reduced trees (Figure 64).

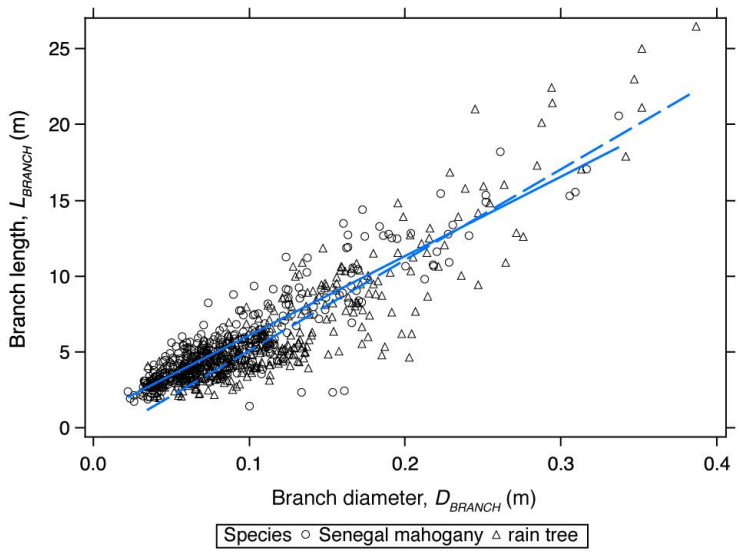

Figure 6: Scatter plot and best-fit lines of branch length, L_{BRANCH}, against branch diameter, D_{BRANCH}, with solid and dashed lines representing species-specific models of the form $y = \beta + \alpha x$ obtained by least squares regression of untransformed observations for Senegal mahogany (*Khaya senegalensis*) and rain tree (*Samanea saman*), respectively. See Table 3 for model sample sizes, parameter estimates, and fit statistics.

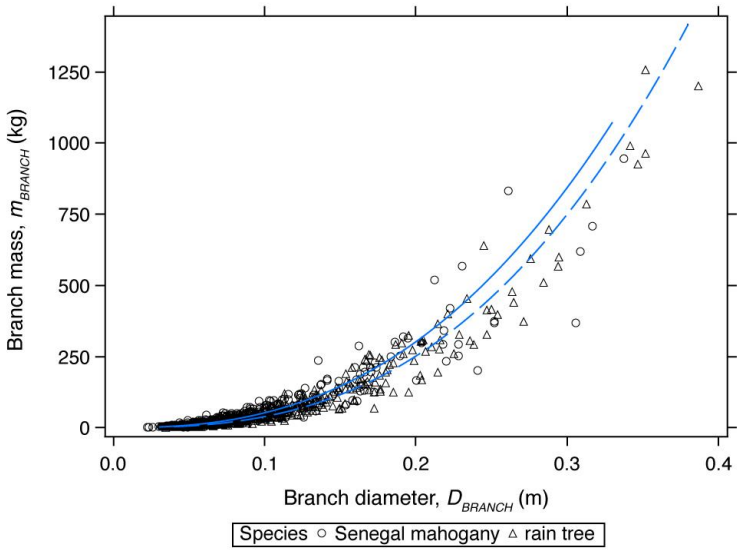

Figure 7: Scatter plot and best-fit lines of total branch mass, m_{BRANCH}, against branch diameter, D_{BRANCH}, with solid and dashed lines representing species-specific models of the form $y = \beta x^{\alpha}$ obtained by least squares regression of $\log_{10}$-transformed observations for Senegal mahogany (*Khaya senegalensis*) and rain tree (*Samanea saman*), respectively. See Table 3 for model sample sizes, parameter estimates, and fit statistics.

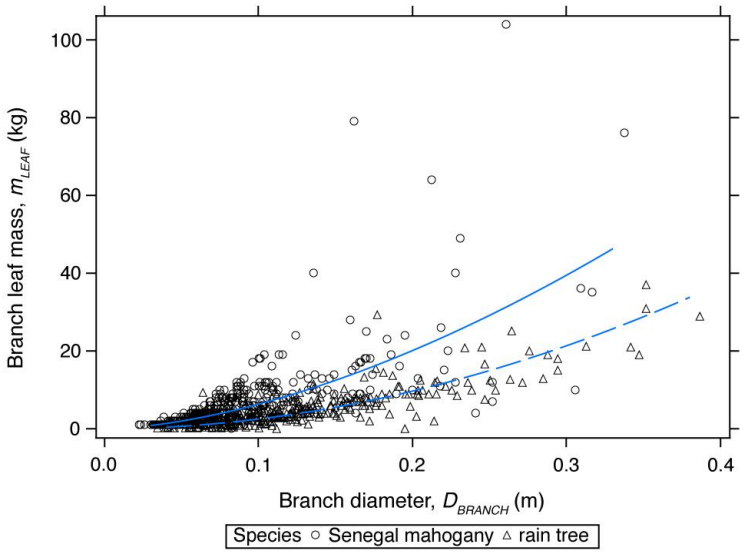

Figure 8: Scatter plot and best-fit lines of branch leaf mass, m_{LEAF}, against branch diameter, D_{BRANCH}, with solid and dashed lines representing species-specific models of the form $y = \beta x^{\alpha}$ obtained by least squares regression of $\log_{10}$-transformed observations for Senegal mahogany (*Khaya senegalensis*) and rain tree (*Samanea saman*), respectively. See Table 3 for model sample sizes, parameter estimates, and fit statistics.

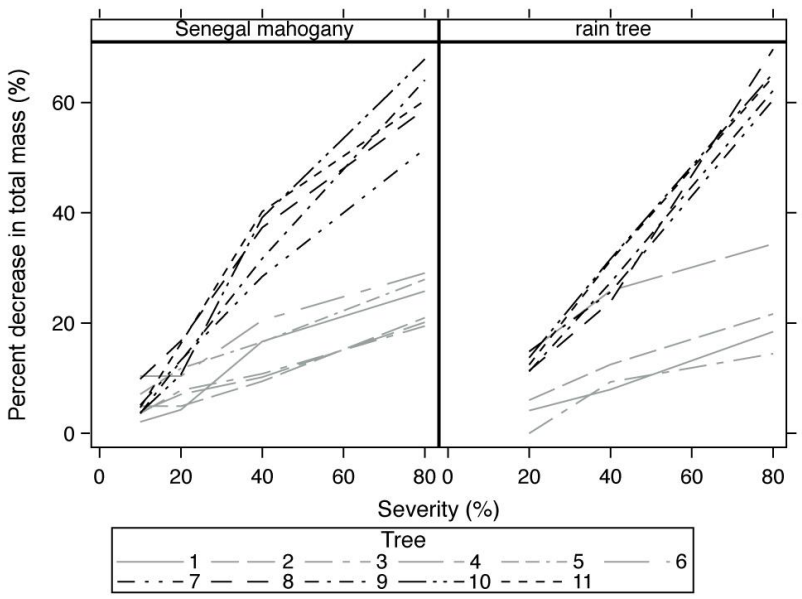

Figure 9: Data profile plot showing repeated measurements of percent decrease in total mass, m_{TREE}, on individual pruned Senegal mahoganies (*Khaya senegalensis*) and rain trees (*Samanea saman*). The percent decrease in total mass was measured repeatedly on six raised and five reduced Senegal mahoganies and four raised and five reduced rain trees. In the legend, trees numbered 1 – 6 and 7 – 11 were raised and reduced, respectively.

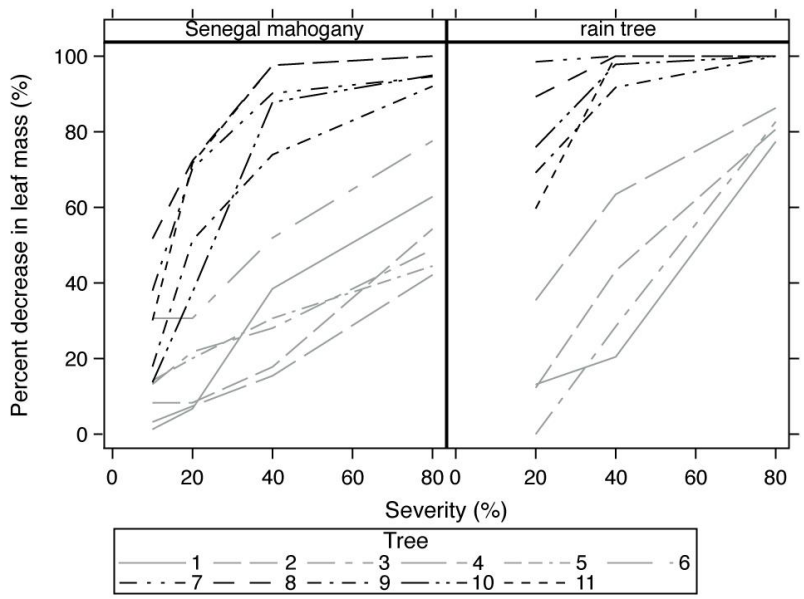

Figure 10: Data profile plot showing repeated measurements of percent decrease in leaf mass, m_{LEAF}, on individual pruned Senegal mahoganies (*Khaya senegalensis*) and rain trees (*Samanea saman*). The percent decrease in leaf mass was measured repeatedly on six raised and five reduced Senegal mahoganies and four raised and five reduced rain trees. In the legend, trees numbered 1 – 6 and 7 – 11 were raised and reduced, respectively.

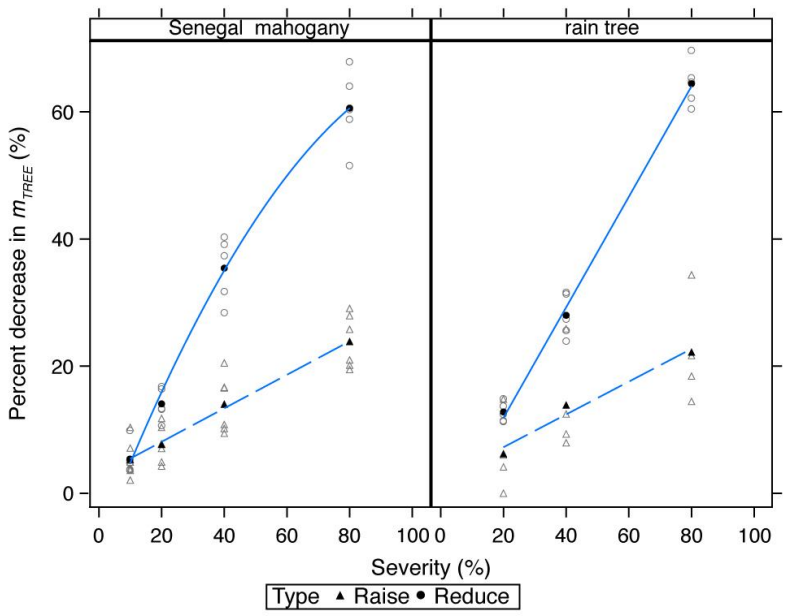

A)

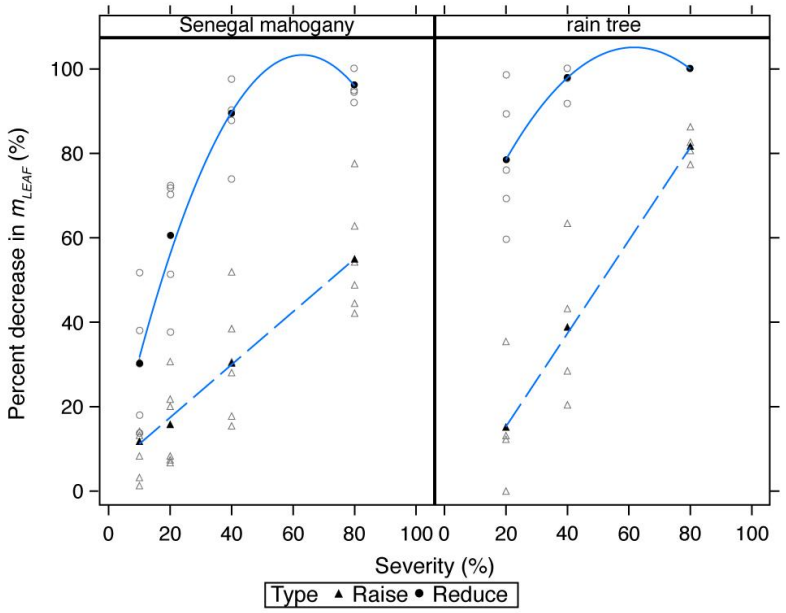

B)

Figure 11: Regression of mean percent decrease in total mass, m_{TREE}, (**A**) and leaf mass, m_{LEAF}, (**B**) against pruning severity for raised (filled triangles) and reduced (filled circles) rain tree (*Samanea saman*) and Senegal mahogany (*Khaya senegalensis*). During the experiment, percent decrease in mass was measured repeatedly on six raised and five reduced Senegal mahoganies and four raised and five reduced rain trees. For Senegal mahogany, least squares regression equations are $y = 0.26\ x + 2.82$ [$r^2 = 0.99$] and $y = (-5.32\times10^{-3})\ x^2 + 1.28\ x - 7.49$ [$R^2 = 0.99$] for the percent decrease in m_{TREE} on raised and reduced trees, respectively, and $y = 0.63\ x + 4.9$ [$r^2 = 0.99$] and $y = -(2.6\times10^{-2})\ x^2 + 3.2\ x + 2.1$ [$R^2 = 0.99$] for the percent decrease in m_{LEAF} on raised and reduced trees, respectively. For rain tree, least squares regression equations are $y = 0.26\ x + 2.08$ [$R^2 = 0.97$] and $y = 0.87\ x - 5.53$ [$R^2 = 0.99$] for the percent decrease in m_{TREE} on raised and reduced trees, respectively, and $y = 1.1\ x - 6.8$ [$r^2 = 0.99$] and $y = (-1.5\times10^{-2})\ x^2 + 1.9\ x + 47$ [$R^2 = 0.99$] for the percent decrease in m_{LEAF} on raised and reduced trees, respectively. For reference, empty gray symbols show observations of individual trees.

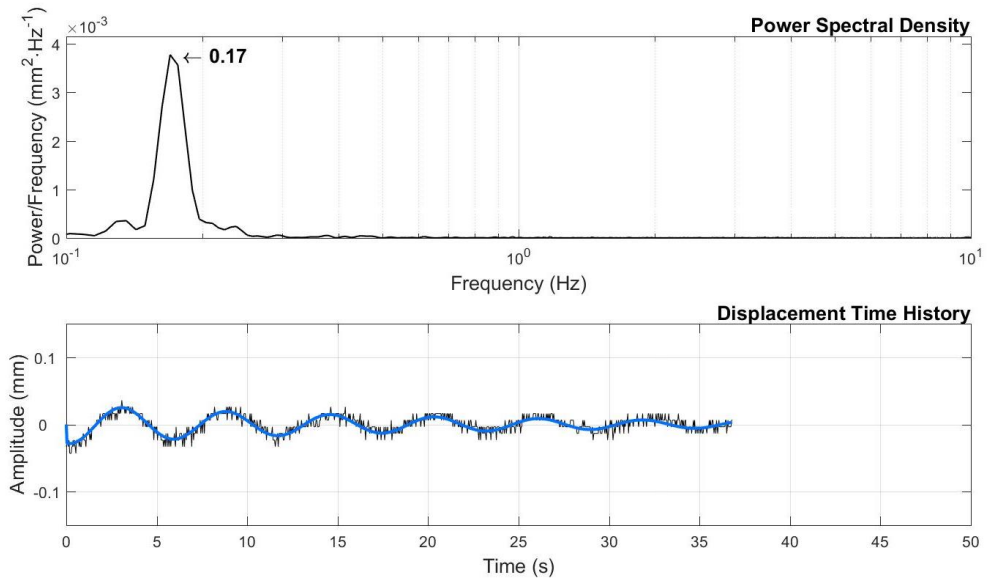

Figure 12: Pre-treatment time history of trunk displacement measured during free vibration on Senegal mahogany (*Khaya senegalensis*) tree number 2, including the equation of motion for a damped harmonic oscillator (solid blue line) fit to recorded observations (bottom); and power spectral density plot with annotation showing peak frequency (top).

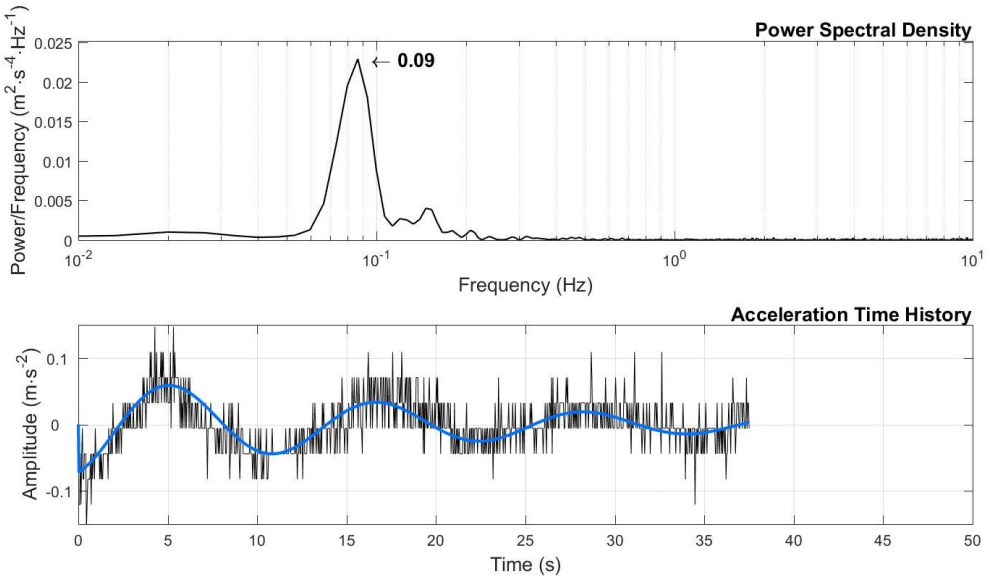

Figure 13: Pre-treatment time history of branch acceleration measured during free vibration on Senegal mahogany (Khaya senegalensis) tree number 7, including the equation of motion for a damped harmonic oscillator (solid blue line) fit to recorded observations (bottom); and power spectral density plot with annotation showing peak frequency (top).

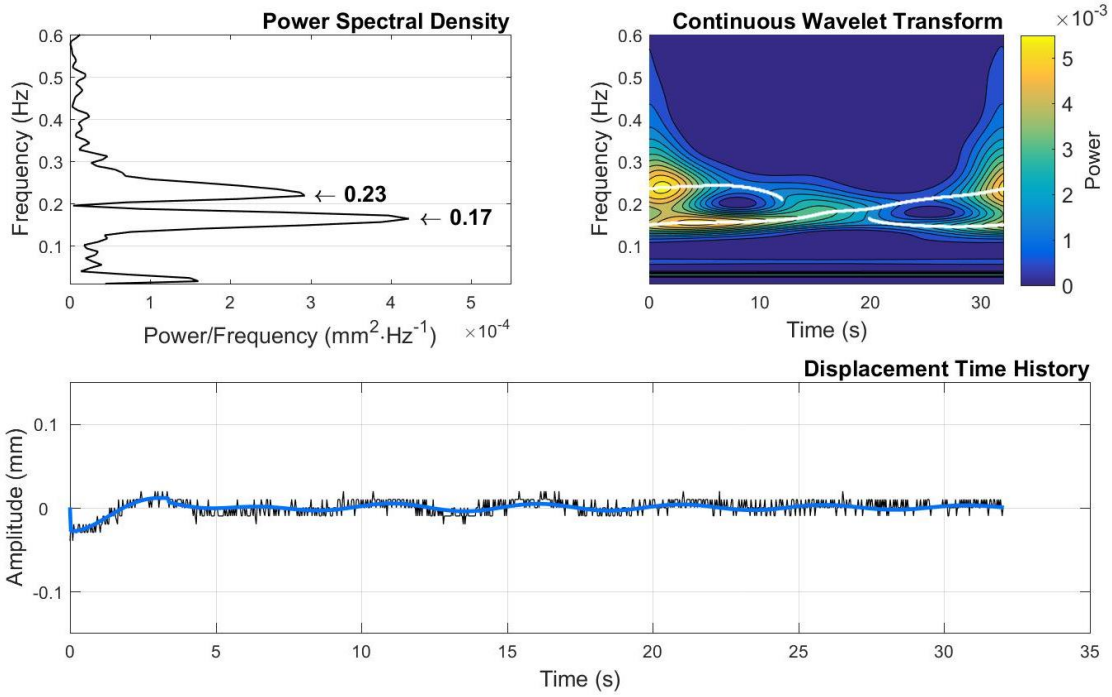

Figure 14: Power spectral density (PSD) plot with annotation showing peak frequencies (top left), wavelet variance spectrum (top right), and pre-treatment time history of trunk displacement measured during free vibration on Senegal mahogany (*Khaya senegalensis*) tree number 8, including the equation of motion for a damped harmonic oscillator (solid blue line) fit to recorded observations (bottom). For the wavelet variance spectrum (top right), contour lines depict level curves on a wavelet power surface representing instantaneous power as a function of time and frequency and white trace lines highlight ridges of chained local maxima designating instantaneous modal frequencies near peaks in PSD.

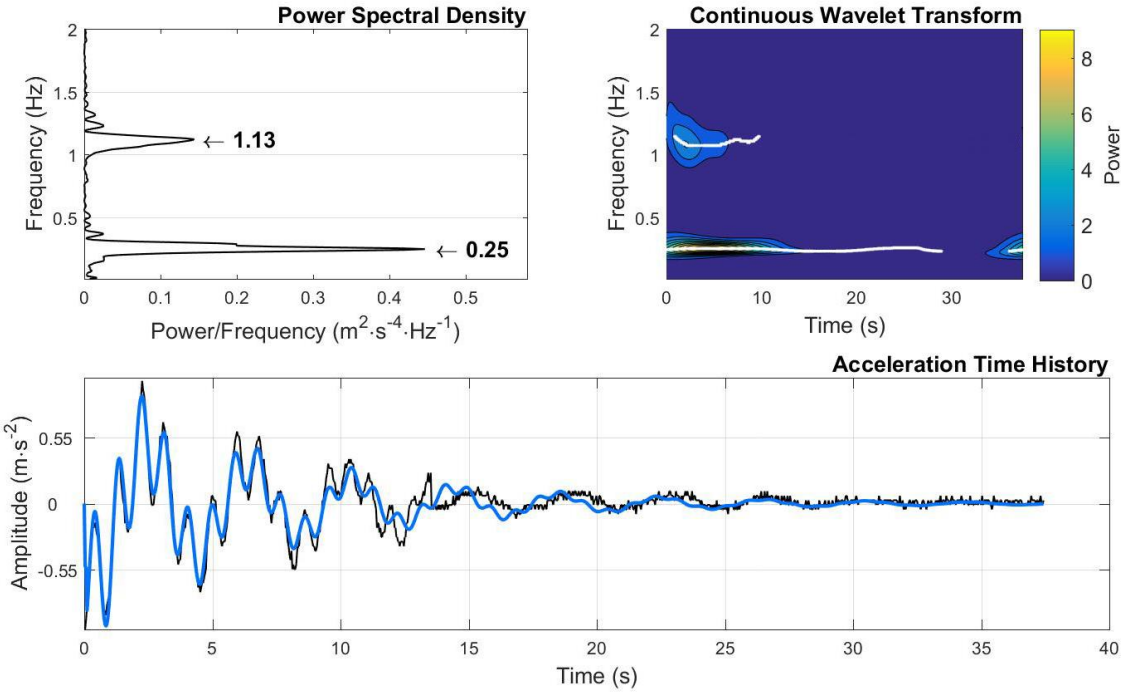

Figure 15: Power spectral density (PSD) plot with annotation showing peak frequencies (top left), wavelet variance spectrum (top right), and time history of branch acceleration measured during free vibration on Senegal mahogany (*Khaya senegalensis*) tree number 1, including the equation of motion for a damped harmonic oscillator (solid blue line) fit to recorded observations (bottom). For the wavelet variance spectrum (top right), contour lines depict level curves on a wavelet power surface representing instantaneous power as a function of time and frequency and white trace lines highlight ridges of chained local maxima designating instantaneous modal frequencies near peaks in PSD.

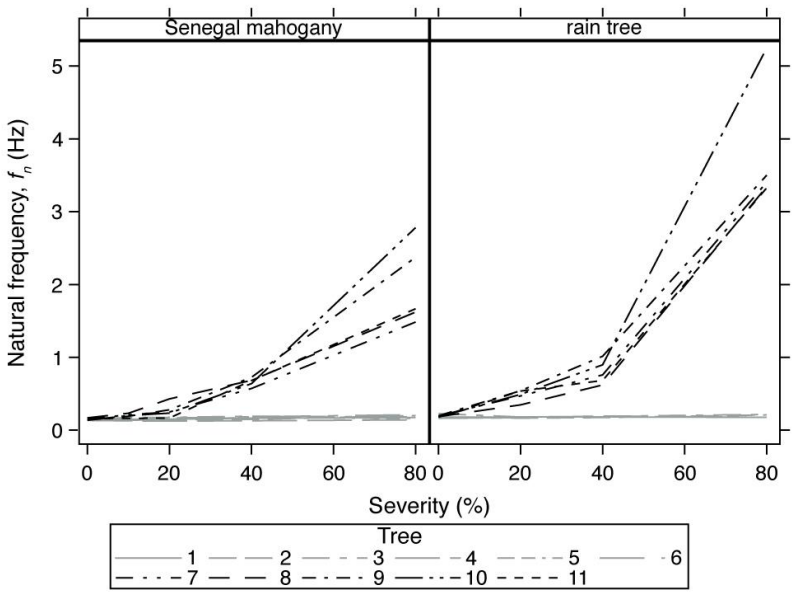

Figure 16: Data profile plot showing repeated measurements of trunk f_n on individual Senegal mahoganies (*Khaya senegalensis*) and rain trees (*Samanea saman*). Trunk f_n was measured repeatedly on six raised and five reduced Senegal mahoganies and four raised and five reduced rain trees. In the legend, trees numbered 1 – 6 and 7 – 11 were raised and reduced, respectively.

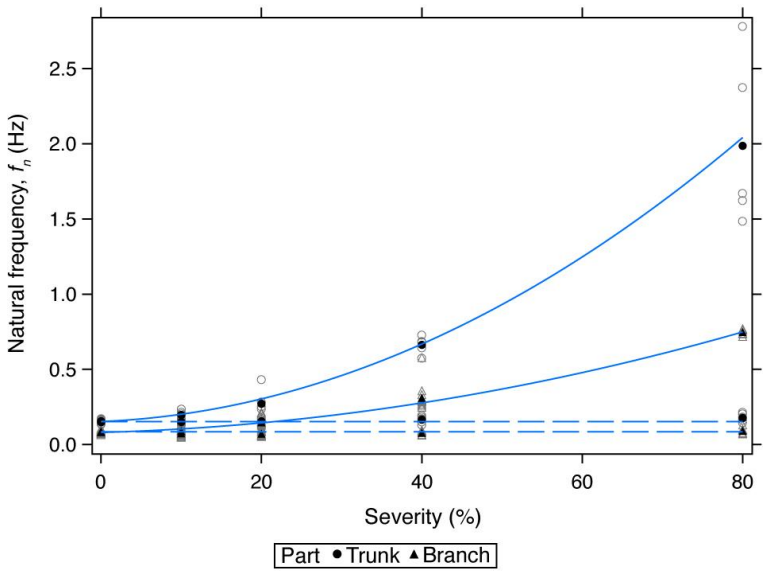

Figure 17: Regression of mean Senegal mahogany (*Khaya senegalensis*) natural frequency, f_n (Hz), against pruning severity for reduced trees (solid line) with data obtained from trunk displacement (filled circle) and branch acceleration (filled triangle) time histories of free vibration tests. Trunk f_n was measured repeatedly on six raised and five reduced Senegal mahoganies; branch f_n was simultaneously measured on 12 and 14 branches, respectively, distributed among raised and reduced trees. Least squares regression equations are $y = (2.7\times10^{-4})\,x^2 + (2.2\times10^{-3})\,x + 0.15$ ($R^2 = 0.99$) and $y = (8.6\times10^{-5})\,x^2 + (1.5\times10^{-3})\,x + 0.08$ ($R^2 = 0.99$) for trunk and branch f_n, respectively. Dashed horizontal lines depict the mean f_n for similar trunk and branch observations on raised trees, for which f_n remained constant across the range of tested pruning severities. For reference, empty gray symbols show observations of individual trees.

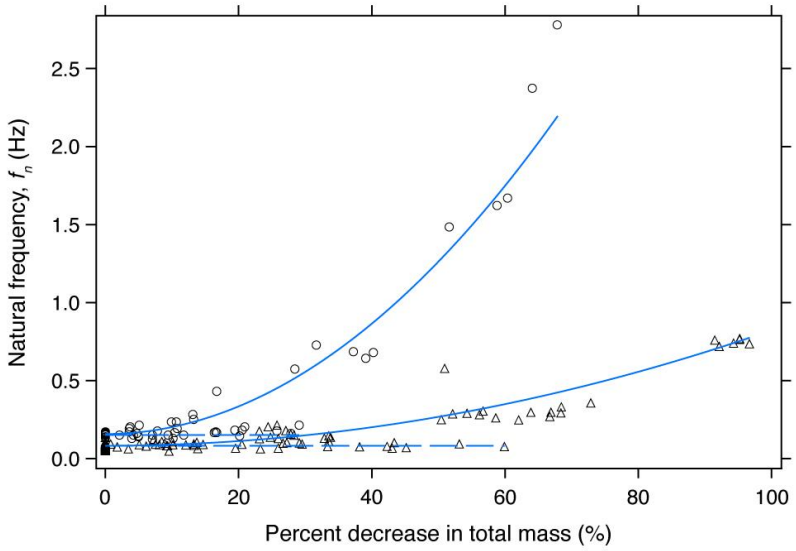

Figure 18: Regression of Senegal mahogany (*Khaya senegalensis*) natural frequency, f_n, on percent decrease in total mass, m_{TREE}, of the relevant tree part for reduced trees (solid line) with data obtained from trunk displacement (circle) and branch acceleration (triangle) time histories of free vibration tests. Trunk f_n was measured repeatedly on six raised and five reduced Senegal mahoganies; branch f_n was simultaneously measured on 12 and 14 branches, respectively, distributed among raised and reduced trees. Least squares regression equations are $y = (4.4\times10^{-4})\ x^2 + (2.4\times10^{-3})\ x + 0.16$ ($R^2 = 0.97$) and $y = (7.4\times10^{-5})\ x^2 + (6.7\times10^{-5})\ x + 0.08$ ($R^2 = 0.91$) for trunk and branch f_n, respectively. Dashed horizontal lines depict the mean f_n for analogous trunk and branch observations on raised trees, for which f_n remained constant across the range of tested pruning severities.

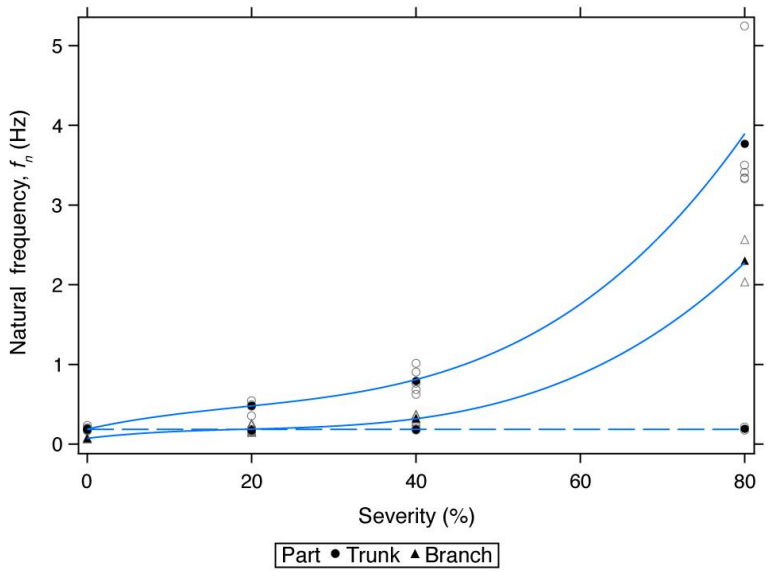

Figure 19: Regression of mean rain tree (*Samanea saman*) natural frequency, f_n (Hz), against pruning severity for reduced trees (solid line) with data obtained from trunk displacement (filled circle) and branch acceleration (filled triangle) time histories of free vibration tests. Trunk f_n was measured repeatedly on four raised and five reduced rain trees; branch f_n was simultaneously measured on six branches in one reduced rain tree. Least squares regression equations are $y = (1.2\times10^{-5})\,x^3 - (6.7\times10^{-4})\,x^2 + (2.3\times10^{-2})\,x + 0.19$ ($R^2 = 0.99$) and $y = (8.6\times10^{-6})\,x^3 - (5.0\times10^{-4})\,x^2 + (1.2\times10^{-2})\,x + 0.07$ ($R^2 = 0.99$) for trunk and branch f_n, respectively. Dashed horizontal line depicts the mean f_n for trunk observations on raised trees, for which f_n remained constant across the range of tested pruning severities. For reference, empty gray symbols show observations of individual trees.

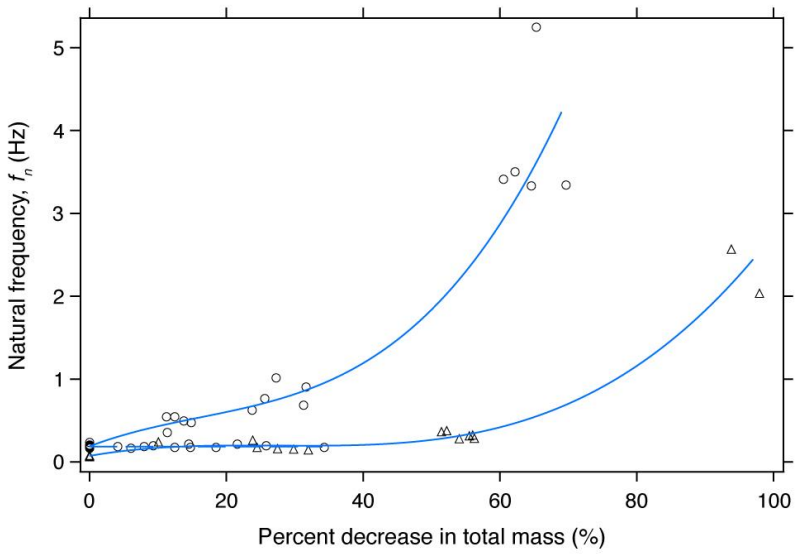

Figure 20: Regression of rain tree (*Samanea saman*) natural frequency, f_n (Hz), on percent decrease in total mass, m_{TREE}, of the relevant tree part for reduced trees (solid line) with data obtained from trunk displacement (circle) and branch acceleration (triangle) time histories of free vibration tests. Trunk f_n was measured repeatedly on four raised and five reduced rain trees; branch f_n was simultaneously measured on six branches in one reduced rain tree. Least squares regression equations are $y = (1.9\times10^{-5})\,x^3 - (9.2\times10^{-4})\,x^2 + (3.2\times10^{-2})\,x + 0.19$ [$R^2 = 0.92$] and $y = (6.7\times10^{-6})\,x^3 - (5.5\times10^{-4})\,x^2 + (1.5\times10^{-2})\,x + 0.07$ [$R^2 = 0.95$] for trunk and branch f_n, respectively. Dashed horizontal line depicts the mean f_n for similar trunk observations on raised trees, for which f_n remained constant across the range of tested pruning severities.

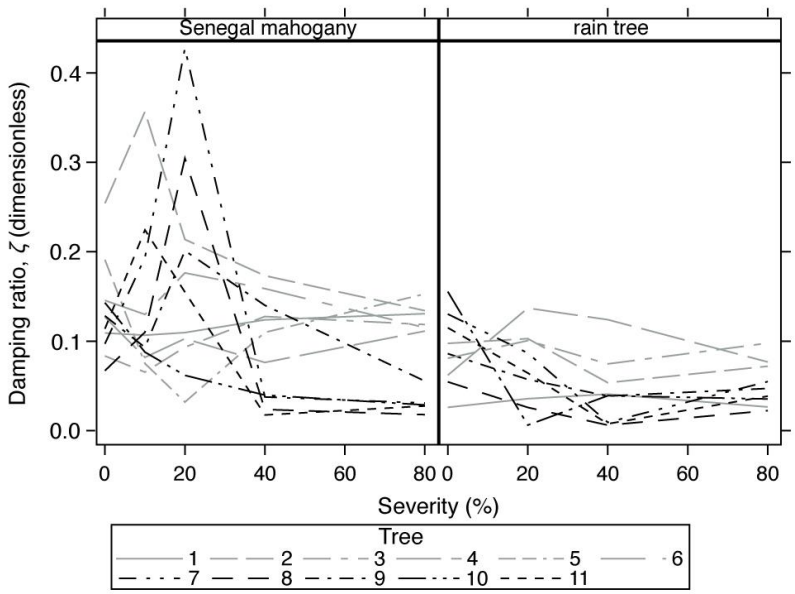

Figure 21: Data profile plot showing repeated measurements of trunk damping ratio, ζ (dimensionless), on individual Senegal mahoganies (*Khaya senegalensis*) and rain trees (*Samanea saman*). Trunk ζ was measured repeatedly on six raised and five reduced Senegal mahoganies and four raised and five reduced rain trees. In the legend, trees numbered 1 – 6 and 7 – 11 were raised and reduced, respectively.

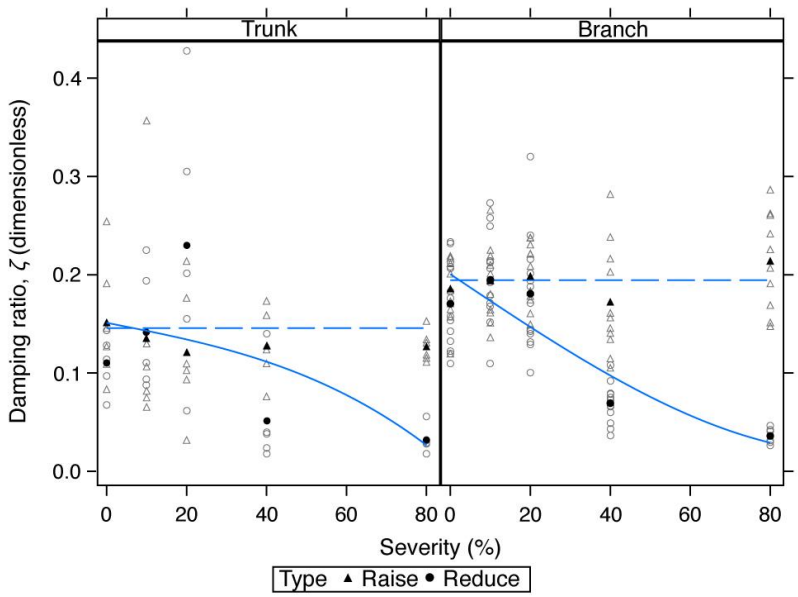

Figure 22: Regression of mean Senegal mahogany (*Khaya senegalensis*) damping ratio, ζ (dimensionless), on pruning severity for reduced trees (filled circle marker, solid line) with data obtained from trunk displacement (left panel) and branch acceleration (right panel) time histories of free vibration tests. Trunk ζ was measured repeatedly on six raised and five reduced Senegal mahoganies; branch ζ was simultaneously measured on 12 and 14 branches, respectively, distributed among these raised and reduced trees. Least squares regression equations are $y = (-1.2\times10^{-7})\,x^3 - (8.0\times10^{-4})\,x + 0.15$ [$R^2 = 0.42$] and $y = (9.0\times10^{-8})\,x^3 - (2.7\times10^{-3})\,x + 0.20$ [$R^2 = 0.85$] for trunk and branch ζ, respectively. Dashed horizontal lines depict the mean ζ for similar trunk and branch observations on raised trees (filled triangle marker), for which ζ remained constant across the range of tested pruning severities. For reference, empty gray symbols show observations of individual trees.

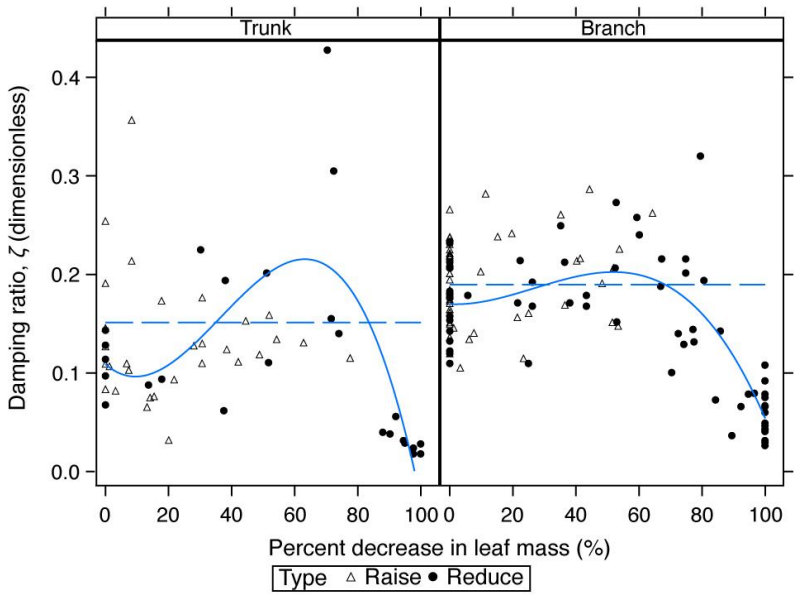

Figure 23: Regression of Senegal mahogany (*Khaya senegalensis*) damping ratio, ζ (dimensionless), on percent decrease in leaf mass, m_{LEAF}, of the relevant tree part for reduced trees (solid line) with data obtained from trunk displacement (left panel) and branch acceleration (right panel) time histories of free vibration tests. During the experiment, trunk ζ was measured repeatedly on six raised and five reduced Senegal mahoganies, and branch ζ was simultaneously measured on 12 and 14 branches, respectively, distributed among the raised and reduced Senegal mahoganies. Least-squares regression equations are $y = (-1.5\times10^{-6})\,x^3 + (1.7\times10^{-4})\,x^2 - (2.8\times10^{-3})\,x + 0.11$ [$R^2 = 0.53$] and $y = (-5.2\times10^{-7})\,x^3 + (4.2\times10^{-5})\,x^2 - (1.5\times10^{-4})\,x + 0.17$ [$R^2 = 0.63$] for trunk and branch ζ, respectively. Dashed horizontal lines depict the mean ζ for analogous trunk and branch observations on raised trees, for which ζ remained constant across the range of tested pruning severities.

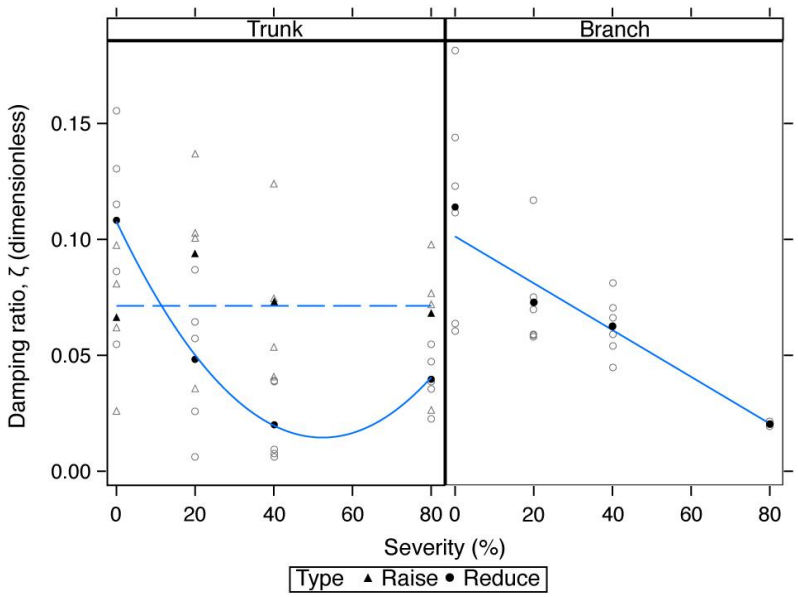

Figure 24: Regression of mean rain tree (*Samanea saman*) damping ratio, ζ (dimensionless), on pruning severity for reduced trees (filled circle marker, solid line) with data obtained from trunk displacement (left panel) and branch acceleration (right panel) time histories of free vibration tests. Trunk ζ was measured repeatedly on four raised and five reduced rain trees; branch ζ was simultaneously measured on six branches in one reduced rain tree. Least squares regression equations are $y = (3.4\times10^{-5})\, x^2 - (3.6\times10^{-3})\, x + 0.11$ [$R^2 = 0.99$] and $y = (-1.0\times10^{-3})\, x + 0.10$ [$r^2 = 0.96$] for trunk and branch ζ, respectively. Dashed horizontal line depicts the mean ζ for similar trunk observations on raised trees (filled triangle marker), for which ζ remained constant across the range of tested pruning severities. For reference, empty gray symbols show observations of individual trees.

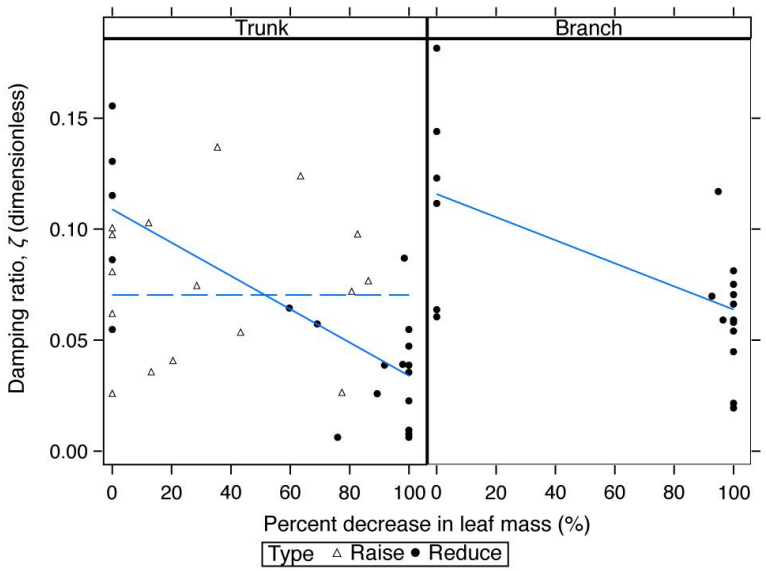

Figure 25: Regression of rain tree (*Samanea saman*) damping ratio, ζ (dimensionless), on percent decrease in leaf mass, m_{LEAF}, of the relevant tree part for reduced trees (solid line) with data obtained from trunk displacement (left panel) and branch acceleration (right panel) time histories of free vibration tests. Trunk ζ was measured repeatedly on four raised and five reduced rain trees, and branch ζ was simultaneously measured on six branches in one reduced rain tree. Least-squares regression equations are $y = (-7.5\times10^{-4})\,x + 0.11$ [$r^2 = 0.59$] and $y = (-5.2\times10^{-4})\,x + 0.12$ [$r^2 = 0.40$] for trunk and branch ζ, respectively. Dashed horizontal line depicts the mean ζ for analogous trunk observations on raised trees, for which ζ remained constant across the range of tested pruning severities.

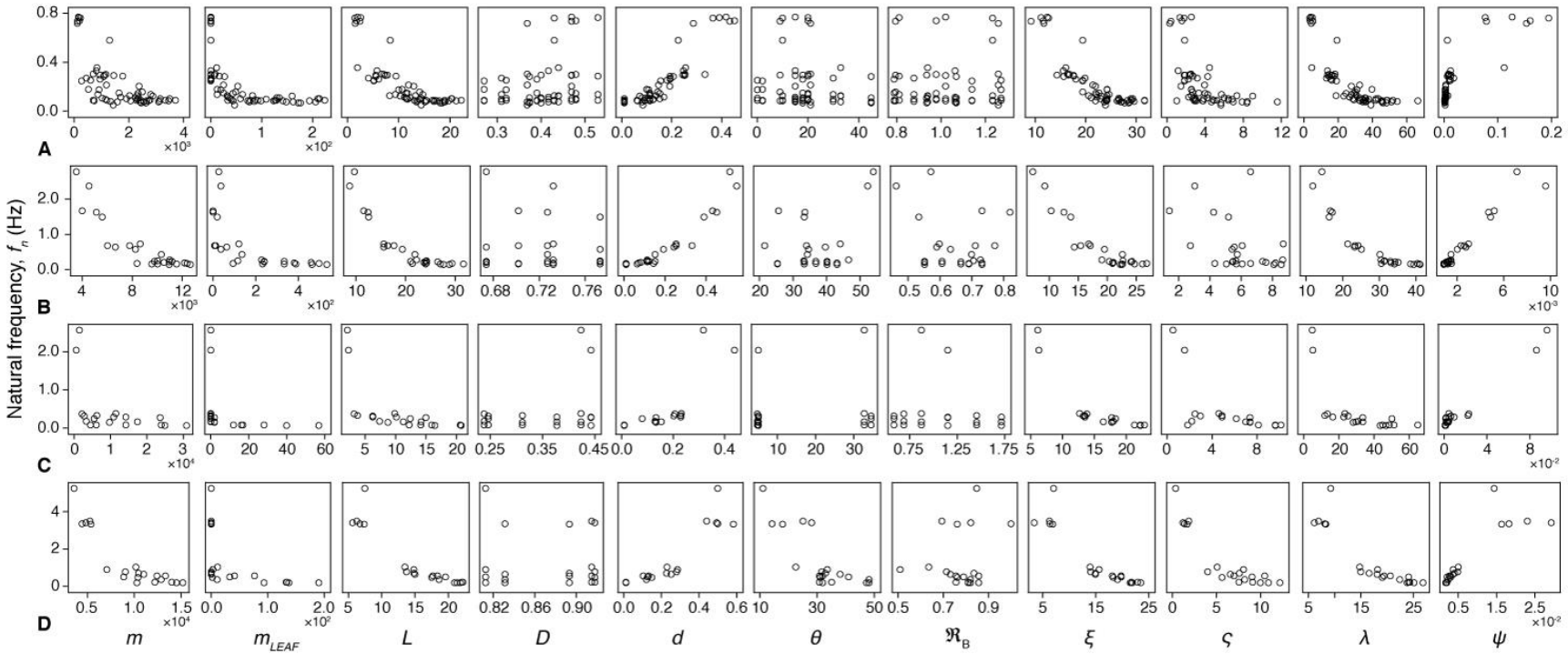

Figure 26: For all pruning severities, scatter plot matrix displaying bivariate relationships between natural frequency, f_n (Hz), and 11 morphometric attributes, including total mass, m (kg); leaf mass, m_{LEAF} (kg); length, L (m); basal diameter, D (m); apical diameter, d (m); branch inclination, θ (°); branch aspect ratio, $\mathfrak{R}_B$ (dimensionless); height of branch apex, ξ (m); spread of branch apex, ς (m); slenderness, λ (dimensionless); and stockiness, ψ (m^{-1}), of the respective tree part. In each row, data are presented separately for f_n measured on the branches (**A**) and trunks (**B**) of Senegal mahogany (*Khaya senegalensis*) and branches (**C**) and trunks (**D**) of rain tree (*Samanea saman*). Data refer only to reduced trees; preliminary analysis indicated no relationships between f_n and any morphometric attributes on raised trees of either species.

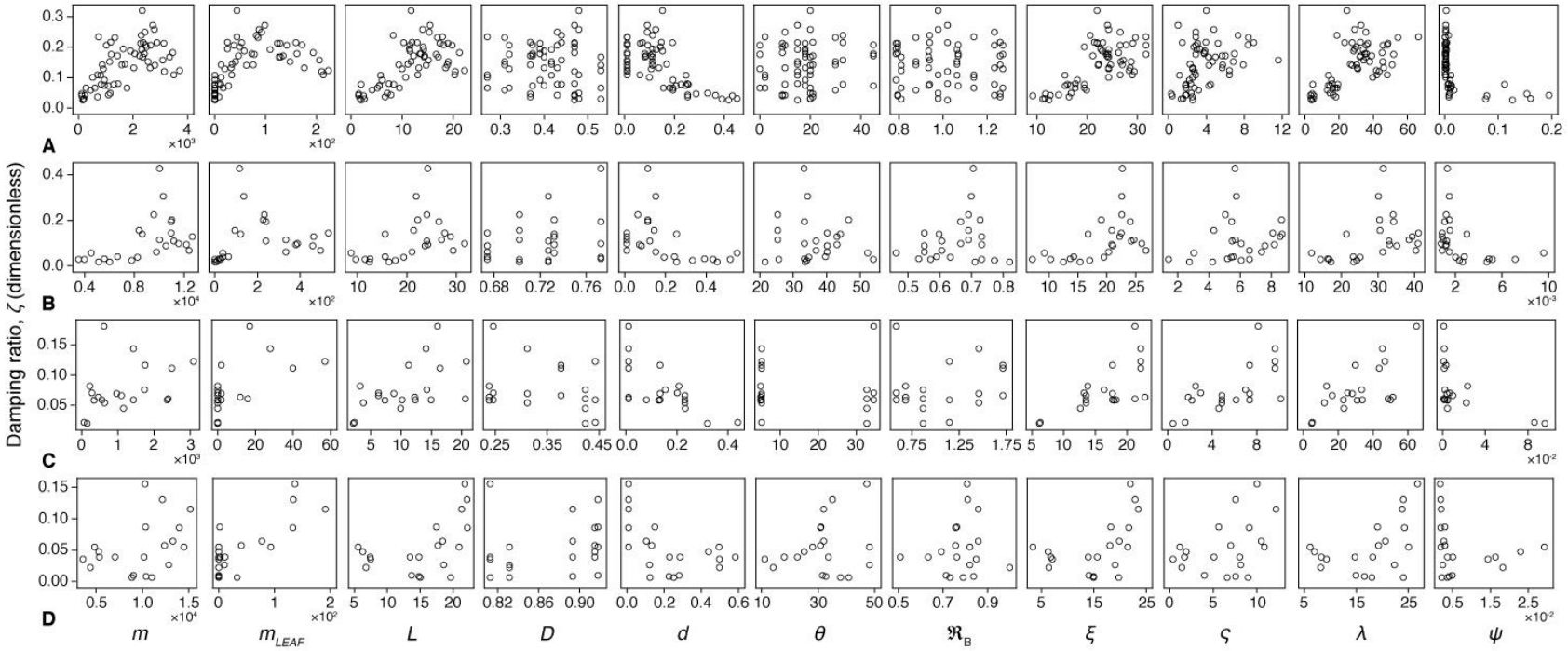

Figure 27: For all pruning severities, scatter plot matrix displaying bivariate relationships between damping ratio, ζ (dimensionless), and and 11 morphometric attributes, including total mass, m (kg); leaf mass, m_{LEAF} (kg); length, L (m); basal diameter, D (m); apical diameter, d (m); branch inclination, θ (°); branch aspect ratio, $\Re_B$ (dimensionless); height of branch apex, ξ (m); spread of branch apex, ς (m); slenderness, λ (dimensionless); and stockiness, ψ (m^{-1}), of the respective tree part. In each row, data are presented separately for ζ measured on the branches (**A**) and trunks (**B**) of Senegal mahogany (*Khaya senegalensis*) and branches (**C**) and trunks (**D**) of rain tree (*Samanea saman*). Data refer only to reduced trees; preliminary analysis indicated not relationships between ζ and any morphometric attributes on raised trees of either species.

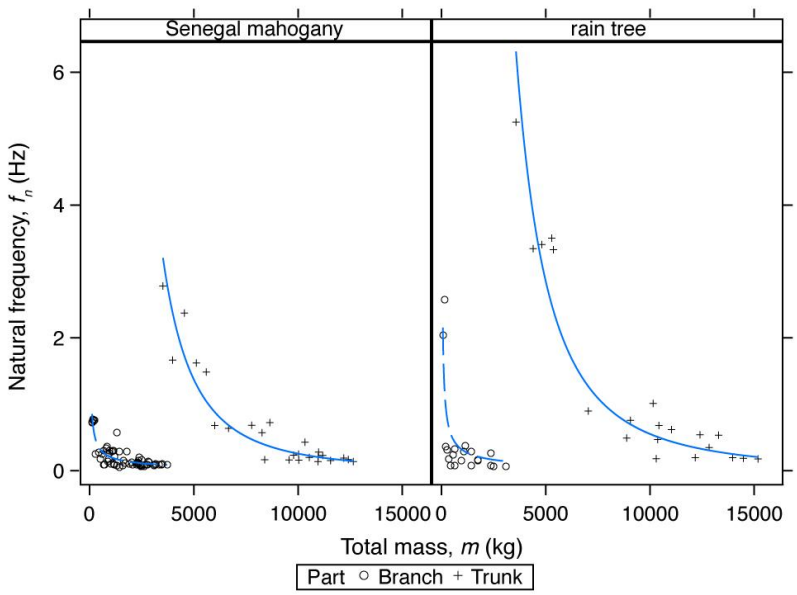

Figure 28: For all pruning severities, scatter plot and best-fit lines of natural frequency, f_n (Hz), against total mass, m (kg), measured on the trunks (solid lines) and branches (dashed lines) of reduced Senegal mahogany (*Khaya senegalensis*) and rain tree (*Samanea saman*). Lines represent power functions of the form $y = \beta x^{\alpha}$ obtained by least squares regression of $\log_{10}$-transformed observations of both f_n and m. See Table 16 for model sample sizes, parameter estimates, and fit statistics.

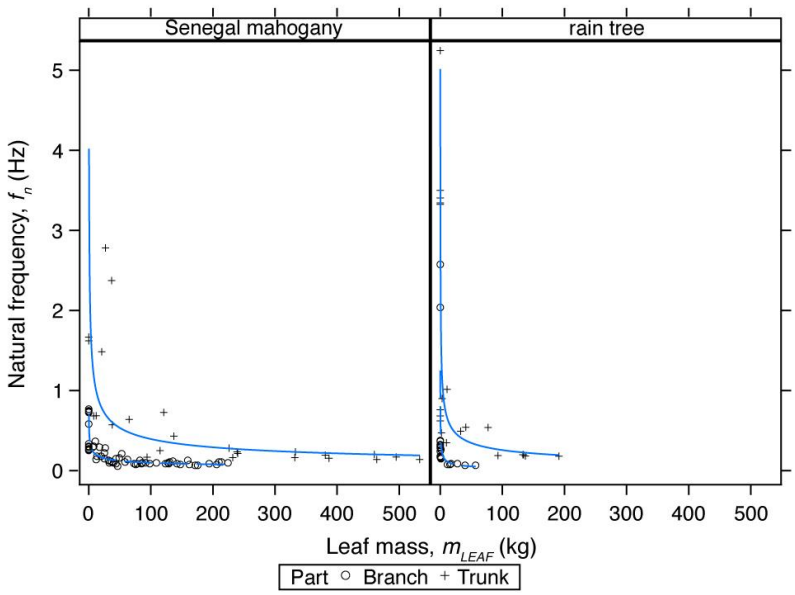

Figure 29: For all pruning severities, scatter plot and best-fit lines of natural frequency, f_n (Hz), against leaf mass, m_{LEAF} (kg), measured on the trunks (solid lines) and branches (dashed lines) of reduced Senegal mahogany (*Khaya senegalensis*) and rain tree (*Samanea saman*). Lines represent power functions of the form $y = \beta x^{\alpha}$ obtained by least squares regression of $\log_{10}$-transformed observations of both f_n and m_{LEAF}. See Table 16 for model sample sizes, parameter estimates, and fit statistics.

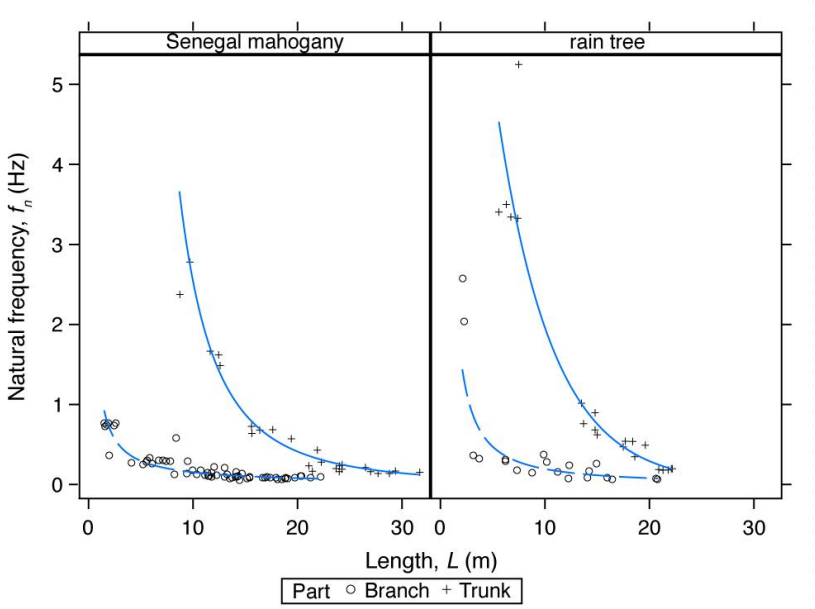

Figure 30: For all pruning severities, scatter plot and best-fit lines of natural frequency, f_n (Hz), against length, L (m), measured on the trunks (solid lines) and branches (dashed lines) of reduced Senegal mahogany (*Khaya senegalensis*) and rain tree (*Samanea saman*). Except for f_n measured on the trunk of rain tree, lines represent power functions of the form $y = \beta x^{\alpha}$ obtained by least squares regression of $\log_{10}$-transformed observations of both f_n and L. For f_n measured on the trunk of rain tree, line represents exponential function of the form $y = \beta e^{\alpha x}$ obtained by least squares regression of $\log_e$-transformed f_n and untransformed L. See Table 16 for model sample sizes, parameter estimates, and fit statistics.

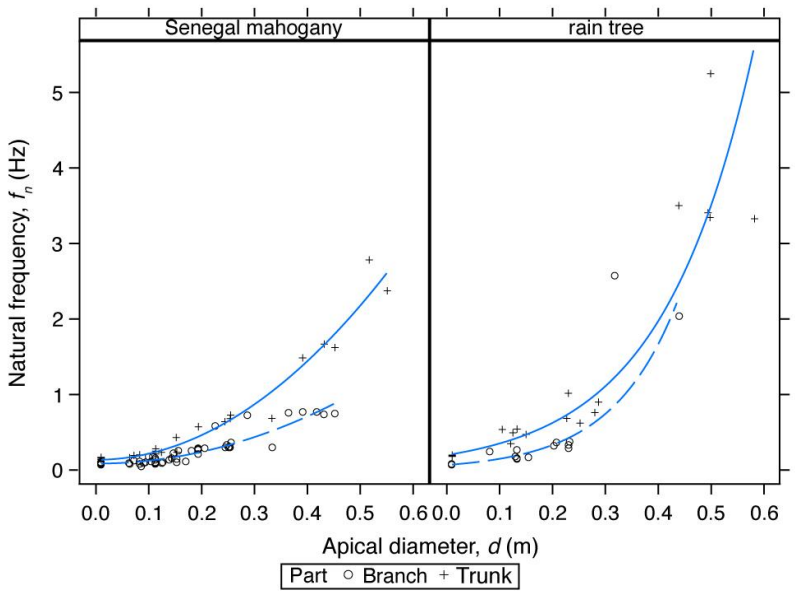

Figure 31: For all pruning severities, scatter plot and best-fit lines of natural frequency, f_n (Hz), against apical diameter, d (m), measured on the trunks (solid lines) and branches (dashed lines) of reduced Senegal mahogany (*Khaya senegalensis*) and rain tree (*Samanea saman*). For Senegal mahogany, lines represent quadratic functions of the form $y = \beta + \alpha x^2$ obtained by least squares regression of untransformed f_n and d^2. For rain tree, lines represent exponential functions of the form $y = \beta e^{\alpha x}$ obtained by least squares regression of $\log_e$-transformed f_n and untransformed d. See Table 16 for model sample sizes, parameter estimates, and fit statistics.

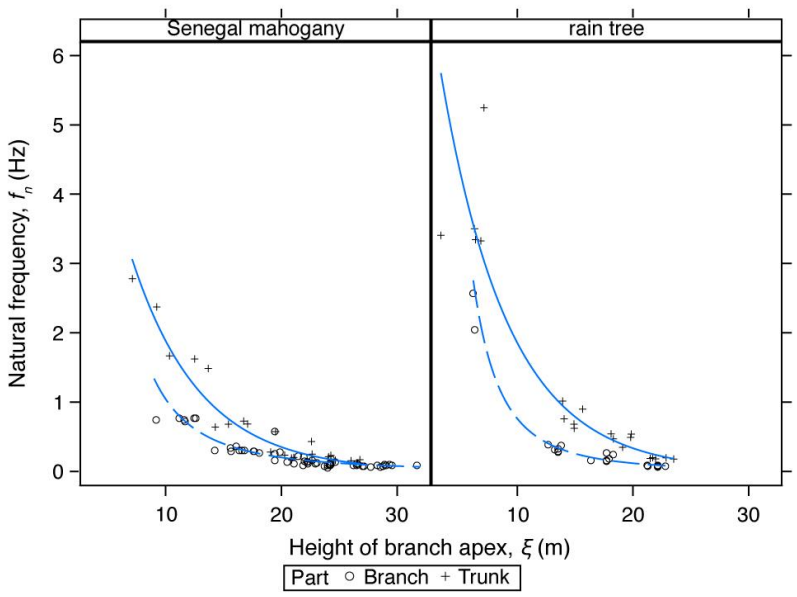

Figure 32: For all pruning severities, scatter plot and best-fit lines of natural frequency, f_n (Hz), against height of branch apex, ξ (m), measured on the trunks (solid lines) and branches (dashed lines) of reduced Senegal mahogany (*Khaya senegalensis*) and rain tree (*Samanea saman*). For branch observations, lines represent power functions of the form $y = \beta x^{\alpha}$ obtained by least squares regression of $\log_{10}$-transformed observations of both f_n and ξ. For trunk observations, lines represent exponential functions of the form $y = \beta e^{\alpha x}$ obtained by least squares regression of $\log_e$-transformed f_n and untransformed ξ. See Table 17 for model sample sizes, parameter estimates, and fit statistics.

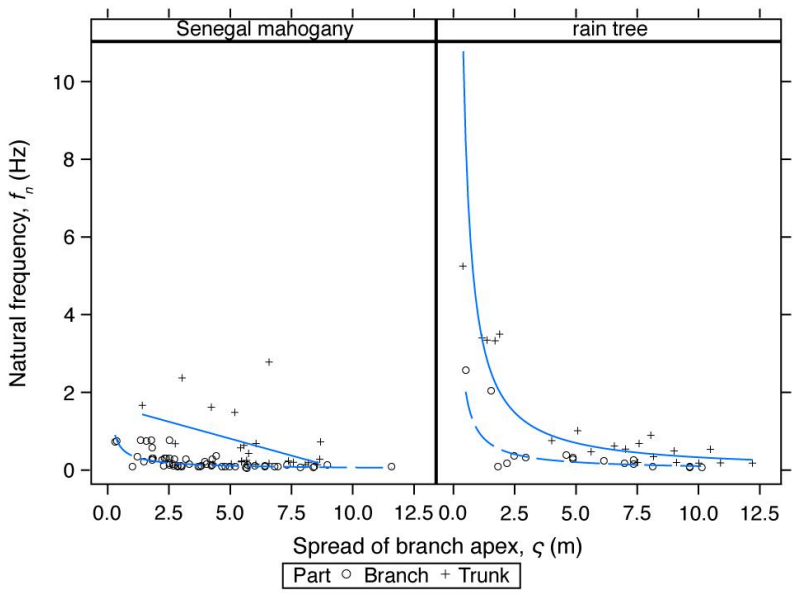

Figure 33: For all pruning severities, scatter plot and best-fit lines of natural frequency, f_n (Hz), against spread of branch apex, ς (m), measured on the trunks (solid line) and branches (dashed lines) of reduced Senegal mahogany (*Khaya senegalensis*) and rain tree (*Samanea saman*). Except for linear functions fit to f_n measured on the trunks of Senegal mahogany, lines represent power functions of the form $y = \beta x^{\alpha}$ obtained by least squares regression of $\log_{10}$-transformed observations of both f_n and ς. See Table 17 for model sample sizes, parameter estimates, and fit statistics.

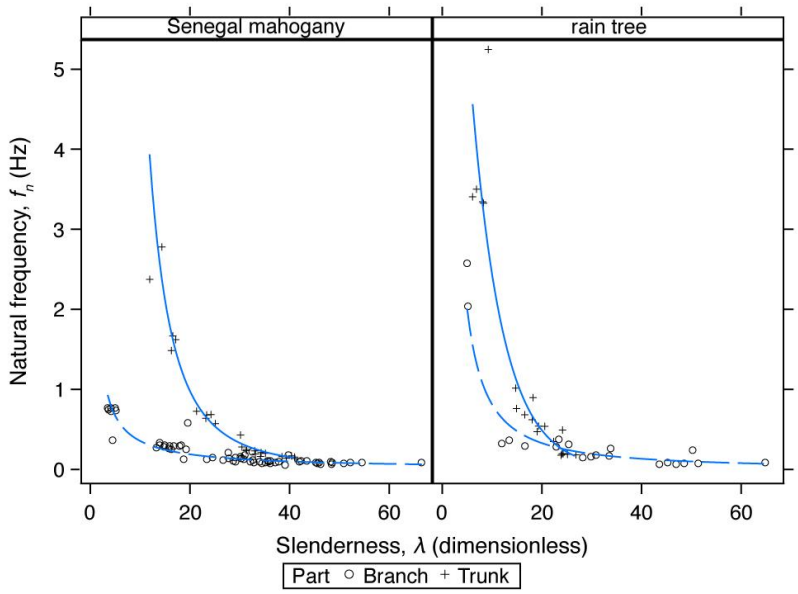

Figure 34: For all pruning severities, scatter plot and best-fit lines of natural frequency, f_n (Hz), against slenderness, λ (dimensionless), measured on the trunks (solid lines) and branches (dashed lines) of reduced Senegal mahogany (*Khaya senegalensis*) and rain tree (*Samanea saman*). Except for f_n measured on the trunks of rain tree, lines represent power functions of the form $y = \beta x^{\alpha}$ obtained by least squares regression of $\log_{10}$-transformed observations of both f_n and λ. For f_n measured on the trunks of rain tree, line represents exponential function of the form $y = \beta e^{\alpha x}$ obtained by least squares regression of $\log_e$-transformed f_n and untransformed λ. See Table 17 for model sample sizes, parameter estimates, and fit statistics.

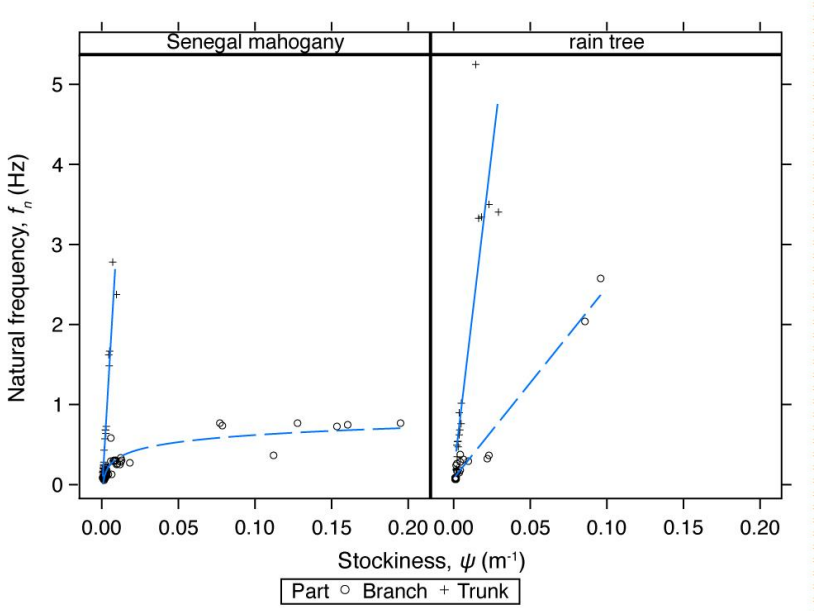

Figure 35: For all pruning severities, scatter plot and best-fit lines of natural frequency, f_n (Hz), against stockiness, ψ (m^{-1}), measured on the trunks (solid lines) and branches (dashed lines) of reduced Senegal mahogany (*Khaya senegalensis*) and rain tree (*Samanea saman*). For f_n measured on the branches of Senegal mahogany, line represents a logarithmic function of the form $y = \beta + \alpha \cdot \ln(x)$ obtained by least-squares regression of untransformed f_n and $\log_e$-transformed ψ. All other lines represent linear functions. See Table 17 for model sample sizes, parameter estimates, and fit statistics.

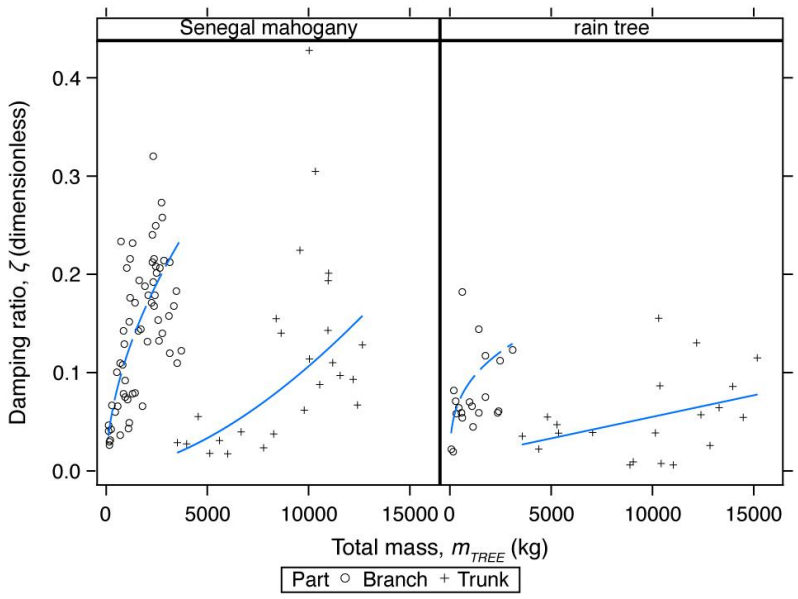

Figure 36: For all pruning severities, scatter plot and best-fit lines of damping ratio, ζ (dimensionless), against total mass, m (kg), measured on the branches (dashed lines) and trunks (solid lines) of reduced Senegal mahogany (*Khaya senegalensis*) and rain tree (*Samanea saman*). Except for a linear function fit to post-pruning ζ measured on the trunks of rain tree, lines represent power functions of the form $y = \beta x^{\alpha}$ obtained by least squares regression of $\log_{10}$-transformed observations of both ζ and m. See Table 18 for model sample sizes, parameter estimates, and fit statistics.

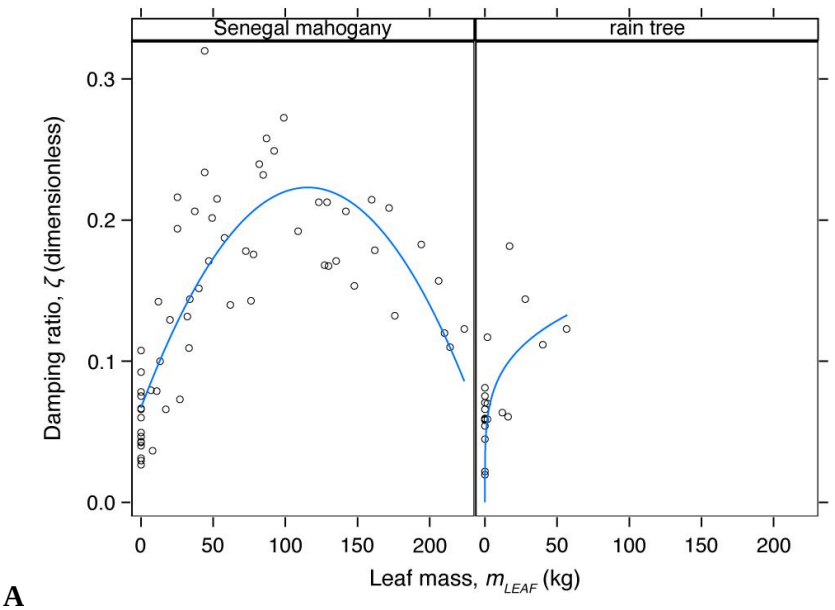

A

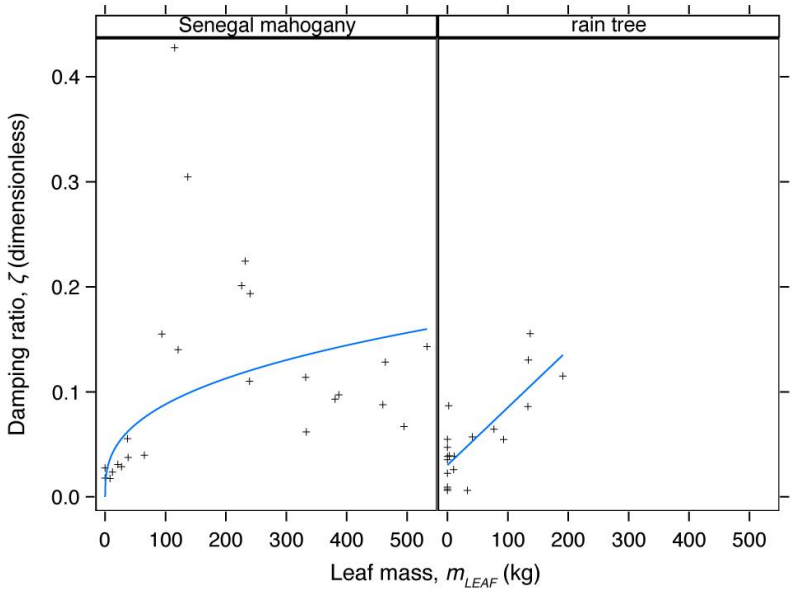

B

Figure 37: For all pruning severities, scatter plot and best-fit lines of damping ratio, ζ (dimensionless), against leaf mass, m_{LEAF} (kg), measured on the branches (**A**) and trunks (**B**) of reduced Senegal mahogany (*Khaya senegalensis*) and rain tree (*Samanea saman*). For ζ measured on the branches of Senegal mahogany, line represents second-order polynomial of the form $y = \beta + \alpha_1 x + \alpha_2 x^2$ obtained by least squares regression of untransformed ζ, m_{LEAF}, and m_{LEAF}^2. Other lines represent power functions of the form $y = \beta x^{\alpha}$ obtained by least squares regression of $\log_{10}$-transformed observations of both ζ and m_{LEAF}, except for a linear function fit to ζ measured on the trunks of rain tree. See Table 18 for model sample sizes, parameter estimates, and fit statistics.

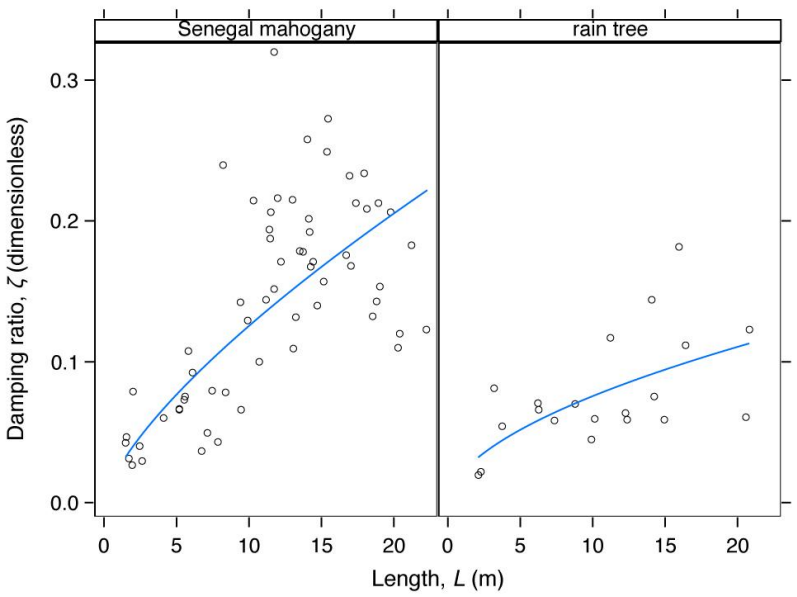

A

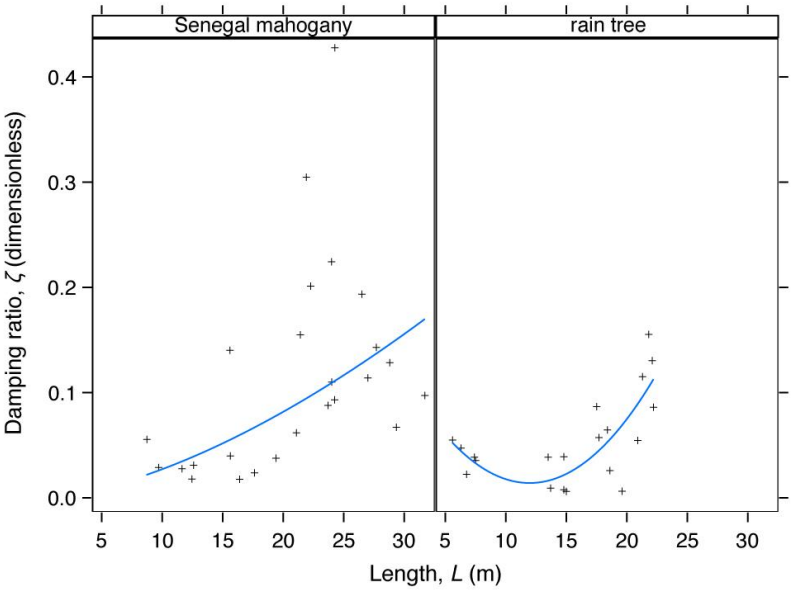

B

Figure 38: For all pruning severities, scatter plot and best-fit lines of damping ratio, ζ (dimensionless), against length, L (m), measured on the branches (**A**) and trunks (**B**) of reduced Senegal mahogany (*Khaya senegalensis*) and rain tree (*Samanea saman*). Except for ζ measured on the trunk of rain tree, lines represent power functions of the form $y = \beta x^{\alpha}$ obtained by least squares regression of $\log_{10}$-transformed observations of both ζ and L. For ζ measured on the trunk of rain tree, line represents second-order polynomial of the form $y = \beta + \alpha_1 x + \alpha_2 x^2$ obtained by least squares regression of untransformed ζ, L, and L^2. See Table 18 for model sample sizes, parameter estimates, and fit statistics.

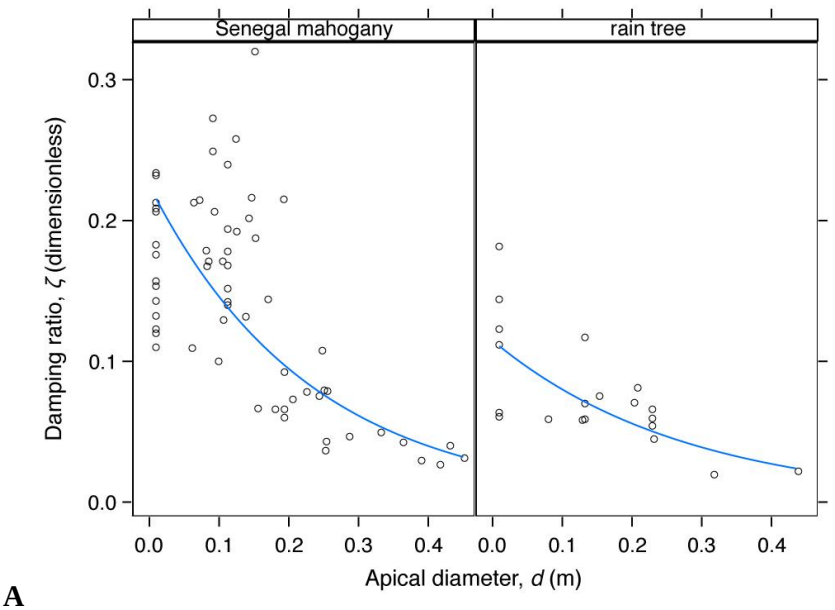

A

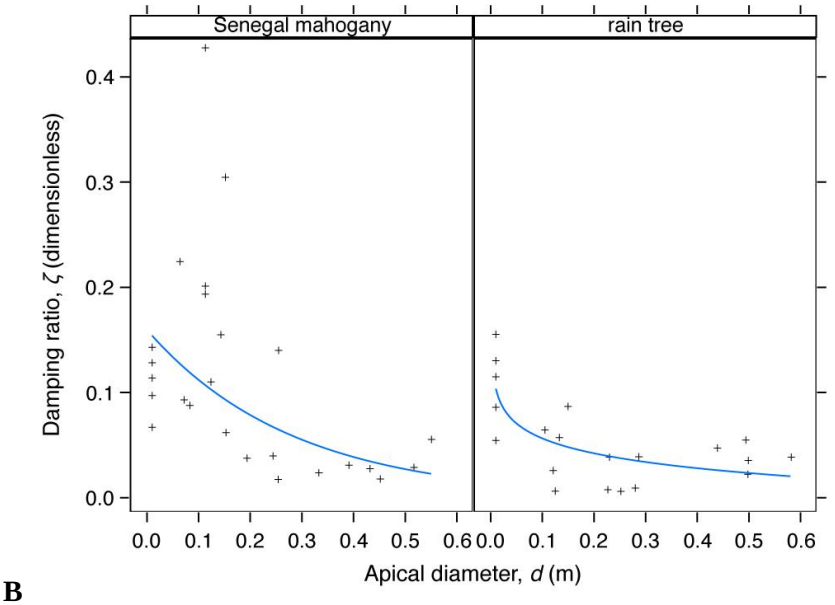

B

Figure 39: For all pruning severities, scatter plot and best-fit lines of damping ratio, ζ (dimensionless), against apical diameter, d (m), measured on the branches (**A**) and trunks (**B**) of reduced Senegal mahogany (*Khaya senegalensis*) and rain tree (*Samanea saman*). Except for ζ measured on the trunk of rain tree, lines represent exponential functions of the form $y = \beta e^{\alpha x}$ obtained by least squares regression of $\log_e$-transformed ζ and untransformed d. For ζ measured on the trunk of rain tree, line represents logarithmic function of the form $y = \beta + \alpha \cdot \ln(x)$ obtained by least squares regression of untransformed ζ and $\log_e$-transformed d. See Table 18 for model sample sizes, parameter estimates, and fit statistics.

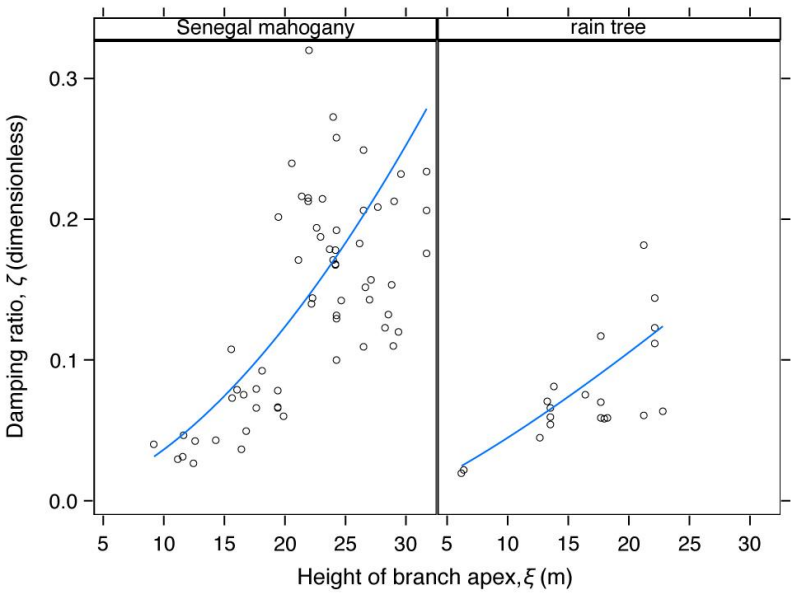

A

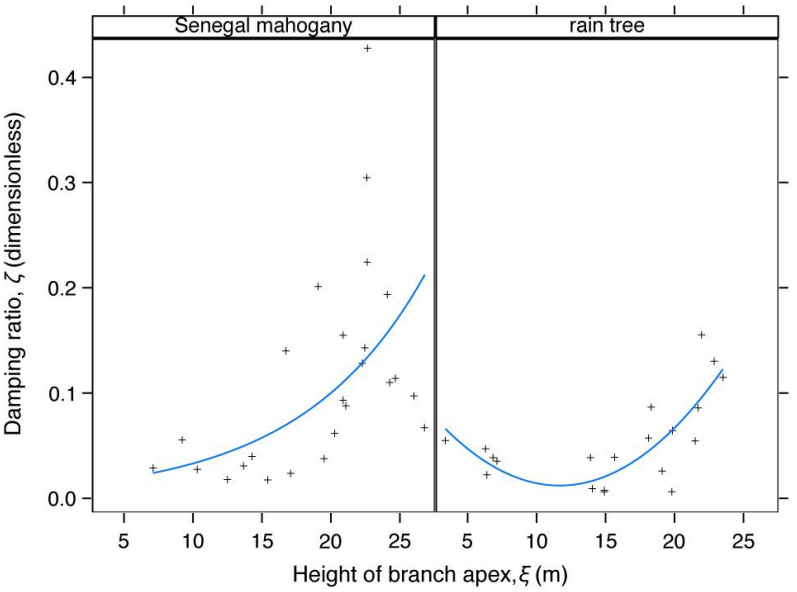

B

Figure 40: For all pruning severities, scatter plot and best-fit lines of damping ratio, ζ (dimensionless), against height of branch apex, ξ (m), measured on the branches (**A**) and trunks (**B**) of reduced Senegal mahogany (*Khaya senegalensis*) and rain tree (*Samanea saman*). For branch observations, lines represent power functions of the form $y = \beta x^{\alpha}$ obtained by least squares regression of $\log_{10}$-transformed observations of both ζ and ξ. For ζ measured on the trunk of Senegal mahogany, line represents exponential function of the form $y = \beta e^{\alpha x}$ obtained by least squares regression of $\log_e$-transformed ζ and untransformed ξ. For ζ measured on the trunk of rain tree, line represents second-order polynomial of the form $y = \beta + \alpha_1 x + \alpha_2 x^2$ obtained by least squares regression of untransformed ζ, ξ, and ξ^2. See Table 19 for model sample sizes, parameter estimates, and fit statistics.

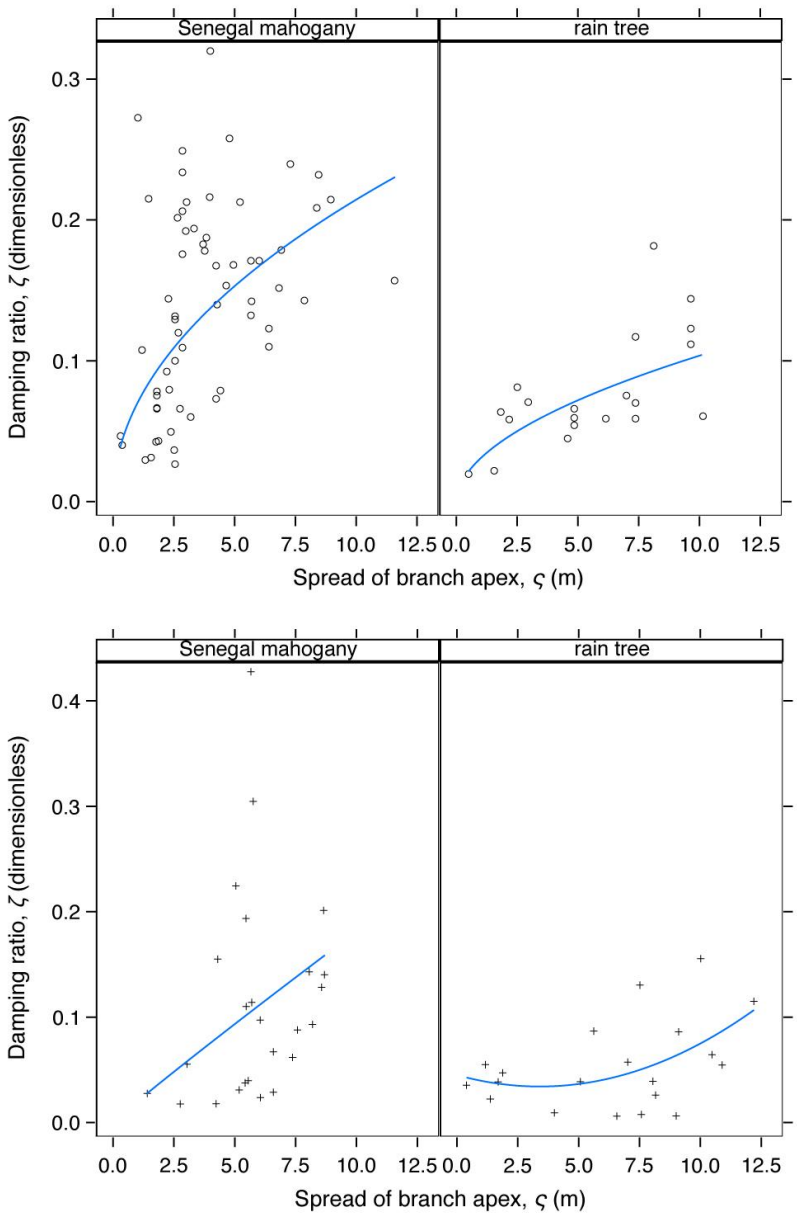

Figure 41: For all pruning severities, scatter plot and best-fit lines of damping ratio, ζ (dimensionless), against spread of branch apex, ς (m), measured on the branches (**A**) and trunks (**B**) of reduced Senegal mahogany (*Khaya senegalensis*) and rain tree (*Samanea saman*). Except for ζ measured on the trunk of rain tree, lines represent power functions of the form $y = \beta x^{\alpha}$ obtained by least squares regression of $\log_{10}$-transformed observations of both ζ and ς. For ζ measured on the trunk of rain tree, line represents second-order polynomial of the form $y = \beta + \alpha_1 x + \alpha_2 x^2$ obtained by least squares regression of untransformed ζ, ς, and ς^2. See Table 19 for model sample sizes, parameter estimates, and fit statistics.

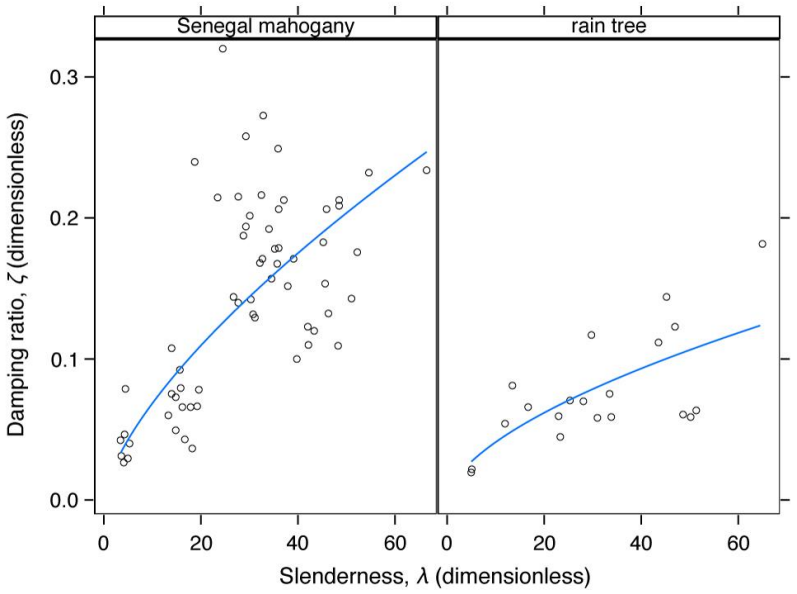

A

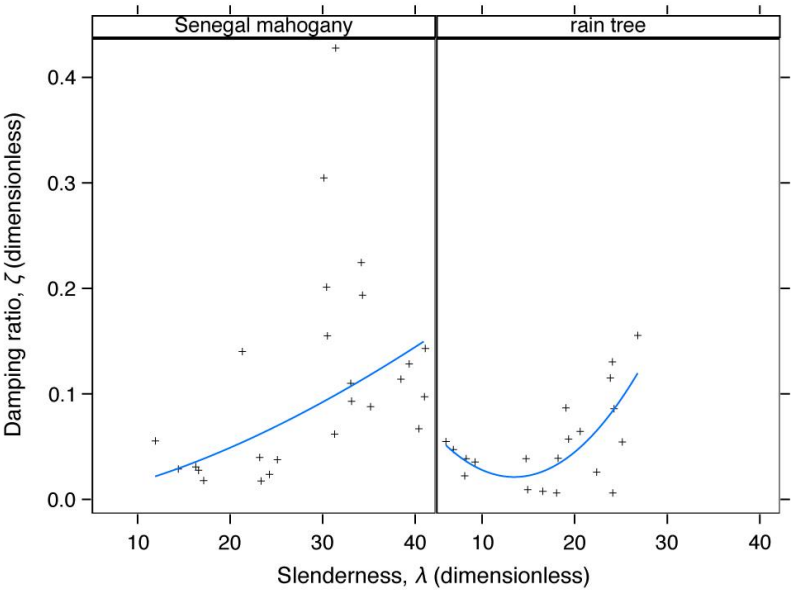

B

Figure 42: For all pruning severities, scatter plot and best-fit lines of damping ratio, ζ (dimensionless), against slenderness, λ (dimensionless), measured on the branches (**A**) and trunks (**B**) of reduced Senegal mahogany (*Khaya senegalensis*) and rain tree (*Samanea saman*). Except for ζ measured on the trunk of rain tree, lines represent power functions of the form $y = \beta x^{\alpha}$ obtained by least squares regression of $\log_{10}$-transformed observations of both ζ and λ. For ζ measured on the trunk of rain tree, line represents second-order polynomial of the form $y = \beta + \alpha_1 x + \alpha_2 x^2$ obtained by least squares regression of untransformed ζ, λ, and λ^2. See Table 19 for model sample sizes, parameter estimates, and fit statistics.

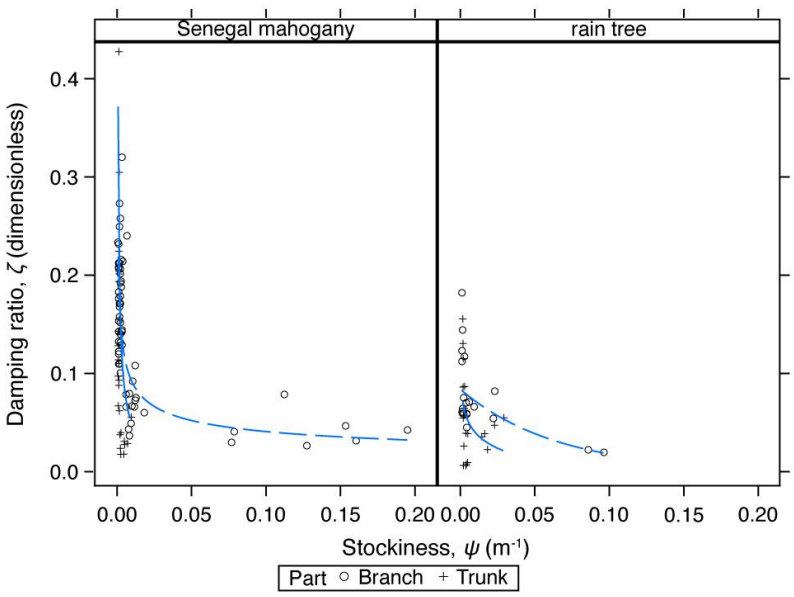

Figure 43: For all pruning severities, scatter plot and best-fit lines of damping ratio, ζ (dimensionless), against stockiness, ψ (m^{-1}), measured on the branches (dashed lines) and trunks (solid lines) of reduced Senegal mahogany (*Khaya senegalensis*) and rain tree (*Samanea saman*). For Senegal mahogany, lines represent power functions of the form $y = \beta x^{\alpha}$ obtained by least squares regression of $\log_{10}$-transformed observations of both ζ and ψ. For ζ measured on the trunk of rain tree, line represents exponential function of the form $y = \beta e^{\alpha x}$ obtained by least squares regression of $\log_e$-transformed ζ and untransformed ψ. For ζ measured on the branches of rain tree, line represents logarithmic function of the form $y = \beta + \alpha \cdot \ln(x)$ obtained by least squares regression of untransformed ζ and $\log_e$-transformed ψ. See Table 19 for model sample sizes, parameter estimates, and fit statistics.

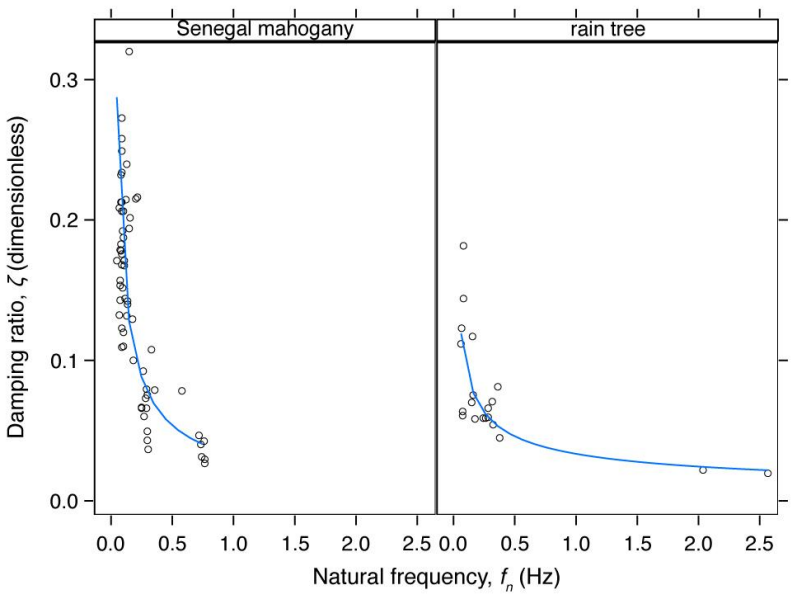

A

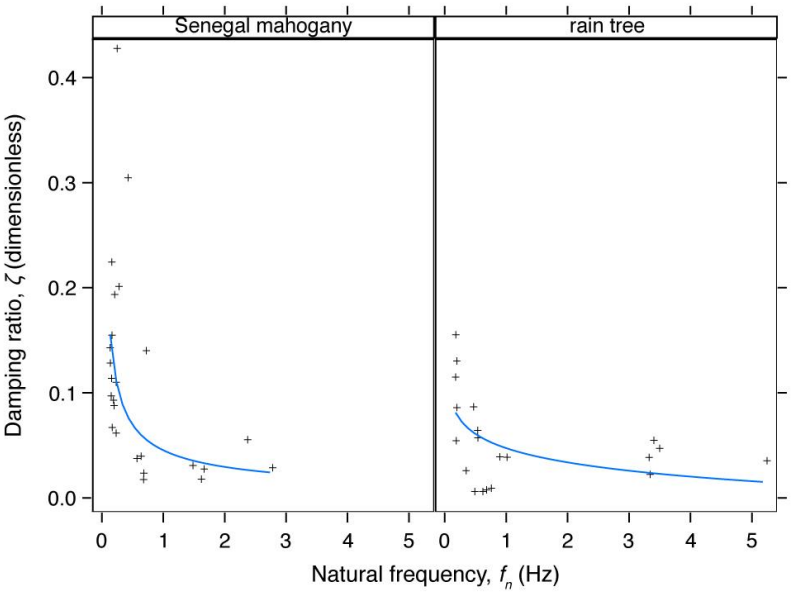

B

Figure 44: For all pruning severities, scatter plot and best-fit lines of damping ratio, ζ (dimensionless), against natural frequency, f_n (Hz), measured on the branches (**A**) and trunks (**B**) of reduced Senegal mahogany and (*Khaya senegalensis*) and rain tree (*Samanea saman*). Except for ζ measured on the trunk of rain tree, lines represent power functions of the form $y = \beta x^{\alpha}$ obtained by least squares regression of $\log_{10}$-transformed observations of both ζ and f_n. For ζ measured on the trunk of rain tree, line represents logarithmic function of the form $y = \beta + \alpha \cdot \ln(x)$ obtained by least squares regression of untransformed ζ and $\log_e$ transformed f_n. See Table 19 for model sample sizes, parameter estimates, and fit statistics.

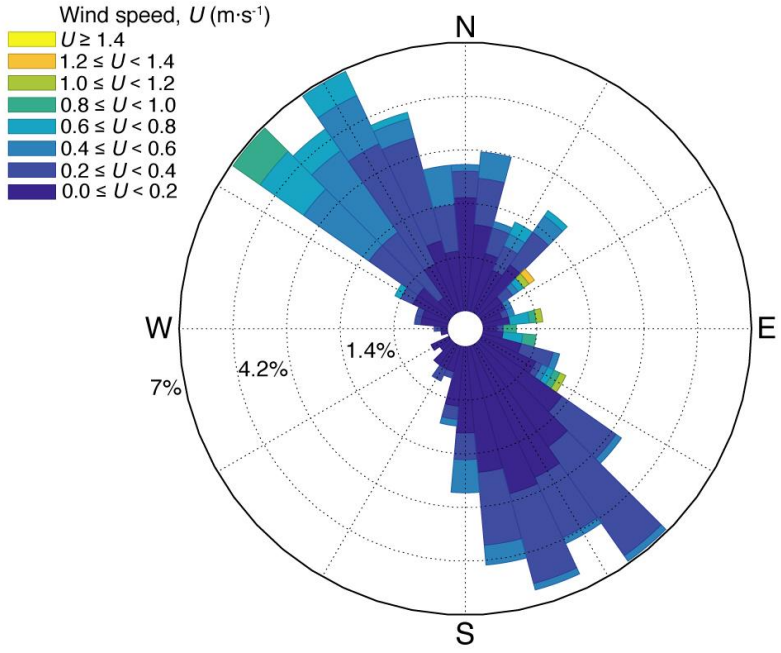

Figure 45: At 0% pruning severity for the Senegal mahoganies, wind rose showing the relative frequency of 30-minute resultant wind speeds and directions for 577 different 30-minute intervals between 2 August and 15 September 2013. For measurements at 18.3 m (z/H_{TREE} = 0.69), the length of spokes depicts the relative frequency of 30-minute resultant wind directions, within 36 incremental 10° bins, for a given wind speed range denoted by color bands. Concentric circles are labeled to show the relative frequency of winds.

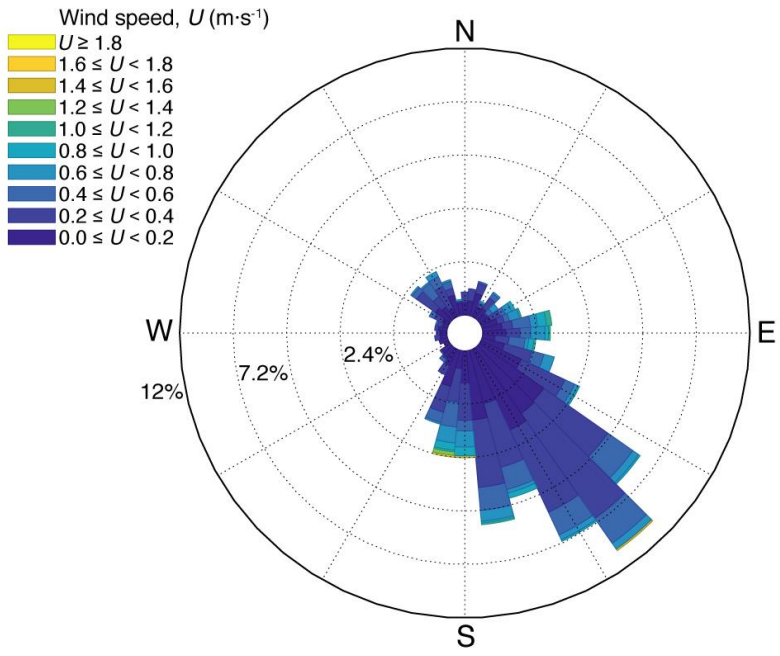

Figure 46: At 10% pruning severity for the Senegal mahoganies, wind rose showing the relative frequency of 30-minute resultant wind speeds and directions for 1,249 different 30-minute intervals between 30 September and 13 November 2013. For measurements at 18.3 m (z/H_{TREE} = 0.69), the length of spokes depicts the relative frequency of 30-minute resultant wind directions, within 36 incremental 10° bins, for a given wind speed range denoted by color bands. Concentric circles are labeled to show the relative frequency of winds.

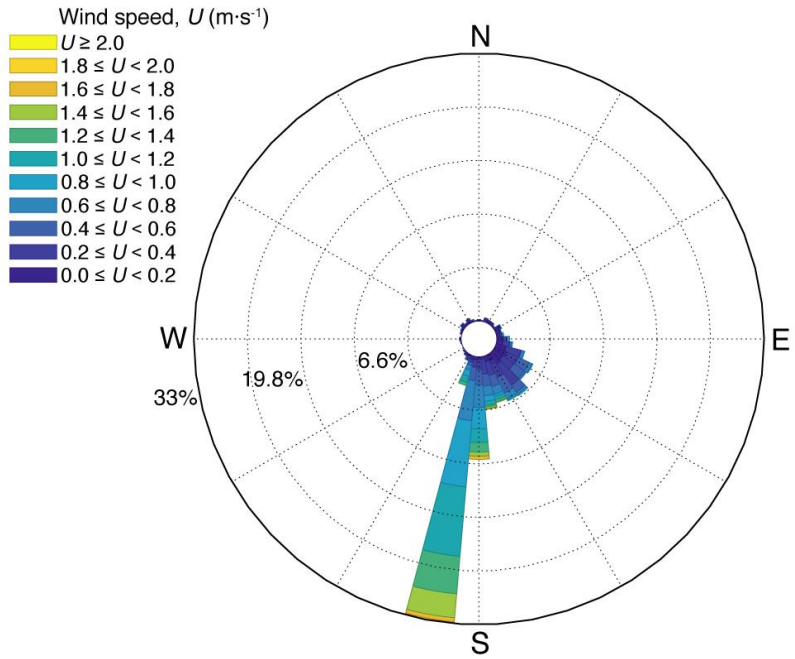

Figure 47: At 20% pruning severity for the Senegal mahoganies, wind rose showing the relative frequency of 30-minute resultant wind speeds and directions for 1,013 different 30-minute intervals between 27 November 2013 and 10 January 2014. For measurements at 18.3 m (z/H_{TREE} = 0.69), the length of spokes depicts the relative frequency of 30-minute resultant wind directions, within 36 incremental 10° bins, for a given wind speed range denoted by color bands. Concentric circles are labeled to show the relative frequency of winds.

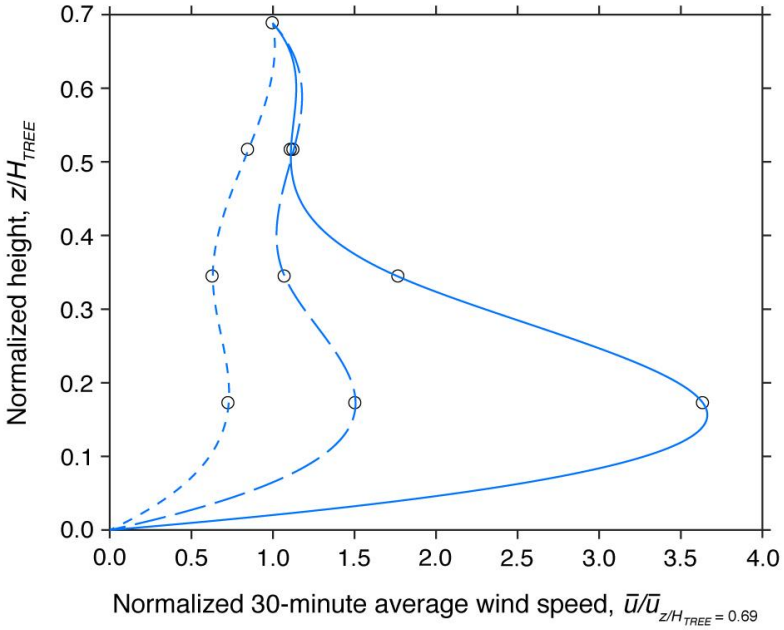

Figure 48: For all measurement heights, z (m), normalized by average tree height, H_{TREE} = 26.9 m, vertical wind profile showing the average 30-minute streamwise wind speed, $\bar{u}$ (m·s^{-1}), normalized by $\bar{u}$ measured at z/H_{TREE} = 0.69. Plotted values are averages of all 30-minute intervals recorded during the 45-day periods corresponding with 0% (solid line; n = 558), 10% (long dash line; n = 803), and 20% (short dash line; n = 226) pruning severity for Senegal mahogany. Wind speeds at heights between discrete measurements were approximated using cubic spline interpolation.

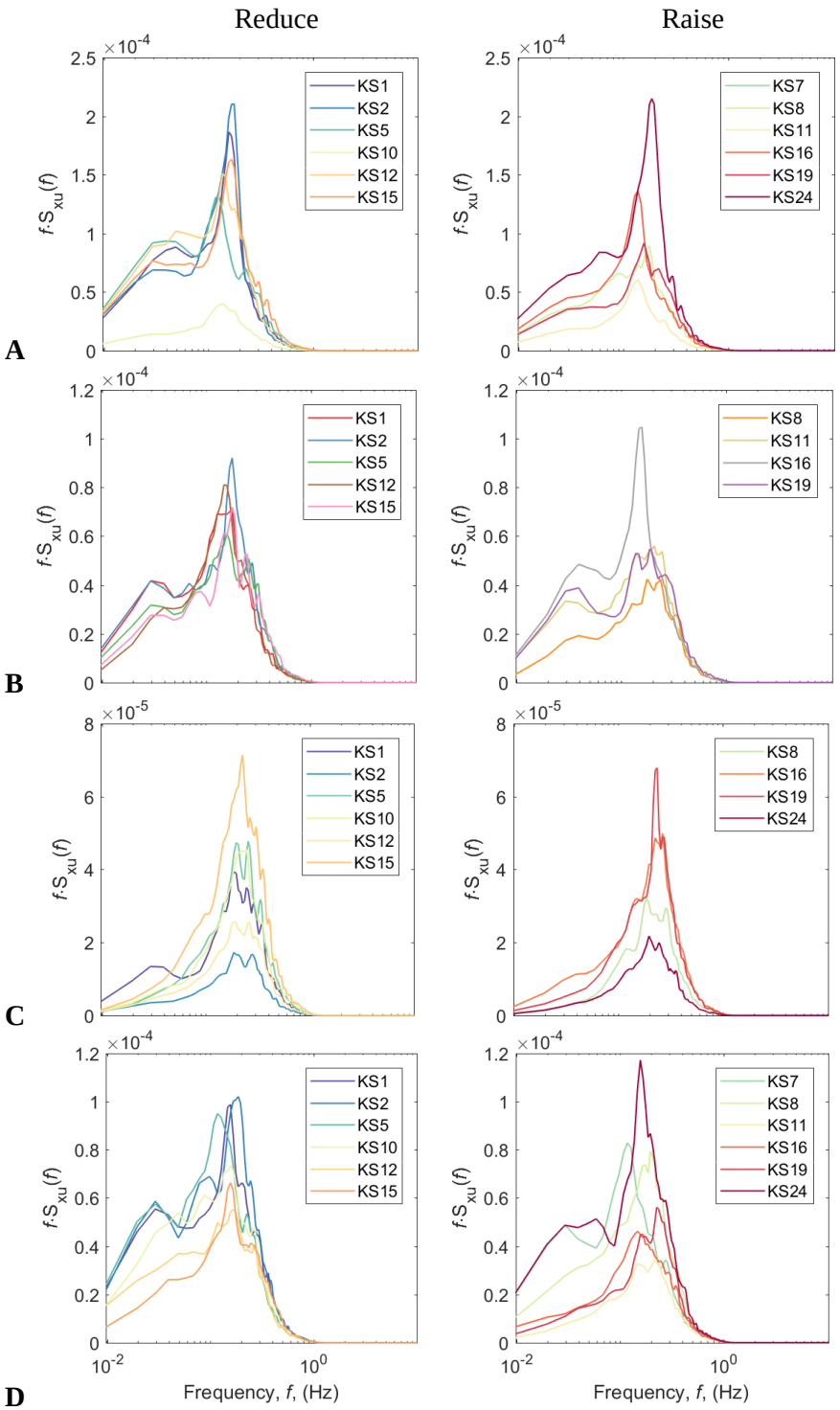

Figure 49: Fourier energy spectra $f \cdot S_{xu}(f)$ for Senegal mahoganies reduced (left column) and raised (right column) by 0% computed using 30-minute time histories of streamwise trunk displacement, x_U, recorded 2319 – 2349H 6 September 2013 (**A**), 1215 – 1245H 7 September 2013 (**B**), 1330 – 1400H 14 September 2013 (**C**), and 1219 – 1249H 15 September 2013 (**D**). During these 30-minute intervals, the resultant wind speeds ($m \cdot s^{-1}$) and directions (°) at 18.3 m (z/H_{TREE} = 0.69) were 1.0 $m \cdot s^{-1}$, 94°; 1.1 $m \cdot s^{-1}$, 80°; 0.8 $m \cdot s^{-1}$, 323°; and 1.0 $m \cdot s^{-1}$, 58°. In the legend, trees are identified by the abbreviation KS (*Khaya senegalensis*) and tree number.

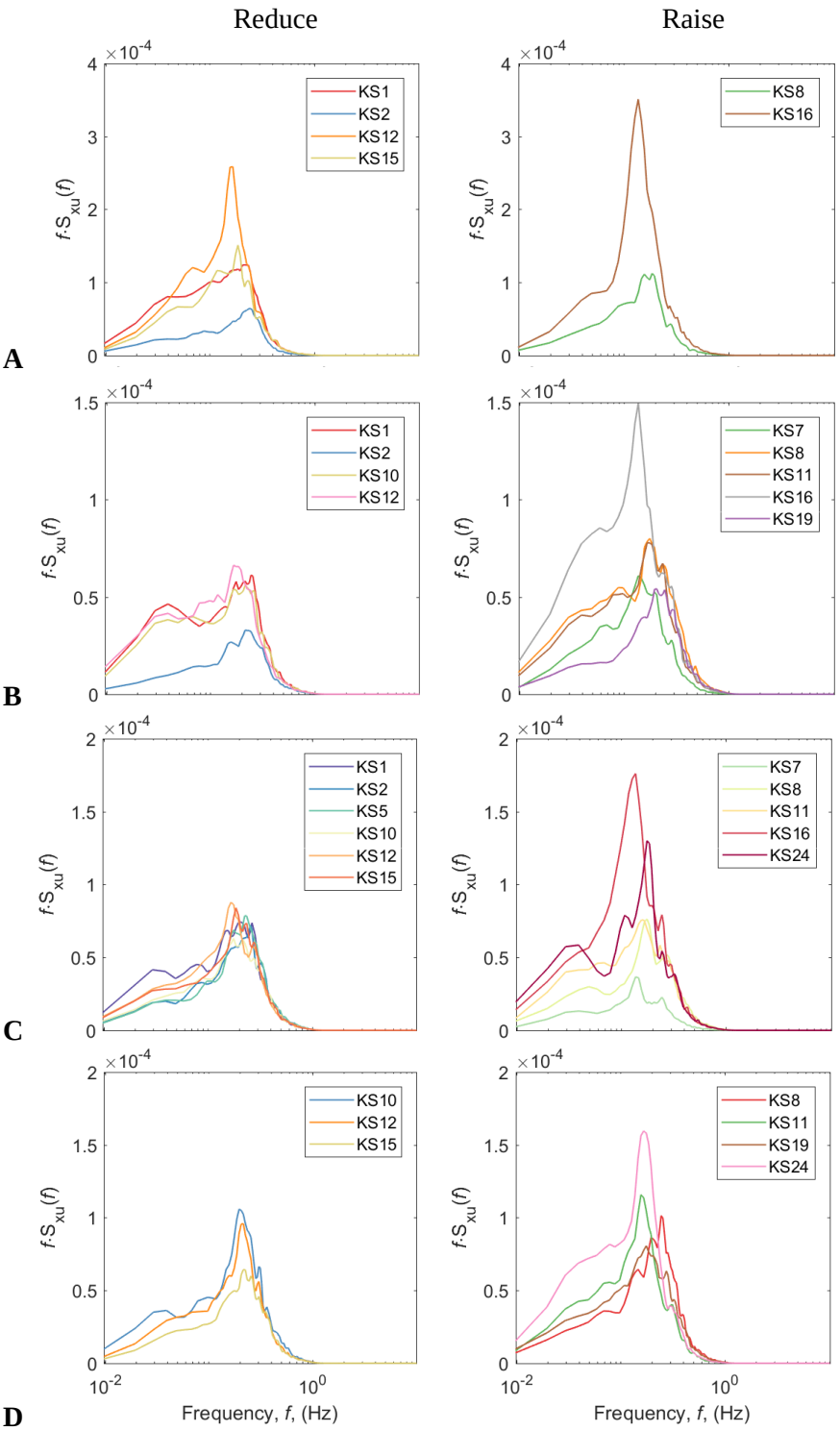

Figure 50: Fourier energy spectra $f \cdot S_{xu}(f)$ for Senegal mahoganies reduced (left column) and raised (right column) by 10% computed using 30-minute time histories of streamwise trunk displacement, x_U, recorded 0501 – 0531H 5 October 2013 (**A**), 1315 – 1345H 11 October 2013 (**B**), 1530 – 1600H 16 October 2013 (**C**), and 1330 – 1400H 20 October 2013 (**D**). During these 30-minute intervals, the resultant wind speeds ($m \cdot s^{-1}$) and directions (°) at 18.3 m ($z/H_{TREE} = 0.69$) were 1.5 $m \cdot s^{-1}$, 139°; 0.5 $m \cdot s^{-1}$, 317°; 0.4 $m \cdot s^{-1}$, 18°; and 1.2 $m \cdot s^{-1}$, 83°. In the legend, trees are identified by the abbreviation KS (*Khaya senegalensis*) and tree number.

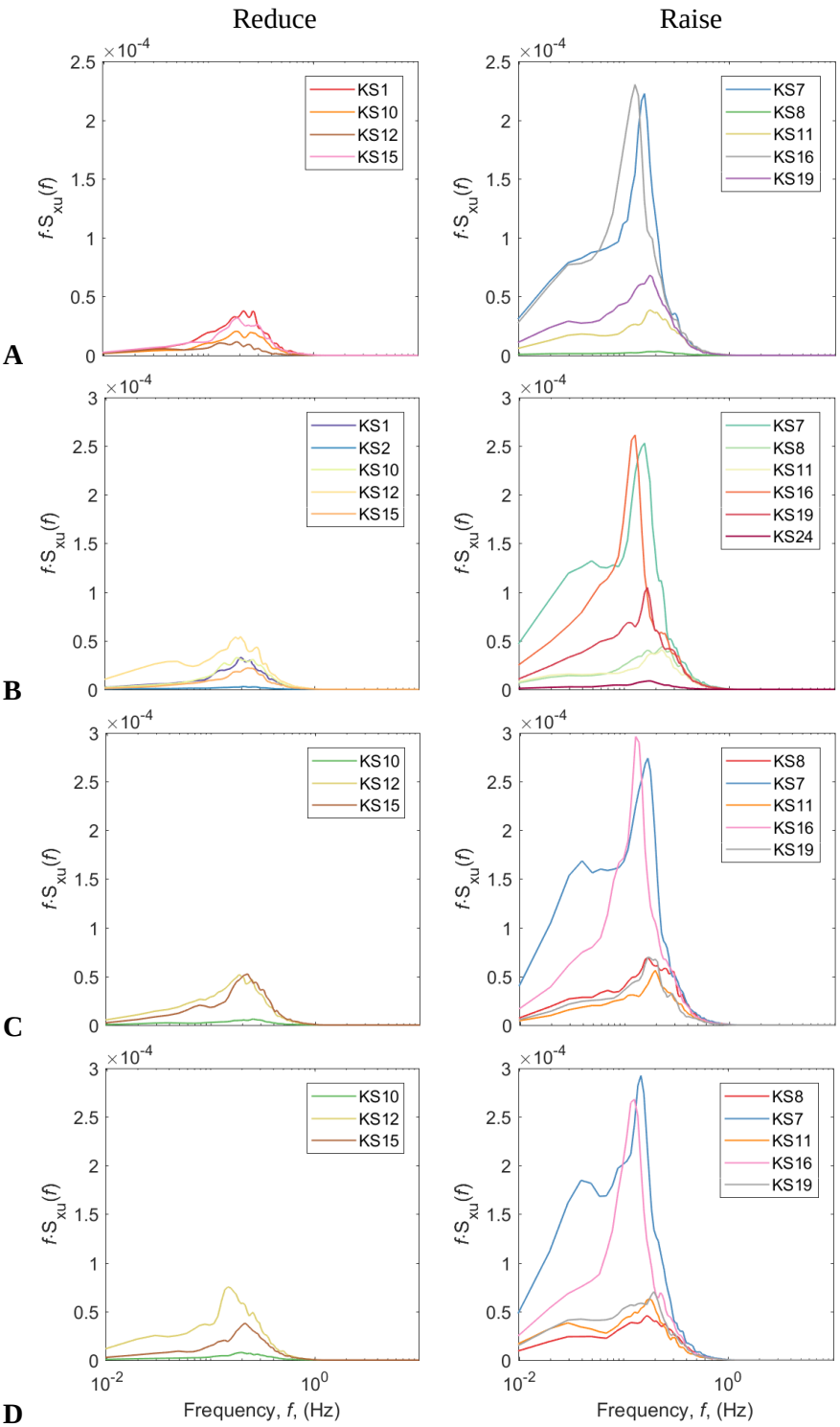

Figure 51: Fourier energy spectra $f \cdot S_{xu}(f)$ for Senegal mahoganies reduced (left column) and raised (right column) by 20% computed using 30-minute time histories of streamwise trunk displacement, x_U, recorded 1519 – 1549H 23 December 2013 (**A**), 0930 – 1000H 7 January 2014 (**B**), 1420 – 1450H 10 January 2014 (**C**), and 1600 – 1630H 10 January 2014 (**D**). During these 30-minute intervals, the resultant wind speeds ($m \cdot s^{-1}$) and directions (°) at 18.3 m (z/H_{TREE} = 0.69) were 1.7 $m \cdot s^{-1}$, 190°; 2.0 $m \cdot s^{-1}$, 187°; 1.8 $m \cdot s^{-1}$, 189°; and 2.1 $m \cdot s^{-1}$, 191°. In the legend, trees are identified by the abbreviation KS (*Khaya senegalensis*) and tree number.

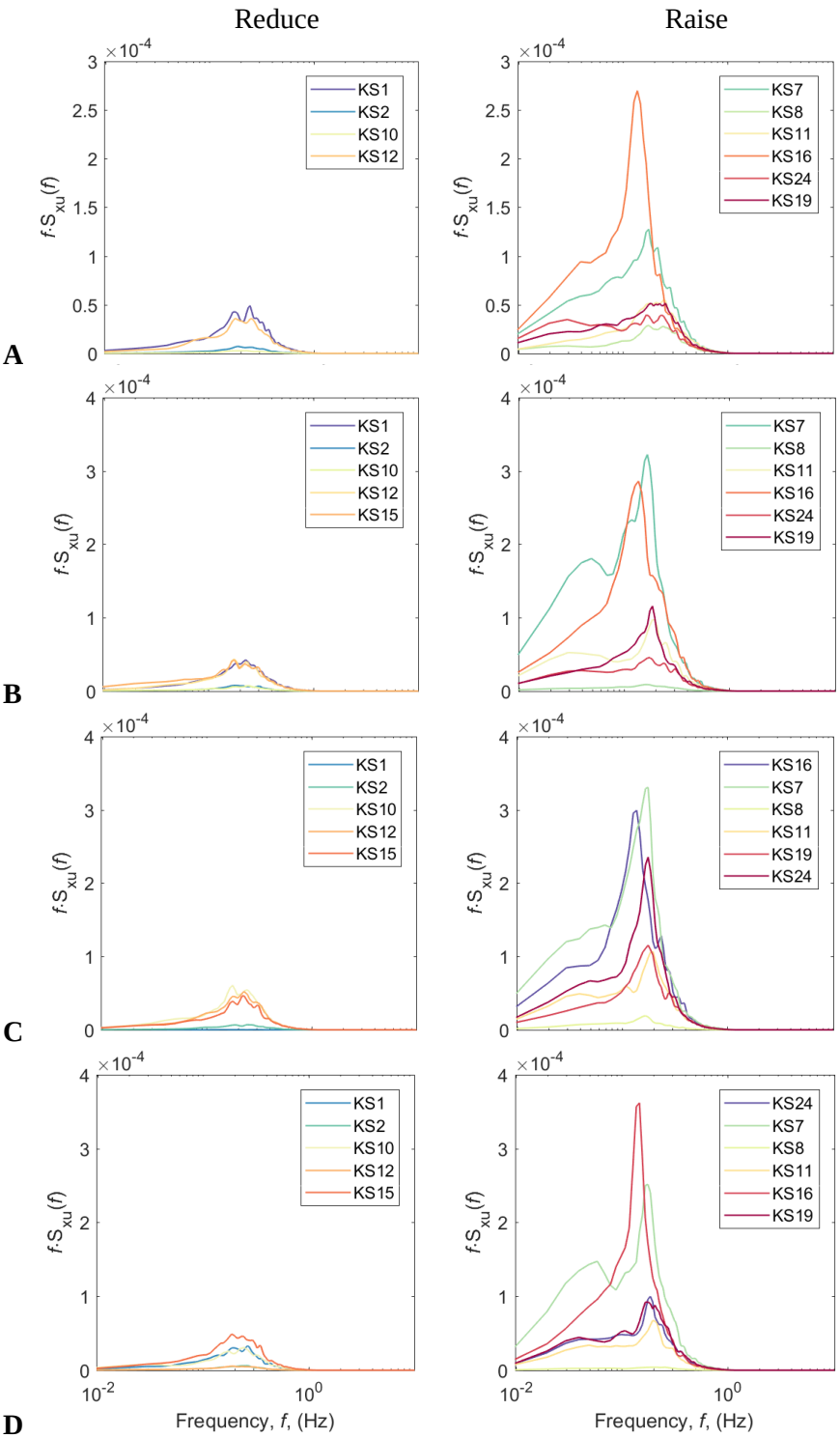

Figure 52: Fourier energy spectra $f \cdot S_{xu}(f)$ for Senegal mahoganies reduced (left column) and raised (right column) by 40% computed using 30-minute time histories of streamwise trunk displacement, x_U, recorded 1607 – 1637H 28 January 2014 (**A**), 1300 – 1330H 22 February 2014 (**B**), 1415 – 1445H 22 February 2014 (**C**), and 1525 – 1555H 22 February 2014 (**D**). During these 30-minute intervals, the resultant wind speeds ($m \cdot s^{-1}$) and directions (°) at 18.3 m (z/H_{TREE} = 0.69) were 1.6 $m \cdot s^{-1}$, 188°; 2.3 $m \cdot s^{-1}$, 189°; 2.2 $m \cdot s^{-1}$, 188°; and 2.0 $m \cdot s^{-1}$, 186°. In the legend, trees are identified by the abbreviation KS (*Khaya senegalensis*) and tree number.

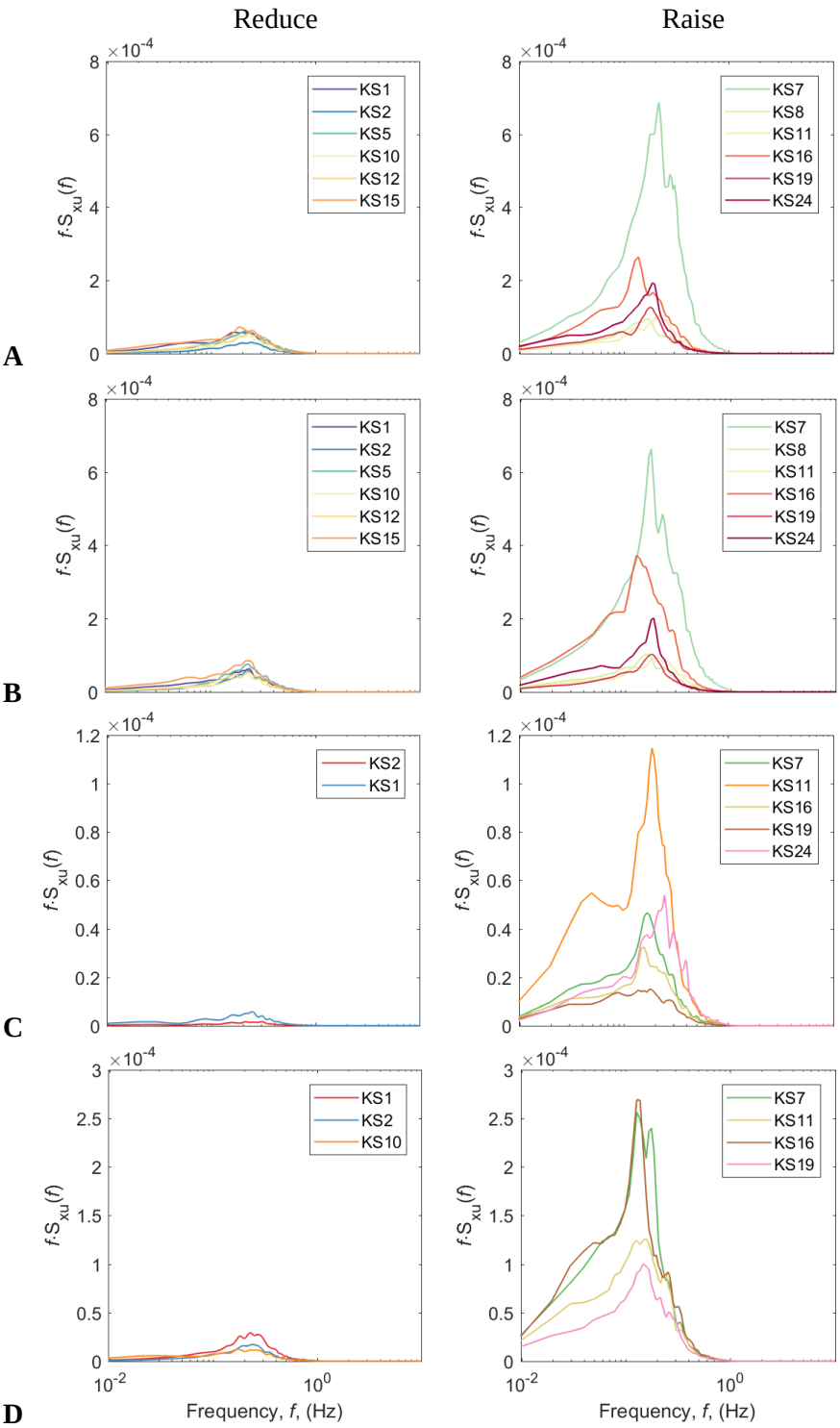

Figure 53: Fourier energy spectra $f \cdot S_{xu}(f)$ for Senegal mahoganies reduced (left column) and raised (right column) by 80% computed using 30-minute time histories of streamwise trunk displacement, x_U, recorded 1015 – 1045H 20 April 2014 (**A**), 1415 – 1445H 26 April 2014 (**B**), 0430 – 0500H 1 May 2014 (**C**), and 1245 – 1315H 6 May 2014 (**D**). During these 30-minute intervals, the resultant wind speeds ($m \cdot s^{-1}$) and directions (°) at 18.3 m (z/H_{TREE} = 0.69) were 1.7 $m \cdot s^{-1}$, 190°; 1.8, 187°; 1.0 $m \cdot s^{-1}$, 75°; and 1.0 $m \cdot s^{-1}$, 330°. In the legend, trees are identified by the abbreviation KS (*Khaya senegalensis*) and tree number.

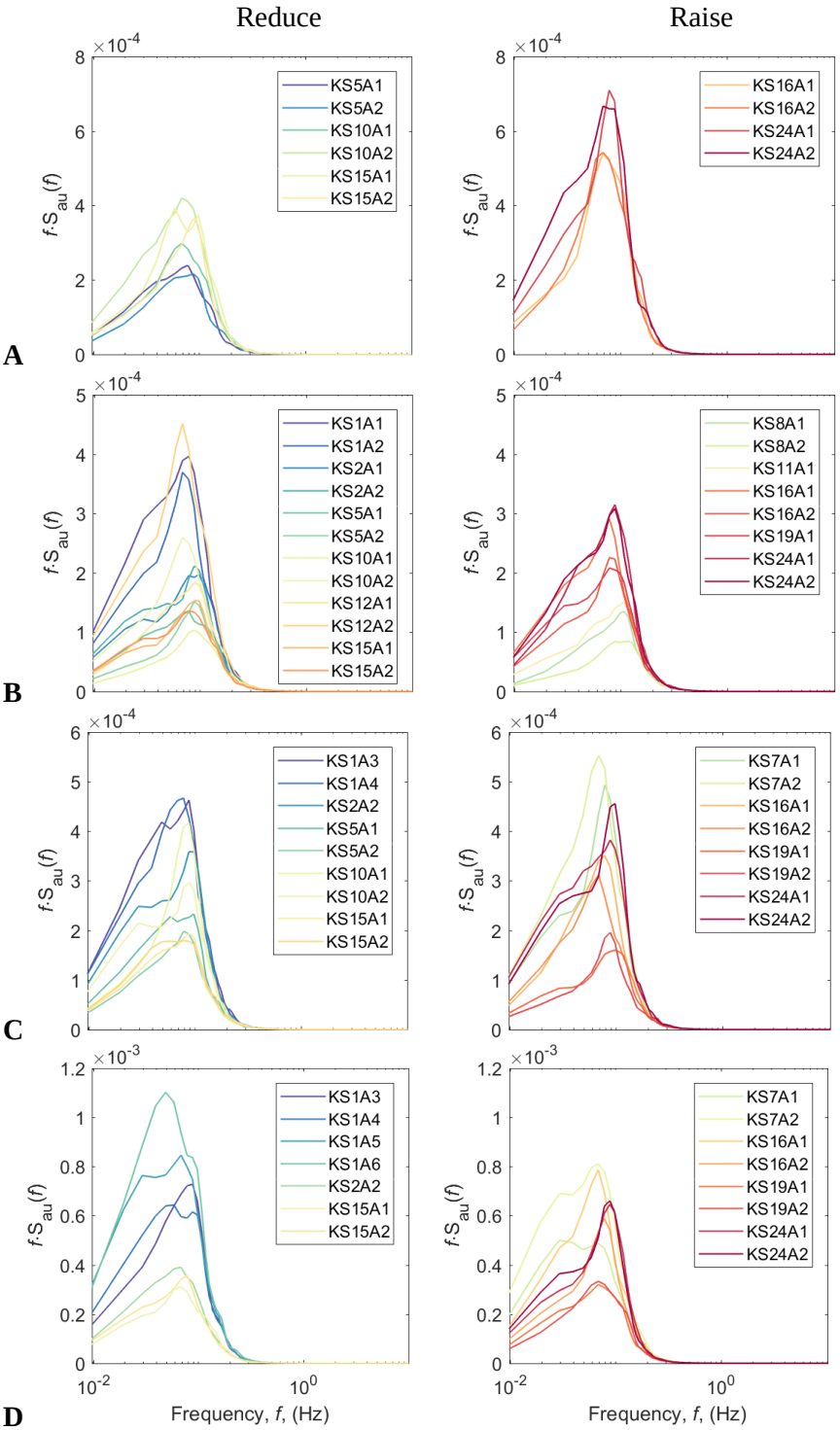

Figure 54: Fourier energy spectra $f \cdot S_{au}(f)$ for Senegal mahoganies reduced (left column) and raised (right column) by 0% computed using 30-minute time histories of streamwise branch acceleration, a_U, recorded 2319 – 2349H 6 September 2013 (**A**), 1215 – 1245H 7 September 2013 (**B**), 1330 – 1400H 14 September 2013 (**C**), and 1219 – 1249H 15 September 2013 (**D**). During these 30-minute intervals, the resultant wind speeds ($m \cdot s^{-1}$) and directions (°) at 18.3 m (z/H_{TREE} = 0.69) were 1.0 $m \cdot s^{-1}$, 94°; 1.1 $m \cdot s^{-1}$, 80°; 0.8 $m \cdot s^{-1}$, 323°; and 1.0 $m \cdot s^{-1}$, 58°. In the legend, trees are identified by the abbreviation KS (*Khaya senegalensis*), tree number, and accelerometer code.

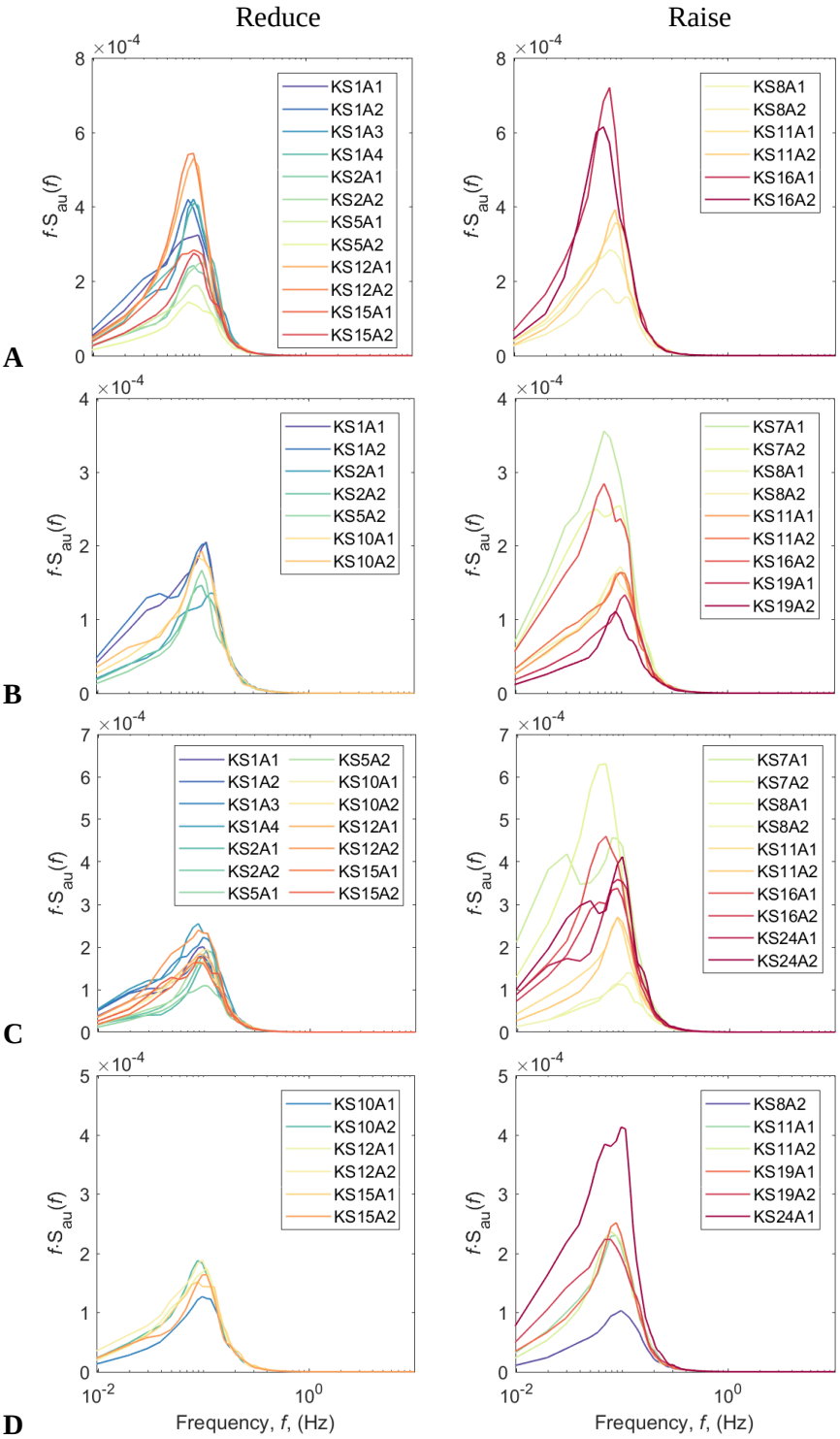

Figure 55: Fourier energy spectra $f \cdot S_{au}(f)$ for Senegal mahoganies reduced (left column) and raised (right column) by 10% computed using 30-minute time histories of streamwise branch acceleration, a_U, recorded 0501 – 0531H 5 October 2013 (**A**), 1315 – 1345H 11 October 2013 (**B**), 1530 – 1600H 16 October 2013 (**C**), and 1330 – 1400H 20 October 2013 (**D**). During these 30-minute intervals, the resultant wind speeds ($m \cdot s^{-1}$) and directions (°) at 18.3 m (z/H_{TREE} = 0.69) were 1.5 $m \cdot s^{-1}$, 139°; 0.5 $m \cdot s^{-1}$, 317°; 0.4 $m \cdot s^{-1}$, 18°; and 1.2 $m \cdot s^{-1}$, 83°. In the legend, trees are identified by the abbreviation KS (*Khaya senegalensis*), tree number, and accelerometer code.

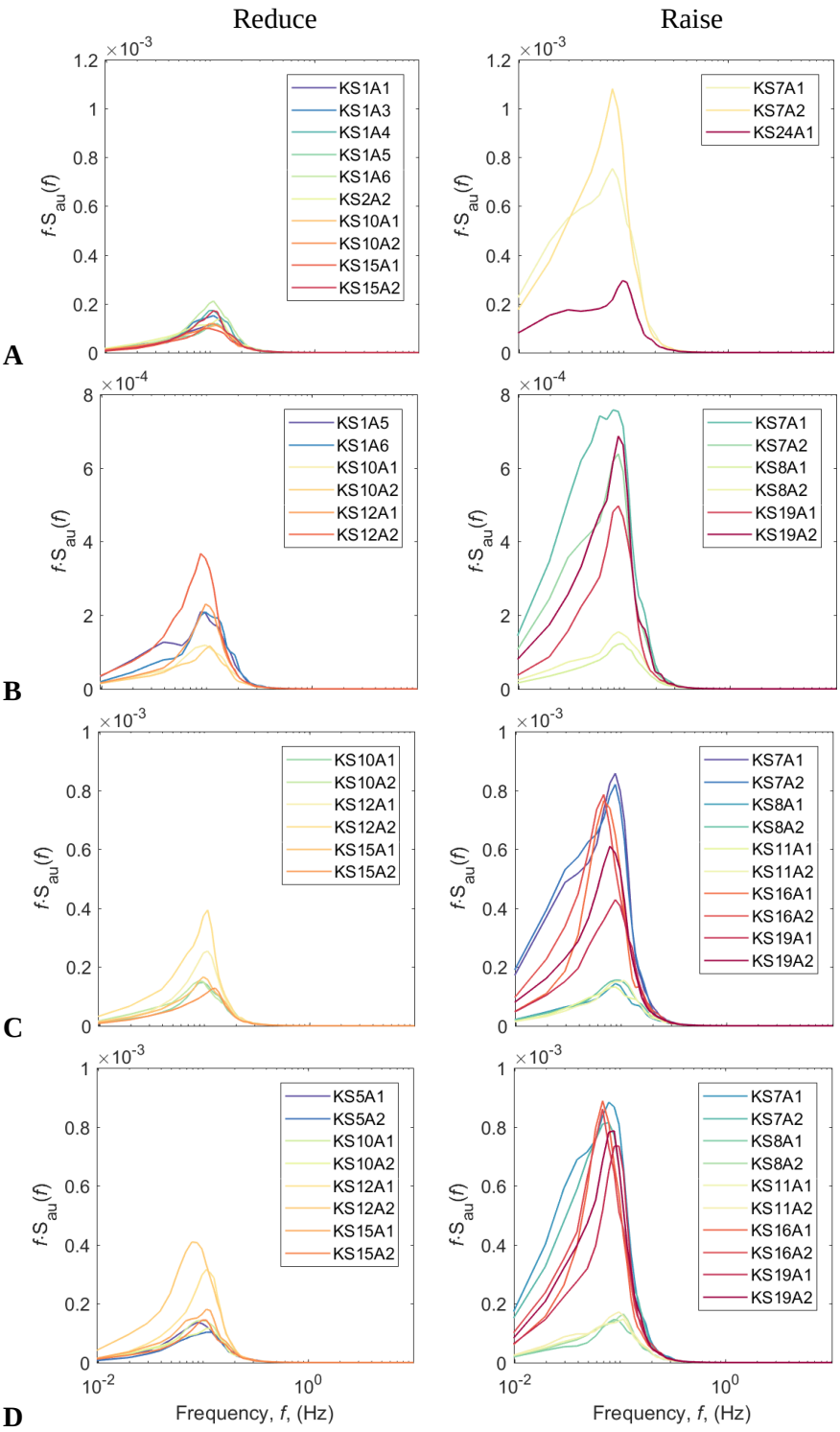

Figure 56: Fourier energy spectra $f{\cdot}S_{au}(f)$ for Senegal mahoganies reduced (left column) and raised (right column) by 20% computed using 30-minute time histories of streamwise branch acceleration, a_U, recorded 1519 – 1549H 23 December 2013 (**A**), 0930 – 1000H 7 January 2014 (**B**), 1420 – 1450H 10 January 2014 (**C**), and 1600 – 1630H 10 January 2014 (**D**). During these 30-minute intervals, the resultant wind speeds ($m{\cdot}s^{-1}$) and directions (°) at 18.3 m (z/H_{TREE} = 0.69) were 1.7 $m{\cdot}s^{-1}$, 190°; 2.0 $m{\cdot}s^{-1}$, 187°; 1.8 $m{\cdot}s^{-1}$, 189°; and 2.1 $m{\cdot}s^{-1}$, 191°. In the legend, trees are identified by the abbreviation KS (*Khaya senegalensis*), tree number, and accelerometer code.

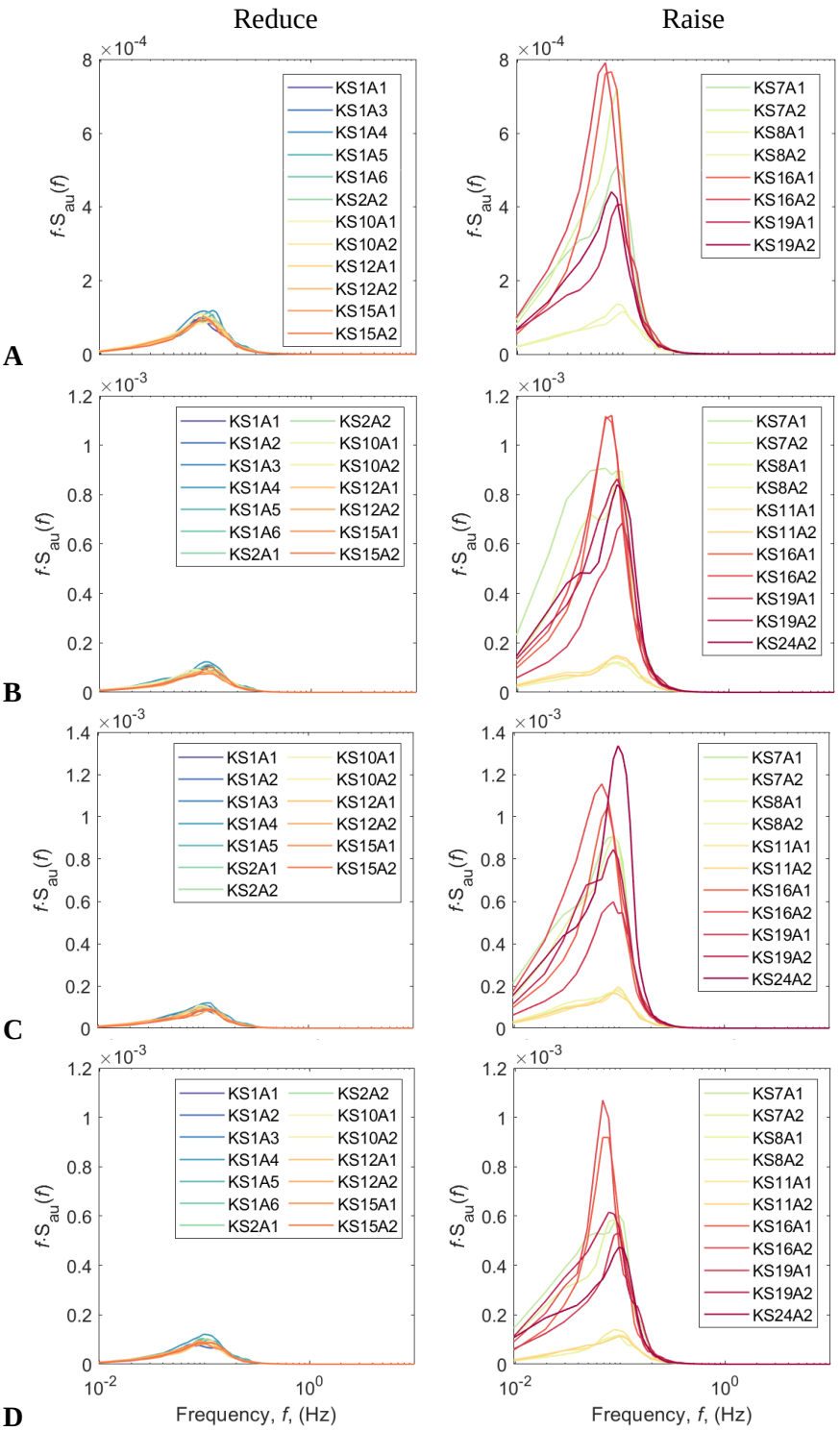

Figure 57: Fourier energy spectra $f \cdot S_{au}(f)$ for Senegal mahoganies reduced (left column) and raised (right column) by 40% computed using 30-minute time histories of streamwise branch acceleration, a_U, recorded 1607 – 1637H 28 January 2014 (**A**), 1300 – 1330H 22 February 2014 (**B**), 1415 – 1445H 22 February 2014 (**C**), and 1525 – 1555H 22 February 2014 (**D**). During these 30-minute intervals, the resultant wind speeds ($m \cdot s^{-1}$) and directions (°) at 18.3 m ($z/H_{TREE} = 0.69$) were 1.6 $m \cdot s^{-1}$, 188°; 2.3 $m \cdot s^{-1}$, 189°; 2.2 $m \cdot s^{-1}$, 188°; and 2.0 $m \cdot s^{-1}$, 186°. In the legend, trees are identified by the abbreviation KS (*Khaya senegalensis*), tree number, and accelerometer code.

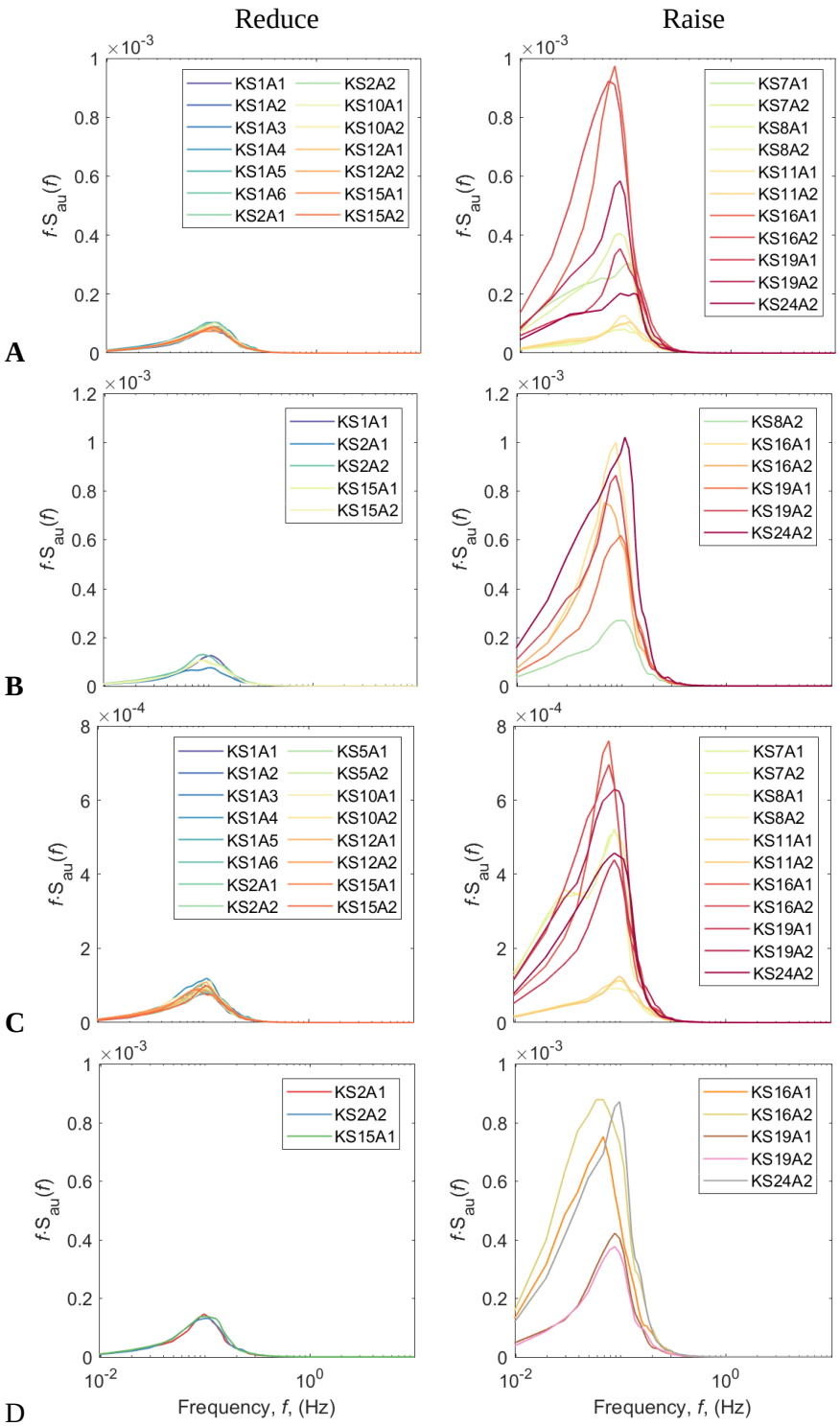

Figure 58: Fourier energy spectra $f \cdot S_{au}(f)$ for Senegal mahoganies reduced (left column) and raised (right column) by 80% computed using 30-minute time histories of streamwise branch acceleration, a_U, recorded 1015 – 1045H 20 April 2014 (**A**), 1415 – 1445H 26 April 2014 (**B**), 0430 – 0500H 1 May 2014 (**C**), and 1245 – 1315H 6 May 2014 (**D**). During these 30-minute intervals, the resultant wind speeds (m·s^{-1}) and directions (°) at 18.3 m (z/H_{TREE} = 0.69) were 1.7 m·s^{-1}, 190°; 1.8, 187°; 1.0 m·s^{-1}, 75°; and 1.0 m·s^{-1}, 330°. In the legend, trees are identified by the abbreviation KS (*Khaya senegalensis*), tree number, and accelerometer code.

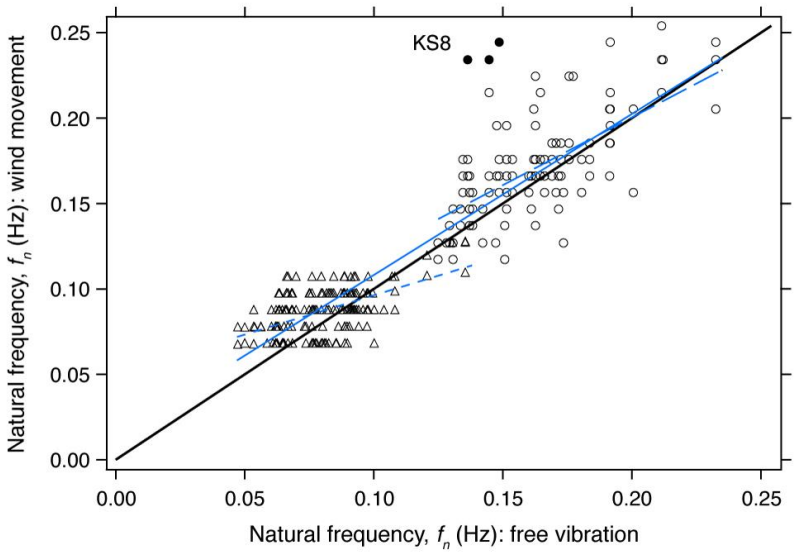

Figure 59: Scatter plot and best-fit lines of the natural frequency, f_n (Hz), measured during wind-induced movement against the same measured in free vibration for Senegal mahogany (*Khaya senegalensis*) branches (triangle) and trunks (circle). For raised trees, the comparisons were made using f_n estimated at all pruning severities, but the same comparisons were only possible at 0% and 10% severity for reduced trees, since the Fourier spectra for trees reduced by greater than 10% did not show a dominant frequency. Most values are located near the solid black 1:1 comparison line, indicating reasonable agreement between these two measurements. In contrast, several observations from Senegal mahogany tree number 8 (solid circles, labeled KS8) were underpredicted, on average, by 36% because different modal frequencies were excited by pull testing and wind loading. Least squares regression equation for branches (short dash blue line), trunks (long dash blue line), and combined set (solid blue line), respectively, is $y = 0.46\ x + 5.0\times10^{-2}$ ($r^2 = 0.34$), $y = 0.79\ x + 4.2\times10^{-2}$ ($r^2 = 0.40$), and $y = 0.94\ x + 1.4\times10^{-2}$ ($r^2 = 0.84$).

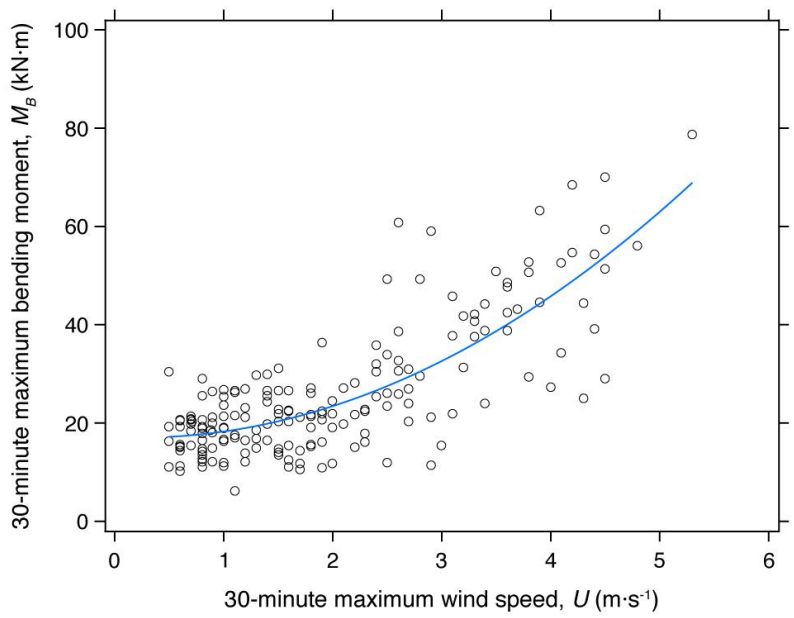

Figure 60: Scatter plot and best-fit line of the 30-minute maximum bending moment, M_B (kN·m), on unpruned Senegal mahogany (*Khaya senegalensis*) tree number 2 against 30-minute maximum wind speed, U (m·s^{-1}), measured 18.3 m above ground (z/H = 0.69) for 180 non-consecutive 30-minute intervals. Least squares regression equation is $y = 2.00\,x^2 - 0.85\,x + 17.1$ (R^2 = 0.63).

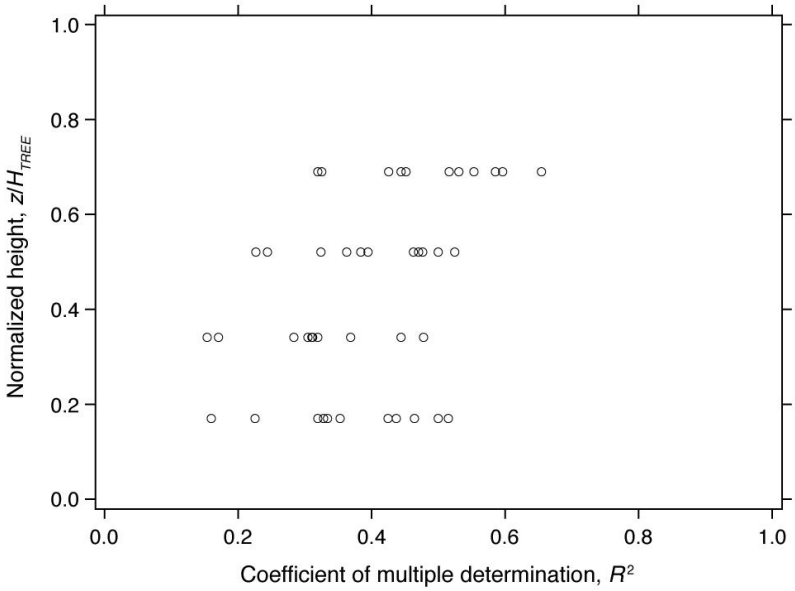

Figure 61: For all unpruned Senegal mahoganies (*Khaya senegalensis*), scatterplot of the coefficient of multiple determination (R^2) describing the proportion of variance in 30-minute maximum bending moment, M_B (kN·m), explained by 30-minute maximum wind speed, U (m·s^{-1}), using a quadratic function for wind speeds measured on four different anemometers installed 4.6, 9.1, 13.7, and 18.3 m above ground. The installation height of anemometers, z (m), was normalized by the average height of all Senegal mahoganies, H_{TREE} = 26.9 m.

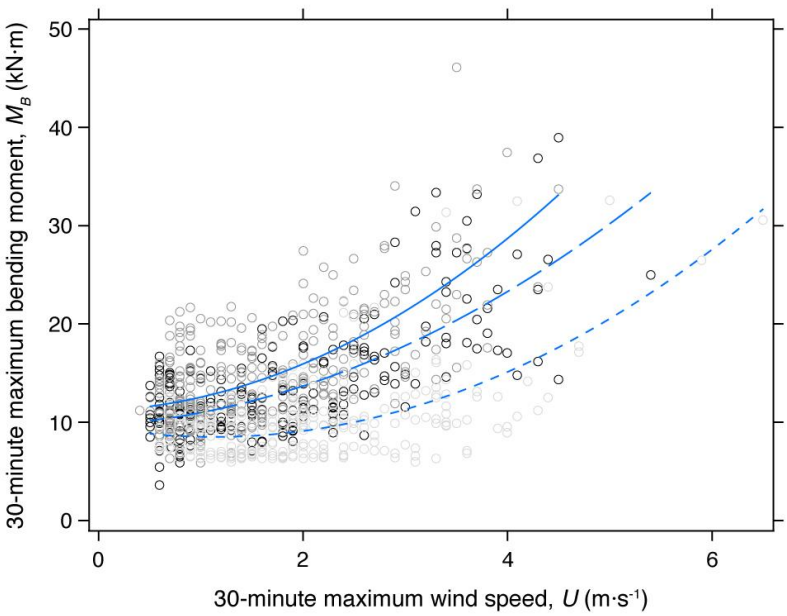

Figure 62: Scatter plot and best-fit lines of the 30-minute maximum bending moment, M_B (kN·m), against 30-minute maximum wind speed, U (m·s^{-1}), measured 18.3 m above ground (z/H_{TREE} = 0.69) for Senegal mahogany (*Khaya senegalensis*) tree number 16 raised by 0% (black empty circle marker, solid line), 10% (dark gray empty circle marker, long dash line), and 20% (light gray empty circle marker, short dash line). At 0%, 10%, and 20% severity, least squares regression equations are $y = 0.70\ x^2 + 0.61\ x + 9.67$ (n = 230; R^2 = 0.52), $y = 1.00\ x^2 + 0.38\ x + 11.2$ (n = 312; R^2 = 0.48), and $y = 0.81\ x^2 – 1.83\ x + 9.55$ (n = 278; R^2 = 0.38), respectively.

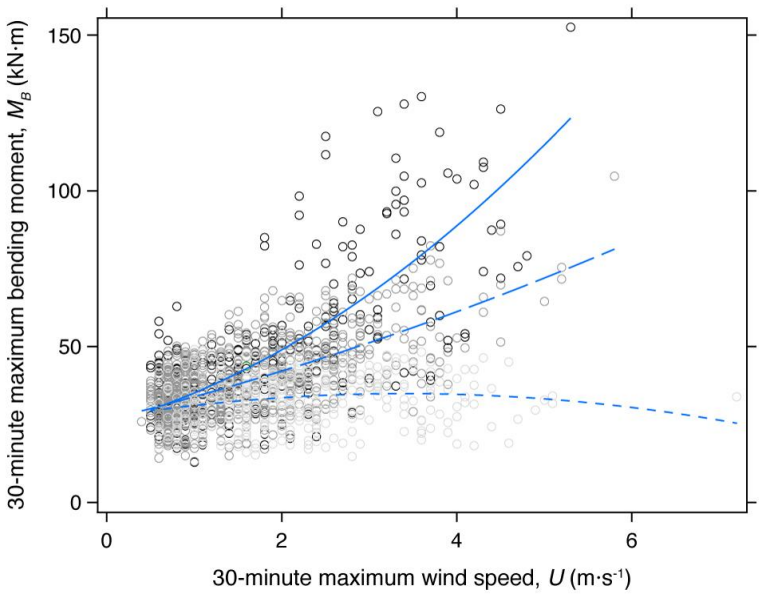

Figure 63: Scatter plot and best-fit lines of the 30-minute maximum bending moment, M_B (kN·m), against 30-minute maximum wind speed, U (m·s^{-1}), measured 18.3 m above ground (z/H_{TREE} = 0.69) for Senegal mahogany (*Khaya senegalensis*) tree number 1 reduced by 0% (black empty circle marker, solid line), 10% (dark gray empty circle marker, long dash line), and 20% (light gray empty circle marker, short dash line). At 0%, 10%, and 20% severity, least squares regression equations are $y = 2.02\ x^2 + 7.80\ x + 25.3$ (n = 288; R^2 = 0.56), $y = 0.43\ x^2 + 6.96\ x + 26.5$ (n = 825; R^2 = 0.41), and $y = -0.66\ x^2 + 4.49\ x + 27.3$ (n = 370; R^2 = 0.03), respectively.

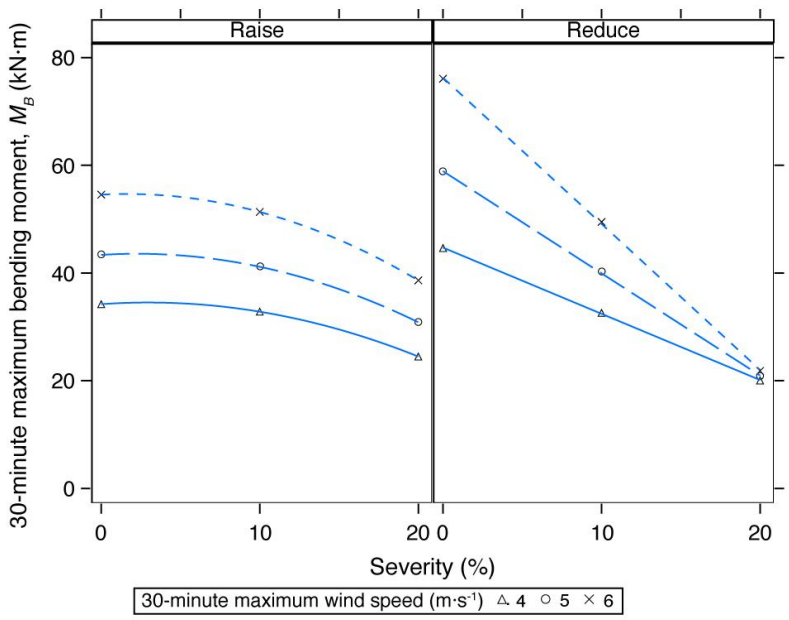

Figure 64: Regression of mean Senegal mahogany (*Khaya senegalensis*) 30-minute maximum bending moment, M_B (kN·m), against pruning severity for raised (left panel) and reduced (right panel) trees at three different values of the covariate 30-minute maximum wind speed, U (m·s^{-1}). During the experiment, wind-induced M_B was measured repeatedly on the lower trunk of six raised and five reduced Senegal mahoganies. For raised trees, least squares regression equations are $y = (-3.46\times10^{-2})\,x^2 + (2.06\times10^{-1})\,x + 34.2$ ($R^2 = 1$), $y = (-4.04\times10^{-2})\,x^2 + (1.83\times10^{-1})\,x + 43.4$ ($R^2 = 1$), and $y = (-4.75\times10^{-2})\,x^2 + (1.54\times10^{-1})\,x + 54.6$ ($R^2 = 1$) at 4, 5, and 6 m·s^{-1}, respectively. For reduced trees, least squares regression equations are $y = -1.23\,x + 44.7$ ($R^2 = 0.99$), $y = -1.90\,x + 58.9$ ($r^2 = 0.99$), and $y = -2.71\,x + 76.3$ ($r^2 = 0.99$) at 4, 5, and 6 m·s^{-1}, respectively.

Table 2: Average tree (**A**) and branch (**B**) attributes of unpruned Senegal mahogany (*Khaya senegalensis*) and rain tree (*Samanea saman*)

	Senegal mahogany	**rain tree**
A) tree attributes		
Trees, n	11	9
Diameter, DBH (m)	0.72 [0.04; 0.67–0.84]	0.92 [0.07; 0.81–1.03]
Height, H_{TREE} (m)	28.9 [1.8; 23.0–31.7]	22.2 [1.0; 20.9–23.7]
Slenderness, λ_{TREE}	37.9 [3.8; 30.3–41.1]	24.3 [1.1; 23.0–26.8]
Tree mass, m_{TREE} (kg)	11523 [1073; 8030–15673]	14135 [1787; 10304–15612]
Leaf mass, m_{LEAF} (kg)	442 [82; 303–643]	144 [28; 93–191]
Crown width, W_{CROWN} (m)	16.7 [4.0; 11.7–24.3]	24.5 [4.1; 18.6–30.0]
Crown length, L_{CROWN} (m)	21.1 [2.4; 16.9–24.1]	19.4 [1.1; 17.9–21.2]
B) branch attributes		
Primary branches, n	10 [2; 7–14]	8 [2; 7–12]
Diameter, D_{BRANCH} (m)	0.21 [0.11; 0.05–0.47]	0.27 [0.17; 0.07–0.73]
Length, L_{BRANCH} (m)	11.3 [5.0; 0.6–23.6]	12.8 [6.7; 2.7–26.5]
Slenderness, λ_{BRANCH}	55.9 [13.8; 10.2–96.6]	49.3 [9.7; 31.2–73.5]
Branch mass, m_{BRANCH} (kg)	489 [596; 5–3152]	947 [1272; 17–5488]
Leaf mass, m_{LEAF} (kg)	36 [39; 1–210]	16 [15; 1–69]
Inclination, θ (°)	54 [17; -10–90]	49 [16; 8–85]
Rotation, γ (°)	174 [103; 0–356]	187 [105; 2–359]
Bifurcation angle, φ (°)	48 [15; 18–95]	53 [24; 12–129]
Aspect ratio, $\Re_B$	0.63 [0.25; 0.21–2.00]	0.83 [0.15; 0.45–1.00]

Note: Values listed are mean [SD; min–max].

Table 3: For Senegal mahogany (*Khaya senegalensis*) (**A**) and rain tree (*Samanea saman*) (**B**), sample sizes, parameter estimates, confidence intervals, and coefficients of determination for regression models fit to branch attributes

Relation	$L_{BRANCH} \propto D_{BRANCH}$	$m_{LEAF} \propto D_{BRANCH}$	$m_{BRANCH} \propto D_{BRANCH}$
Form	$y = \beta + \alpha x$	$y = \beta x^{\alpha}$	$y = \beta x^{\alpha}$
A) Senegal mahogany			
α	52.3	1.7	2.50
(95% CI)	(± 2.27)	(1.6 – 1.8)	(2.46 – 2.61)
β	0.8	290	17800
(95% CI)	(± 0.22)	(230 – 380)	(14700 – 21600)
n	458	457	458
r^2	0.82	0.72	0.91
B) rain tree			
α	59.9	1.9	2.7
(95% CI)	(± 3.21)	(1.8 – 2.1)	(2.62– 2.77)
β	-1.0	220	19200
(95% CI)	(± 0.45)	(160 – 310)	(16400 – 22500)
n	313	311	313
r^2	0.81	0.70	0.95

Note: Branch attributes included basal diameter, D_{BRANCH} (m); length, L_{BRANCH} (m); leaf mass, m_{LEAF} (kg); and branch mass, m_{BRANCH} (kg). m_{LEAF} and m_{BRANCH} were determined using fresh leaves and branches, respectively.

Table 4: For Senegal mahogany (*Khaya senegalensis*) (**A**) and rain tree (*Samanea saman*) (**B**), average tree height, H_{TREE} (m); crown length, L_{CROWN} (m); tree slenderness, λ_{TREE}; total fresh mass, m_{TREE} (kg); and fresh leaf mass, m_{LEAF} (kg) of raised and reduced trees at each pruning severity

	H_{TREE}		L_{CROWN}		λ_{TREE}		m_{TREE}		m_{LEAF}	
Severity	Raise	Reduce	Raise	Reduce	Raise	Reduce	Raise	Reduce	Raise	Reduce
A) Senegal mahogany										
0%	25.8 (2.2)	28.9 (1.8)	21.5 (2.8)	22.3 (1.8)	36.0 (4.4)	40.1 (1.1)	10583 (2982)	11420 (992)	391 (135)	454 (79)
10%	25.8 (2.2)	24.5 (1.1)	18.8 (2.9)	17.8 (1.7)	36.0 (4.4)	34.0 (0.9)	10013 (2764)	10735 (939)	343 (116)	308 (90)
20%	25.8 (2.2)	22.2 (1.2)	18.4 (2.9)	15.5 (1.6)	36.0 (4.4)	30.8 (0.6)	9749 (2614)	9802 (891)	328 (108)	186 (89)
40%	25.8 (2.2)	16.9 (1.6)	17.5 (4.4)	10.3 (1.1)	36.0 (4.4)	23.4 (1.4)	9105 (2578)	7344 (1041)	277 (105)	58 (48)
80%	25.8 (2.2)	11.0 (1.7)	17.3 (4.7)	4.4 (0.8)	36.0 (4.4)	15.3 (2.1)	8021 (2148)	4525 (752)	178 (98)	23 (21)
B) rain tree										
0%	23.0 (0.8)	21.6 (0.6)	20.1 (1.2)	18.9 (0.8)	23.7 (0.6)	24.8 (1.2)	16083 (1850)	12960 (1852)	200 (14)	139 (23)
20%	23.0 (0.8)	18.4 (0.8)	20.1 (1.2)	15.6 (0.7)	23.7 (0.6)	21.1 (2.1)	14716 (1434)	11326 (1711)	195 (50)	36 (31)
40%	23.0 (0.8)	14.4 (0.7)	20.1 (1.2)	11.6 (0.5)	23.7 (0.6)	16.5 (1.6)	13432 (1497)	9207 (1172)	154 (42)	4 (10)
80%	23.0 (0.8)	6.7 (0.8)	20.1 (1.2)	4.0 (0.7)	23.7 (0.6)	7.7 (1.2)	12116 (1487)	4686 (735)	80 (28)	0 (0)

Note: Values listed are mean (SD). Fresh mass of wood, m_{WOOD} (kg), is the difference between m_{TREE} and m_{LEAF}. Measurements were made on six raised and five reduced Senegal mahoganies (n = 11) and four raised and five reduced rain trees (n = 9).

Table 5: Information criteria on covariance structures for the Senegal mahogany (*Khaya senegalensis*) (**A**) and rain tree (*Samanea saman*) (**B**) analyses of variance considering the effect of pruning treatments on percent decrease in total mass, m_{TREE}, and percent decrease in leaf mass, m_{LEAF}

		Covariance Structures				
Dataset	**Fit Statistics**	ANTE(1)	AR(1)	ARMA(1,1)	CS	HF
A) Senegal mahogany						
percent decrease in m_{TREE}	AICC	212.6	207.9	209.9	–	217.6
	BIC	211.4	208.4	210.4	–	217.6
percent decrease in m_{LEAF}	AICC	284.6	275.5	277.8	281.7	287.2
	BIC	285.4	275.9	278.3	282.1	287.1
B) rain tree						
percent decrease in m_{TREE}	AICC	–	132.6	134.2	131.5	134.3
	BIC	–	132.3	133.4	131.2	132.6
percent decrease in m_{LEAF}	AICC	158.1	#155.8	–	#158.4	155.0
	BIC	155.1	#154.1	–	#156.7	153.3

Note: Fit statistics include AICC, corrected Akaike information criteria, and BIC, Schwarz's Bayesian information criteria. Covariance structures include ANTE(1), first-order ante dependent; AR(1), first-order autoregressive; ARMA(1,1), first-order autoregressive moving average; CS, compound symmetry; and HF, Huynh-Feldt. # denotes values for a heterogeneous version of the same covariance structure fit to the data. Null values in empty cells (–) indicate model failure to converge.

Table 6: Analysis of variance of the percent decrease in total mass, m_{TREE}, (%) for Senegal mahogany (*Khaya senegalensis*)

Effect	**df**	***F***	***p***	**Level**	**Mean (SE)**
Type	1, 9.78	74.78	< 0.001	Raise	12.7 (1.3)a
				Reduce	28.8 (1.4)b
Severity	3, 26.2	199.1	< 0.001		
Type × Severity	3, 26.2	47.84	< 0.001		
Severity:Type$_1$(Raise)	3, 26.2	28.88	< 0.001		
Orthogonal polynomial comparisons					
Linear	1, 19.6	117.9	< 0.001		
Quadratic	1, 14.7	0.35	0.560		
Cubic	1, 12.4	0.54	0.477	10%	5.3 (1.7)
				20%	7.7 (1.7)
				40%	14.0 (1.7)
				80%	23.9 (1.7)
Severity:Type$_2$(Reduce)	3, 26.2	202.3	< 0.001		
Orthogonal polynomial comparisons					
Linear	1, 15.8	416.1	< 0.001		
Quadratic	1, 11.8	9.31	0.010		
Cubic	1, 8.1	2.12	0.183	10%	5.4 (1.8)
				20%	14.0 (1.8)
				40%	35.4 (1.8)
				80%	60.5 (1.8)

Note: Fixed effects include pruning type: raise, reduce; severity: 10, 20, 40, 80%; and their interaction: type × severity. Percent decrease in m_{TREE} was measured repeatedly on six raised and five reduced Senegal mahoganies. Means followed by the same letter are not significantly different at the $\alpha = 0.05$ level. Orthogonal polynomial comparisons test the significance of an nth-order polynomial multiple regression of percent decrease in m_{TREE} against pruning severity; the corresponding regression coefficients were determined separately using least squares regression (Figure 11).

Table 7: Analysis of variance of the percent decrease in total mass, m_{TREE}, (%) for rain tree (*Samanea saman*)

Effect	**df**	***F***	***p***	**Level**	**Mean (SE)**
Type	1, 7	37.45	< 0.001	Raise	14.1 (2.5)a
				Reduce	35.0 (2.3)b
Severity	2, 14	363.5	< 0.001		
Type × Severity	2, 14	108.8	< 0.001		
Severity:$Type_1$(Raise)	2, 14	35.24	< 0.001		
Orthogonal polynomial comparisons					
Linear	1, 6	139.1	< 0.001		
Quadratic	1, 6	3.94	0.095	20%	6.2 (2.8)
				40%	13.9 (2.8)
				80%	22.2 (2.8)
Severity:$Type_2$(Reduce)	2, 14	487.3	< 0.001		
Orthogonal polynomial comparisons					
Linear	1, 8	704.7	< 0.001		
Quadratic	1, 8	1.30	0.287	20%	12.7 (2.5)
				40%	28.0 (2.5)
				80%	64.5 (2.5)

Note: Fixed effects include pruning type: raise, reduce; severity: 20, 40, 80%; and their interaction: type × severity. Percent decrease in m_{TREE} was measured repeatedly on four raised and five reduced rain trees. Means followed by the same letter are not significantly different at the α = 0.05 level. Orthogonal polynomial comparisons test the significance of an *n*th-order polynomial multiple regression of percent decrease in m_{TREE} against pruning severity; the corresponding regression coefficients were determined separately using least squares regression (Figure 11).

Table 8: Analysis of variance of the percent decrease in leaf mass, m_{LEAF}, (%) for Senegal mahogany (*Khaya senegalensis*)

Effect	**df**	***F***	***p***	**Level**	**Mean (SE)**
Type	1, 9.96	46.2	< 0.001	Raise	28 (4.1)a
				Reduce	69 (4.4)b
Severity	3, 26.9	61.7	< 0.001		
Type × Severity	3, 26.9	14.0	< 0.001		
Severity:$Type_1$(Raise)	3, 26.9	26.0	< 0.001		
Orthogonal polynomial comparisons					
Linear	1, 18.9	76.0	< 0.001		
Quadratic	1, 14.5	0.01	0.943		
Cubic	1, 12.8	0.76	0.400	10%	12 (4.8)
				20%	16 (4.8)
				40%	30 (4.8)
				80%	55 (4.8)
Severity:$Type_2$(Reduce)	3, 26.9	47.7	< 0.001		
Orthogonal polynomial comparisons					
Linear	1, 15.9	84.5	< 0.001		
Quadratic	1, 12	55.7	< 0.001		
Cubic	1, 9.86	2.57	0.140	10%	30 (5.3)
				20%	61 (5.3)
				40%	89 (5.3)
				80%	96 (5.3)

Note: Fixed effects include pruning type: raise, reduce; severity: 10, 20, 40, 80%; and their interaction: type × severity. Percent decrease in m_{LEAF} was measured repeatedly on six raised and five reduced Senegal mahoganies. Means followed by the same letter are not significantly different at the $\alpha = 0.05$ level. Orthogonal polynomial comparisons test the significance of an *n*th-order polynomial multiple regression of percent decrease in m_{LEAF} against pruning severity; the corresponding regression coefficients were determined separately using least squares regression (Figure 11).

Table 9: Analysis of variance of the percent decrease in leaf mass, m_{LEAF}, (%) for rain tree (*Samanea saman*)

Effect	**df**	***F***	***p***	**Level**	**Mean (SE)**
Type	1, 12.9	54.7	< 0.001	Raise	45 (4.7)a
				Reduce	92 (4.2)b
Severity	2, 14	51.7	< 0.001		
Type × Severity	2, 14	16.5	< 0.001		
Severity:$Type_1$(Raise)	2, 14	54.6	< 0.001		
Orthogonal polynomial comparisons					
Linear	1, 9	46.4	< 0.001		
Quadratic	1, 9	0.03	0.867	20%	15 (7.0)
				40%	39 (7.6)
				80%	82 (1.4)
Severity:$Type_2$(Reduce)	2, 14	8.44	0.004		
Orthogonal polynomial comparisons					
Linear	1, 12	10.9	0.006		
Quadratic	1, 12	5.69	0.034	20%	79 (6.2)
				40%	98 (6.8)
				80%	100 (1.2)

Note: Fixed effects include pruning type: raise, reduce; severity: 20, 40, 80%; and their interaction: type × severity. Percent decrease in m_{LEAF} was measured repeatedly on four raised and five reduced rain trees. Means followed by the same letter are not significantly different at the α = 0.05 level. Orthogonal polynomial comparisons test the significance of an *n*th-order polynomial multiple regression of percent decrease in m_{LEAF} against pruning severity; the corresponding regression coefficients were determined separately using least squares regression (Figure 11).

Table 10: Information criteria on covariance structures for the Senegal mahogany (*Khaya senegalensis*) (**A**) and rain tree (*Samanea saman*) (**B**) analyses of variance considering the effect of pruning treatments on natural frequency, f_n (Hz)

		Covariance Structures				
Dataset	**Fit Statistics**	ANTE(1)	ARH(1)	CSH	UN(1)	VC
A) Senegal mahogany						
trunk f_n	AICC	-112.9	-117.7	–	-112.1	-11.6
	BIC	-114.5	-117.5	–	-111.7	-11.3
branch f_n	AICC	-469.6	-472.5	-474.3	-474.5	-406.1
	BIC	-460.0	-465.8	-467.5	-468.8	-404.9
B) rain tree						
trunk f_n	AICC	-22.0	-26.6	-25.6	-27.8	32.4
	BIC	-32.8	-32.9	-32.0	-32.5	31.1
branch f_n	AICC	–	–	–	-50.7	-19.7
	BIC	–	–	–	-55.2	-20.2

Note: Fit statistics include AICC, corrected Akaike information criteria, and BIC, Schwarz's Bayesian information criteria. Covariance structures include ANTE(1), first-order ante dependent; ARH(1), heterogeneous first-order autoregressive; CSH, heterogeneous compound symmetry; UN(1), first-order banded diagonal; and VC, variance components. Null values in empty cells (–) indicate model failure to converge.

Table 11: Analysis of variance of natural frequency, f_n (Hz), measured on the trunks (**A**) and branches (**B**) of Senegal mahogany (*Khaya senegalensis*)

Effect	df	*F*	*p*	Level	Mean (SE)
A) trunk f_n					
Type	1, 9	84.5	< 0.001	Raise	0.16 (0.04)a
				Reduce	0.65 (0.04)b
Severity	4, 36	91.7	< 0.001		
Type × Severity	4, 36	83.3	< 0.001		
Severity:Type$_1$(Raise)	4, 36	0.20	0.938		
Severity:Type$_2$(Reduce)	4, 36	160	< 0.001		
Orthogonal polynomial comparisons					
Linear	1, 4.07	52.1	0.002		
Quadratic	1, 3.98	14.0	0.020		
Cubic	1, 7.89	0.31	0.591		
Quartic	1, 4.49	0.65	0.460	0%	0.15 (0.01)
				10%	0.20 (0.01)
				20%	0.27 (0.03)
				40%	0.66 (0.02)
				80%	1.99 (0.18)
B) branch f_n					
Type	1, 44.9	1040	< 0.001	Raise	0.08 (0.01)a
				Reduce	0.28 (0.01)b
Severity	4, 47.3	1080	< 0.001		
Type × Severity	4, 47.3	1030	< 0.001		
Severity:Type$_1$(Raise)	4, 48.5	1.59	0.191		
Severity:Type$_2$(Reduce)	4, 46.6	1720	< 0.001		
Orthogonal polynomial comparisons					
Linear	1, 10.2	5230	< 0.001		
Quadratic	1, 15.8	43.1	< 0.001		
Cubic	1, 17.7	3.08	0.097		
Quartic	1, 30.3	1.16	0.290	0%	0.08 (0.01)
				10%	0.09 (0.01)
				20%	0.15 (0.01)
				40%	0.31 (0.02)
				80%	0.75 (0.01)

Note: Fixed effects include pruning type: raise, reduce; severity: 0, 10, 20, 40, 80%; and their interaction: type × severity. Trunk f_n was measured repeatedly on six raised and five reduced Senegal mahoganies; branch f_n was simultaneously measured on 12 and 14 branches distributed among raised and reduced trees, respectively. Means followed by the same letter are not significantly different at the $\alpha = 0.05$ level. For reduced trees, orthogonal polynomial comparisons test the significance of an *n*th-order polynomial multiple regression of f_n against pruning severity; the corresponding regression coefficients were determined separately using least squares regression (Figure 17).

Table 12: Analysis of variance of natural frequency, f_n (Hz), measured on the trunks (**A**) and branches (**B**) of rain tree (*Samanea saman*)

Effect	df	*F*	*p*	Level	Mean (SE)
A) trunk f_n					
Type	1, 8.37	98.9	< 0.001	Raise	0.18 (0.08)a
				Reduce	1.3 (0.08)b
Severity	3, 8.62	37.9	< 0.001		
Type × Severity	3, 8.62	39.7	< 0.001		
Severity:$Type_1$(Raise)	3, 8.62	0.05	0.986		
Severity:$Type_2$(Reduce)	3, 8.62	87.3	< 0.001		
Orthogonal polynomial comparisons					
Linear	1, 4.33	92.6	0.001		
Quadratic	1, 4.16	48.2	0.002		
Cubic	1, 7.17	26.2	0.001	0%	0.19 (0.01)
				20%	0.48 (0.03)
				40%	0.80 (0.05)
				80%	3.8 (0.28)
B) branch f_n					
Severity	3, 11	110	< 0.001		
Orthogonal polynomial comparisons					
Linear	1, 11	69.3	< 0.001		
Quadratic	1, 11	41.8	< 0.001		
Cubic	1, 11	25.7	0.001	0%	0.07 (0.01)
				20%	0.19 (0.02)
				40%	0.32 (0.02)
				80%	2.3 (0.27)

Note: For trunk f_n, fixed effects include pruning type: raise, reduce; severity: 0, 20, 40, 80%; and their interaction: type × severity. For branch f_n, insufficient observations of branch acceleration on raised trees resulted in a single fixed effect: pruning severity for reduced trees. Trunk f_n was measured repeatedly on four raised and five reduced rain trees; branch f_n was simultaneously measured on six branches in one reduced rain tree. Means followed by the same letter are not significantly different at the $\alpha = 0.05$ level. For reduced trees, orthogonal polynomial comparisons test the significance of an nth-order polynomial multiple regression of f_n against pruning severity; the corresponding regression coefficients were determined separately using least squares regression (Figure 19).

Table 13: Information criteria on covariance structures for the Senegal mahogany (*Khaya senegalensis*) (**A**) and rain tree (*Samanea saman*) (**B**) analyses of variance considering the effect of pruning treatments on damping ratio, ζ (dimensionless)

		Covariance Structures				
Dataset	**Fit Statistics**	ANTE(1)	ARH(1)	CSH	UN(1)	VC
A) Senegal mahogany						
trunk ζ	AICC	-111.9	-119.0	-115.8	-113.7	-93.1
	BIC	-113.4	-118.8	-115.6	-113.3	-92.8
branch ζ	AICC	-356.8	-355.4	-355.4	-357.6	-364.5
	BIC	-347.3	-348.7	-348.6	-351.8	-363.3
B) rain tree						
trunk ζ	AICC	-89.5	-92.9	-99.4	-93.9	-98.8
	BIC	-97.8	-99.2	-104.0	-98.5	-100.1
branch ζ	AICC	–	-57.3	-57.3	-61.7	-58.5
	BIC	–	-64.4	-64.3	-66.1	-59.0

Note: Fit statistics include AICC, corrected Akaike information criteria, and BIC, Schwarz's Bayesian information criteria. Covariance structures include ANTE(1), first-order ante dependent; ARH(1), heterogeneous first-order autoregressive; and CSH, heterogeneous compound symmetry; UN(1), first-order banded diagonal; and VC, variance components. Null values in empty cells (–) indicate model failure to converge.

Table 14: Analysis of variance of damping ratio, ζ (dimensionless), measured on the trunks (**A**) and branches (**B**) of Senegal mahogany (*Khaya senegalensis*)

Effect	df	*F*	*p*	Level	Mean (SE)
A) trunk ζ					
Type	1, 9	0.55	0.479		
Severity	4, 36	4.29	0.006		
Type × Severity	4, 36	2.78	0.041		
Severity:Type$_1$(Raise)	4, 36	0.43	0.789		
Severity:Type$_2$(Reduce)	4, 36	6.12	0.001		
Orthogonal polynomial comparisons					
Linear	1, 16	28.0	< 0.001		
Quadratic	1, 16	1.24	0.281		
Cubic	1, 16	7.08	0.017		
Quartic	1, 16	2.29	0.150	0%	0.11 (0.02)
				10%	0.14 (0.04)
				20%	0.23 (0.05)
				40%	0.05 (0.02)
				80%	0.03 (0.01)
B) branch ζ					
Type	1, 110	66.8	< 0.001	Raise	0.19 (0.01)a
				Reduce	0.13 (0.01)b
Severity	4, 110	17.3	< 0.001		
Type × Severity	4, 110	16.7	< 0.001		
Severity:Type$_1$(Raise)	4, 110	1.58	0.183		
Severity:Type$_2$(Reduce)	4, 110	31.8	< 0.001		
Orthogonal polynomial comparisons					
Linear	1, 57	78.3	< 0.001		
Quadratic	1, 57	0.54	0.465		
Cubic	1, 57	28.7	< 0.001		
Quartic	1, 57	0.09	0.761	0%	0.17 (0.01)
				10%	0.19 (0.01)
				20%	0.18 (0.01)
				40%	0.07 (0.01)
				80%	0.04 (0.02)

Note: Fixed effects include pruning type: raise, reduce; severity: 0, 10, 20, 40, 80%; and their interaction: type × severity. Trunk ζ was measured repeatedly on six raised and five reduced Senegal mahoganies; branch ζ was simultaneously measured on 12 and 14 branches, respectively, distributed among these raised and reduced trees. Means followed by the same letter are not significantly different at the $\alpha = 0.05$ level. For reduced trees, orthogonal polynomial comparisons test the significance of an *n*th-order polynomial multiple regression of ζ against pruning severity; the corresponding regression coefficients were determined separately using least squares regression (Figure 22).

Table 15: Analysis of variance of damping ratio, ζ (dimensionless), measured on the trunks (**A**) and branches (**B**) of rain tree (*Samanea saman*)

Effect	df	*F*	*p*	Level	Mean (SE)
A) trunk ζ					
Type	1, 6.96	1.88	0.213		
Severity	3, 12.1	4.13	0.031		
Type × Severity	3, 12.1	5.33	0.014		
Severity:$Type_1$(Raise)	3, 12.1	0.87	0.483		
Severity:$Type_2$(Reduce)	3, 12.1	9.56	0.002		
Orthogonal polynomial comparisons					
Linear	1, 5.96	15.9	0.007		
Quadratic	1, 7.25	20.0	0.003		
Cubic	1, 6.18	0.03	0.868	0%	0.11 (0.02)
				20%	0.05 (0.02)
				40%	0.02 (0.02)
				80%	0.04 (0.01)
B) branch ζ					
Severity	3, 7.21	32.0	< 0.001		
Orthogonal polynomial comparisons					
Linear	1, 5.51	31.6	0.002		
Quadratic	1, 6.82	0.55	0.483		
Cubic	1, 11.4	1.34	0.271	0%	0.11 (0.02)
				20%	0.07 (0.01)
				40%	0.06 (0.01)
				80%	0.02 (0.01)

Note: For trunk ζ, fixed effects include pruning type: raise, reduce; severity: 0, 20, 40, 80%; and their interaction: type × severity. For branch ζ, insufficient observations of branch acceleration on raised trees resulted in a single fixed effect: pruning severity for reduced trees. Trunk ζ was measured repeatedly on four raised and five reduced rain trees; branch ζ was simultaneously measured on six branches in one reduced rain tree. For reduced trees, orthogonal polynomial comparisons test the significance of an *n*th-order polynomial multiple regression of ζ against pruning severity; the corresponding regression coefficients were determined separately using least squares regression (Figure 24).

Table 16: Sample sizes, functional forms, parameter estimates, confidence intervals, and coefficients of determination for regression models that describe the correlation between natural frequency, f_n (Hz), and morphometric attributes at all pruning severities for reduced Senegal mahogany (*Khaya senegalensis*) and rain tree (*Samanea saman*)

	Senegal mahogany		**rain tree**	
	branch	**trunk**	**branch**	**trunk**
n	62	25	20	20
Total mass, *m*				
Form	$y = \beta x^{\alpha}$	$y = \beta x^{\alpha}$	$y = \beta x^{\alpha}$	$y = \beta x^{\alpha}$
α	-6.56×10^{-1}	-2.41	-0.70	-2.36
(95% CI)	$-(7.88 – 5.24)\times10^{-1}$	-(2.84 – 1.99)	-(1.03 – 0.37)	-(2.84 – 1.89)
β	19.2	1.15×10^{9}	39.7	1.58×10^{9}
(95% CI)	(7.41 – 49.7)	$(0.25 – 54.0)\times10^{9}$	(4.18 – 376)	$0.20\times10^{8} – 1.22\times10^{11}$
r^2	0.62	0.86	0.52	0.86
Leaf mass, m_{LEAF}				
Form	$y = \beta x^{\alpha}$	$y = \beta x^{\alpha}$	$y = \beta x^{\alpha}$	$y = \beta x^{\alpha}$
α	-0.33	-0.44	-0.51	-0.43
(95% CI)	-(0.38 – 0.28)	-(0.57 – 0.30)	-(0.74 – 0.28)	-(0.58 – 0.28)
β	0.45	3.0	0.39	1.9
(95% CI)	(0.38 – 0.53)	(1.5 – 5.7)	(0.25 – 0.59)	(1.2 – 2.9)
r^2	0.77	0.66	0.55	0.67
Length, *L*				
Form	$y = \beta x^{\alpha}$	$y = \beta x^{\alpha}$	$y = \beta x^{\alpha}$	$y = \beta e^{\alpha x}$
α	-0.95	-2.62	-1.28	-0.19
(95% CI)	-(1.06 – 0.83)	-(2.92 – 2.33)	-(1.64 – 0.92)	-(0.21 – 0.17)
β	1.36	1.07×10^{3}	3.73	13.1
(95% CI)	(1.03 – 1.79)	$(0.44 – 2.60)\times10^{3}$	(1.64 – 8.44)	(9.56 – 18.1)
r^2	0.82	0.94	0.76	0.96
Apical diameter, *d*				
Form	$y = \beta + \alpha x^2$	$y = \beta + \alpha x^2$	$y = \beta e^{\alpha x}$	$y = \beta e^{\alpha x}$
α	3.90	8.17	8.08	5.75
(95% CI)	(3.49 – 4.32)	(7.46 – 8.87)	(6.58 – 9.57)	(5.10 – 6.40)
β	8.42×10^{-2}	0.13	6.59×10^{-2}	0.20
(95% CI)	$(6.03 – 10.8)\times10^{-2}$	(0.06 – 0.21)	$(4.99 – 8.70)\times10^{-2}$	(0.16 – 0.24)
r^2	0.86	0.96	0.88	0.95

Note: Branch attributes used to predict f_n measured on the trunk were determined as the mean of all primary branches.

Table 17: Sample sizes, functional forms, parameter estimates, confidence intervals, and coefficients of determination for regression models that describe the correlation between natural frequency, f_n (Hz), and morphometric attributes at all pruning severities for reduced Senegal mahogany (*Khaya senegalensis*) and rain tree (*Samanea saman*)

	Senegal mahogany		**rain tree**	
	branch	**trunk**	**branch**	**trunk**
n	62	25	20	20
Height of branch apex, ξ				
Form	$y = \beta x^{\alpha}$	$y = \beta e^{\alpha x}$	$y = \beta x^{\alpha}$	$y = \beta e^{\alpha x}$
α	-2.37	-0.17	-2.69	-0.17
(95% CI)	-(2.64 – 2.09)	-(0.20 – 0.14)	-(2.99 – 2.39)	-(0.19 – 0.15)
β	243	10.1	372	10.3
(95% CI)	(104 – 571)	(5.76 – 17.6)	(161 – 859)	(7.25 – 14.6)
r^2	0.83	0.87	0.95	0.94
Spread of branch apex, ς				
Form	$y = \beta x^{\alpha}$	$y = \beta + \alpha x$	$y = \beta x^{\alpha}$	$y = \beta x^{\alpha}$
α	-0.74	-0.17	-0.99	-1.08
(95% CI)	-(0.95 – 0.53)	-(0.33 – 0.02)	-(1.41 – 0.57)	-(1.33 – 0.83)
β	0.37	1.68	1.01	4.00
(95% CI)	(0.28 – 0.49)	(0.73 – 2.63)	(0.50 – 2.07)	(2.53 – 6.32)
r^2	0.46	0.19	0.58	0.82
Slenderness, λ				
Form	$y = \beta x^{\alpha}$	$y = \beta x^{\alpha}$	$y = \beta x^{\alpha}$	$y = \beta e^{\alpha x}$
α	-0.92	-2.68	-1.31	-0.16
(95% CI)	-(1.02 – 0.81)	-(2.93 – 2.42)	-(1.58 – 1.03)	-(0.18 – 0.14)
β	2.93	2.99×10^{3}	16.4	12.2
(95% CI)	(2.07 – 4.15)	$(1.29 – 6.94)\times10^{3}$	(6.58 – 40.9)	(8.11 – 18.2)
r^2	0.83	0.95	0.85	0.93
Stockiness, ψ				
Form	$y = \beta + \alpha\cdot\ln(x)$	$y = \beta + \alpha x$	$y = \beta + \alpha x$	$y = \beta + \alpha x$
α	0.13	324	23.9	161
(95% CI)	(0.11 – 0.14)	(286 – 362)	(21.6 – 26.2)	(115 – 206)
β	0.91	-0.15	7.54×10^{-2}	-0.14
(95% CI)	(0.83 – 1.00)	-(0.27 – 0.02)	$(0.69 – 14.4)\times10^{-2}$	(-0.35 – 0.63)
r^2	0.84	0.93	0.96	0.76

Note: Branch attributes used to predict f_n measured on the trunk were determined as the mean of all primary branches.

Table 18: Sample sizes, functional forms, parameter estimates, confidence intervals, and coefficients of determination for regression models that describe the correlation between damping ratio, ζ (dimensionless), and morphometric attributes at all pruning severities for reduced Senegal mahogany (*Khaya senegalensis*) and rain tree (*Samanea saman*)

	Senegal mahogany		**rain tree**	
	branch	**trunk**	**branch**	**trunk**
n	62	25	20	20
Total mass, m				
Form	$y = \beta x^{\alpha}$	$y = \beta x^{\alpha}$	$y = \beta x^{\alpha}$	$y = \beta + \alpha x$
α	0.54	1.67	0.31	4.38×10^{-6}
(95% CI)	(0.43 – 0.66)	(0.92 – 2.42)	(0.11 – 0.52)	$(0.98 – 9.75)\times10^{-6}$
β	2.71×10^{-3}	2.24×10^{-8}	1.05×10^{-2}	1.13×10^{-2}
(95% CI)	$(1.17 – 6.26)\times10^{-3}$	2.57×10^{-11} – 1.95×10^{-5}	$(0.26 – 4.24)\times10^{-2}$	$(-4.43 – 6.68)\times10^{-2}$
r^2	0.59	0.48	0.36	0.14
Leaf mass, m_{LEAF}				
Form	$y = \beta + \alpha x + \alpha_2 x^2$	$y = \beta x^{\alpha}$	$y = \beta x^{\alpha}$	$y = \beta + \alpha x$
α	2.7×10^{-3}	0.36	0.23	5.5×10^{-4}
(95% CI)	$(2.2 – 3.2)\times10^{-3}$	(0.20 – 0.51)	(0.09 – 0.37)	$(3.4 – 7.5)\times10^{-4}$
α_2	-1.2×10^{-5}	–	–	–
(95% CI)	$-(1.4 – 0.91)\times10^{-5}$			
β	6.7×10^{-2}	1.7×10^{-2}	5.2×10^{-2}	3.0×10^{-2}
(95% CI)	$(4.9 – 8.5)\times10^{-2}$	$(0.83 – 3.5)\times10^{-2}$	$(4.0 – 6.8)\times10^{-2}$	$(1.5 – 4.6)\times10^{-2}$
r^2	0.67	0.51	0.39	0.64
Length, L				
Form	$y = \beta x^{\alpha}$	$y = \beta x^{\alpha}$	$y = \beta x^{\alpha}$	$y = \beta + \alpha x + \alpha_2 x^2$
α	0.71	1.59	0.55	-2.25×10^{-2}
(95% CI)	(0.57 – 0.85)	(0.75 – 2.43)	(0.27 – 0.83)	$-(3.76 – 0.75)\times10^{-2}$
α_2	–	–	–	9.42×10^{-4}
(95% CI)				$(4.07 – 14.8)\times10^{-4}$
β	2.45×10^{-2}	7.00×10^{-4}	2.14×10^{-2}	0.15
(95% CI)	$(1.76 – 3.39)\times10^{-2}$	$(0.57 – 85.8)\times10^{-4}$	$(1.12 – 4.06)\times10^{-2}$	(0.05 – 0.24)
r^2	0.64	0.40	0.48	0.59
Apical diameter, d				
Form	$y = \beta e^{\alpha x}$	$y = \beta e^{\alpha x}$	$y = \beta e^{\alpha x}$	$y = \beta + \alpha \cdot \ln(x)$
α	-4.33	-3.54	-3.60	-2.05×10^{-2}
(95% CI)	-(5.19 – 3.46)	-(5.29 – 1.79)	-(5.04 – 2.17)	$-(2.97 – 1.12)\times10^{-2}$
β	0.22	0.16	0.11	9.32×10^{-3}
(95% CI)	(0.19 – 0.26)	(0.10 – 0.25)	(0.09 – 0.15)	$(-1.50 – 3.37)\times10^{-2}$
r^2	0.63	0.43	0.61	0.55

Note: Branch attributes used to predict ζ measured on the trunk were determined as the mean of all primary branches.

Table 19: Sample sizes, functional forms, parameter estimates, confidence intervals, and coefficients of determination for regression models that describe the correlation between damping ratio, ζ (dimensionless), and morphometric attributes at all pruning severities for reduced Senegal mahogany (*Khaya senegalensis*) and rain tree (*Samanea saman*)

	Senegal mahogany		**rain tree**	
	branch	**trunk**	**branch**	**trunk**
n	62	25	20	20
Height of branch apex, ξ				
Form	$y = \beta x^{\alpha}$	$y = \beta e^{\alpha x}$	$y = \beta x^{\alpha}$	$y = \beta + \alpha x + \alpha_2 x^2$
α	1.76	0.11	1.23	-1.84×10^{-2}
(95% CI)	(1.42 – 2.11)	(0.06 – 0.16)	(0.82 – 1.64)	$-(2.99 – 0.70)\times10^{-2}$
α_2	–	–	–	7.89×10^{-4}
(95% CI)				$(3.80 – 12.0)\times10^{-4}$
β	6.30×10^{-4}	1.10×10^{-2}	2.62×10^{-3}	0.12
(95% CI)	$(2.19 – 18.1)\times10^{-4}$	$(0.38 – 3.16)\times10^{-2}$	$(0.85 – 8.06)\times10^{-3}$	(0.05 – 0.19)
r^2	0.64	0.44	0.69	0.62
Spread of branch apex, ς				
Form	$y = \beta x^{\alpha}$	$y = \beta x^{\alpha}$	$y = \beta x^{\alpha}$	$y = \beta + \alpha x + \alpha_2 x^2$
α	0.49	0.96	0.53	-6.39×10^{-3}
(95% CI)	(0.28 – 0.69)	(0.10 – 1.81)	(0.30 – 0.76)	$(-2.67 – 1.39)\times10^{-2}$
α_2	–	–	–	9.38×10^{-4}
(95% CI)				$(-0.72 – 2.60)\times10^{-3}$
β	6.99×10^{-2}	2.00×10^{-2}	3.08×10^{-2}	4.50×10^{-2}
(95% CI)	$(5.33 – 9.17)\times10^{-2}$	$(0.45 – 8.93)\times10^{-2}$	$(2.09 – 4.56)\times10^{-2}$	$-(0.83 – 9.84)\times10^{-2}$
r^2	0.28	0.19	0.56	0.22
Slenderness, λ				
Form	$y = \beta x^{\alpha}$	$y = \beta x^{\alpha}$	$y = \beta x^{\alpha}$	$y = \beta + \alpha x + \alpha_2 x^2$
α	0.68	1.56	0.59	-1.49×10^{-2}
(95% CI)	(0.54 – 0.81)	(0.70 – 2.42)	(0.35 – 0.83)	$-(2.93 – 0.05)\times10^{-2}$
α_2	–	–	–	5.53×10^{-4}
(95% CI)				$(1.12 – 9.93)\times10^{-4}$
β	1.45×10^{-2}	4.59×10^{-4}	1.05×10^{-2}	0.12
(95% CI)	$(0.93 – 2.25)\times10^{-2}$	$(0.26 – 80.1)\times10^{-4}$	$(0.48 – 2.33)\times10^{-2}$	(0.02 – 0.23)
r^2	0.63	0.38	0.60	0.45
Stockiness, ψ				
Form	$y = \beta x^{\alpha}$	$y = \beta x^{\alpha}$	$y = \beta e^{\alpha x}$	$y = \beta + \alpha \cdot \ln(x)$
α	-0.35	-0.79	-15.5	-1.76×10^{-2}
(95% CI)	-(0.42 – 0.28)	-(1.22 – 0.37)	-(21.9 – 9.07)	$-(3.80 – 0.29)\times10^{-2}$
β	1.81×10^{-2}	1.28×10^{-3}	8.38×10^{-2}	-4.10×10^{-2}
(95% CI)	$(1.24 – 2.66)\times10^{-2}$	$(0.08 – 18.8)\times10^{-3}$	$(6.92 – 10.2)\times10^{-2}$	-(0.15 – 0.07)
r^2	0.64	0.39	0.59	0.15
Natural frequency, f_n				
Form	$y = \beta x^{\alpha}$	$y = \beta x^{\alpha}$	$y = \beta x^{\alpha}$	$y = \beta + \alpha \cdot \ln(x)$
α	-0.71	-0.62	-0.46	-1.95×10^{-2}
(95% CI)	-(0.83 – 0.59)	-(0.92 – 0.32)	-(0.60 – 0.32)	$-(3.54 – 0.36)\times10^{-2}$
β	3.28×10^{-2}	4.54×10^{-2}	3.34×10^{-2}	4.74×10^{-2}
(95% CI)	$(2.58 – 4.17)\times10^{-2}$	$(3.07 – 6.72)\times10^{-2}$	$(2.58 – 4.32)\times10^{-2}$	$(2.92 – 6.56)\times10^{-2}$
r^2	0.70	0.45	0.72	0.27

Note: Branch attributes used to predict ζ measured on the trunk were determined as the mean of all primary branches.

Table 20: Relative importance of morphometric attributes for predicting vibration properties at all pruning severities for reduced Senegal mahogany (*Khaya senegalensis*) and rain tree (*Samanea saman*)

	Tree and branch attributes							
	m	m_{LEAF}	L	d	ξ	ς	λ	ψ
Natural frequency, f_n								
Khaya senegalensis								
Branch	0.114	0.106	0.125	0.144	0.125	0.056	0.138	0.131
Trunk	0.147	0.043	0.151	0.167	0.159	0.026	0.144	0.155
Samanea saman								
Branch	0.095	0.023	0.133	0.100	0.184	0.127	0.167	0.170
Trunk	0.169	0.066	0.146	0.120	0.115	0.139	0.128	0.115
Damping ratio, ζ								
Khaya senegalensis								
Branch	0.103	0.245	0.079	0.054	0.061	0.028	0.075	0.081
Trunk	0.061	0.021	0.059	0.045	0.047	0.010	0.056	0.057
Samanea saman								
Branch	0.049	0.128	0.084	0.091	0.088	0.133	0.102	0.052
Trunk	0.040	0.177	0.125	0.125	0.149	0.072	0.083	0.027

Note: Morphometric attributes include, total mass, m (kg); leaf mass, m_{LEAF} (kg); length, L (m); apical diameter, d (m); height of branch apex, ξ (m); spread of branch apex, ς (m); slenderness, λ (dimensionless); and stockiness, ψ (m^{-1}), of the respective tree part. For vibration properties measured on the trunk and branches of each species, relative importance was estimated as the average squared semipartial correlation coefficient associated with each variable in all candidate subset models.

Table 21: Model parameters and fit statistics for the best subset of multiple regression models fit to natural frequency, f_n (Hz), of reduced Senegal mahogany (*Khaya senegalensis*) and rain tree (*Samanea saman*) at all pruning severities

	Variables	Adjusted R^2	AIC	BIC
Senegal mahogany				
Branch f_n	m_{LEAF}, d, ς, λ	0.966	-358.4	-356.0
	m, m_{LEAF}, L, ς, λ, ψ	0.967	-358.7	-355.1
	m_{LEAF}, d, ξ, λ	0.966	-357.4	-355.1
	m, m_{LEAF}, d, ς, λ	0.966	-357.9	-355.1
	m, m_{LEAF}, d, λ	0.966	-357.2	-354.9
	m, m_{LEAF}, L, d, λ	0.966	-357.4	-354.7
	β, m, m_{LEAF}, L, ς, λ	0.930	-358.4	-354.7
	m, m_{LEAF}, L, λ, ψ	0.966	-357.1	-354.7
All subsets		0.92 (0.05)	-335.1 (21.0)	-334.7 (19.7)
Trunk f_n				
	L, d, ξ, λ	0.992	-117.8	-115.1
	m, m_{LEAF}, L, d, ψ	0.992	-118.9	-114.7
	m, m_{LEAF}, d, ς	0.992	-117.1	-114.6
	β, L, d, ξ, λ	0.986	-117.0	-114.1
	β, m, d, ς, ψ	0.986	-116.8	-114.0
	L, d, ξ, ς, λ	0.992	-117.4	-113.8
	L, d, ξ, λ, ψ	0.992	-116.9	-113.5
	β, m, L, d, ς, ψ	0.987	-118.2	-113.5
All subsets		0.97 (0.07)	-99.2 (15.6)	-100.3 (13.6)
rain tree				
Branch f_n				
	m_{LEAF}, d, ξ	0.997	-127.8	-123.6
	m_{LEAF}, d, ξ, ψ	0.998	-128.6	-122.4
	m_{LEAF}, L, d, ξ	0.998	-127.8	-121.9
	m_{LEAF}, d, ξ, λ	0.998	-127.4	-121.7
	m, m_{LEAF}, d, ξ	0.997	-125.9	-120.9
	m_{LEAF}, d, ξ, ς	0.997	-125.8	-120.8
	β, m_{LEAF}, d, ξ	0.997	-126.0	-120.8
	m_{LEAF}, d, ξ, λ, ψ	0.998	-126.9	-119.2
All subsets		0.97 (0.08)	-96.4 (23.8)	-97.7 (20.0)
Trunk f_n				
	L, d, ξ, ς	0.997	-87.3	-82.0
	m_{LEAF}, L, d, ξ, ς	0.997	-86.6	-79.6
	L, d, ξ, ς, ψ	0.997	-86.0	-79.3
	L, d, ξ, ς, λ	0.997	-85.4	-79.1
	m, L, d, ξ, ς	0.997	-85.4	-79.1
	β, L, d, ξ, ς	0.995	-85.4	-78.4
	m, d, ξ, ς, λ	0.996	-81.3	-77.4
	m_{LEAF}, L, d, ξ, ς, ψ	0.997	-85.1	-76.6
All subsets		0.96 (0.06)	-50.9 (21.2)	-54.0 (18.5)

Note: For f_n measured on the trunks and branches of both species, eight multiple regression models are displayed with the lowest BIC among all candidate subset models. Fit statistics for all subsets were computed from 510 different multiple parameter models consisting of unique combinations of morphometric attributes fit to f_n measured on the trunk and branches of each species. Fit statistics for all subsets are listed as mean (SD).

Table 22: Model parameters and fit statistics for the best subset of multiple regression models fit to damping ratio, ζ (dimensionless), of reduced Senegal mahogany (*Khaya senegalensis*) and rain tree (*Samanea saman*) at all pruning severities

	Variables	Adjusted R^2	AIC	BIC
Senegal mahogany				
Branch ζ				
	m_{LEAF}, ξ	0.936	-396.2	-394.1
	m_{LEAF}, ψ	0.935	-396.0	-393.9
	m_{LEAF}, λ	0.935	-395.8	-393.8
	m_{LEAF}, L	0.935	-395.8	-393.8
	m, m_{LEAF}	0.935	-395.6	-393.5
	m_{LEAF}	0.934	-395.2	-393.2
	m_{LEAF}, d, ξ	0.936	-395.1	-392.9
	m, m_{LEAF}, L, ς, ψ	0.938	-396.1	-392.9
All subsets		0.74 (0.19)	-378.5 (14.9)	-377.6 (13.2)
Trunk ζ				
	m	0.648	-120.4	-118.1
	ξ	0.639	-119.8	-117.5
	L	0.633	-119.4	-117.1
	ψ	0.626	-118.9	-116.6
	d	0.626	-118.9	-116.6
	λ	0.618	-118.4	-116.2
	m, ξ	0.638	-118.8	-115.9
	m, m_{LEAF}	0.636	-118.6	-115.8
All subsets		0.34 (0.27)	-114.2 (2.1)	-109.6 (3.3)
rain tree				
Branch ζ				
	m_{LEAF}, L, ς, λ	0.922	-145.4	-139.9
	m, d, ς	0.908	-143.1	-139.9
	m, ξ, ς	0.907	-142.9	-139.8
	L, d, ς	0.905	-142.5	-139.5
	L, ς, λ	0.905	-142.4	-139.5
	d, ς	0.895	-141.3	-139.3
	d	0.888	-140.9	-139.2
	ξ	0.887	-140.7	-139.0
All subsets		0.67 (0.22)	-137.7 (2.7)	-134.0 (2.7)
Trunk ζ				
	β, m_{LEAF}, ς	0.686	-147.1	-143.5
	ξ	0.853	-145.0	-143.0
	β, m_{LEAF}	0.615	-143.9	-141.9
	β, m_{LEAF}, ξ, ς	0.695	-147.0	-141.9
	β, m, m_{LEAF}	0.645	-144.7	-141.8
	m_{LEAF}, ξ	0.852	-144.0	-141.7
	β, m, m_{LEAF}, ς	0.688	-146.5	-141.6
	L	0.841	-143.5	-141.6
All subsets		0.70 (0.15)	-139.9 (3.3)	-136.4 (2.7)

Note: For ζ measured on the trunks and branches of both species, eight multiple regression models are displayed with the lowest BIC among all candidate subset models. Fit statistics for all subsets were computed from 510 different multiple parameter models consisting of unique combinations of morphometric attributes fit to ζ measured on the trunk and branches of each species. Fit statistics for all subsets are listed as mean (SD).

Table 23: Information criteria on covariance structures for the analysis of covariance considering the effect of pruning treatments on maximum 30-minute bending moment, M_B (kNm), for Senegal mahogany (*Khaya senegalensis*)

	Covariance Structures			
Fit Statistics	AR(1)	ARMA(1,1)	CS	VC
AICC	229465.1	228911.9	231241.1	240846.8
BIC	229466.3	228913.5	231241.9	240847.2

Note: Fit statistics include AICC, corrected Akaike Information criteria, and BIC, Schwarz's Bayesian Information criteria. Covariance structures include AR(1), first-order autoregressive; ARMA(1,1) first-order autoregressive moving average; CS, compound symmetry; and VC, variance components. Null values in empty cells (-) indicate model failure to converge.

Table 24: Model coefficients for covariate fit to 30-minute maximum M_B (kN·m) and 30-minute maximum U^2 (m·s^{-1})

Effect	**Level**	**Parameter Estimate (95% CI)**	***p***
U^2 × Type × Severity	Raise 0%	1.02 (0.90 – 1.13)	< 0.001
	Raise 10%	0.93 (0.82 – 1.03)	< 0.001
	Raise 20%	0.71 (0.63 – 0.79)	< 0.001
	Reduce 0%	1.57 (1.48 – 1.67)	< 0.001
	Reduce 10%	0.84 (0.77 – 0.92)	< 0.001
	Reduce 20%	0.09 (0.01 – 0.16)	0.025

Note: Parameter estimates for covariates describe the slope of a linear relationship between 30-minute maximum M_B and 30-minute maximum U^2 for all combinations of pruning type and severity. See Table 25 for the full model and tests of fixed effects.

Table 25: Analysis of covariance of 30-minute maximum bending moment, M_B (kN·m), measured on the lower trunk of Senegal mahogany (*Khaya senegalensis*), after accounting for 30-minute maximum wind speed, U ($m \cdot s^{-1}$)

Effect	df	F	p	Level	Mean (SE)
Type	1, 9.4	0.07	0.796		
Severity	2, 6218	308	< 0.001		
Type × Severity	2, 6218	72.6	< 0.001		
U^2 × Type × Severity	6, 8539	407	< 0.001		
Severity:Type$_1$(Raise) at U = 4	2, 3207	56.0	< 0.001		
Orthogonal polynomial comparisons					
Linear	1, 614	79.3	< 0.001		
Quadratic	1, 963	14.3	< 0.001	0%	34.2 (3.8)
				10%	32.8 (3.8)
				20%	24.5 (3.8)
Severity:Type$_2$(Reduce) at U = 4	2, 2672	394	< 0.001		
Orthogonal polynomial comparisons					
Linear	1, 2124	680	< 0.001		
Quadratic	1, 3301	6.72	0.010	0%	44.6 (4.1)
				10%	32.6 (4.1)
				20%	20.0 (4.1)
Severity:Type$_1$(Raise) at U = 5	2, 6565	39.6	< 0.001		
Orthogonal polynomial comparisons					
Linear	1, 1831	64.3	< 0.001		
Quadratic	1, 2673	9.41	0.002	0%	43.4 (3.9)
				10%	41.2 (3.9)
				20%	30.9 (3.8)
Severity:Type$_2$(Reduce) at U = 5	2, 5715	395	< 0.001		
Orthogonal polynomial comparisons					
Linear	1, 4154	754	< 0.001		
Quadratic	1, 5710	3.38	0.066	0%	58.8 (4.2)
				10%	40.2 (4.2)
				20%	20.8 (4.1)
Severity:Type$_1$(Raise) at U = 6	2, 8175	29.7	< 0.001		
Orthogonal polynomial comparisons					
Linear	1, 3061	52.1	< 0.001		
Quadratic	1, 3591	6.70	0.010	0%	54.6 (4.2)
				10%	51.3 (4.1)
				20%	38.6 (3.9)
Severity:Type$_2$(Reduce) at U = 6	2, 7257	373	< 0.001		
Orthogonal polynomial comparisons					
Linear	1, 5212	753	< 0.001		
Quadratic	1, 6614	1.95	0.163	0%	76.1 (4.4)
				10%	49.5 (4.3)
				20%	21.8 (4.2)

Note: Fixed effects include pruning type: raise, reduce; severity: 0, 10, 20%; and their interaction: type × severity. Statistical inferences about fixed effects were made with the covariate equal to 5 $m \cdot s^{-1}$. During the experiment, 30-minute maximum M_B was measured repeatedly on six raised and five reduced Senegal mahoganies. Orthogonal polynomial comparisons test the significance of an nth-order polynomial multiple regression of 30-minute maximum M_B against pruning severity after accounting for 30-minute maximum U; the corresponding regression coefficients were determined separately using least squares regression (Figure 64).

CHAPTER 5

DISCUSSION

Tree and branch attributes

Among more than a dozen existing studies considering the effect of pruning on vibration properties or wind loads, the size and mass of most trees were much smaller than those used in this study. The size of rain trees and Senegal mahoganies used in this study was similar to those frequently considered during tree risk assessment, and the results are useful for arborists considering the use of pruning treatments to mitigate risk presented by large trees.

Using the branch allometric models presented in this study, arborists can relate the measured diameter of a pruning cut to the size and mass of an excised branch, and these estimates can be used to practically determine the cumulative severity of pruning. Despite countless allometric models relating various size-dependent tree attributes, relatively few allometric models exist for the branch attributes of any species, and these are the first branch allometric models developed for rain tree and Senegal mahogany. Practically, pruning severity is often estimated visually as the percentage of foliage removed (TCIA 2017b), but the accuracy of these subjective visual estimates is questionable (Pavlis et al. 2008). Since the mass of trees and leaves correlates strongly with vibration properties (Bruchert and Gardiner 2006) and drag (Vollsinger et al. 2005; Kane et al. 2008b), authors should further examine and facilitate the use of mass as a measure of pruning severity by practitioners.

Structural Young's modulus

Senegal mahogany and rain tree E_{STRUCT} was the same order of magnitude as values reported for excurrent conifers (Milne and Blackburn 1989; Milne 1991; Bruchert et al. 2000; Peltola et al. 2000) and open-grown decurrent trees (Kane 2014). In existing attempts to determine E_{STRUCT} on standing trees subjected to static bending, authors reported similar variability in estimates for

multiple trees of the same species (Milne and Blackburn 1989; Peltola et al. 2000; Kane 2014). Senegal mahogany E_{STRUCT} was similar to values reported for green milled specimens obtained from congeneric African mahoganies measured in three-point bending (Kretschmann 2010). However, the use of outer bark diameter to estimate σ likely resulted in a small underestimation of E_{STRUCT} (Cannell and Morgan 1987; Lundstrom et al. 2008). For the trees in this study, a uniform bark thickness of 1 cm, for example, would have caused an error of approximately 5% in E_{STRUCT} from the overestimate of a, b, and I in Eq. 38.

Effect of pruning treatments on mass and vibration properties

The greater percent decrease in m_{TREE} on reduced trees was expected because this pruning type removed all tree parts from a portion of L_{CROWN}, while only higher-order branches were removed from raised trees to retain the trunk and most primary branches. A distal concentration of leaves on the branches of both species resulted in a faster rate of decrease in m_{LEAF} for reduced trees, and this was especially true for rain tree. The distinct form of polynomial regression functions fit to the percent decrease in m_{LEAF} on reduced trees, especially the large negative quadratic term, depicted the unique defoliation of these trees. This finding suggests that, especially for rain trees, arborists must use good judgment when prescribing the severity of reduction pruning to avoid defoliation. It should be noted, however, that the polynomials fit to the percent decrease in m_{LEAF} are not well-suited for prediction because the functions unrealistically exceed 100% over part of their range. The polynomial regression models used to separate means should be regarded as describing trends in measurements over the range of tested pruning severities, rather than predictive models.

Before pruning, trunk f_n measured during free vibration on Senegal mahogany and rain tree occupied the lower limit of values reported for excurrent conifers (Moore and Maguire 2004; Jonsson et al. 2007) and fell short of similar values reported for other unmodified in-leaf

decurrent trees (Roodbaraky et al. 1994; Kane and James 2011; Kane et al. 2014; Miesbauer et al. 2014). Differences in size account for much of the disparity between these measurements. Previously measured trees had a smaller *DBH* and most were shorter, and it is likely that they had a lower mass since $m_{TREE} \propto DBH^2 \cdot H_{TREE}$ (Chave et al. 2005). Although most existing studies did not measure m_{TREE}, Baker (1997) analogously reported that f_n was inversely proportional to *DBH* for 18 European lindens. The lower f_n of large trees agrees with the behavior of a SDOF mass-spring system, whose f_n is inversely proportional to its mass according to Eq. 15.

However, Reiland et al. (2015) reported that unmodified, in-leaf red oaks had a trunk f_n between 0.18 and 0.23 Hz during free vibration, and these values partially overlapped the range of observations for Senegal mahogany and rain tree in this study. The red oaks were also smaller, on average, than trees included in this study and, assuming a proportional difference in m_{TREE}, a comparable decrease in stiffness must have existed in order to maintain parity between measurements according to Eq. 15. The authors attributed the disparity between the red oaks and existing reports, in part, to factors associated with the sheltered location in which the trees were growing (Reiland et al. 2015). Specifically, the trees were expected to have experienced greater wind shelter and competition for resources from neighbors, resulting in more slender trees containing a greater proportion of branches in the upper crown (Reiland et al. 2015).

Before pruning, there was little difference between branch f_n measured in free vibration on Senegal mahogany and rain tree. There are few existing measurements of branch f_n for unmodified in-leaf decurrent trees undergoing free vibration. Campiformio (2012) reported that six branches in one white ash [*Fraxinus americana* L. (Oleaceae)] vibrated at a narrow range of frequencies near the fundamental mode of the entire tree. Likewise, Kane (2018) observed that the trunk and large codominant stems of seven red oaks vibrated at similar frequencies.

Overall, the similar trends in the vibration properties of pruned trees for both species did not suggest that post-pruning growth confounded the analysis of Senegal mahogany vibration properties. For both species tested in this study, trunk and branch f_n increased continually with pruning severity only for reduced trees, consistent with existing reports of small (Kane and James 2011; Miesbauer et al. 2014) and large (Kane 2018) trees. In contrast, trunk and branch f_n remained constant on raised trees of both species for all pruning severities tested in this study. Previous studies have similarly documented the minimal change in f_n on raised trees (Kane and James 2011) unless a substantial proportion of crown mass was removed (Moore and Maguire 2005). These findings are physically intuitive since f_n of a cantilever beam is inversely proportional to the square of its length but only to the square root of its mass (Niklas 1992); tree parts were shortened only on reduced trees and m_{TREE} decreased on reduced trees at a rate nearly twice that for raised trees. On raised Douglas-firs, Moore and Maguire (2005) did not observe an increase in f_n until more than 80% of m_{CROWN} was removed. For Senegal mahogany and rain tree, m_{TREE} decreased on raised trees, at most, by only 24%, and it would have been practically challenging to further decrease m_{TREE} without removing very large branches. Such severe pruning is unlikely in most arboricultural settings.

Although trunk and branch f_n increased curvilinearly on reduced trees for both species, the unit difference in the degree of polynomials indicated that post-pruning f_n increased faster on rain tree than Senegal mahogany, and this was likely caused by the smaller λ for rain tree originating from the larger basal diameter of most tree parts and shorter tree height. In addition, the absence of the 10% pruning severity from the rain tree experiment may have contributed to a difference in the modeled trend for the two species; a difference in the concavity of the two functions existed only between 0 and 19% pruning severity. Still, the general pattern of the two functions is similar over the entire range of tested pruning severities. For both species, the absence of a difference in f_n and

ζ between pruning types at 0% severity suggests that it was not necessary to include a covariate to account for the initial condition of trees in statistical models.

Although pruning affected trunk and branch f_n similarly, these measurements differed from existing reports that branches vibrated at a higher f_n than the trunk on a given tree (Rodriguez et al. 2008, 2012). The reasons for this discrepancy are not immediately clear, but it is useful to consider whether differences in the torsional stiffness of attachments between tree parts may have contributed to variability in their f_n. Most existing uses of beam theory to consider the vibration of tree parts have assumed classical fixed-free boundary conditions (Spatz and Speck 2002). The fundamental f_n of truncated cylindrical cones (Conway and Dubil 1965) in transverse free vibration increases nonlinearly between the classical fixed-free and pinned-free boundary conditions (Yan et al. 2013), with intermediate conditions approximated by a torsional spring with varying stiffness at the restrained end. If the difference between the trunk and branch f_n of trees measured in this study was caused by these boundary conditions, the torsional stiffness of branch attachments must have been higher than for the root-soil system. However, there are few reported measurements of the torsional stiffness of attachments between tree parts available for consideration. Among four Sitka spruce, Neild and Wood (1999) estimated that the resultant torsional root-anchorage stiffness was, on average, 33 times greater than trunk stiffness. In addition, anatomical evidence of the increased lateral flexibility of branch attachments (Farber et al. 2001; Jungnikl et al. 2009) diminishes the possibility that the difference between trunk and branch f_n was caused by a disparity in their attachment stiffness.

Before pruning, trunk ζ measured during free vibration on Senegal mahogany and rain tree was similar to values reported for excurrent conifers (Moore and Maguire 2005; Jonsson et al. 2007) and open-grown decurrent trees (Kane and Clouston 2008; Kane and James 2011; Miesbauer et al. 2014; Reiland et al. 2015). Trunk ζ, however, was consistently lower for rain tree than Senegal

mahogany, and the relatively low m_{LEAF} for rain tree explains the difference, in agreement with other reports on the significance of aerodynamic drag generated by leaves towards damping (Bruchert et al. 2003).

Before pruning, branch ζ measured during free vibration on Senegal mahogany and rain tree were slightly different from one another, but no similar reports are available in the literature for comparison. On rain tree, mean trunk and branch ζ were initially similar to one another, but mean branch ζ was initially greater than measured on the trunk of Senegal mahogany. These observations support the common assertion that kinetic energy is dissipated more efficiently in the branches (Speck and Spatz 2004), since ζ measured on Senegal mahogany was greater for the branches than trunk. Comparatively, the estimates of branch ζ for Senegal mahogany are more representative of the variability among experimental trees, since they were based on a larger sample than for rain tree.

The accelerated rate of leaf loss on reduced trees likely explained the exclusive decline in ζ for reduced trees, consistent with studies that demonstrated the effect of leaves on damping (Sellier and Fourcaud 2005; Kane and James 2011). Distal tree parts also experience larger wind-induced displacements, undergo extended periods of motion, and usually interact with faster moving air because the horizontal wind speed increases nonlinearly above ground (Oliver 1971). Since drag is proportional to the square of wind velocity, ignoring reconfiguration, the outsized contribution of leaves at the top of the crown to total damping was expected. Despite an average 61% decrease in m_{LEAF} for raised trees, the preservation of distal branches and leaves on these trees offers one explanation for the observed difference between pruning types.

Although ζ generally decreased with pruning severity for reduced trees, the change was, except for rain tree branch ζ, not constant. For reduced Senegal mahogany, mean trunk and branch ζ

increased between 0 and 20% pruning severity before decreasing to similar values, and this explains the lack of an overall difference in trunk ζ between pruning types. The local increase in trunk ζ for Senegal mahoganies reduced by 20% was unexpected but similar to selected observations of raised Douglas-firs (Moore and Maguire 2005) and reduced maritime pines (Sellier and Fourcaud 2005). For the maritime pines, ζ increased by 15% to 25% after the removal of tertiary branches that comprised less than 1% of each sapling's biomass, and the authors suggested that the flexibility and topological position of these tertiary branches might have explained their negative influence on ζ (Sellier and Fourcaud 2005). However, this effect is not always observed after shortening tree parts by different methods; Kane (2018) reported a large decrease in ζ after all primary branches were shortened by one-third on a single red oak.

The increase in ζ observed on multiple reduced trees in this experiment was likely caused by a shift in the relative contribution from various damping sources. On reduced trees, greater leaf area per unit mass was removed at low pruning severity, decreasing contributions from aerodynamic drag on damping. Recalling that inter-crown collisions were restricted in this study, the remaining sources of damping that could have contributed to this post-pruning increase in ζ include internal wood friction, root-soil friction, intra-crown collisions, and structural damping (Spatz et al. 2007). Among these sources, an increase in structural damping is the most plausible since m_{WOOD} decreased and the root-soil system was not modified on any trees. A post-pruning increase in intra-crown collisions was not visually observed or detected as shocks in acceleration time histories during free vibration testing. Practically, the increase in ζ on some trees reduced by 20% was significant because it should attenuate tree movement under external loading, and it should be a priority to attempt to replicate and examine these conditions in future studies.

However, the relationship between ζ and pruning severity was clarified by regressing ζ against the percent decrease in m_{LEAF} rather than percent decrease in L_{CROWN} (i.e., pruning severity). One

distinction was apparent between the observations for each species: ζ generally increased on selected trees until a majority of m_{LEAF} was removed from reduced Senegal mahoganies, but ζ decreased linearly between observations mostly constrained near 0% and 100% decrease in m_{LEAF} on reduced rain trees, since leaves were removed quickly from these trees. Although the source and mechanism of increased damping on reduced Senegal mahoganies remains unclear, it uniquely occurred on reduced trees that retained most of their leaves. In the future, researchers should reduce trees to progressively remove leaves over a series of small increments when examining pruning-induced changes to ζ.

These results demonstrate a complicated, species-specific response pattern to ζ on the reduced trees of each species, and there was considerable variability in ζ among trees subjected to the same pruning treatment. Under certain conditions, the kinematics of reduced branches undergoing free vibration likely created greater interference from out-of-phase movement that dissipated total kinetic energy. In addition to a smaller initial value, the data suggest that rain tree ζ is more sensitive to reduction than Senegal mahogany, a distinction that can be similarly attributed to its relatively sparse crown. Practically, rain tree should be reduced carefully to avoid a large decrease in damping; preservation of ζ is important since trees are generally underdamped ($\zeta < 1$) structures (Moore and Maguire 2004). Senegal mahoganies reduced by $\leq 20\%$, on the other hand, may benefit from the increased post-pruning trunk and branch ζ by better dissipating motion energy compared to their unmodified counterparts.

Relationship between vibration properties and morphometric attributes of trees at all pruning severities

The lack of correlation between vibration properties and morphometric attributes at all pruning severities was expected for raised trees, since pruning treatments did not affect the vibration properties of these trees. For reduced trees, on the other hand, the significant correlations between

vibration properties and morphometric attributes at all pruning severities reflected the significant changes in both variables on these trees. Among reduced trees, the direction of correlation between vibration properties and morphometric attributes at all pruning severities was reversed for f_n and ζ, and the observed trends agree with theoretical expectations (de Langre 2008) and previous measurements of unpruned trees (Moore and Maguire 2004; Kane et al. 2014).

In many cases, analytical functions poorly described the complex patterns observed in data, especially for ζ measured on the trunks and branches of both species. Distinctively, morphometric attributes consistently accounted for the least variance in ζ measured on the trunk of Senegal mahogany, and this showed the limitations of the analytical functions at depicting the increased damping near 20% severity on these trees. For each combination of variables, the functional form of relationships often differed among the trunk and branch observations of each species, and this suggested that the observed patterns in vibration properties at all pruning severities on reduced trees were not easily generalized. Considering these differences, it is unlikely that generic pruning recommendations are appropriate for all trees, and additional studies are needed to examine changes in the post-pruning vibration properties of other species.

Among the bivariate regression models fit to f_n, the concentration of outliers at higher pruning severities was consistent with the increased variance observed under the same conditions while evaluating covariance structures for these data. In the models using d and ψ to predict f_n, extreme outliers strongly influenced the regression model in every case, and the form and coefficients of these models may have differed significantly without these observations. As a result, these model predictions should be viewed cautiously, especially at higher pruning severities. In contrast, the relatively few outliers identified in models fit to ζ was surprising, especially since there was an obvious local increase in post-pruning ζ on the trunks of both species.

Consistent with other findings, the regression models generally showed a greater rate of change in vibration properties on reduced rain trees than Senegal mahoganies. Despite the similar initial f_n of both species, the greater increase in post-pruning f_n measured on the trunk of rain trees was likely caused by a smaller λ resulting from their shorter height and larger *DBH*. On the other hand, the relatively sparse crown of rain tree, compared to Senegal mahogany, likely explained its smaller initial ζ and faster decrease in post-pruning ζ. In combination, these findings suggest that a smaller range of pruning severities should be considered for rain tree than Senegal mahogany.

For the relationships between vibration properties and morphometric attributes, there was stronger correlation between f_n and morphometric attributes of reduced trees at all pruning severities, and the difficulty predicting ζ from morphometric attributes was consistent with existing reports (Jonsson et al. 2007; Kane et al. 2014). In previous studies, most authors attributed difficulty modeling ζ to the complexity of damping processes in trees (Moore and Maguire 2004), and the bivariate regression models fit in this study explained a similar proportion of variance compared to existing attempts to model ζ on unpruned trees (Kane et al. 2014). Despite large confidence intervals about estimates, the models accurately depicted trends between ζ and morphometric attributes at all severities on reduced trees, and they can be used by arborists to guide expectations about changes in damping for reduced trees. More work is needed to understand the mechanisms that affect damping in open-grown trees.

In addition to morphometric attributes, bivariate regression showed that f_n could be used to predict ζ on reduced trees at all pruning severities. Notably for the branch observations of both species, f_n accounted for greater variability in ζ at all pruning severities than any other morphometric attribute, but the same was not true for the trunk observations of both species, which contained large local increases in ζ at some pruning severities. Since f_n is generally easier

to estimate than ζ, this relationship can be conveniently used to anticipate post-pruning changes in ζ on reduced trees.

In contrast with existing reports for excurrent conifers (Moore and Maguire 2004; Jonsson et al. 2007), some recent studies showed there was not a significant relationship between f_n and ψ for unpruned, open-grown decurrent trees (Kane et al. 2014; Kane 2018). Conversely, there was a significant relationship between f_n and ψ for trunk and branch measurements of both species in this study. However, the logarithmic relationship observed between f_n and ψ for Senegal mahogany branch measurements did not agree with theoretical expectations or existing reports of unpruned trees (Moore and Maguire 2004; Jonsson et al. 2007). Since this relationship was linear for all other measurements, the difference was likely caused by the large increase in ψ as the length of branches became very short on reduced Senegal mahoganies. Practically, this showed the limitations of ψ, derived from beam theory, for predicting the f_n of shortened tree parts with a low λ.

Comparatively, ξ consistently explained more variability in the vibration properties of both species than ς at all pruning severities. Despite a sizeable difference in the branch architecture and crown size of the two species, this difference consistently showed the importance of a change in the vertical extent of reduced crowns towards a change in post-pruning vibration properties. In practice, arborists often reduce the height and spread of tree crowns to mitigate the likelihood of failure, but the experimental pruning treatments primarily affected the vertical extent of reduced trees in this study. In future studies, it may be useful to examine changes in the post-pruning vibration properties of reduced trees after a change in the height and width of crowns separately.

For several functions fit to vibration properties and m_{LEAF} at all pruning severities, the asymptotic approach of functions towards zero implied a large rate of change in vibration properties for trees

near defoliation. Although this was a reasonable description of the relationship between ζ and m_{LEAF}, it may have been an artefact of the lack of correlation between vibration properties and m_{LEAF} after defoliation. In contrast, the persistent covariation between vibration properties and other morphometric attributes after defoliation suggests that m_{LEAF} is poorly suited to predict the vibration properties of severely reduced, leafless trees.

There was some evidence for the consistently large contributions of some morphometric attributes to predicting vibration properties at all pruning severities. Among all morphometric attributes, d and m_{LEAF} repeatedly accounted for the largest, or nearly so, amount of additional variance in f_n and ζ, respectively, and the important contributions of these variables supports their inclusion in predictive models. Since d scales with the length and mass of removed tree parts, this suggests that changes to f_n on reduced trees can be anticipated by knowing the size of parts removed from these trees. Still, this is the first report of a relationship between these variables, and it will be important to confirm these observations with additional measurements in future studies.

In contrast, the importance of m_{LEAF} for explaining changes in ζ at all pruning severities largely confirms existing reports (Kane and James 2011; Reiland et al. 2015), and this suggests that changes to ζ on reduced trees can be anticipated by knowing the remaining m_{LEAF} on these trees. Still, the important contributions of m_{LEAF} to predicting ζ at all pruning severities was somewhat surprising, since there was no covariation between these variables after defoliation, and this suggests that the latter mostly varied before removing all leaves. Although d intrinsically accounted for the difference between pruning types, since d remained unchanged on raised trees, the same was not true for m_{LEAF} – a change in m_{LEAF} did not cause an equivalent change in ζ on raised and reduced trees. As a result, it will be important to account for the difference between pruning types in any models based on m_{LEAF}.

Although multiple regression showed that many models were suitable for explaining the observed changes in vibration properties at all pruning severities, there were several issues that prevented the selection and use of a single best model in each case. First, the equivalent fit statistics among the subset of models with the lowest BIC showed that many different combinations of morphometric attributes were equally suitable for predicting changes in the vibration properties of reduced trees at all pruning severities, and the inconsistent form and composition of these models did not reveal an obviously superior choice. Second, the practical use of models was limited by the awkward interpretation of regression coefficients fit to variables after linearization necessary for multiple regression, and the suitability of the underlying transformations for prediction using other data is questionable. In the future, it will be important to collect similar data on other species to validate these models. Third, the unsurprising dependencies among many morphometric attributes on reduced trees contributed to degrading collinearity in many candidate models, and this effectively precluded some highly-correlated variables from consideration in multiple regression models. Although alternatives exist to multiple regression based on ordinary least squares (e.g., ridge, principal components, and partial least squares regression), these procedures lack an equally rigorous theoretical foundation and, in some cases, produce estimates without a straightforward practical interpretation.

To anticipate changes in the vibration properties of reduced trees at all pruning severities, a parsimonious model is desirable for many reasons. The error of prediction often increases with the number of parameters in a model, and it is more economical, in terms of the cost and difficulty of measurement, to model vibration properties with as few morphometric attributes as possible. In practice, it would likely be onerous for an arborist to measure several tree and branch attributes during pruning operations, and the increased confidence of prediction derived from additional measurements must be carefully weighed against the additional time and energy requirements. For some post-pruning tree and branch attributes, the additional measurements

would require a costly deviation from ordinary work activities to move around the tree crown. Uniquely, however, *d* was conveniently measured and explained considerable variation in the vibration properties of both species. Practically, *d* represented the size of the largest reduction or heading cut made on a reduced tree or branch. Since it is straightforward for arborists to measure the size of a pruning wound immediately after removing a branch, it would be easy to measure this attribute in the course of existing practice.

With few exceptions, most morphometric attributes were significantly correlated with vibration properties at all pruning severities, and many attributes accounted for considerable proportions of variance in f_n and ζ. However, *d* was consistently present in many of the multiple parameter models fit to vibration properties with the lowest BIC, and it explained the greatest additional variance, on average, in f_n across all subset models more often than other variables. These varied considerations, taken together, suggest that *d* can be easily used by practitioners to anticipate changes in the vibration properties of pruned trees. For f_n, this study has produced models that can be directly used for this purpose on rain tree and Senegal mahogany, but more work is needed to examine and facilitate the use of *d* to predict changes in the vibration properties, especially ζ, on other species. Still, most evidence in this study suggested that m_{LEAF} was better suited for predicting ζ at all pruning severities, and this variable should be used in experimental settings where direct measurement is possible. Likewise, the size of pruning cuts should be considered more broadly as a possible measure of pruning severity, in light of the scaling relationships between the diameter, length, and mass of tree parts.

Effect of pruning treatments on wind-induced vibration and bending moments

The low wind speeds predominantly observed in this study were consistent with meteorological observations in Singapore (Micheline and Ng 2012) and similar studies in other climates (Schindler 2008; Schindler et al. 2013b). Along the vertical gradient surveyed by the anemometer

mast, the shift in the location of the highest relative wind speeds was likely caused by seasonal changes in the prevailing wind direction. At the site, the anemometer mast was located in a small clearing near a stand edge exposed to the northeast. During the experiment, the wind measurements between August and January coincided with the seasonal transitions between the southwest monsoon, inter-monsoon period, and northeast monsoon. At 0 and 10% severity, the wind mostly flowed over the woodland stand before reaching the anemometers, and this likely caused an attenuation of flow through the crown relative to the permeable trunk space below the crown. At 20%, the wind consistently approached the anemometers from the exposed edge of the woodland after flowing through a heterogenous urban landscape, and the lack of forest vegetation along the upwind fetch explains the shift in the highest relative wind speeds to the highest measurement position.

Before pruning, the predominant vibration of tree parts near their fundamental frequency during wind-induced motion is consistent with existing reports (Sellier et al. 2008; Schindler et al. 2010). Although the magnitude of peaks in Fourier energy was not consistent among spectra computed for all trees in a given wind event, it was expected that variability in the exposure of trees to a heterogenous wind field contributed to differences in excitation. Several reports have demonstrated that, during low wind speeds, trees are mostly excited by gusts arising from coherent structures occurring at frequencies below their fundamental mode (Gardiner 1995; Schindler et al. 2013a; Schindler and Mohr 2019). Since the interval between wind gusts is generally much longer than the sway period of most trees, vibration at the tree's natural frequency mostly results from the stored energy created by wind-induced deflection (Schindler and Mohr 2019). If consistent, the decoupling of wind excitation from energy dissipation should valuably diminish the possibility of destructive harmonic resonance (Ciftci et al. 2013). Especially at 0% severity, the secondary peaks observed in Fourier spectra were likely associated with the momentum transferred by coherent structures at lower frequencies. Although few observations

exist of tree movement at high wind speeds, Schindler and Mohr (2018) provided some evidence that the vibratory response of trees is replaced by quasi-static displacement under these conditions, but more work is needed to elucidate wind-tree interaction for a variety of species and wind conditions.

In agreement with free vibration tests, spectral analysis showed there was no change in the fundamental mode of raised trees at any pruning severity, indicating that these trees continued to dissipate wind energy by swaying at their fundamental mode. Although it was possible to use free vibration tests to estimate f_n for reduced trees at each severity, wind loads acting on these trees were increasingly insufficient, as severity increased, to cause trunk deflection needed to induce vibration near the fundamental mode. Differences in wind conditions prevented a straightforward comparison among spectra computed from separate 30-minute intervals, but the spectra showed a marked difference between the vibration behavior of raised and reduced trees. Overall, reduced trees vibrated less than raised trees at all analyzed frequencies, and the amplitude of vibration for reduced trees at all analyzed frequencies was progressively less than raised trees at each severity. Some higher frequencies were detected on trees reduced by 10%, but there was insufficient wind excitation on trees reduced at greater severities to cause measurable trunk vibration at the fundamental mode. Although residual power in the range of analyzed frequencies suggested that vibration did not completely cease for reduced trees, some of this was caused by instrument noise.

Consistent with previous observations (Scannell 1983), the broad agreement between frequencies measured in free and wind-induced vibration showed that free vibration tests provide a reasonable estimate of f_n for unpruned trees. It was not possible to compare these estimates on trees reduced by greater than 10%, since the reduced trees experienced smaller wind loads, but it is likely that similar agreement would have been demonstrated if measurements were available. In the future,

authors should use LVDT displacement probes offering precise measurements (James and Kane 2008), as far as practicable, to facilitate the measurement of higher frequencies with smaller amplitudes under similar conditions.

The use of period maxima to characterize wind-induced M_B on trees is consistent with existing work (Wellpott 2008; Jackson et al. 2019). Although material fatigue caused by cyclical loading over time may precede tree failure in some cases (Rodgers et al. 1995), most authors assume that extreme (maximum) wind loads are the most frequent cause of failures (Gardiner et al. 2008). Schindler et al. (2016) showed that maximum gust speeds were the most important predictor of storm damage caused by a winter storm in southwest Germany, and other authors have similarly assumed that natural disturbances are driven by extreme value processes (Denny and Gaines 1990).

Although the observed quadratic relationship between 30-minute maxim M_B and 30-minute maximum U agreed with theory (de Langre 2008) and existing experimental observations (Hale et al. 2012), the functions fit to Senegal mahoganies explained less variance in 30-minute maximum M_B than reported in previous studies (Wellpott 2008; Hale et al. 2012), and there could be several reasons for the greater variability observed in this study. First, the heterogenous wind field likely affected trees uniquely depending on their exposure, and it was expected that wind measurements at a single location would only approximate the wind conditions experienced by individual trees, since the distance between the anemometers and trees ranged between 22 and 147 m. Second, Schindler (2008) reported that wind conditions near the crown apex are most closely associated with tree movement. Although a similar trend was observed in this study, the anemometers used in this study were all positioned below the crown apex at 18.3 m (z/H_{TREE} = 0.69). Third, some authors estimated wind loads using Reynold's stress (Mayer 1987) or momentum flux (Schindler and Mohr 2018), in addition to U (Peltola 1996; Flesch and Wilson

1999), but it was not possible to compute these higher-order statistics in this study using two-dimensional wind measurements. In the future, authors should measure three-dimensional wind flow near the crown apex and, as far as possible, ensure close proximity between wind flow and tree measurements.

In this study, the relatively low strain resolution of displacement probes (James and Kane 2008) and mild wind conditions resulted in the sensors operating near their limits of detection and contributed additional, unknown variability to observations. The low strain resolution of displacement probes caused similarly coarse M_B measurements. In terms of C_1, James (2010) measured M_B in much smaller increments, between 0.01 and 1.13 kNm, than possible in this study. In the future, authors should carefully consider measurement resolution in light of anticipated wind loading conditions. Still, the estimation of maximum M_B should be less affected than mean M_B by this limitation (Gardiner 1995). The maximum M_B observed in this study was slightly greater than measured on a 23 m tall tree in 22 $m \cdot s^{-1}$ wind flow (James et al. 2006) and much greater than existing measurements of excurrent conifers (Gardiner et al. 1997; Hale et al. 2012), but this difference was expected, even in lower wind speeds, because of the relatively large size of trees used in this study.

The covariates fit to describe 30-minute maximum M_B as a function of 30-minute maximum U for each treatment combination show that wind-tree interaction was more drastically altered on reduced than raised trees. Although both pruning types decreased the size of the crown exposed to the wind, the length of tree parts was simultaneously shortened on reduced trees, and this distinction likely explains the observed difference in wind loads between the two pruning types. Although several studies demonstrated that drag is proportional to mass (Rudnicki et al. 2004; Vollsinger et al. 2005), others have shown a greater decrease in wind-induced M_B, per unit decrease in mass, on reduced than raised trees. Leaves contribute significantly to total drag, and

they were removed faster on reduced than raised trees because pruning removed leaves concentrated near the canopy apex on these trees. Vollsinger et al. (2005) observed that leaves contributed approximately half of total drag on small black cottonwood and red alder. Reduced tree parts were also less exposed to faster-moving air at higher positions, since wind speed increases non-linearly above the ground in forests (Raupach et al. 1996). In addition, the average height at which drag acted, corresponding to the center of pressure height, was lowered on reduced trees, shortening the distance over which drag causes M_B on reduced trees. Pavlis et al. (2008) similarly observed a greater decrease in wind-induced M_B, per unit mass removed, on reduced than thinned and raised trees, and the authors explained the observed difference in terms of the combined effect of a decrease in drag, proportional to removed mass, and a lower center of pressure. In addition to the decreased wind load, the increased stiffness of shortened tree parts, illustrated by their greater f_n, and associated smaller deflections conferred greater wind resistance to reduced trees. For end-loaded cantilever beams, tip deflection is proportional to the cube of beam length (Niklas 1992), and this demonstrates the importance of a change in length towards a change in mechanical behavior. Analogously, Jackson et al. (2019) estimated that a higher critical wind speed was needed to cause trunk fracture on trees with a larger diameter for a given height than their more slender counterparts, and the stockiness of trees exclusively increased for reduced trees in this study.

The lack of an overall difference in the average 30-minute maximum M_B at 5 $m \cdot s^{-1}$ between pruning types was caused by the initial difference in wind loads experienced by raised and reduced trees. At 0% severity, the average 30-minute maximum M_B at 5 $m \cdot s^{-1}$ was significantly greater on reduced than raised trees, but the average 30-minute maximum M_B at 5 $m \cdot s^{-1}$ decreased more on reduced than raised trees over the range of tested severities to diminish this initial difference. For the four analyzed 30-minute intervals, Fourier energy spectra showed a similar initial difference in wind excitation between trees assigned to each pruning type.

These observations agree with existing reports that M_B decreased more on reduced than raised trees (Smiley and Kane 2006; Pavlis et al. 2008), and the consistency of findings for small and large trees gives assurance to arborists contemplating the use of pruning as a risk mitigation strategy. Since M_B decreased more, per unit mass removed, on reduced than raised trees, less mass needs to be removed from a reduced tree to cause a unit decrease in wind-induced M_B, usefully preserving more of the existing branches and leaves. Although this study did not examine all pruning methods tested in other studies, most existing reports consistently showed that M_B decreased most, at a given severity, on reduced trees compared to others pruned differently (Smiley and Kane 2006; Pavlis et al. 2008). At high severities, the form of raised trees in this study was increasingly similar to lion tailed trees, and it is unfortunate that missing data for these conditions prevented comparisons with existing observations of small lion tailed trees (Smiley and Kane 2006; Gilman et al. 2008a).

It will be important to examine other pruning types in future work, but authors must address important issues of repeatability in future experiments. For example, two related studies reported that visual estimates of pruning severity were poorly related to the measured change in tree mass (Smiley and Kane 2006; Pavlis et al. 2008), and a reliable estimate of the change in mass at a given pruning severity is needed, especially since mass correlates strongly with post-pruning vibration properties and drag (Vollsinger et al. 2005). Similarly, two related studies reported conflicting results about the wind-induced movement of trees thinned in different ways (Gilman et al. 2008a, b), and it will be important to elaborate on existing standards to describe pruning treatments using a set of detailed procedures, despite challenges arising from species-specific differences in crown architecture. Authors should also examine the mechanical consequences of pruning treatments affecting part of the crown or individual branches, which have received relatively little attention (Gilman et al. 2015).

Some studies reported important species-specific differences in reconfiguration during high wind speeds after pruning, but it was not possible to examine reconfiguration in the mild wind conditions encountered in this study. If possible, authors should examine reconfiguration after pruning treatments on large trees experiencing higher wind speeds in the future. Although smaller trees (Rudnicki et al. 2004; Vollsinger et al. 2005; Kane et al. 2008b) and tree parts (Vogel 1989) have been shown to reconfigure extensively in wind flow, it is not clear whether pruning treatments will alter the reconfiguration of larger, and much stiffer, trees.

Conclusion

This is the first study to clearly demonstrate a consistent and practically meaningful difference between pruning types over a wide range of pruning severities. Wind loads decreased more on reduced than raised Senegal mahoganies because the two pruning types altered both the size, location, and vibration properties of tree parts differently. The effect of pruning was greater, in terms of mass, vibration properties, wind-induced vibration, and wind-induced M_B, on reduced than raised trees in every comparison made in this study. Although wind loads were only measured on Senegal mahogany, the similar effect of pruning on the vibration properties of both species suggests that a comparable difference in wind-induced M_B can be expected between raised and reduced rain trees. Assuming no change in the load-bearing capacity of the remaining tree parts, these results indicate that the likelihood of failure will decrease more for reduced than raised trees at a given severity of pruning, in proportion to the decrease in loads acting on these trees. In practice, trees are pruned to meet specific objectives, and there are often multiple reasons for pruning a tree in a landscape. If tree risk mitigation is a reason for pruning, these results suggest that arborists should reduce the size of the crown by shortening the length of tree parts.

For reduced trees, the results suggest that the mechanical benefits of pruning are realized at low severities ($\leq 20\%$). Exposed to a 30-minute maximum wind speed of 6 $m \cdot s^{-1}$, Senegal mahoganies

reduced by 10% and 20% showed meaningful decreases in wind-indced M_B compared to the same trees before pruning. In addition to the increased f_n, the decrease to ζ was minimized after trees were reduced by relatively small amounts, and ζ increased for many reduced Senegal mahoganies up to 20% severity. However, trees with sparse foliage situated near the crown apex, such as the rain trees used in this study, should be reduced carefully by smaller amounts to prevent a large decrease in ζ. This important distinction suggests that pruning treatments should take into account the unique branch and leaf attributes of each species, and there is a need for additional studies on the pruning-induced changes to the mechanical properties and wind loads of other species.

Although this study acknowledges that trees are often pruned to reduce risk, it is equally important to consider the long-term implications of pruning on tree health and vitality. The results demonstrated a meaningful improvement in safety for reduced trees, but several studies have documented the adverse consequences of some methods, especially topping, used to reduce the size of a tree crown. Topping, the practice of arbitrarily shortening tree parts without considering tree anatomy, removes apical control to favor the production of neformed sprouts at the expense of secondary growth (Fini et al. 2015), and there is compelling evidence against the indiscriminate use of heading cuts during topping (Grabosky and Gilman 2007). At the same time, practical experience suggests that excessive pruning is unnecessary and possibly detrimental to trees – professional standards discourage removing more branches and leaves than necessary to meet pruning objectives (TCIA 2017b). Severe defoliation can alter resource allocation patterns and diminish stored carbohydrates available for future growth and defense (Landhausser and Lieffers 2012), and most studies show that removing small branches with properly-executed pruning cuts will minimize similar issues (Fini et al. 2015; Ramirez et al. 2018).

In scientific and practical settings, many continue to visually assess the severity of pruning, and the lack of a widely accepted measure of pruning severity, especially one closely related to

important changes in the post-pruning condition of trees, remains a problem. In this study, several tree and branch attributes were significantly related to the post-pruning vibration properties of reduced, but not raised, trees. The post-pruning f_n of reduced trees could be reasonably predicted with many different tree and branch attributes using basic analytical functions, but the same attributes and functions often poorly described complex patterns in the post-pruning ζ of reduced trees. In the future, it will be important to evaluate alternative approaches to modeling these changes. Still, based on a variety of considerations, post-pruning d and m_{LEAF} usefully explained considerable variation in post-pruning f_n and ζ, respectively, for most measurements, and the predictive utility of these variables should be examined in future studies on tree pruning.

The long-term effects of pruning on the mechanical properties of trees were not studied in this project. In future work, it will be important to examine post-pruning changes to mechanical properties as trees grow over longer periods to determine the persistence of these outcomes over time. This information is especially important for arborists, urban foresters, and policymakers considering an appropriate interval of time between pruning treatments. At the same time, researchers should examine the long-term effects of pruning on tree growth and vitality, since this regulates the magnitude of benefits and services rendered by trees in communities (Song et al. 2018).

APPENDIX A

EXPERIMENTAL TREE CROWN ARCHITECTURE MODELS AND PHOTOGRAPHS

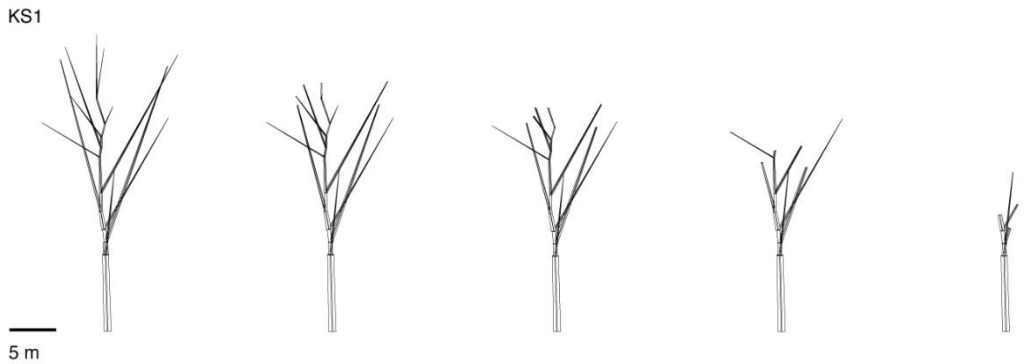

Figure 65: Crown architecture models showing the dimensions and arrangement of primary branches on Senegal mahogany (Khaya senegalensis) number 1 reduced by 0%, 10%, 20%, 40%, and 80% (L – R).

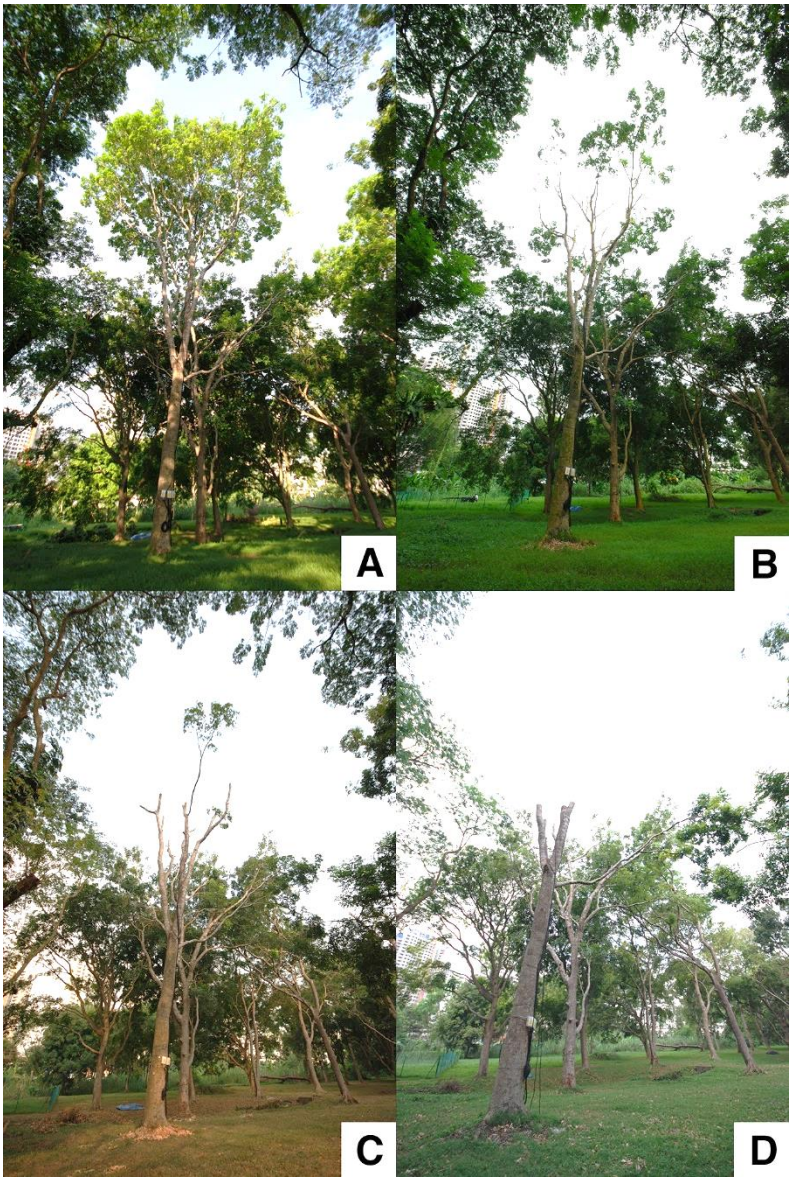

Figure 66: Photographs of Senegal mahogany (*Khaya senegalensis*) number 1 reduced by (**A**) 0%, (**B**) 20%, (**C**) 40%, and (**D**) 80%.

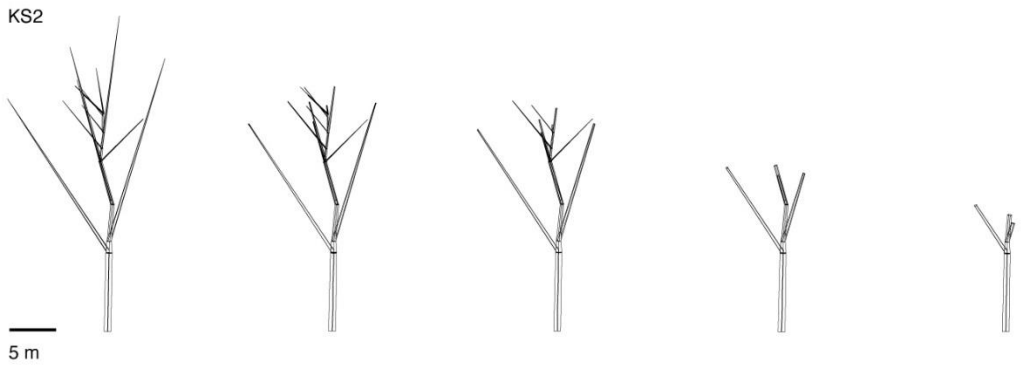

Figure 67: Crown architecture models showing the dimensions and arrangement of primary branches on Senegal mahogany (*Khaya senegalensis*) number 2 reduced by 0%, 10%, 20%, 40%, and 80% (L – R).

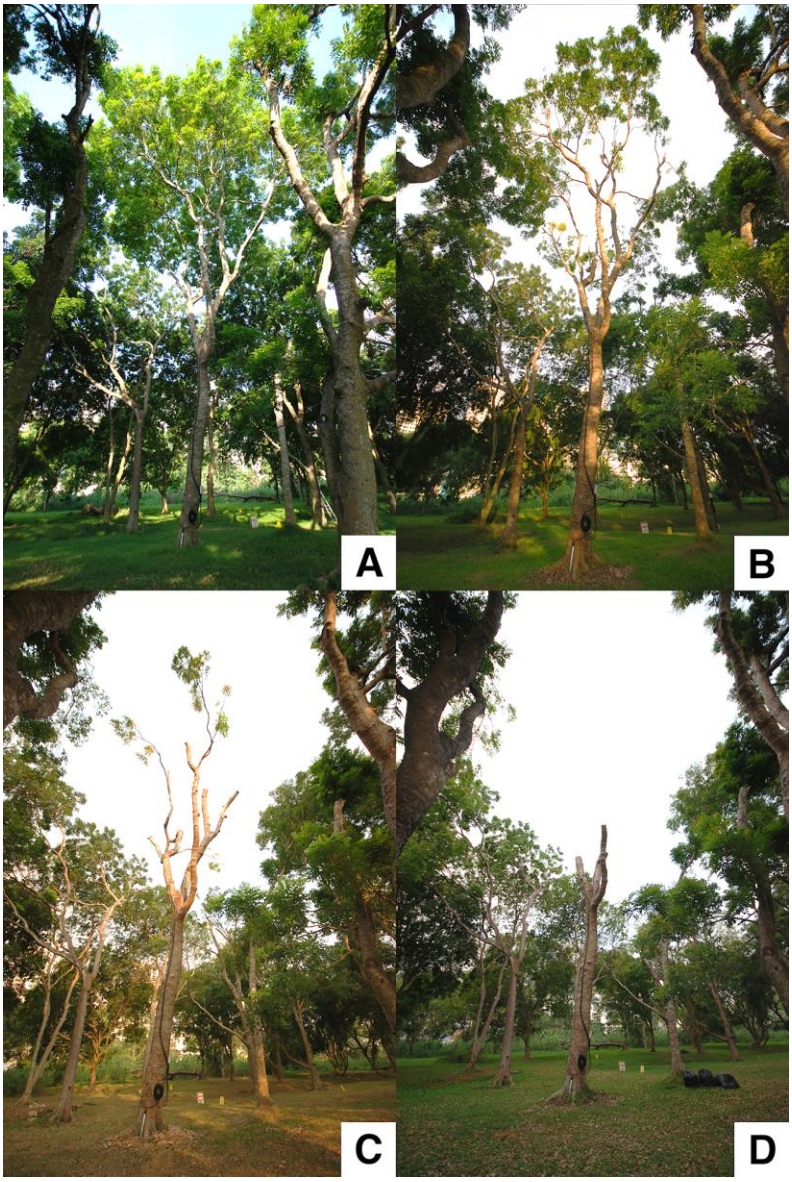

Figure 68: Photographs of Senegal mahogany (*Khaya senegalensis*) number 2 reduced by (**A**) 0%, (**B**) 20%, (**C**) 40%, and (**D**) 80%.

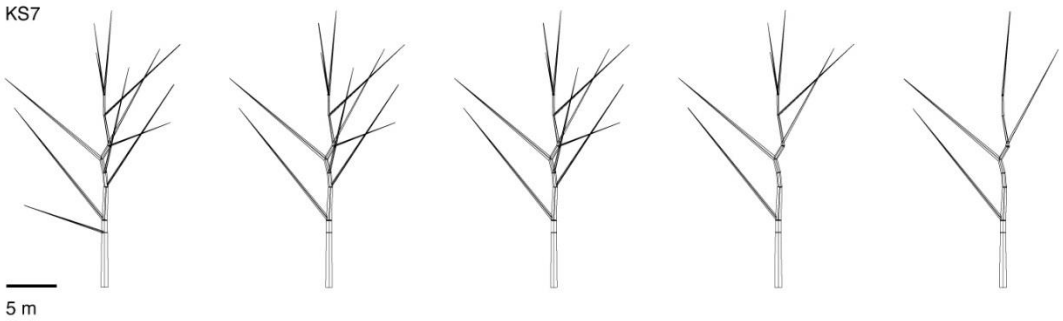

Figure 69: Crown architecture models showing the dimensions and arrangement of primary branches on Senegal mahogany (*Khaya senegalensis*) number 7 raised by 0%, 10%, 20%, 40%, and 80% (L – R).

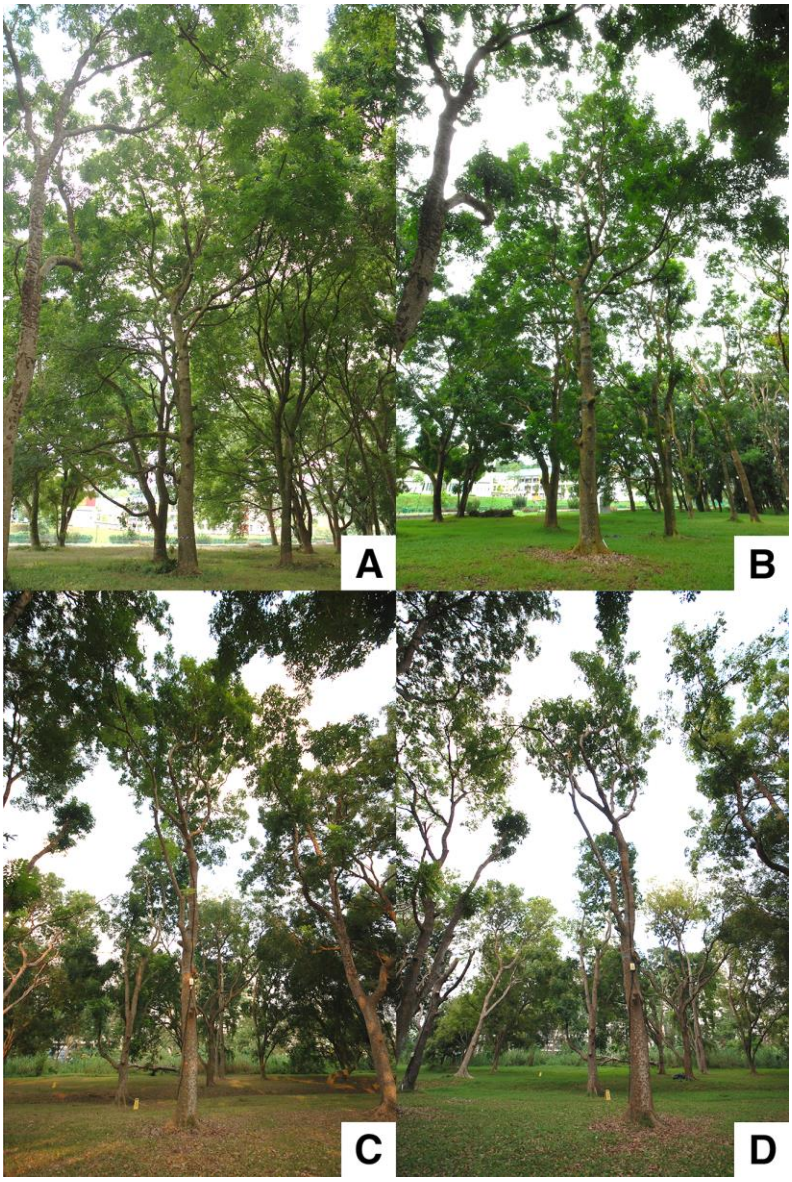

Figure 70: Photographs of Senegal mahogany (*Khaya senegalensis*) number 7 raised by (**A**) 0%, (**B**) 20%, (**C**) 40%, and (**D**) 80%.

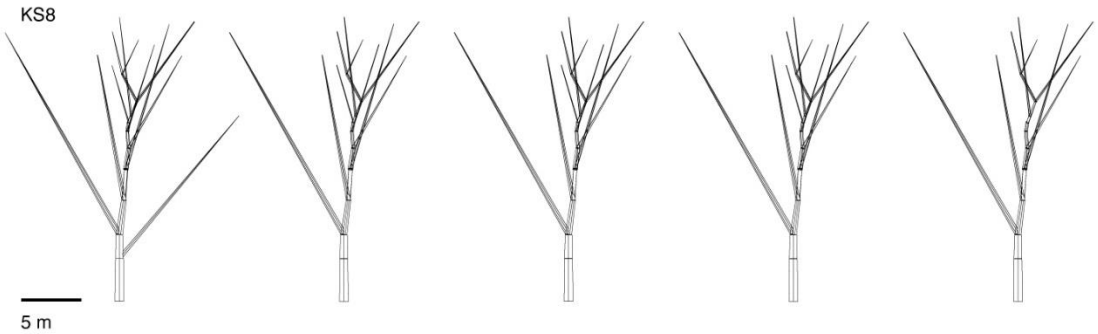

Figure 71: Crown architecture models showing the dimensions and arrangement of primary branches on Senegal mahogany (*Khaya senegalensis*) number 8 raised by 0%, 10%, 20%, 40%, and 80% (L – R).

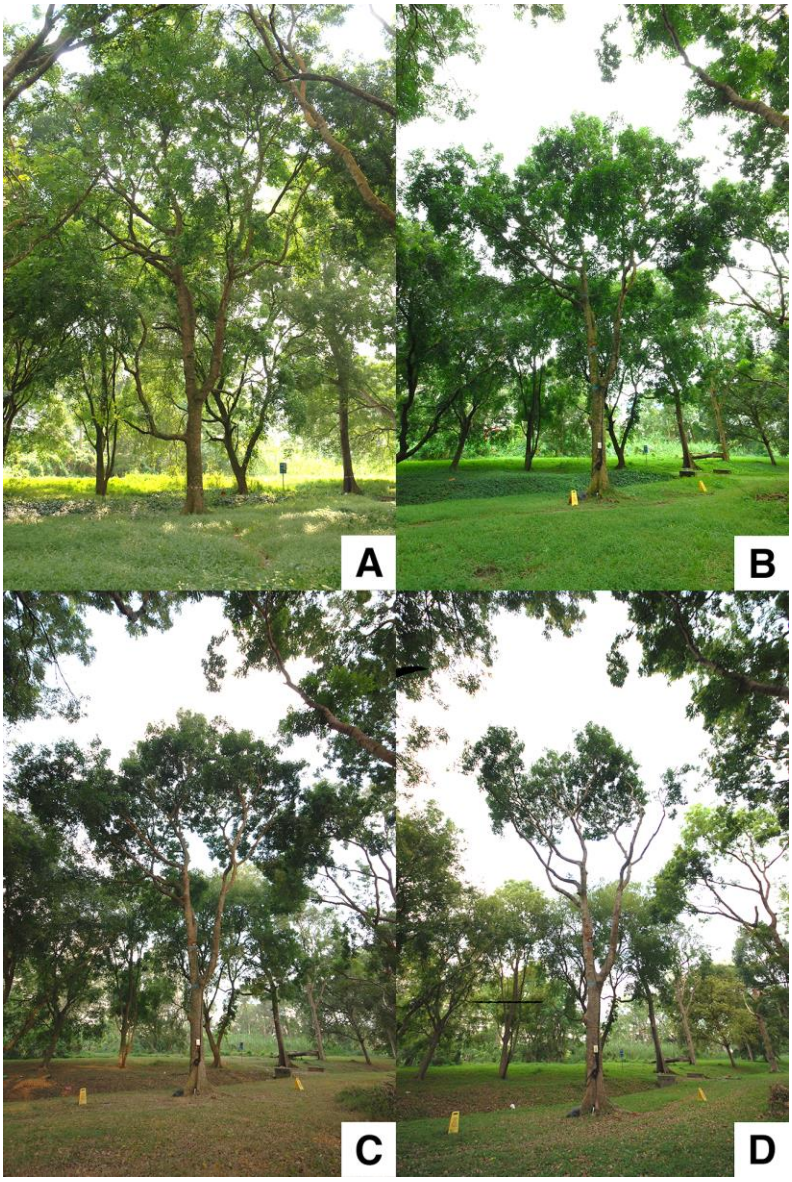

Figure 72: Photographs of Senegal mahogany (*Khaya senegalensis*) number 8 raised by (**A**) 0%, (**B**) 20%, (**C**) 40%, and (**D**) 80%.

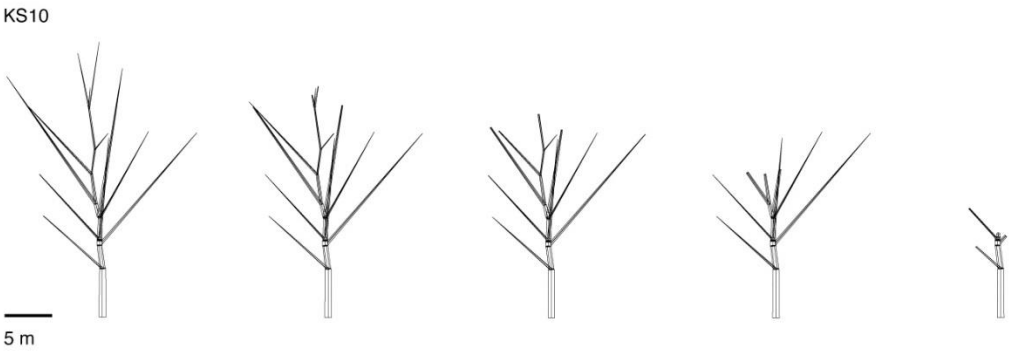

Figure 73: Crown architecture models showing the dimensions and arrangement of primary branches on Senegal mahogany (*Khaya senegalensis*) number 10 reduced by 0%, 10%, 20%, 40%, and 80% (L – R).

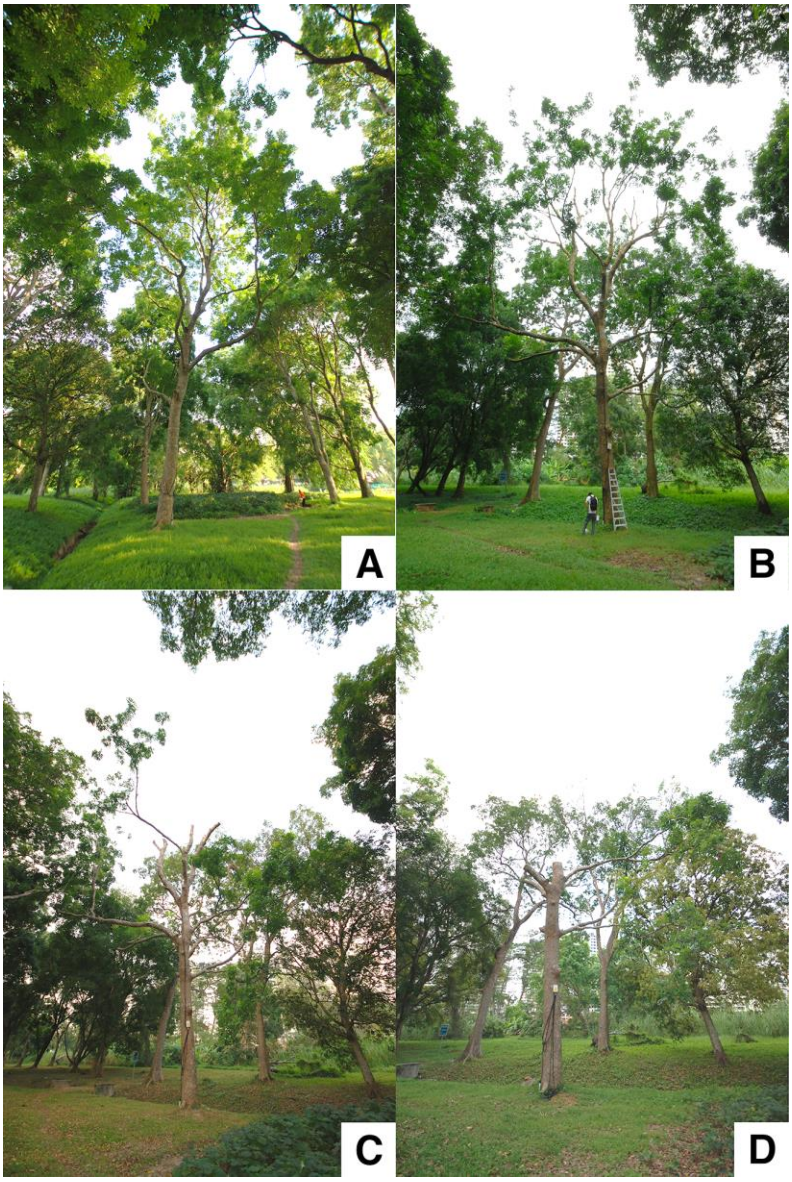

Figure 74: Photographs of Senegal mahogany (*Khaya senegalensis*) number 10 reduced by (**A**) 0%, (**B**) 20%, (**C**) 40%, and (**D**) 80%.

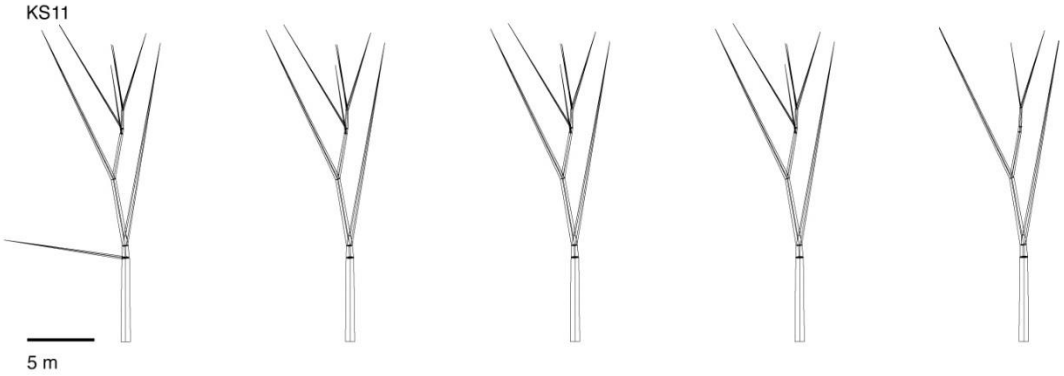

Figure 75: Crown architecture models showing the dimensions and arrangement of primary branches on Senegal mahogany (*Khaya senegalensis*) number 11 raised by 0%, 10%, 20%, 40%, and 80% (L – R).

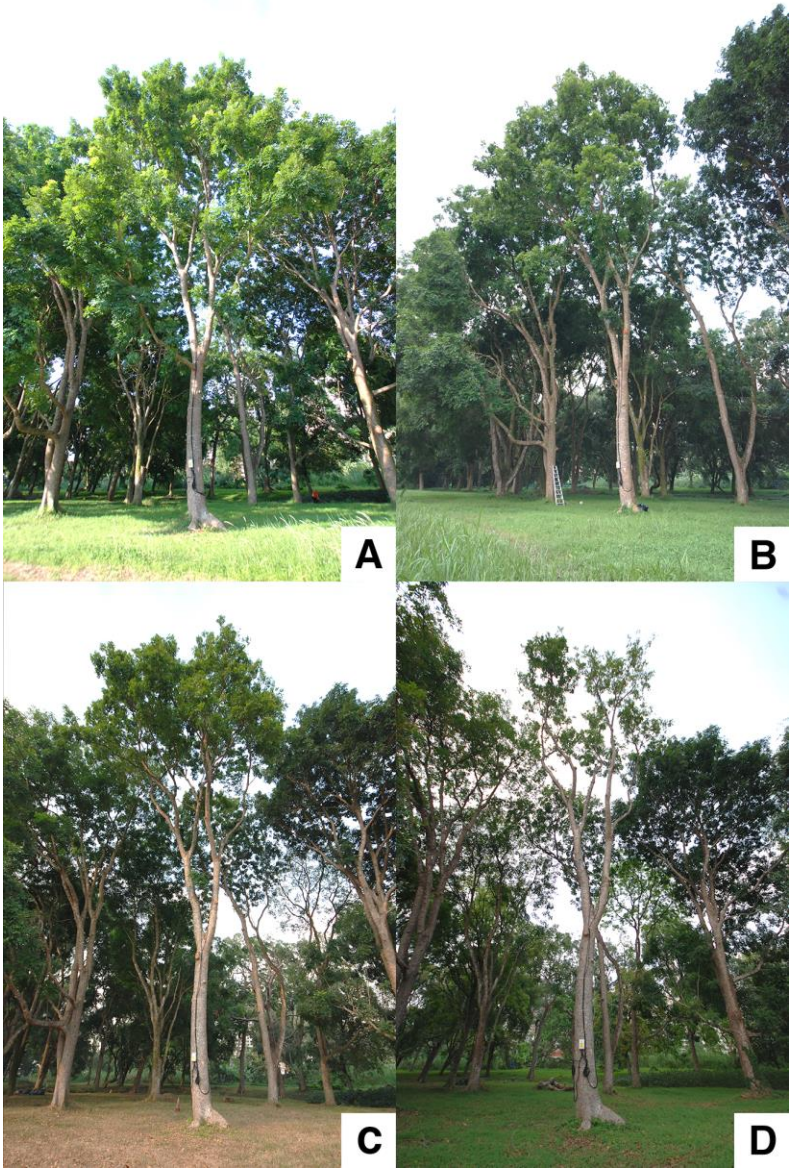

Figure 76: Photographs of Senegal mahogany (*Khaya senegalensis*) number 11 raised by (**A**) 0%, (**B**) 20%, (**C**) 40%, and (**D**) 80%.

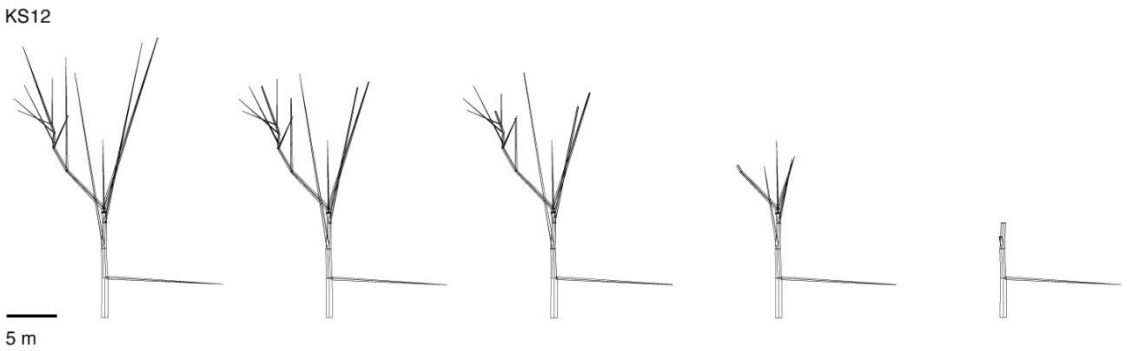

Figure 77: Crown architecture models showing the dimensions and arrangement of primary branches on Senegal mahogany (*Khaya senegalensis*) number 12 reduced by 0%, 10%, 20%, 40%, and 80% (L – R).

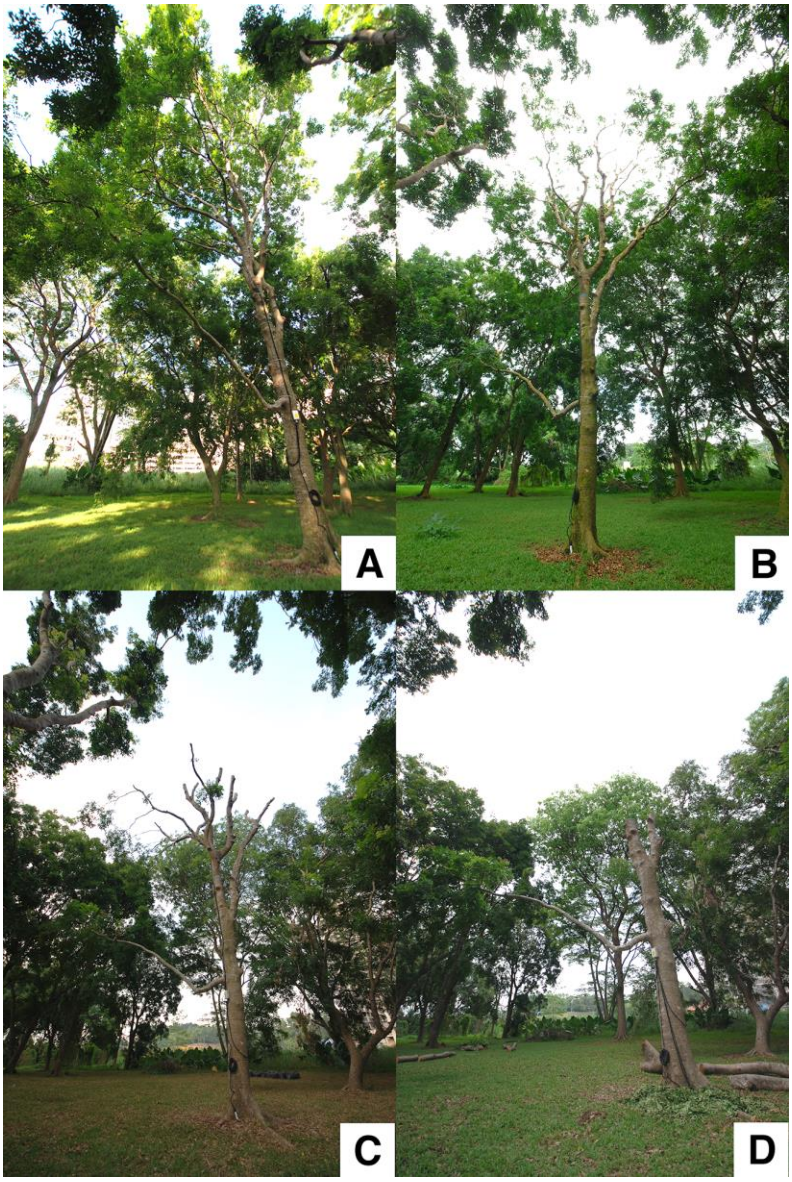

Figure 78: Photographs of Senegal mahogany (*Khaya senegalensis*) number 12 reduced by (**A**) 0%, (**B**) 20%, (**C**) 40%, and (**D**) 80%.

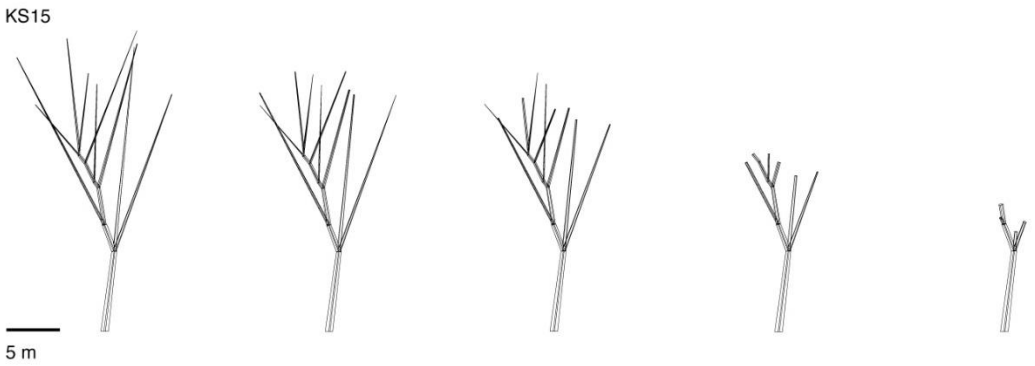

Figure 79: Crown architecture models showing the dimensions and arrangement of primary branches on Senegal mahogany (*Khaya senegalensis*) number 15 reduced by 0%, 10%, 20%, 40%, and 80% (L – R).

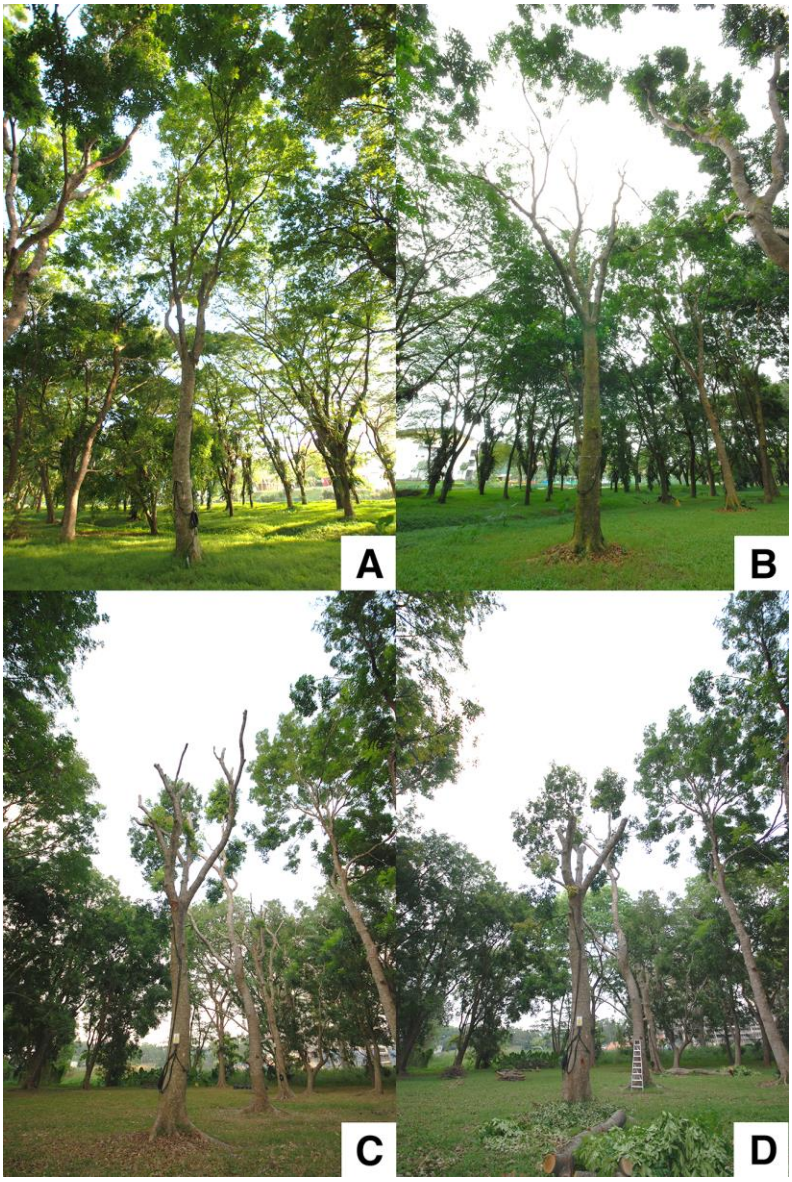

Figure 80: Photographs of Senegal mahogany (*Khaya senegalensis*) number 15 reduced by (**A**) 0%, (**B**) 20%, (**C**) 40%, and (**D**) 80%.

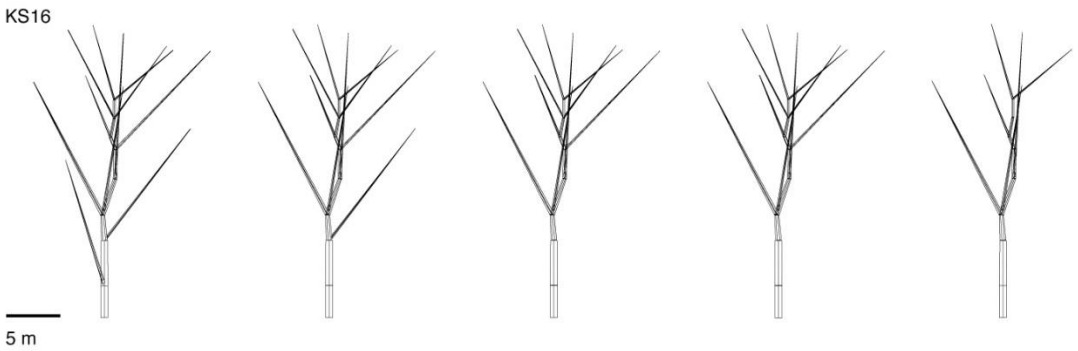

Figure 81: Crown architecture models showing the dimensions and arrangement of primary branches on Senegal mahogany (*Khaya senegalensis*) number 16 raised by 0%, 10%, 20%, 40%, and 80% (L – R).

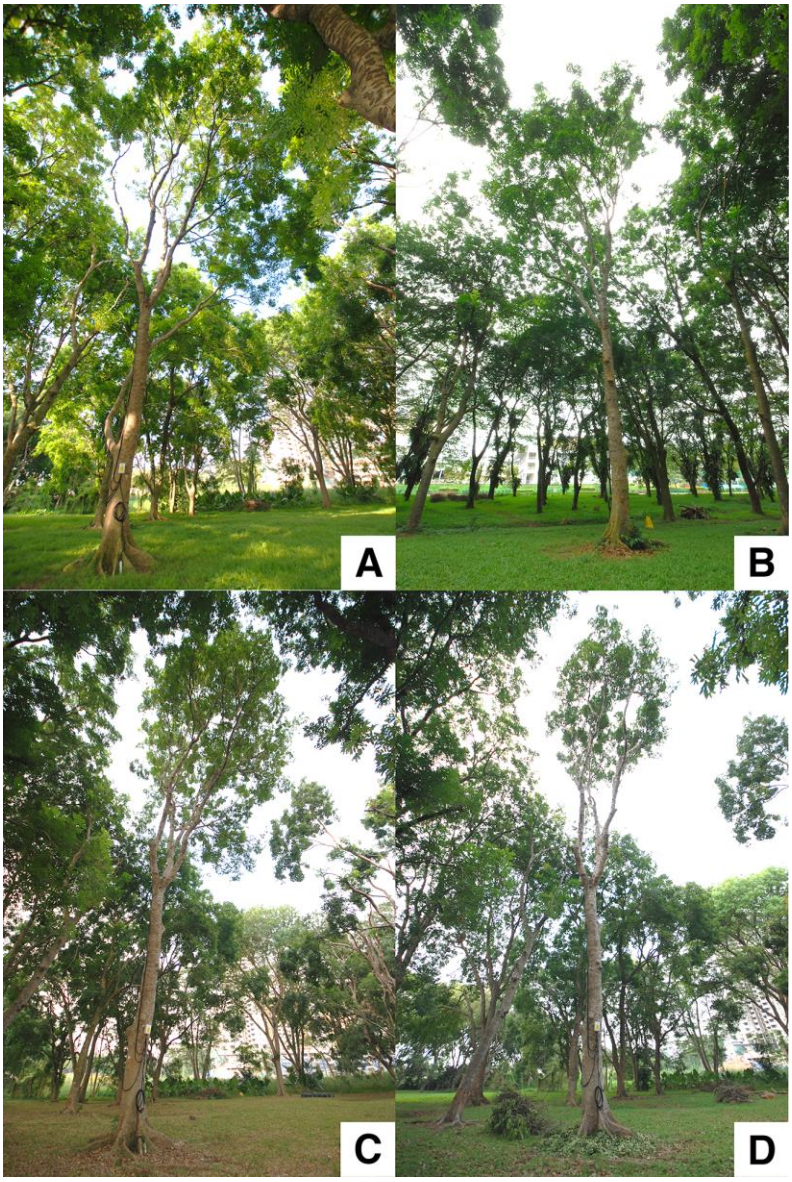

Figure 82: Photographs of Senegal mahogany (*Khaya senegalensis*) number 16 raised by (**A**) 0%, (**B**) 20%, (**C**) 40%, and (**D**) 80%.

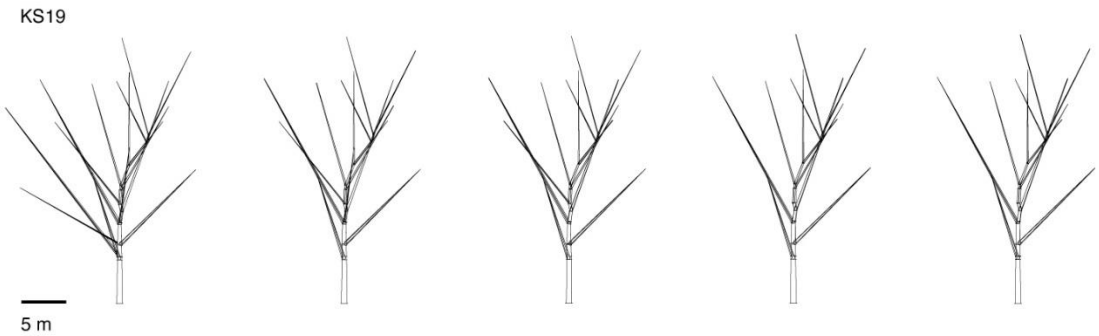

Figure 83: Crown architecture models showing the dimensions and arrangement of primary branches on Senegal mahogany (*Khaya senegalensis*) number 19 raised by 0%, 10%, 20%, 40%, and 80% (L – R).

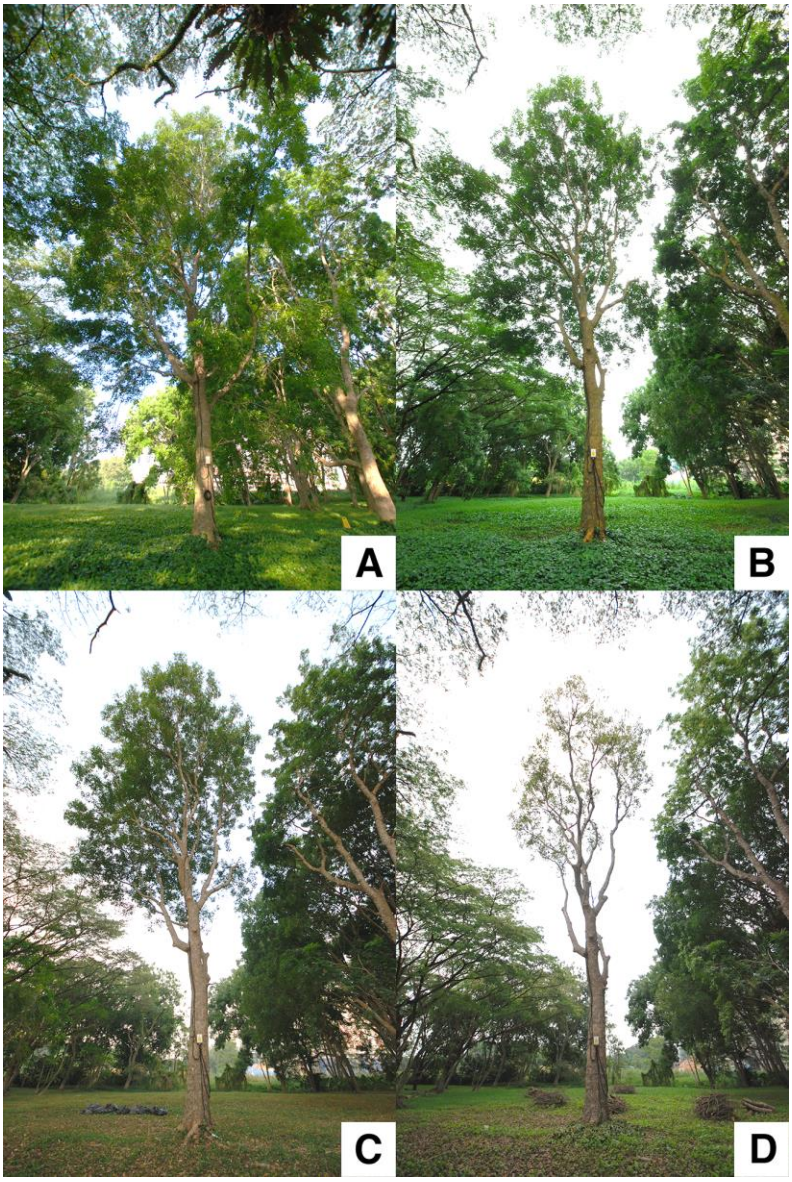

Figure 84: Photographs of Senegal mahogany (*Khaya senegalensis*) number 19 raised by (**A**) 0%, (**B**) 20%, (**C**) 40%, and (**D**) 80%.

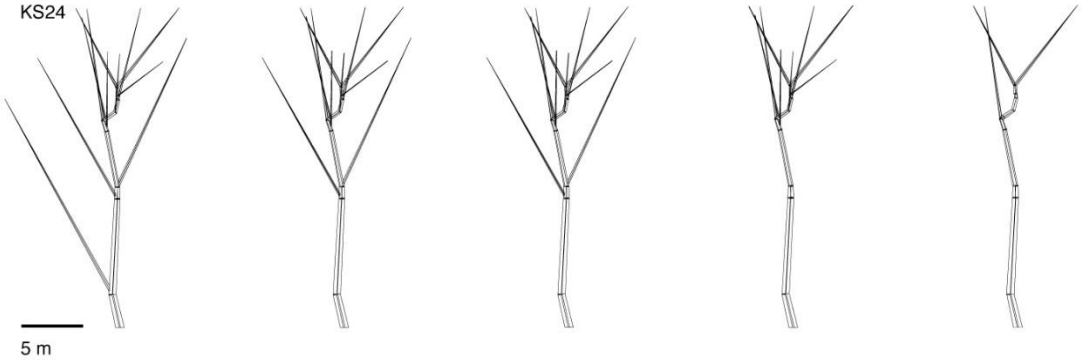

Figure 85: Crown architecture models showing the dimensions and arrangement of primary branches on Senegal mahogany (*Khaya senegalensis*) number 24 raised by 0%, 10%, 20%, 40%, and 80% (L – R).

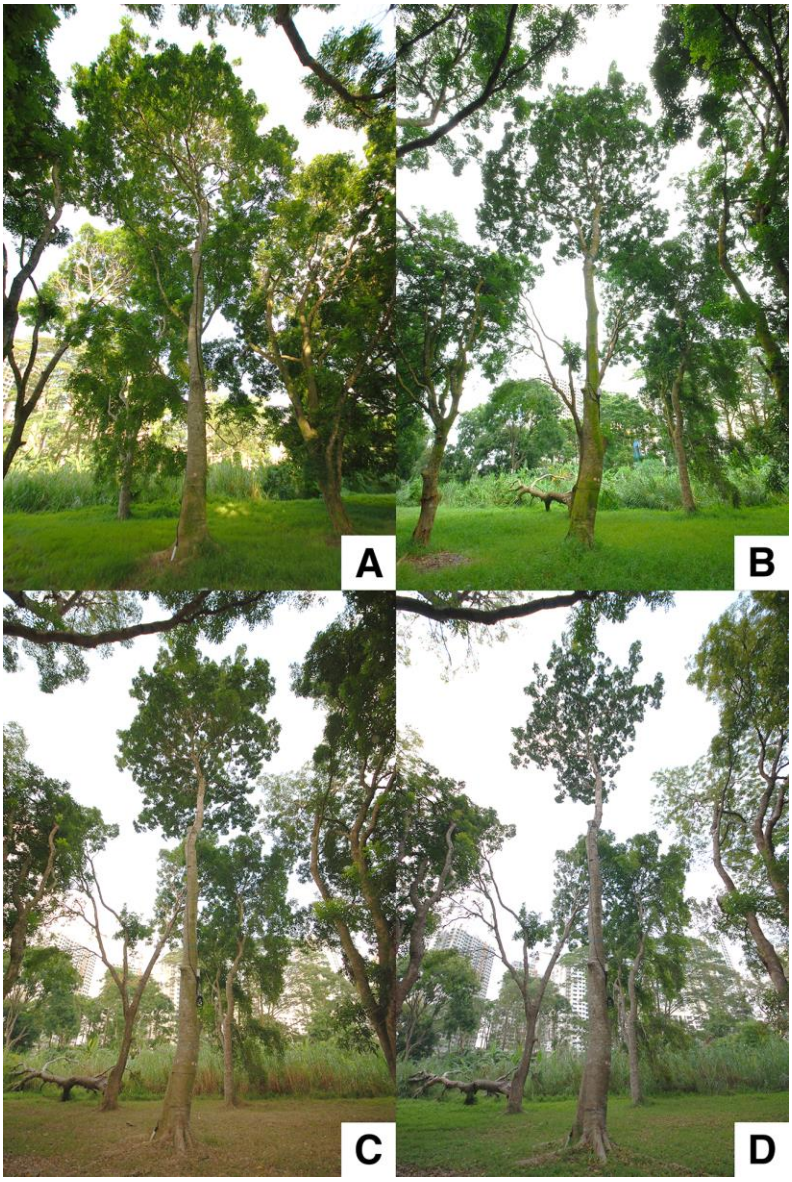

Figure 86: Photographs of Senegal mahogany (*Khaya senegalensis*) number 24 raised by (**A**) 0%, (**B**) 20%, (**C**) 40%, and (**D**) 80%.

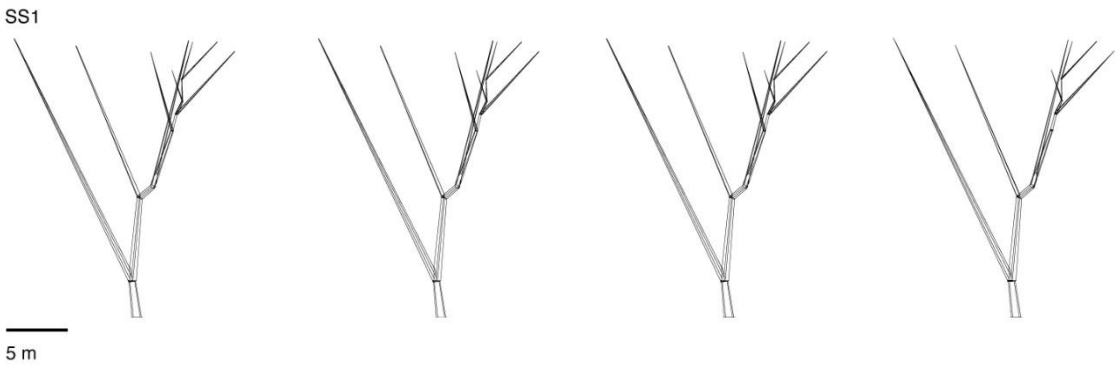

Figure 87: Crown architecture models showing the dimensions and arrangement of primary branches on rain tree (*Samanea saman*) number 1 raised by 0%, 20%, 40%, and 80% (L – R).

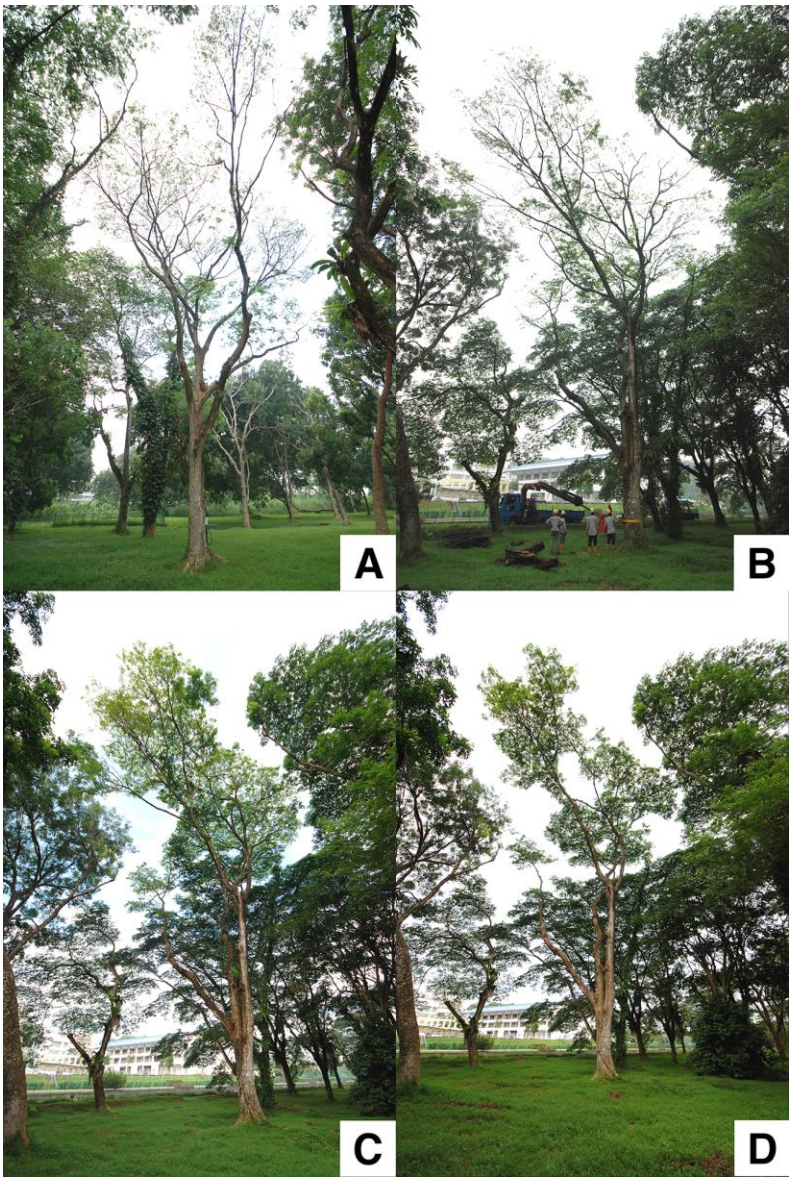

Figure 88: Photographs of rain tree (*Samanea saman*) number 1 raised by (**A**) 0%, (**B**) 20%, (**C**) 40%, and (**D**) 80%.

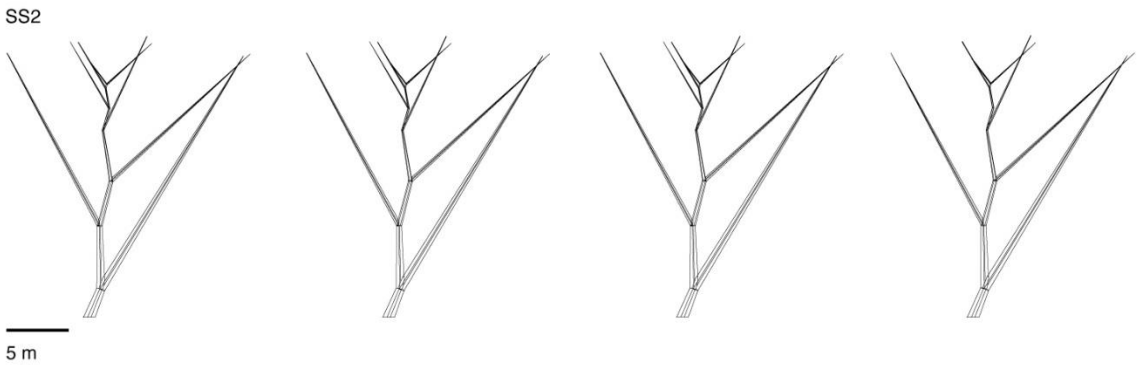

Figure 89: Crown architecture models showing the dimensions and arrangement of primary branches on rain tree (*Samanea saman*) number 2 raised by 0%, 20%, 40%, and 80% (L – R).

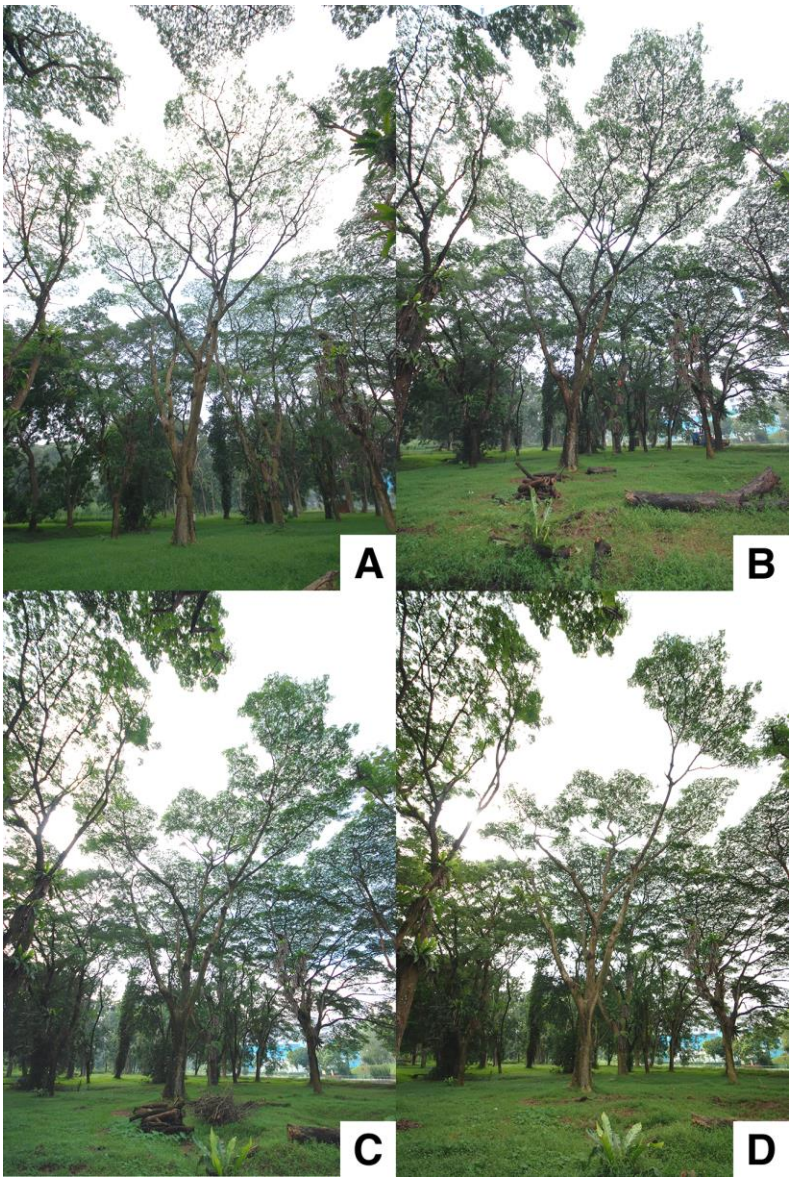

Figure 90: Photographs of rain tree (*Samanea saman*) number 2 raised by (**A**) 0%, (**B**) 20%, (**C**) 40%, and (**D**) 80%.

Figure 91: Crown architecture models showing the dimensions and arrangement of primary branches on rain tree (*Samanea saman*) number 3 reduced by 0%, 20%, 40%, and 80% (L – R).

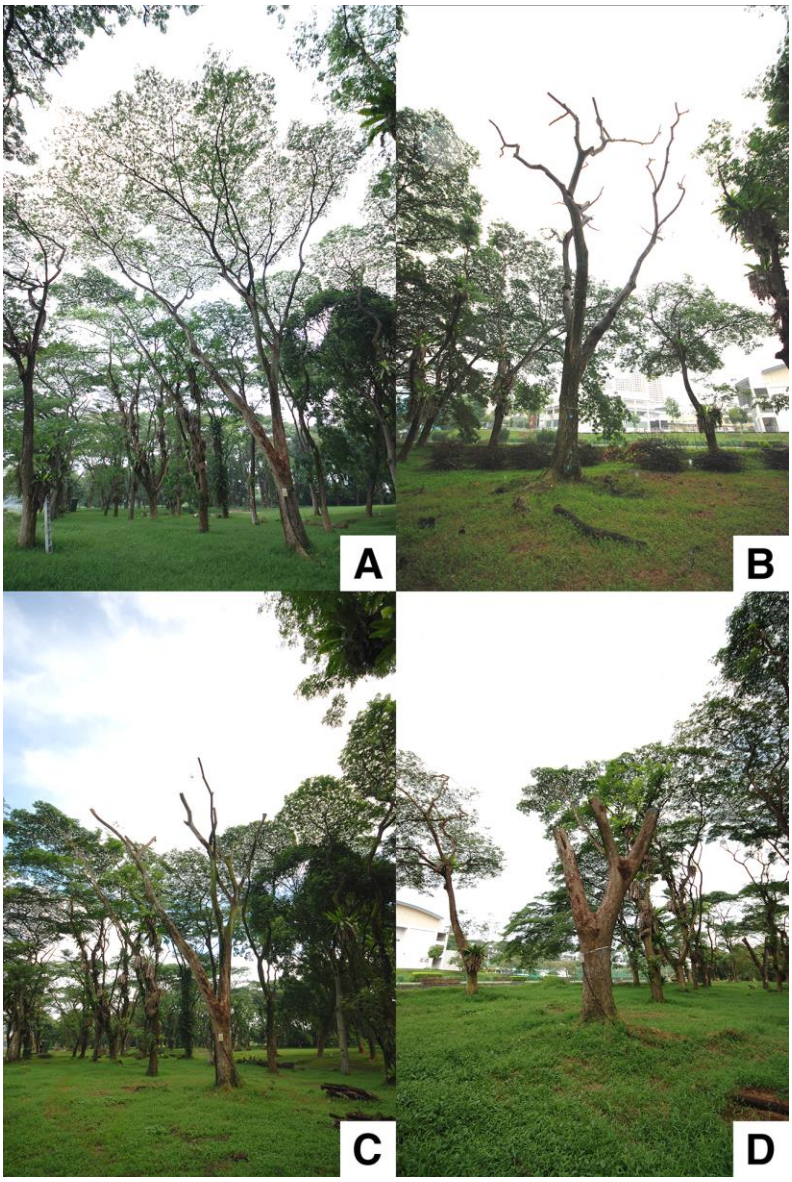

Figure 92: Photographs of rain tree (*Samanea saman*) number 3 reduced by (**A**) 0%, (**B**) 20%, (**C**) 40%, and (**D**) 80%.

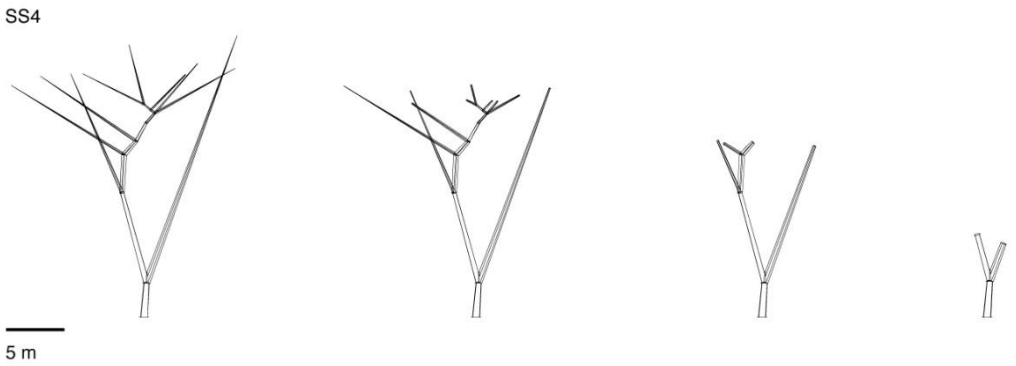

Figure 93: Crown architecture models showing the dimensions and arrangement of primary branches on rain tree (*Samanea saman*) number 4 reduced by 0%, 20%, 40%, and 80% (L – R).

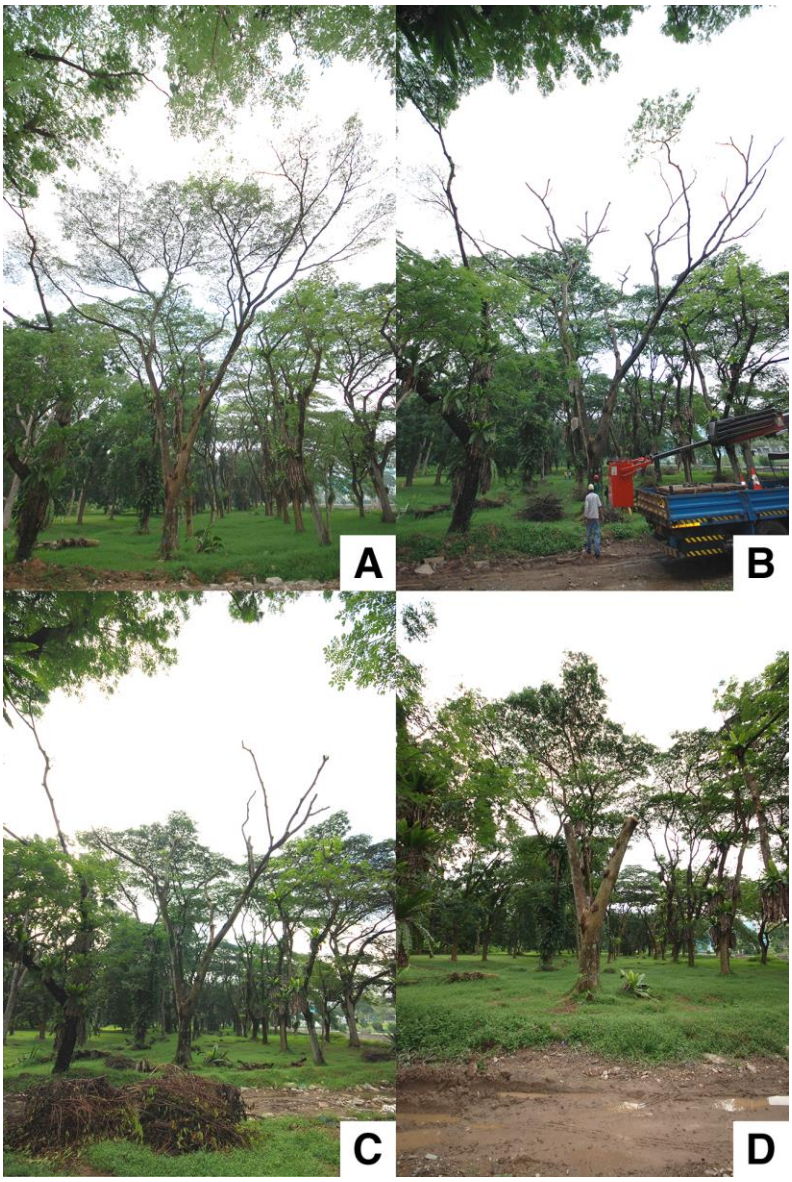

Figure 94: Photographs of rain tree (*Samanea saman*) number 4 reduced by (**A**) 0%, (**B**) 20%, (**C**) 40%, and (**D**) 80%.

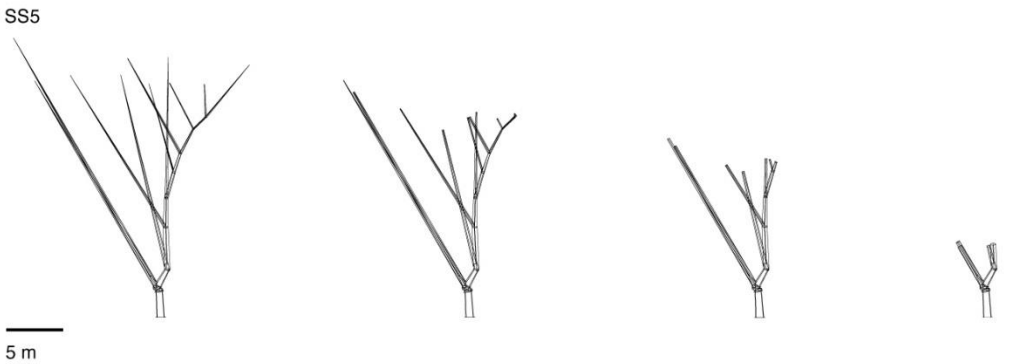

Figure 95: Crown architecture models showing the dimensions and arrangement of primary branches on rain tree (*Samanea saman*) number 5 reduced by 0%, 20%, 40%, and 80% (L – R).

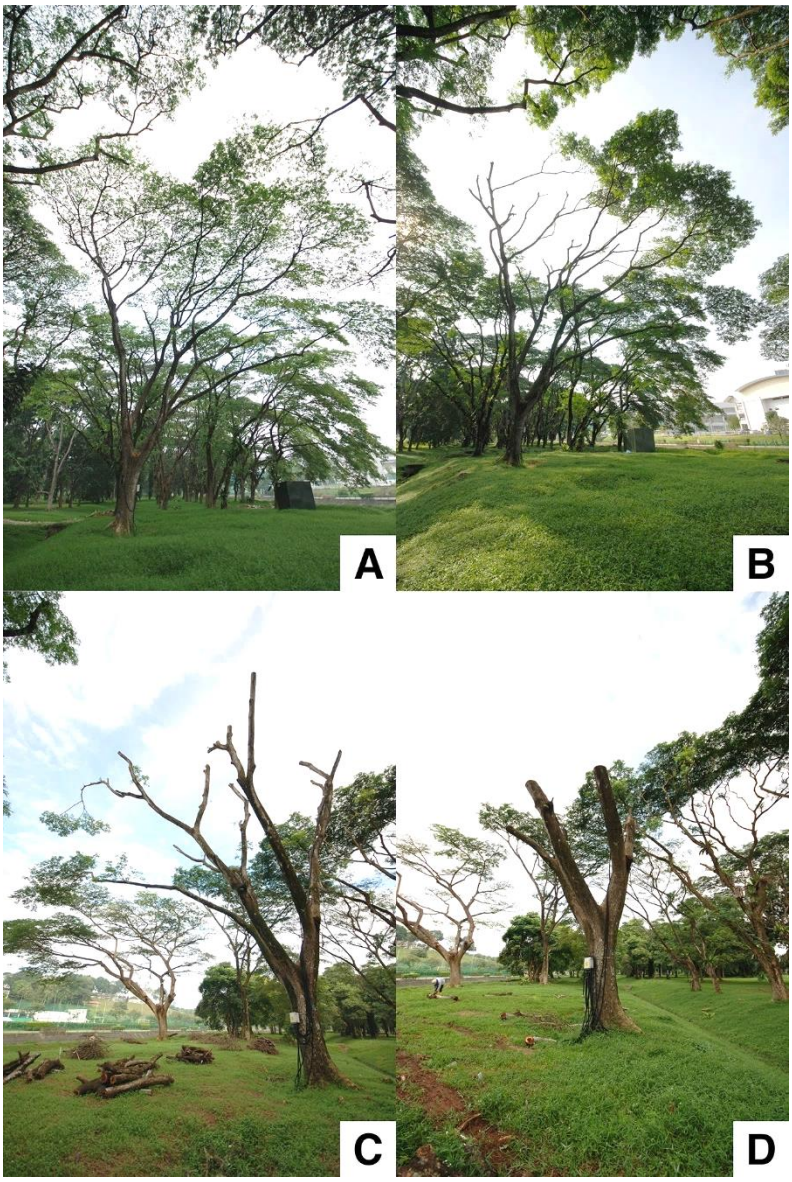

Figure 96: Photographs of rain tree (*Samanea saman*) number 5 reduced by (**A**) 0%, (**B**) 20%, (**C**) 40%, and (**D**) 80%.

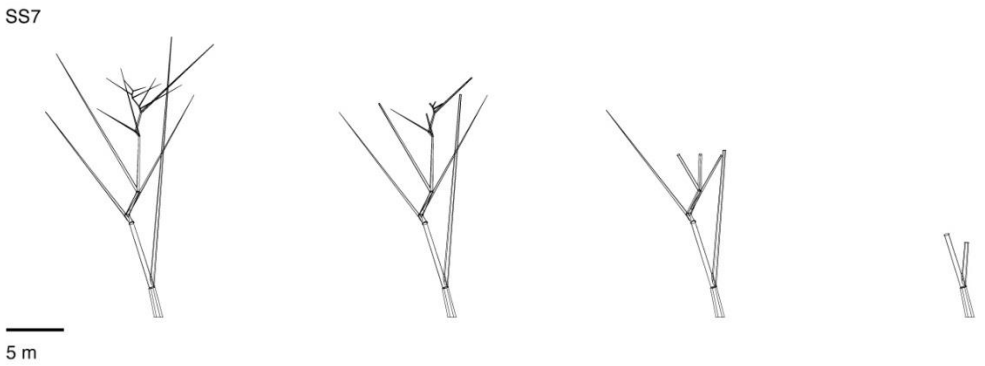

Figure 97: Crown architecture models showing the dimensions and arrangement of primary branches on rain tree (*Samanea saman*) number 7 reduced by 0%, 20%, 40%, and 80% (L – R).

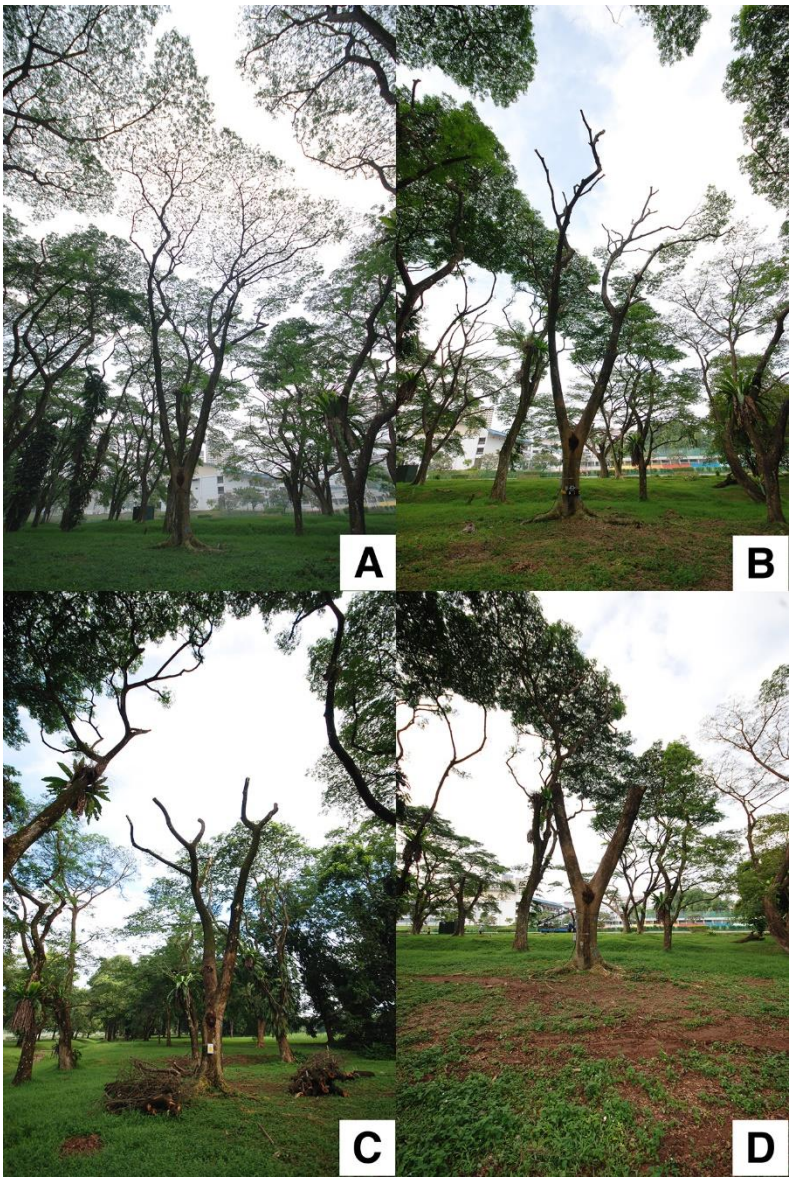

Figure 98: Photographs of rain tree (*Samanea saman*) number 7 reduced by (**A**) 0%, (**B**) 20%, (**C**) 40%, and (**D**) 80%.

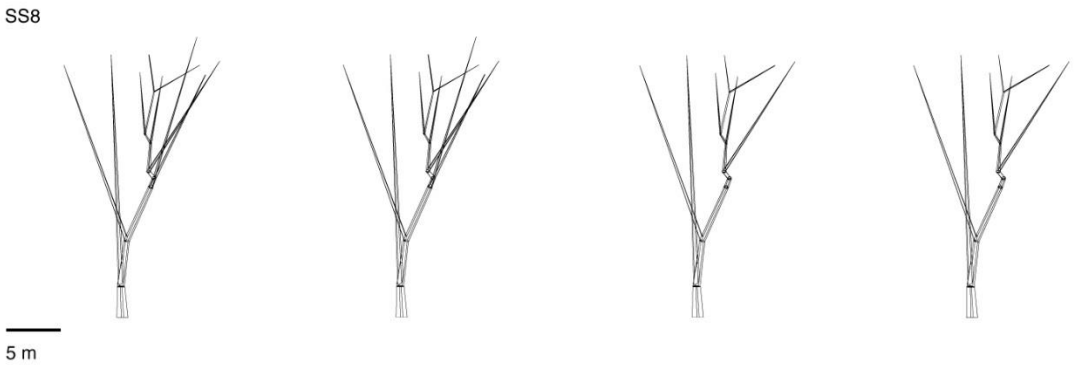

Figure 99: Crown architecture models showing the dimensions and arrangement of primary branches on rain tree (*Samanea saman*) number 8 raised by 0%, 20%, 40%, and 80% (L – R).

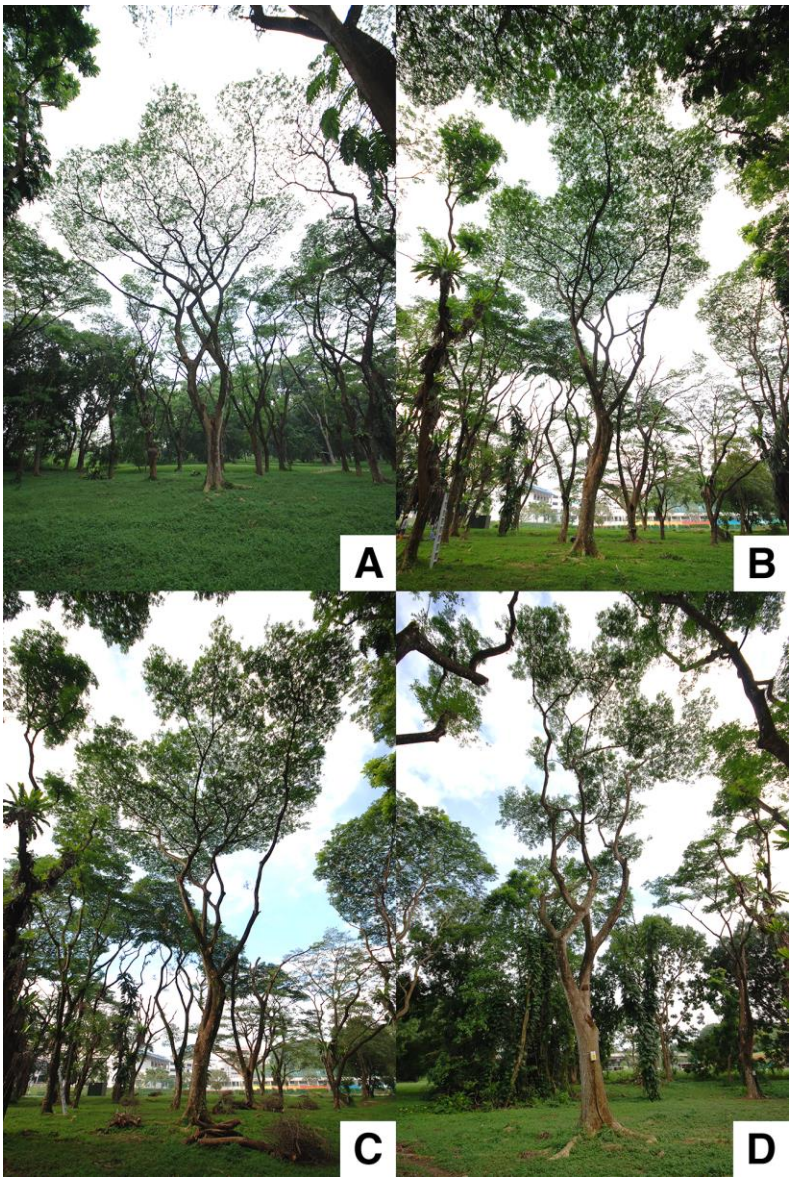

Figure 100: Photographs of rain tree (*Samanea saman*) number 8 raised by (**A**) 0%, (**B**) 20%, (**C**) 40%, and (**D**) 80%.

Figure 101: Crown architecture models showing the dimensions and arrangement of primary branches on rain tree (*Samanea saman*) number 9 raised by 0%, 20%, 40%, and 80% (L – R).

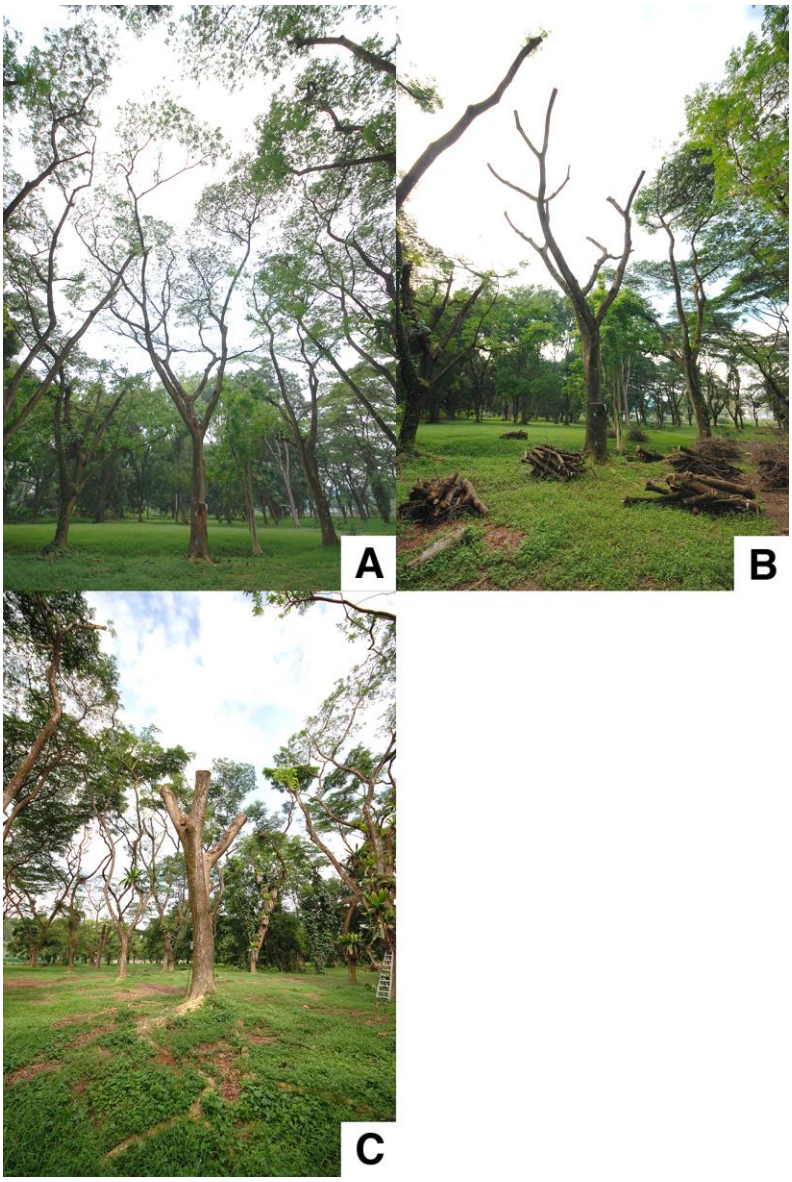

Figure 102: Photographs of rain tree (*Samanea saman*) number 9 reduced by (**A**) 0%, (**B**) 40%, and (**C**) 80%.

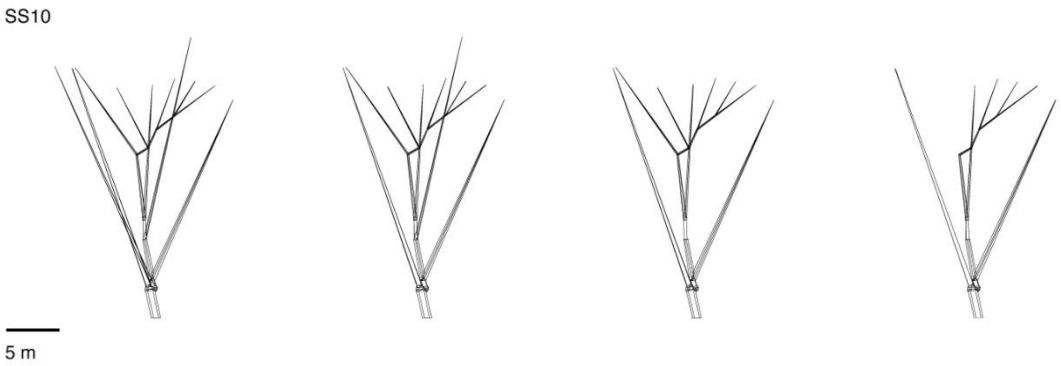

Figure 103: Crown architecture models showing the dimensions and arrangement of primary branches on rain tree (*Samanea saman*) number 10 raised by 0%, 20%, 40%, and 80% (L – R).

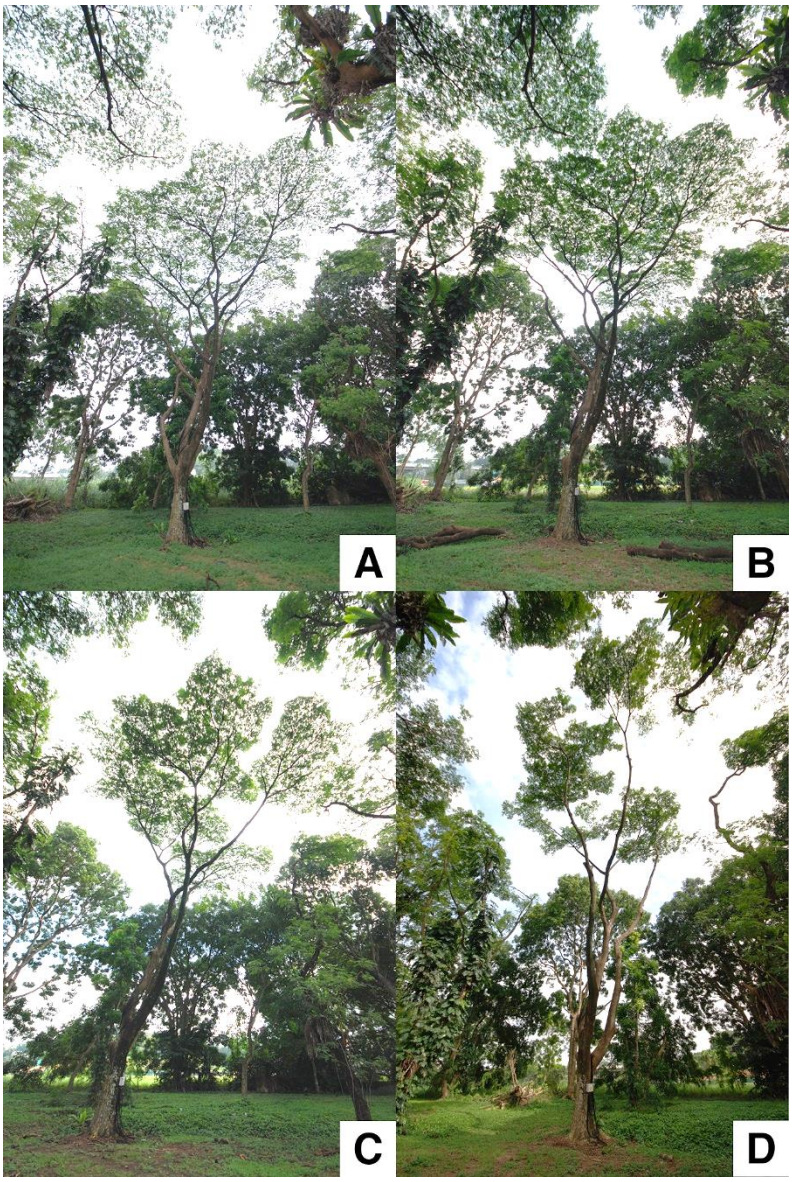

Figure 104: Photographs of rain tree (*Samanea saman*) number 10 raised by (**A**) 0%, (**B**) 20%, (**C**) 40%, and (**D**) 80%.

APPENDIX B

SCATTER PLOTS FOR 30-MINUTE MAXIMUM BENDING MOMENT AND 30-MINUTE MAXIMUM WIND SPEED FOR ALL SENEGAL MAHOGANIES

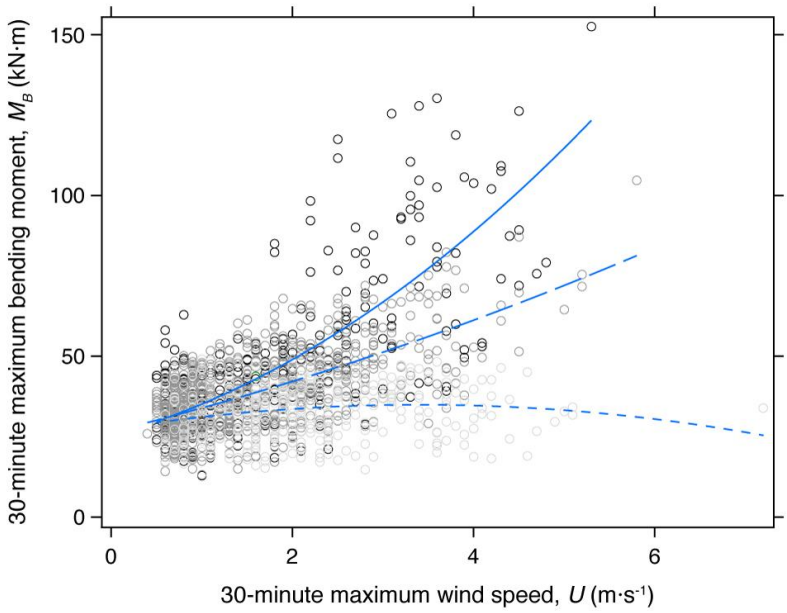

Figure 105: Scatter plot and best-fit lines of the 30-minute maximum bending moment, M_B (kN·m), against 30-minute maximum wind speed, U (m·s^{-1}), measured 18.3 m above ground (z/H_{TREE} = 0.69) for Senegal mahogany (*Khaya senegalensis*) tree number 1 reduced by 0% (black empty circle marker, solid line), 10% (dark gray empty circle marker, long dash line), and 20% (light gray empty circle marker, short dash line). At 0%, 10%, and 20% severity, least squares regression equations are $y = 2.02\ x^2 + 7.80\ x + 25.3$ (n = 288; R^2 = 0.56), $y = 0.43\ x^2 + 6.96\ x + 26.5$ (n = 825; R^2 = 0.41), and $y = -0.66\ x^2 + 4.49\ x + 27.3$ (n = 370; R^2 = 0.03), respectively.

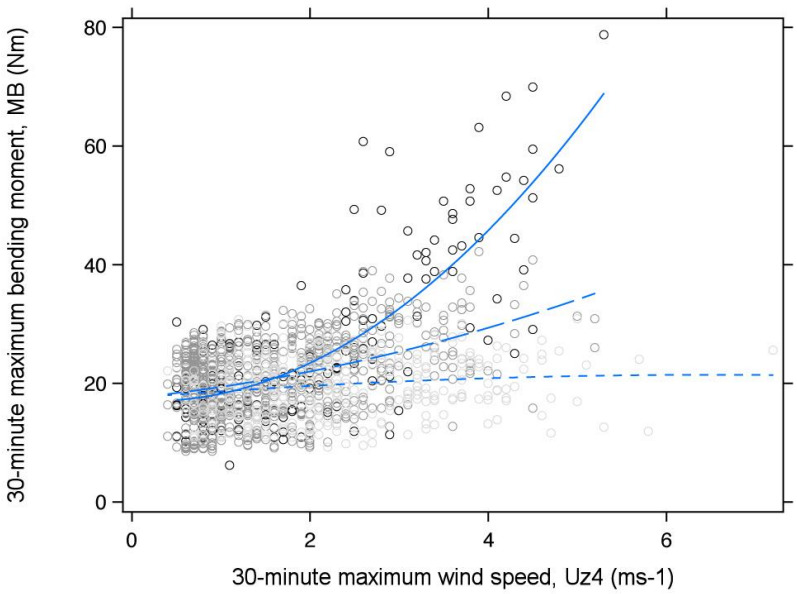

Figure 106: Scatter plot and best-fit lines of the 30-minute maximum bending moment, M_B (kN·m), against 30-minute maximum wind speed, U (m·s^{-1}), measured 18.3 m above ground (z/H_{TREE} = 0.69) for Senegal mahogany (*Khaya senegalensis*) tree number 2 reduced by 0% (black empty circle marker, solid line), 10% (dark gray empty circle marker, long dash line), and 20% (light gray empty circle marker, short dash line). At 0%, 10%, and 20% severity, least squares regression equations are $y = 2.00\ x^2 - 0.85\ x + 17.1$ (n = 180; R^2 = 0.63), $y = 0.36\ x^2 + 1.53\ x + 17.5$ (n = 729; R^2 = 0.18), and $y = -0.09\ x^2 + 1.20\ x + 17.5$ (n = 449; R^2 = 0.03), respectively.

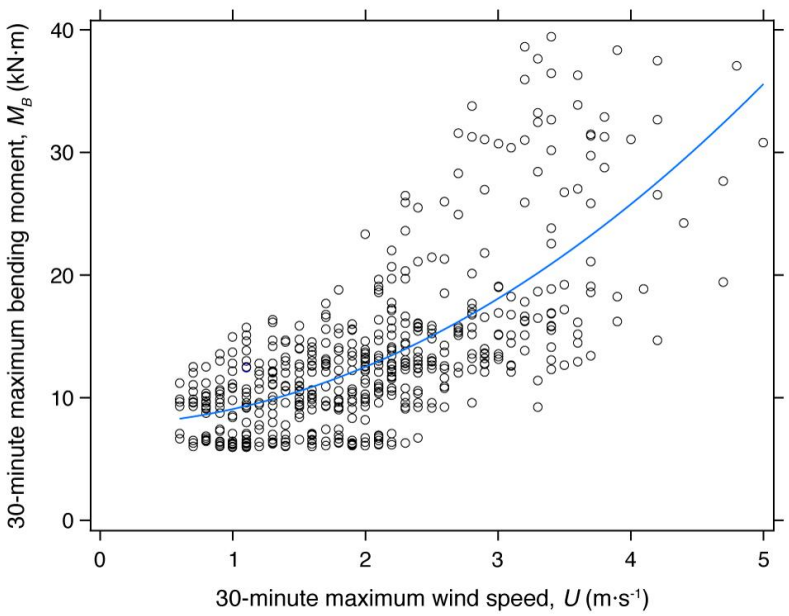

Figure 107: Scatter plot and best-fit lines of the 30-minute maximum bending moment, M_B (kN·m), against 30-minute maximum wind speed, U (m·s^{-1}), measured 18.3 m above ground (z/H_{TREE} = 0.69) for Senegal mahogany (*Khaya senegalensis*) tree number 7 reduced by 20%. Due to instrumentation failures, no observations were available at 0% and 10% severity for this tree. Least squares regression equation is $y = 1.06\,x^2 + 0.26\,x + 7.75$ (n = 507; R^2 = 0.48).

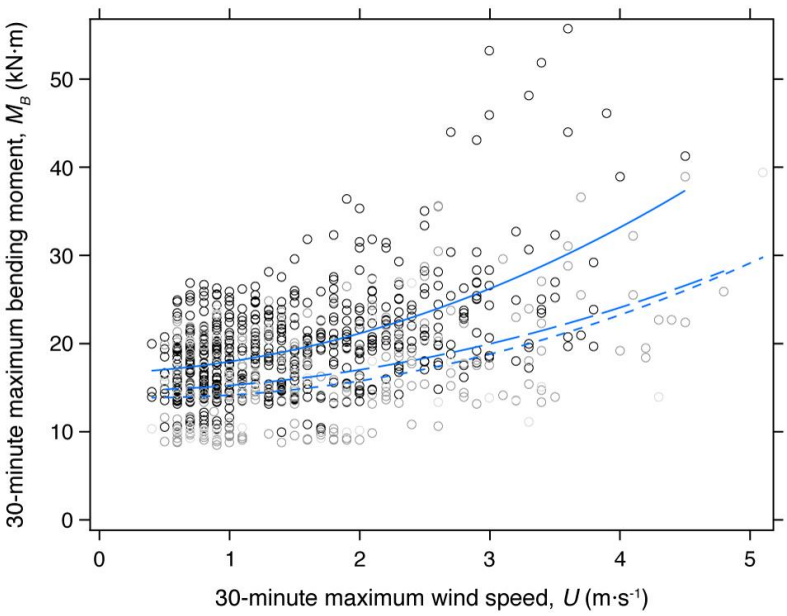

Figure 108: Scatter plot and best-fit lines of the 30-minute maximum bending moment, M_B (kN·m), against 30-minute maximum wind speed, U (m·s^{-1}), measured 18.3 m above ground (z/H_{TREE} = 0.69) for Senegal mahogany (*Khaya senegalensis*) tree number 8 raised by 0% (black empty circle marker, solid line), 10% (dark gray empty circle marker, long dash line), and 20% (light gray empty circle marker, short dash line). At 0%, 10%, and 20% severity, least squares regression equations are $y = 0.94\ x^2 + 0.40\ x + 16.6$ (n = 551; R^2 = 0.29), $y = 0.59\ x^2 + 0.01\ x + 14.7$ (n = 243; R^2 = 0.20), and $y = 0.71\ x^2 – 0.53\ x + 14.0$ (n = 48; R^2 = 0.26), respectively.

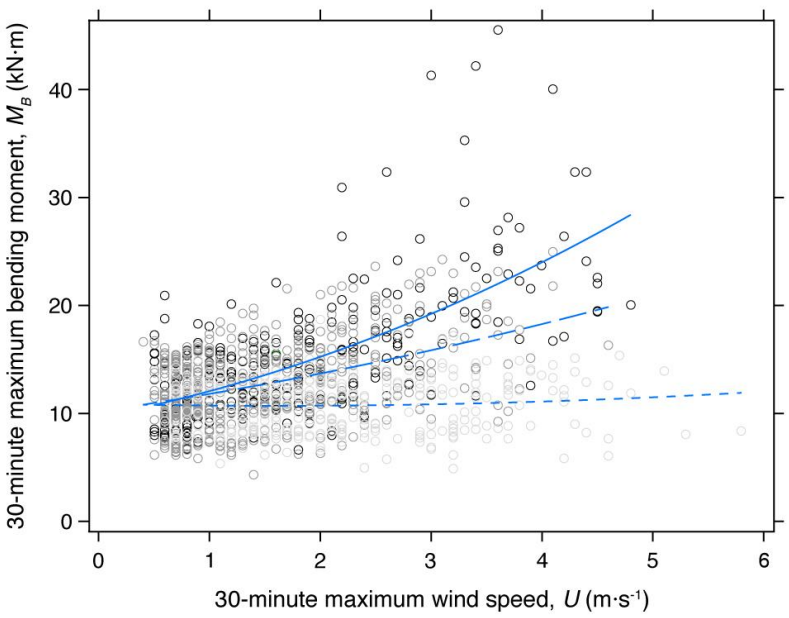

Figure 109: Scatter plot and best-fit lines of the 30-minute maximum bending moment, M_B (kN·m), against 30-minute maximum wind speed, U (m·s^{-1}), measured 18.3 m above ground (z/H_{TREE} = 0.69) for Senegal mahogany (*Khaya senegalensis*) tree number 10 reduced by 0% (black empty circle marker, solid line), 10% (dark gray empty circle marker, long dash line), and 20% (light gray empty circle marker, short dash line). At 0%, 10%, and 20% severity, least squares regression equations are $y = 0.70\ x^2 + 0.61\ x + 9.67$ (n = 230; R^2 = 0.52), $y = 1.00\ x^2 + 0.38\ x + 11.2$ (n = 312; R^2 = 0.48), and $y = 0.81\ x^2 – 1.83\ x + 9.55$ (n = 278; R^2 = 0.38), respectively.

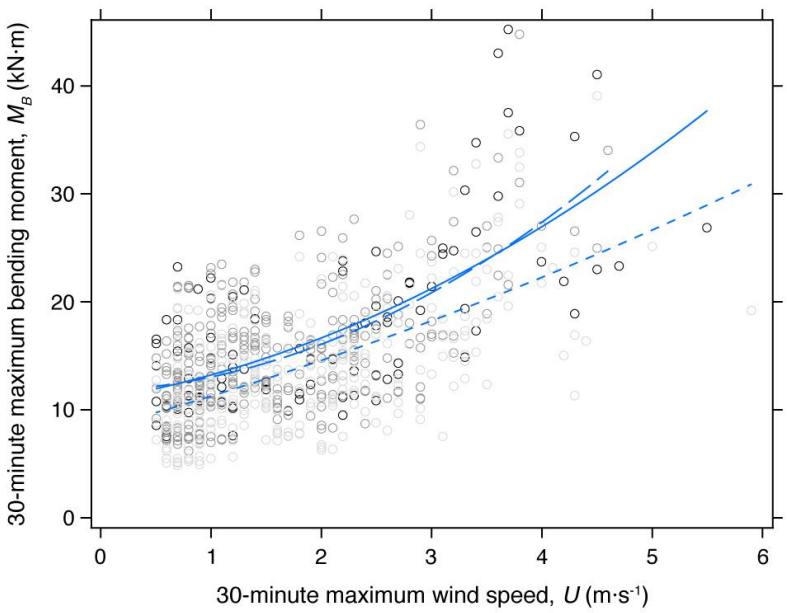

Figure 110: Scatter plot and best-fit lines of the 30-minute maximum bending moment, M_B (kN·m), against 30-minute maximum wind speed, U (m·s^{-1}), measured 18.3 m above ground (z/H_{TREE} = 0.69) for Senegal mahogany (*Khaya senegalensis*) tree number 11 raised by 0% (black empty circle marker, solid line), 10% (dark gray empty circle marker, long dash line), and 20% (light gray empty circle marker, short dash line). At 0%, 10%, and 20% severity, least squares regression equations are $y = 0.58\ x^2 + 1.69\ x + 11.0$ (n = 109; R^2 = 0.48), $y = 0.87\ x^2 + 0.41\ x + 11.7$ (n = 288; R^2 = 0.36), and $y = 0.18\ x^2 + 2.78\ x + 8.31$ (n = 297; R^2 = 0.36), respectively.

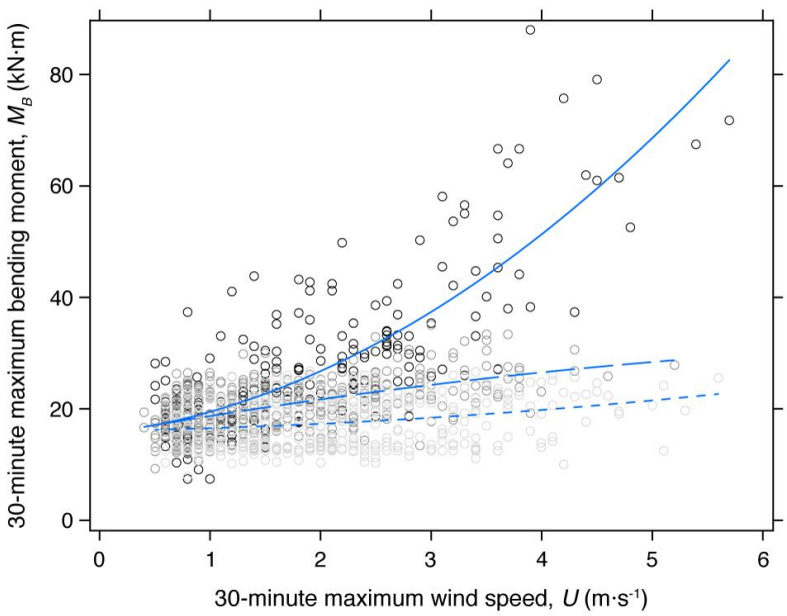

Figure 111: Scatter plot and best-fit lines of the 30-minute maximum bending moment, M_B (kN·m), against 30-minute maximum wind speed, U (m·s^{-1}), measured 18.3 m above ground (z/H_{TREE} = 0.69) for Senegal mahogany (*Khaya senegalensis*) tree number 12 reduced by 0% (black empty circle marker, solid line), 10% (dark gray empty circle marker, long dash line), and 20% (light gray empty circle marker, short dash line). At 0%, 10%, and 20% severity, least squares regression equations are $y = 1.66\ x^2 + 2.32\ x + 15.5$ (n = 233; R^2 = 0.64), $y = -0.19\ x^2 + 3.54\ x + 15.4$ (n = 386; R^2 = 0.32), and $y = 0.15\ x^2 + 0.33\ x + 16.1$ (n = 441; R^2 = 0.06), respectively.

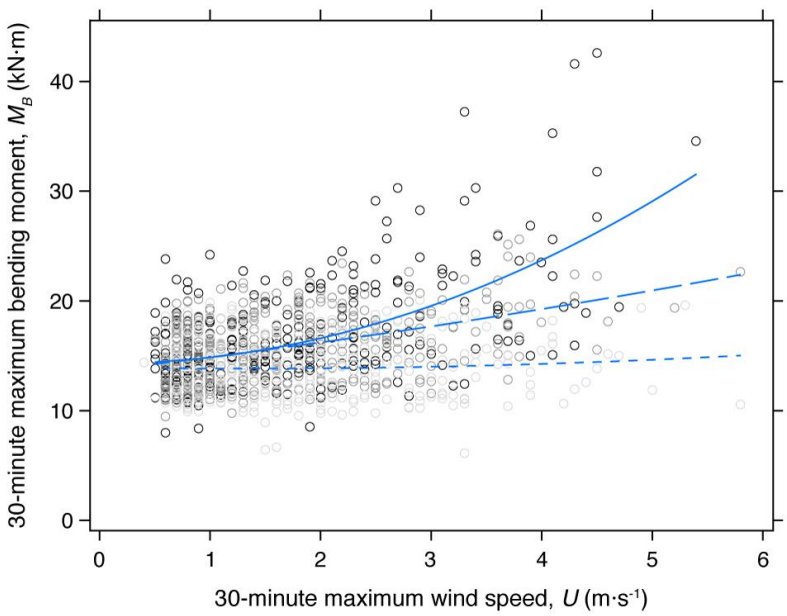

Figure 112: Scatter plot and best-fit lines of the 30-minute maximum bending moment, M_B (kN·m), against 30-minute maximum wind speed, U (m·s^{-1}), measured 18.3 m above ground (z/H_{TREE} = 0.69) for Senegal mahogany (*Khaya senegalensis*) tree number 15 reduced by 0% (black empty circle marker, solid line), 10% (dark gray empty circle marker, long dash line), and 20% (light gray empty circle marker, short dash line). At 0%, 10%, and 20% severity, least squares regression equations are $y = 0.60\ x^2 - 0.07\ x + 14.3$ (n = 305; R^2 = 0.33), $y = 0.06\ x^2 + 1.17\ x + 13.6$ (n = 416; R^2 = 0.18), and $y = 0.06\ x^2 - 0.15\ x + 13.9$ (n = 250; R^2 = 0.00), respectively.

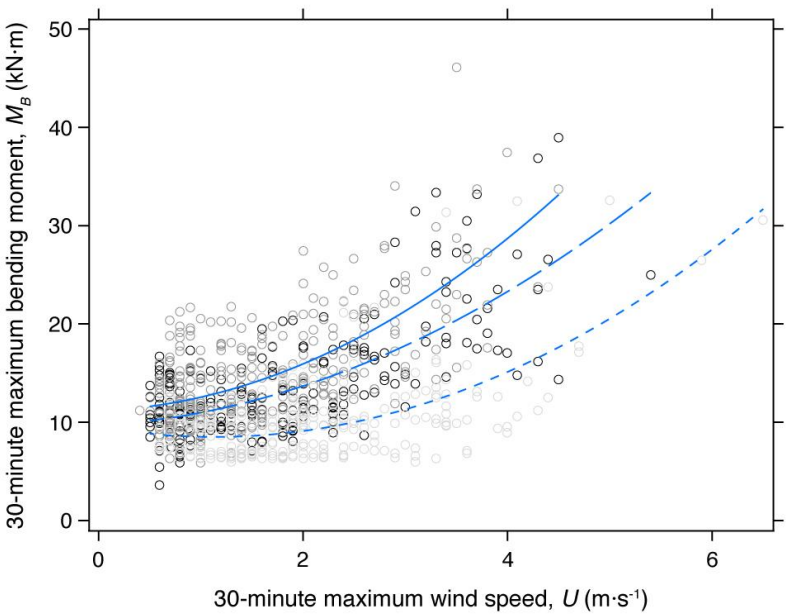

Figure 113: Scatter plot and best-fit lines of the 30-minute maximum bending moment, M_B (kN·m), against 30-minute maximum wind speed, U (m·s^{-1}), measured 18.3 m above ground (z/H_{TREE} = 0.69) for Senegal mahogany (*Khaya senegalensis*) tree number 16 raised by 0% (black empty circle marker, solid line), 10% (dark gray empty circle marker, long dash line), and 20% (light gray empty circle marker, short dash line). At 0%, 10%, and 20% severity, least squares regression equations are $y = 0.70\ x^2 + 0.61\ x + 9.67$ (n = 230; R^2 = 0.52), $y = 1.00\ x^2 + 0.38\ x + 11.2$ (n = 312; R^2 = 0.48), and $y = 0.81\ x^2 – 1.83\ x + 9.55$ (n = 278; R^2 = 0.38), respectively.

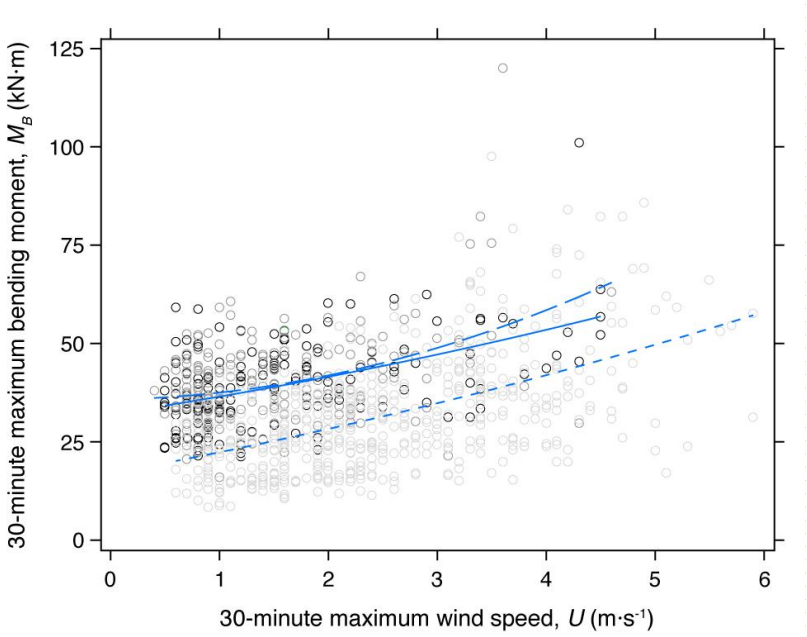

Figure 114: Scatter plot and best-fit lines of the 30-minute maximum bending moment, M_B (kN·m), against 30-minute maximum wind speed, U (m·s^{-1}), measured 18.3 m above ground (z/H_{TREE} = 0.69) for Senegal mahogany (*Khaya senegalensis*) tree number 19 raised by 0% (black empty circle marker, solid line), 10% (dark gray empty circle marker, long dash line), and 20% (light gray empty circle marker, short dash line). At 0%, 10%, and 20% severity, least squares regression equations are $y = 0.31\ x^2 + 4.11\ x + 32.1$ (n = 175; R^2 = 0.26), $y = 1.31\ x^2 + 0.45\ x + 35.8$ (n = 213; R^2 = 0.17), and $y = 0.30\ x^2 + 5.03\ x + 17.0$ (n = 543; R^2 = 0.29), respectively.

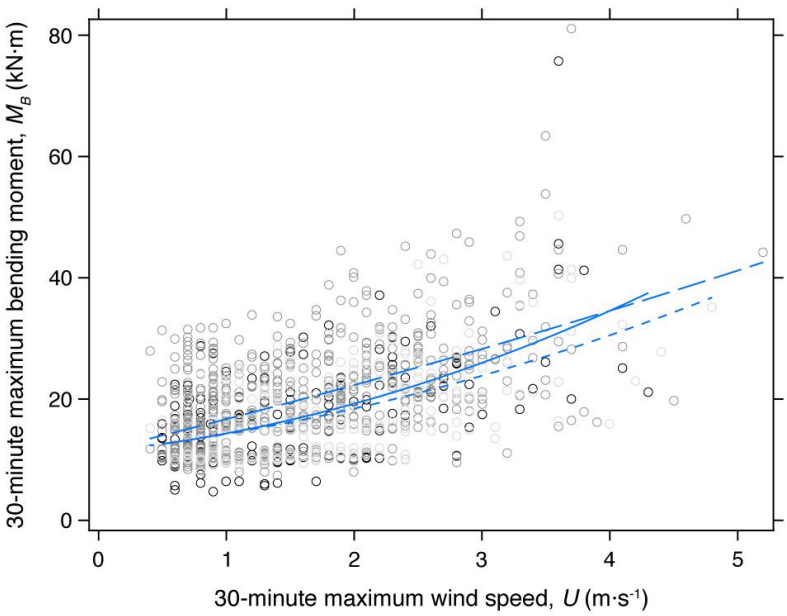

Figure 115: Scatter plot and best-fit lines of the 30-minute maximum bending moment, M_B (kN·m), against 30-minute maximum wind speed, U (m·s^{-1}), measured 18.3 m above ground (z/H_{TREE} = 0.69) for Senegal mahogany (*Khaya senegalensis*) tree number 24 raised by 0% (black empty circle marker, solid line), 10% (dark gray empty circle marker, long dash line), and 20% (light gray empty circle marker, short dash line). At 0%, 10%, and 20% severity, least squares regression equations are $y = 0.92\ x^2 + 2.14\ x + 11.3$ (n = 177; R^2 = 0.34), $y = 0.17\ x^2 + 5.12\ x + 11.4$ (n = 620; R^2 = 0.31), and $y = 0.62\ x^2 + 2.32\ x + 11.3$ (n = 244; R^2 = 0.33), respectively.

BIBLIOGRAPHY

Achim A, Ruel JC, Gardiner BA, et al (2005a) Modelling the vulnerability of balsam fir forests to wind damage. For Ecol Manag 204:37–52

Achim A, Ruel JC, Gardiner BA (2005b) Evaluating the effect of precommercial thinning on the resistance of balsam fir to windthrow through experimentation, modelling, and development of simple indices. Can J For Res 35:1844–1853

Alben S, Zhang J, Shelley M (2002) Drag reduction through self-similar bending of a flexible body. Nature 420:479–481

Allen LH (1968) Turbulence and wind speed spectra within a Japanese larch plantation. J Appl Meteorol 7:73–78

Amiro BD (1990) Comparison of turbulence statistics within three boreal forest canopies. Bound-Layer Meteorol 51:99–121

Amiro BD, Davis PA (1988) Statistics of atmospheric turbulence with a natural black spruce forest canopy. Bound-Layer Meteorol 44:267–283

Ancelin P, Courbaud B, Fourcaud T (2004) Development of an individual tree-based mechanical model to predict wind damage within forest stands. For Ecol Manag 203:101–121

Angelou N, Dellwik E, Mann J (2019) Wind load estimation on an open-grown European oak tree. Forestry 1–12. https://doi.org/10.1093/forestry/cpz026

Anten NPR, Barton KE, Boege K, et al (2011) Size- and Age-Related Changes to Tree Structure and Function. Springer, Dordrecht, The Netherlands

Arfken GB, Weber HJ (2005) Mathematical methods for physicists, 6th edn. Elsevier, Amsterdam, Netherlands

Arnold SJ (1983) Morphology, performance and fitness. Am Zool 23:347–361

ASTM (2014) Standard Test Methods for Density and Specific Gravity (Relative Density) of Wood and Wood-Based Materials. ASTM International, West Conshohocken, PA, USA

Auty D, Achim A, Macdonald E, et al (2014) Models for predicting wood density variation in Scots pine. Forestry 87:449–458

Azen R, Budescu DV (2003) The dominance analysis approach for comparing predictors in multiple regression. Psychol Methods 8:129–148

Baker CJ (1997) Measurements of the natural frequencies of trees. J Exp Bot 48:1125–1132

Baker CJ, Bell HJ (1992) The aerodynamics of urban trees. J Wind Eng Ind Aerodyn 44:2655–2666

Baldocchi DD, Hutchinson BA (1987) Turbulence in an almond orchard: Vertical variations in turbulent statistics. Bound-Layer Meteorol 40:127–146

Baldocchi DD, Meyers TP (1988) Turbulence structure in a deciduous forest. Bound-Layer Meteorol 43:345–364

Barbacci A, Diener J, Hemon P, et al (2014) A robust videogrametric method for the velocimetry of wind-induced motion in trees. Agric For Meteorol 184:220–229

Barry KM, Pearce RB, Mohammed CL (2000) Properties of reaction zones associated with decay from pruning wounds in plantation-grown *Eucalyptus nitens*. For Pathol 30:233–245

Baskerville GL (1972) Use of logarithmic regression in the estimation of plant biomass. Can J For Res 2:49–53

Baum S, Schwarze FWMR (2002) Large-leaved lime (*Tilia platyphyllos*) has a low ability to compartmentalize decay fungi via reaction zone formation. New Phytol 154:481–490

Belsley DA, Kuh E, Welsh RE (2004) Regression Diagnostics. John Wiley & Sons, Hoboken, NJ, USA

Bergeron C, Ruel JC, Elie JG, Mitchell SJ (2009) Root anchorage and stem strength of black spruce (*Picea mariana*) trees in regular and irregular stands. Forestry 82:29–41

Bergstrom H, Hogstrom U (1989) Turbulent exchange above a pine forest II. Organized structures. Bound-Layer Meteorol 49:231–263

Bisset DK, Antonia RA, Browne LWB (1990) Spatial organization of large structures in the turbulent far wake of a cylinder. J Fluid Mech 218:439–461

Blackburn P, Petty JA, Miller KF (1988) An assessment of the static and dynamic factors involved in windthrow. Forestry 61:29–43

Blevins RD (1979) Formulas for natural frequency and mode shape. Van Nostrand Reinhold Co, New York, NY, USA

Bogard DG, Tiederman WG (1986) Burst detection with single-point velocity measurements. J Fluid Mech 162:389–413

Bonnesoeur V, Constant T, Moulia B, Fournier M (2016) Forest trees filter chronic wind-signals to acclimate to high winds. New Phytol 210:850–860

Brazee NJ, Marra RE, Gocke L, Wassenaer PV (2011) Non-destructive assessment of internal decay in three hardwood species of northeastern North America using sonic and electrical impedance tomography. Forestry 84:33–39

Bredenkamp BV, Malan FS, Conradie WE (1980) Some effects of pruning on growth and timber quality of *Eucalyptus grandis* in Zululand. South Afr For J 114:29–34

Bruchert F, Becker G, Speck T (2000) The mechanics of Norway spruce [*Picea abies* (L.) Karst]: Mechanical properties of standing trees from different thinning regimes. For Ecol Manag 135:45–62

Bruchert F, Gardiner BA (2006) The effect of wind exposure on the tree aerial architecture and biomechanics of Sitka spruce (*Picea sitchensis*, Pinaceae). Am J Bot 93:1512–1521

Bruchert F, Speck O, Spatz HC (2003) Oscillations of plants' stems and their damping: Theory and experimentation. Philos Trans R Soc Lond B-Biol Sci 358:1487–1492

Brunet Y, Finnigang JJ, Raupach MR (1994) A wind tunnel study of air flow in waving wheat: Single-point velocity statistics. Bound-Layer Meteorol 70:95–132

Brunet Y, Irvine M (2000) The control of coherent eddies in vegetation canopies: Streamwise structure spacing, canopy shear scale and atmospheric stability. Bound-Layer Meteorol 94:139–163

Burcham DC, Brazee NJ, Marra RE, Kane B (2019) Can sonic tomography predict loss in load-bearing capacity for trees with internal defects? A comparison of sonic tomograms with destructive measurements. Trees Struct Funct 33:681–695. https://doi.org/10.1007/s00468-018-01808-z

Burns LA, Mouritz AP, Pook D, Feih S (2012) Bio-inspired design of aerospace composite joints for improved damage tolerance. Compos Struct 94:995–1004

Burton JD, Smith DM (1972) Guying to prevent wind sway influences loblolly pine growth and wood properties. Forest Service, US Department of Agriculture, Crossett, AR, USA

Butler DW, Gleason SM, Davidson I, et al (2012) Safety and streamlining of woody shoots in wind: An empirical study across 39 species in tropical Australia. New Phytol 193:137–149

Campiformio AT (2012) An investigation of *Fraxinus americana* branch sway using a three-dimensional motion capture system. PhD Thesis

Cannell MGR, Morgan J (1987) Young's modulus of sections of living branches and tree trunks. Tree Physiol 3:355–364

Castro-Garcia S, Blanco-Roldan GL, Gil-Ribes JA, Aguera-Vega J (2008) Dynamic analysis of olive trees in intensive orchards under forced vibration. Trees Struct Funct 22:795–802

Cavanagh JE, Zawar-Reza P, Wilson JG (2009) Spatial attenuation of ambient particulate matter air pollution within an urbanised native forest patch. Urban For Urban Green 8:21–30

Chave J, Andalo C, Brown S, et al (2005) Tree allometry and improved estimation of carbon stocks and balance in tropical forests. Oecologia 145:87–99

Chave J, Coomes DA, Jansen S, et al (2009) Towards a worldwide wood economics spectrum. Ecol Lett 12:351–366

Choi ECC (2000) Wind characteristics of tropical thunderstorms. J Wind Eng Ind Aerodyn 84:215–226

Choi ECC (2004) Field measurement and experimental study of wind speed profile during thunderstorms. J Wind Eng Ind Aerodyn 92:275–290

Chopra AK (2012) Dynamics of Structures: Theory and Applications to Earthquake Engineering, Fourth. Prentice-Hall, Inc, Englewood Cliffs, NJ, USA

Ciftci C, Brena SF, Kane B, Arwade SR (2013) The effect of crown architecture on dynamic amplification factor of an open-grown sugar maple (*Acer saccharum* L.). Trees Struct Funct 27:1175–1189

Ciftci C, Kane B, Brena SF, Arwade SR (2014) Loss in moment capacity of tree stems induced by decay. Trees Struct Funct 28:517–529

Cionco RM (1965) A mathematical model for air flow in a vegetative canopy. J Appl Meteorol 4:517–522

Collineau S, Brunet Y (1993a) Detection of turbulent coherent motions in a forest canopy, Part I: Wavelet analysis. Bound-Layer Meteorol 65:357–379

Collineau S, Brunet Y (1993b) Detection of turbulent coherent motions in a forest canopy, Part II: Time-scales and conditional averages. Bound-Layer Meteorol 66:49–73

Conway HD, Dubil JF (1965) Vibration frequencies of truncated-cone and wedge beams. J Appl Mech 32:932–934

Coutand C (2010) Mechanosensing and thigmomorphogenesis, a physiological and biomechanical point of view. Plant Sci 179:168–182

Coutand C, Moulia B (2000) Biomechanical study of the effect of a controlled bending on tomato stem elongation: Local strain sensing and spatial integration of the signal. J Exp Bot 51:1825–1842

Coutts MP (1986) Components of tree stability in sitka spruce on peaty gley soil. Forestry 59:173–197

Crawford SB, Kosinski AS, Lin HM, et al (2007) Computer programs for the concordance correlation coefficient. Comput Methods Programs Biomed 88:62–74

Dakin AJ (1982) Pruning trial with sugi (*Cryptomeria japonica*). New Zeal J For 27:89–100

Danescu A, Ehring A, Bauhus J, et al (2015) Modelling discoloration and duration of branch occlusion following green pruning in *Acer pseudoplatanus* and *Fraxinus excelsior*. For Ecol Manag 335:87–98

Dawson KS, Gennings C, Carter WH (1997) Two graphical techniques useful in detecting correlation structure in repeated measures data. Am Stat 51:275–283

de Langre E (2008) Effects of wind on plants. Annu Rev Fluid Mech 40:141–168

de Langre E (2012) Methodological advances in predicting flow-induced dynamics of plants using mechanical-engineering theory. J Exp Biol 215:914–921

Deflorio G, Barry KM, Johnson C, Mohammed CL (2007) The influence of wound location on decay extent in plantation-grown *Eucalyptus globulus* and *Eucalyptus nitens*. For Ecol Manag 242:353–362

Deflorio G, Fink S, Schwarze FWMR (2008a) Detection of incipient decay in tree stems with sonic tomography after wounding and fungal inoculation. Wood Sci Technol 42:117–132

Deflorio G, Franz E, Beadle C, Mohammed C (2011) Defence responses in plantation-grown *Eucalyptus globulus* and *Eucalyptus nitens* after artificial fungal inoculation. For Pathol 41:398–406

Deflorio G, Franz E, Fink S, Schwarze FWMR (2009) Host responses in the xylem of trees after inoculation with six wood-decay fungi differing in invasiveness. Can J Bot 87:26–35

Deflorio G, Johnson C, Fink S, Schwarze FWMR (2008b) Decay development in living sapwood of coniferous and deciduous trees inoculated with six wood decay fungi. For Ecol Manag 255:2373–2383

Den Hartog JP (1985) Mechanical Vibrations, Fourth. Dover, Mineola, NY, USA

Den Hartog JP (1948) Moments of Inertia. Dover Publications, Inc., New York, NY, USA, pp 211–230

Denny MW (1987) Life in the maelstrom: The biomechanicsof wave-swept rocky shores. Trends Ecol Evol 2:61–66

Denny MW, Gaines SD (1990) On the prediction of maximal intertidal wave forces. Limnol Oceanogr 35:1–15

Der Loughian C, Tadrist L, Allain JM, et al (2014) Measuring local and global vibration modes in model plants. Comptes Rendus Mec 342:1–7

Donovan GH, Butry DT, Michael YL, et al (2013) The relationship between trees and human health. Am J Prev Med 44:139–145

Downer AJ, Shaw M, Pittenser D (1994) The effect of pruning on branch growth in two oak species. p 550

Dunster JA, Smiley TE, Matheny N, Lilly S (2017) Tree Risk Assessment Manual, 2nd edn. International Society of Arboriculture, Champaign, IL, USA

Dupont S, Bonnefond JM, Irvine MR, et al (2011) Long-distance edge effects in a pine forest with a deep and sparse trunk space: In situ and numerical experiments. Agric For Meteorol 151:328–344

Dupont S, Irvine MR, Bonnefond JM, et al (2012) Turbulent structures in a pine forest with a deep and sparse trunk space: Stand and edge regions. Bound-Layer Meteorol 143:309–336

Dupont S, Patton EG (2012a) Influence of stability and seasonal canopy changes on micrometeorology within and above an orchard canopy: The CHATS experiment. Agric For Meteorol 157:11–29

Dupont S, Patton EG (2012b) Momentum and scalar transport within a vegetation canopy following atmospheric stability and seasonal canopy changes: the CHATS experiment. Atmospheric Chem Phys 12:5913–5935

Dupuy L, Fourcaud T, Stokes A (2005) A numerical investigation into the influence of soil type and root architecture on tree anchorage. Plant Soil 278:119–134

Duryea ML, Kampf E, Littell RC (2007a) Hurricanes and the urban forest: I. Effects on southeastern United States coastal plain tree species. Arboric Urban For 33:83–97

Duryea ML, Kampf E, Littell RC, Rodriguez-Pedraza CD (2007b) Hurricanes and the urban forest: II. Effects on tropical and subtropical tree species. Arboric Urban For 33:98–112

Eisner NJ, Gilman EF, Grabosky JC (2002) Branch morphology impacts compartmentalization of pruning wounds. J Arboric 28:99–105

Ennos AR (2012) Solid Biomechanics, 1st edn. Princeton University Press, Princeton, NJ, USA

Ennos AR, van Casteren A (2010) Transverse stresses and modes of failure in tree branches and other beams. Proc R Soc B-Biol Sci 277:1253–1258

Evert RF (2006) Esau's Plant Anatomy, 3rd edn. John Wiley & Sons, Inc., Hoboken, NJ, USA

Farber J, Lichtenegger HC, Reiterer A, et al (2001) Cellulose microfibril angles in a spruce branch and mechanical implications. J Mater Sci 36:5087–5092

Farge M (1992) Wavelet transforms and their applications to turbulence. Annu Rev Fluid Mech 24:395–457

Farnsworth KD, Niklas KJ (1995) Theories of optimization, form and function in branching architecture in plants. Funct Ecol 9:355–363

Farquhar T, Yong Z (2006) Fracture mechanics and its relevance to botanical structures. Am J Bot 93:1449–1454

Feigenwinter C, Vogt R (2005) Detection and analysis of coherent structures in urban turbulence. Theor Appl Climatol 81:219–230

Feldman M (2011) Hilbert transform in vibration analysis. Mech Syst Signal Process 25:735–802

Fini A, Frangi P, Faoro M, et al (2015) Effects of different pruning methods on an urban tree species: A four-year-experiment scaling down from the whole tree to the chloroplasts. Urban For Urban Green 14:664–674

Finnigan JJ (1979a) Turbulence in waving wheat: I. Mean statistics and honami. Bound-Layer Meteorol 16:181–211

Finnigan JJ (1979b) Turbulence in waving wheat: II. Structure of momentum transfer. Bound-Layer Meteorol 16:213–236

Finnigan JJ (2000) Turbulence in plant canopies. Annu Rev Fluid Mech 32:519–571

Finnigan JJ (2007) The turbulent wind in plant and forest canopies. In: Johnson EA, Miyanishi K (eds). Academic Press, Inc, Burlington, MA, USA, pp 15–58

Finnigan JJ, Brunet Y (1995) Turbulent airflow in forests on flat and hilly terrain. In: Coutts MP, Grace J (eds). University of Cambridge Press, Cambridge, England, UK, pp 3–40

Finnigan JJ, Shaw RH, Patton EG (2009) Turbulence structure above a vegetation canopy. J Fluid Mech 637:387–424

Flesch TK, Wilson JD (1999) Wind and remnant tree sway in forest cutblocks. II. Relating measured tree sway to wind statistics. Agric For Meteorol 93:243–258

Fons WL (1940) Influence of forest cover on wind velocity. J For 38:481–486

Fraser AI (1962) The soil and roots as factors in tree stability. Forestry 35:117–127

Fraser AI, Gardiner JBH (1967) Rooting and stability in Sitka spruce. Forestry Commission

Fredericksen TS, Hedden RL, Williams SA (1993) Testing loblolly pine wind firmness with simulated wind stress. Can J For Res 23:1760–1765

Gao W, Shaw RH, Paw U KT (1989) Observation of organized structure in turbulent flow within and above a forest canopy. Bound-Layer Meteorol 47:349–377

Gardiner BA (1991) Mathematical modelling of the static and dynamic characteristics of plantation trees. In: Franke J, Roeder A (eds) Mathematical Modelling of Forest Ecosystems: Proceedings of a Workshop Organized by Forstliche Versuchsanstalt Rheinland-Pfalz und Zentrum fur Praktische Mathematik. J.D. Sauerlander's Verlag, Frankfurt, Germany, pp 40–61

Gardiner BA (1994) Wind and wind forces in a plantation spruce forest. Bound-Layer Meteorol 67:161–186

Gardiner BA (1995) The interactions of wind and tree movement in forest canopies. In: Coutts MP, Grace J (eds). University of Cambridge, Cambridge, UK, pp 41–59

Gardiner BA, Byrne K, Hale S, et al (2008) A review of mechanistic modelling of wind damage risk to forests. Forestry 81:447–463

Gardiner BA, Leban J-M, Auty D, Simpson H (2011) Models for predicting wood density of British-grown Sitka spruce. Forestry 84:119–132

Gardiner BA, Peltola H, Kellomaki S (2000) Comparison of two models for predicting the critical wind speeds required to damage coniferous trees. Ecol Model 129:1–23

Gardiner BA, Stacey GR, Belcher RE, Wood CJ (1997) Field and wind tunnel assessments of the implications of respacing and thinning for tree stability. Forestry 70:233–252

Georgiou PN (1990) The Singapore wind climate. University of Sydney, School of Civil and Mining Engineering

Gibbs JN, Greig BJW (1990) Survey of parkland trees after the great storm of October 16 1987. Arboric J 14:321–347

Gidlof-Gunnarsson A, Ohrstrom E (2007) Noise and well-being in urban residential environments: The potential role of perceived availability to nearby green areas. Landsc Urban Plan 83:115–126

Gilbert EA, Smiley ET (2004) Picus sonic tomography for the quantification of decay in white oak (*Quercus alba*) and hickory (*Carya* spp.). J Arboric 30:277–281

Gilman EF (2003) Branch-to-stem diameter ratio affects strength of attachment. J Arboric 29:291–294

Gilman EF (2015a) Pruning severity and crown position influence aspect ratio change. Arboric Urban For 41:69–74

Gilman EF (2015b) Pruning *Acer rubrum* at planting impacts structure and growth after three growing seasons. Arboric Urban For 41:11–17

Gilman EF, Grabosky JC (2006) Branch union morphology affects decay following pruning. Arboric Urban For 32:74–79

Gilman EF, Grabosky JC, Jones S, Harchick C (2008a) Effects of pruning dose and type on trunk movement in tropical storm winds. Arboric Urban For 34:13–19

Gilman EF, Lilly SJ (2008) Tree Pruning, 2nd edn. International Society of Arboriculture, Champaign, Illinois

Gilman EF, Masters F, Grabosky JC (2008b) Pruning affects tree movement in hurricane force wind. Arboric Urban For 34:20–28

Gilman EF, Miesbauer JW, Masters FJ (2015) Structural pruning effects on stem and trunk strain in wind. Arboric Urban For 41:3–10

Godin C, Costes E, Sinoquet H (1999) A method for describing plant architecture which integrates topology and geometry. Ann Bot 84:343–357

Gosselin FP, de Langre E (2011) Drag reduction by reconfiguration of a poroelastic system. J Fluids Struct 27:1111–1123

Gosselin FP, de Langre E, Machado-Almeida BA (2010) Drag reduction of flexible plates by reconfiguration. J Fluid Mech 650:319–341

Grabosky JC, Gilman EF (2007) Response of two oak species to reduction pruning cuts. Arboric Urban For 33:360–366

Granucci D, Rudnicki M, Hiscox A, et al (2013) Quantifying the effects of freezing on tree sway frequencies. Agric For Meteorol 168:10–14

Grinsted A, Moore JC, Jevrejeva S (2004) Application of the cross wavelet transform and wavelet coherence to geophysical time series. Nonlinear Process Geophys 11:561–566

Guerin L, Stroup W (2000) A simulation study to evaluate PROC MIXED analysis of repeated measures data. In: Proceedings of the Twelfth Annual Conference on Applied Statistics in Agriculture. Kansas State University, Manhattan, KS

Hale SE, Gardiner BA, Wellpott A, et al (2012) Wind loading of trees: Influence of tree size and competition. Eur J For Res 131:203–217

Halle F, Oldeman RAA, Tomlinson PB (1978) Tropical Trees and Forests: An Architectural Analysis. Springer-Verlag, New York, NY, USA

Hamada S, Takeshi O (2010) Seasonal variations in the cooling effect of urban green areas on surrounding urban areas. Urban For Urban Green 9:15–24

Harder D, Speck O, Hurd C, Speck T (2004) Reconfiguration as a prerequisite for survival in highly unstable flow-dominated habitats. J Plant Growth Regul 23:98–107. https://doi.org/10.1007/s00344-004-0043-1

Harris RW, Clark JR, Matheny NP (2004) Arboriculture: Integrated Management of Landscape Trees, Shrubs, and Vines, Fourth. Pearson Education, Upper Saddle River, NJ

Hassinen A, Lemettinen M, Peltola H, et al (1998) A prism-based system for monitoring the swaying of trees under wind loading. Agric For Meteorol 90:187–194

Hein S, Spiecker H (2007) Comparative analysis of occluded branch characteristics for *Fraxinus excelsior* and *Acer pseudoplatanus* with natural and artificial pruning. Can J For Res 37:1414–1426

Hoag DL, Fridley RB, Hutchinson JR (1971) Experimental measurement of internal and external damping properties of tree limbs. Trans Am Soc Agric Eng 14:20–24

Holbo R (1980) Aeromechanical behavior of selected Douglas-fir. Agric Meteorol 21:81–91

Hommema SE, Adrian RJ (2003) Packet structure of surface eddies in the atmospheric boundary layer. Bound-Layer Meteorol 106:147–170

Huang Y-S, Chen S-S, Kuo-Huang L-L, Lee CM (2005) Growth strain in the trunk and branches of *Chamaecyparis formosensis* and its influence on tree form. Tree Physiol 25:1119–1126

Hunt WF, Smith JT, Jadlocki SJ, et al (2008) Pollutant removal and peak flow mitigation by a bioretention cell in urban Charlotte, N.C. J Environ Eng 134:403–408

Jackson T, Shenkin A, Wellpott A, et al (2019) Finite element analysis of trees in the wind based on terrestrial laser scanning data. Agric For Meteorol 265:137–144

James KR (2014) A study of branch dynamics on an open-grown tree. Arboric Urban For 40:125–134

James KR (2010) A dynamic structural analysis of trees subjected to wind loading. PhD Thesis

James KR, Hallam C, Spencer C (2013) Measuring tilt of tree structural root zones under static and wind loading. Agric For Meteorol 168:160–167

James KR, Haritos N, Ades PK (2006) Mechanical stability of trees under dynamic loads. Am J Bot 93:1522–1530

James KR, Kane B (2008) Precision digital instruments to measure dynamic wind loads on trees during storms. Agric For Meteorol 148:1055–1061

Jeffers WA, Abbott RE (1979) A new system developed for guying trees. J Arboric 5:121–123

Jeronimidis G (1980) The fracture behaviour of wood and the relations between toughness and morphology. Proc R Soc B-Biol Sci 208:447–460

Jevrejeva S, Moore JC, Grinsted A (2003) Influence of the Arctic Oscillation and El Nino-Southern Oscillation (ENSO) on ice conditions in the Baltic Sea: The wavelet approach. J Geophys Res 108:1–11

Johnson AD, Gerhold HD (2003) Carbon storage by urban tree cultivars, in roots and above-ground. Urban For Urban Green 2:65–72

Johnstone DM, Ades PK, Moore GM, Smith IW (2007) Predicting wood decay in eucalypts using an expert system and IML-Resistograph drill. Arboric Urban For 33:76–82

Johnstone DM, Moore GM, Tausz M, Nicolas M (2010) The measurement of wood decay in landscape trees. Arboric Urban For 36:121–127

Jonsson MJ, Foetzki A, Kalberer M, et al (2006) Root-soil rotational stiffness of Norway spruce (*Picea abies* (L.) Karst) growing on subalpine forested slopes. Plant Soil 285:267–277

Jonsson MJ, Foetzki A, Kalberer M, et al (2007) Natural frequencies and damping ratios of Norway spruce (*Picea abies* (L.) Karst) growing on subalpine forested slopes. Trees Struct Funct 21:541–548

Jungnikl K, Goebbels J, Burgert I, Fratzl P (2009) The role of material properties for the mechanical adaptation at branch junctions. Trees Struct Funct 23:605–610

Kane B (2008) Tree failure following a windstorm in Brewster, Massachusetts, USA. Urban For Urban Green 7:15–23

Kane B (2014) Determining parameters related to the likelihood of failure of red oak (*Quercus rubra* L.) from winching tests. Trees Struct Funct 28:1667–1677

Kane B (2007) Branch strength of Bradford pear (*Pyrus calleryana* var. 'Bradford'). Arboric Urban For 33:283–291

Kane B (2018) The effect of simulated trunk splits, pruning, and cabling on sways of *Quercus rubra* L. Trees Struct Funct 32:985–1000. https://doi.org/10.1007/s00468-018-1690-3

Kane B (2002) Assessing the applicability of formulas to detect hazard trees: Callus wood improvement in red maple (*Acer rubrum*). PhD Thesis

Kane B (2011) Withdrawal resistance of J-lags from three hardwood species. Arboric Urban For 37:139–145

Kane B, Autio W (2014) Installing cables did not affect annual radial increment in co-dominant stems of red oaks. Urban For Urban Green 13:443–449

Kane B, Clouston P (2008) Tree pulling tests of large shade trees in the genus Acer. Arboric Urban For 34:101–109

Kane B, Farrell R, Zedaker SM, et al (2008a) Failure mode and prediction of the strength of branch attachments. Arboric Urban For 34:308–316

Kane B, James KR (2011) Dynamic properties of open-grown deciduous trees. Can J For Res 41:321–330

Kane B, Modarres-Sadeghi Y, James KR, Reiland M (2014) Effects of crown structure on the sway characteristics of large decurrent trees. Trees Struct Funct 28:151–159

Kane B, Pavlis M, Harris JR, Seiler JR (2008b) Crown reconfiguration and trunk stress in deciduous trees. Can J For Res 38:1275–1289

Kane B, Ryan HDP (2004) The accuracy of formulas used to assess strength loss due to decay in trees. J Arboric 30:347–356

Kane B, Ryan HDP (2002) Discoloration and decay associated with hardware installation in trees. J Arboric 28:187–193

Kane B, Ryan HDP, Bloniarz DV (2001) Comparing formulae that assess strength loss due to decay in trees. J Arboric 27:78–87

Kane B, Smiley ET (2006) Drag coefficients and crown area estimation of red maple. Can J For Res 36:1951–1958

Kennedy EI (1965) Strength and Related Properties of Woods Grown in Canada. Department of Forestry, Ottawa, ON, Canada

Kenward MG, Roger JH (1997) Small sample inference for fixed effects from restricted maximum likelihood. Biometrics 53:983–997

Kerzenmacher T, Gardiner BA (1998) A mathematical model to describe the dynamic response of a spruce tree to the wind. Trees Struct Funct 12:385–394

Knio OM, Ghoniem AF (1992) The three-dimensional structure of periodic vorticity layers under non-symmetric conditions. J Fluid Mech 243:353–392

Koizumi A, Motoyama J, Sawata K, et al (2010) Evaluation of drag coefficients of poplar-tree crowns by a field test method. J Wood Sci 56:189–193

Kollmann FFP, Cote WA (1968) Principles of Wood Science and Technology I. Solid Wood. Springer-Verlag, Berlin, Germany

Kretschmann DE (2010) Mechanical properties of wood. In: Centennial Edition. Forest Products Laboratory, Madison, WI, USA, pp 5.1-5.44

Kreyszig E (2011) Advanced Engineering Mathematics, 10th edn. John Wiley & Sons, Inc., Hoboken, NJ, USA

Krusche N, Oliveira AP de (2004) Characterization of coherent structures in the atmospheric surface layer. Bound-Layer Meteorol 110:191–211

Kruskal W (1987) Relative importance by averaging over orderings. Am Stat 41:6–10

Kuo FE (2001) Coping with poverty: Impacts of environment and attention in the inner city. Environ Behav 33:5–34

Kutner MH, Nachtsheim CJ, Neter J (2004) Applied Linear Regression Models, 4th edn. McGraw-Hill Irwin, Boston, MA, USA

Lachenbruch B, McCulloh KA (2014) Traits, properties, and performance: How woody plants combine hydraulic and mechanical functions in a cell, tissue, or whole plant. New Phytol 204:747–764

Lai W (1955) Aerodynamic crown drag of several broadleaf tree species. USDA Forest Service

Landhausser SM, Lieffers VJ (2012) Defoliation increases risk of carbon starvation in root systems of mature aspen. Trees Struct Funct 26:653–661

Landsberg JJ, James GB (1971) Wind profiles in plant canopies: Studies on an analytical model. J Appl Ecol 8:729–741

Larson PR (1965) Stem form of young larix as influenced by wind and pruning. For Sci 11:412–424

Launiainen S, Vesala T, Molder M, et al (2007) Vertical variability and effect of stability on turbulence characteristics down to the floor of a pine forest. Tellus Ser B - Chem Phys Meteorol 59:919–936

Lawrence HW (2006) City Trees: A Historical Geography from the Renaissance through the Nineteenth Century, 1st edn. University of Virginia Press, Charlottesville, VA, USA

Lee JK, Park YS (1992) Modal parameter estimation in structural systems using complex envelope signal. In: Proceedings of the 10th International Modal Analysis Conference. pp 167–172

Lilly S, Sydnor TD (1995) Comparison of branch failure during static loading of silver and Norway maples. J Arboric 21:302–305

Lopez D, Eloy C, Michelin S, de Langre E (2014) Drag reduction, from bending to pruning. Europhys Lett 108:1–5

Lopez D, Michelin S, de Langre E (2011) Flow-induced pruning of branched systems and brittle reconfiguration. J Theor Biol 284:117–124

Lovasi GS, Quinn JW, Neckerman KM, et al (2008) Children living in areas with more street trees have lower prevalence of asthma. J Epidemiol Community Health 62:647–649

Lundstrom T, Jonas T, Stockli V, Ammann W (2007) Anchorage of mature conifers: Resistive turning moment, root-soil plate geometry and root growth orientation. Tree Physiol 27:1217–1227

Lundstrom T, Jonsson MJ, Volkwein A, Stoffel M (2009) Reactions and energy absorption of trees subject to rockfall: A detailed assessment using a new experimental method. Tree Physiol 29:345–359

Lundstrom T, Stoffel M, Stockli V (2008) Fresh-stem bending of silver fir and Norway spruce. Tree Physiol 28:355–366

Mahrt L, Sun J, Blumen W, et al (1998) Nocturnal boundary-layer regimes. Bound-Layer Meteorol 88:255–278

Mallard S (2009) A Wavelet Tour of Signal Processing: The Sparse Way, 3rd edn. Academic Press, Burlington, MA

Marasinghe MG, Kennedy WJ, Chambers J, et al (eds) (2008) SAS for Data Analysis: Intermediate Statistical Methods. Springer, New York, NY, USA

Matheny N, Clark J (1994) A Photographic Guide to the Evaluation of Hazard Trees in Urban Areas, 2nd Ed. International Society of Arboriculture, Champaign, IL, USA

Mayer H (1987) Wind-induced tree sways. Trees Struct Funct 1:195–206

Mayer H, Raupach MR, Kohsiek W, et al (1989) Windthrow [and Discussion]. Philos Trans R Soc Lond B-Biol Sci 324:267–281

Mayhead GJ (1973a) Sway periods of forest trees. Scott For 27:19–23

Mayhead GJ (1973b) Some drag coefficients for British forest trees derived from wind tunnel studies. Agric Meteorol 12:123–130

Mayhead GJ, Gardiner JBH, Durrant DW (1975) A report on the physical properties of conifers in relation to plantation stability. Forestry Commission, Edinburgh, United Kingdom

McPherson EG, Simpson JR, Xiao Q, Wu C (2011) Million trees Los Angeles canopy cover and benefit assessment. Landsc Urban Plan 99:40–50

Meng SX, Lieffers VJ, Reid DEB, et al (2006) Reducing stem bending increases the height growth of tall pines. J Exp Bot 57:3175–3182

Meriam JL, Kraige LG (2012) Engineering Mechanics: Dynamics, 7th edn. John Wiley and Sons, Inc, Hoboken, NJ, USA

Micheline F, Ng LK (2012) The Weather and Climate of Singapore. Meteorological Service Singapore, National Environment Agency, Singapore

Miesbauer JW, Gilman EF, Giurcanu M (2014) Effects of tree crown structure on dynamic properties of *Acer rubrum* L. 'Florida Flame'™. Arboric Urban For 40:218–229

Milne R (1991) Dynamics of swaying *Picea sitchensis*. Tree Physiol 9:383–399

Milne R, Blackburn P (1989) The elasticity and vertical distribution of stress within stems of *Picea sitchensis*. Tree Physiol 5:195–205

Mohr M, Schindler D (2016) Coherent momentum exchange above and within a Scots pine forest. Atmosphere 7:61–81

Moore JR (2000) Differences in maximum resistive bending moments of *Pinus radiata* trees grown on a range of soil types. For Ecol Manag 135:63–71

Moore JR, Gardiner BA, Blackburn GRA, et al (2005) An inexpensive instrument to measure the dynamic response of standing trees to wind loading. Agric For Meteorol 132:78–83

Moore JR, Maguire DA (2005) Natural sway frequencies and damping ratios of trees: Influence of crown structure. Trees Struct Funct 19:363–373

Moore JR, Maguire DA (2004) Natural sway frequencies and damping ratios of trees: Concepts, review and synthesis of previous studies. Trees Struct Funct 18:195–203

Mortimer MJ, Kane B (2004) Hazard tree liability in the United States: Uncertain risks for owners and professionals. Urban For Urban Green 2:159–165

Muhairwe CK (1994) Tree form and taper variation over time for interior lodgepole pine. Can J For Res 24:1904–1913

Muller U, Gindl W, Jeronidimis G (2006) Biomechanics of a branch-stem junction in softwood. Trees Struct Funct 20:643–648

Nathan GK, Goh TN (1981) Wind measurements in an equatorial region (Singapore). Sol Energy 26:275–278

Neely D (1979) Tree wounds and wound closure. J Arboric 5:135–140

Neild SA, Wood CJ (1999) Estimating stem and root-anchorage flexibility in trees. Tree Physiol 19:141–151

Netusil NR, Chattopadhyay S, Kovacs KF (2010) Estimating the demand for tree canopy: A second-stage hedonic price analysis in Portland, Oregon. Land Econ 86:281–293

Nicolescu VN, Sandi M, Paun M (2012) Occlusion of pruning wounds on northern red oak (*Quercus rubra*) trees in Romania. Scandanavian J For Res 28:1–6. https://doi.org/10.1080/02827581.2012.747621

Nicoll BC, Gardiner BA, Peace AJ (2008) Improvements in anchorage provided by the acclimation of forest trees to wind stress. Forestry 81:389–398

Nicoll BC, Gardiner BA, Rayner B, Peace AJ (2006) Anchorage of coniferous trees in relation to species, soil type, and rooting depth. Can J For Res 36:1871–1883

Nicoll BC, Ray D (1996) Adaptive growth of tree root systems in response to wind action and site conditions. Tree Physiol 16:891–898

Niklas KJ (1992) Plant Biomechanics: An Engineering Approach to Plant Form and Function, 1st edn. University of Chicago Press, Chicago, IL, USA

Niklas KJ (1997) Mechanical properties of black locust (*Robinia pseudoacacia*) wood: Correlations among elastic and rupture moduli, proportional limit, and tissue density and specific gravity. Ann Bot 79:479–485

Niklas KJ, Kerchner V (1984) Mechanical and photosynthetic constraints on the evolution of plant shape. Paleobiology 10:79–101

Niklas KJ, Spatz HC (2010) Worldwide correlations of mechanical properties and green wood density. Am J Bot 97:1587–1594

Niklas KJ, Spatz HC (2012) Mechanical properties of wood disproportionately increase with increasing density. Am J Bot 99:169–170

Oliver HR (1971) Wind profiles in and above a forest canopy. Q J R Meteorol Soc 97:548–553

Oliver HR (1975) Ventilation in a forest. Agric Meteorol 14:347–355

Oliver HR, Mayhead GJ (1974) Wind measurements in a pine forest during a destructive gale. Forestry 47:185–194

Ostrovsky R, Kobza M, Gazo J (2017) Extensively damaged trees tested with acoustic tomography considering tree stability in urban greenery. Trees Struct Funct 31:1015–1023

O'Sullivan MF, Ritchie RM (1992) An apparatus to apply dynamic loads to forest trees. J Agric Eng Res 51:153–156

Ow LF, Ghosh S, Sim EK (2013) Mechanical injury and occlusion: An urban, tropical perspective. Urban For Urban Green 12:255–261

Ozyhar T, Hering S, Niemz P (2013) Moisture-dependent orthotropic tension-compression asymmetry of wood. Holzforschung 67:395–404

Paatalo ML, Peltola H, Kellomaki S (1999) Modelling the risk of snow damage to forests under short-term snow loading. For Ecol Manag 116:51–70

Packard GC (2014) Assessing allometric growth by leaves and the hypothesis of diminishing returns. Int J Plant Sci 175:742–753

Packard GC (2009) On the use of logarithmic transformations in allometric analyses. J Theor Biol 257:515–518

Packard GC, Birchard GF, Boardman TJ (2011) Fitting statistical models in bivariate allometry. Biol Rev 86:549–563

Page DH, El-Hosseiny F (1983) The mechanical properties of single wood pulp fibres. Part IV: Fibril angle and the shape of the stress-strain curve. J Pulp Pap Sci 9:99–100

Page DH, El-Hosseiny F, Winkler K (1971) Behaviour of single wood fibres under axial tensile strain. Nature 229:252–253

Pandit R, Laband DN (2010) Energy savings from tree shade. Ecol Econ 69:1324–1329

Pandit R, Polyakov M, Tapsuwan S, Moran T (2013) The effect of street trees on property value in Perth, Western Australia. Landsc Urban Plan 110:134–142

Papesch AJG (1997) Mechanical stability of *Pinus radiata* trees at Eyrewell Forest investigated using static tests. N Z J For Sci 27:188–204

Pavlis M, Kane B, Harris JR, Seiler JR (2008) The effects of pruning on drag and bending moment of shade trees. Arboric Urban For 34:207–215

Paw U KT, Brunet Y, Collineau S, et al (1992) On coherent structures in turbulence above and within agricultural plant canopies. Agric For Meteorol 61:55–68

Pearce RB (1996) Antimicrobial defences in the wood of living trees. New Phytol 132:203–233

Peltola H (1995) Studies on the mechanism of wind-induced damage of Scots pine. PhD Thesis

Peltola H (2006) Mechanical stability of trees under static loads. Am J Bot 93:1501–1511

Peltola H (1996) Swaying of trees in response to wind and thinning in a stand of Scots pine. Bound-Layer Meteorol 77:285–304

Peltola H, Kellomaki S, Hassinen A, et al (1993) Swaying of trees as caused by the wind: Analysis of field measurements. Silva Fenn 27:113–126

Peltola H, Kellomaki S, Hassinen A, Granander M (2000) Mechanical stability of Scots pine, Norway spruce and birch: An analysis of tree-pulling experiments in Finland. For Ecol Manag 135:143–153

Peltola H, Kellomaki S, Vaisanen H, Ikonen VP (1999) A mechanistic model for assessing the risk of wind and snow damage to single trees and stands of Scots pine, Norway spruce, and birch. Can J For Res 29:647–661

Pennycuick CJ (1988) Conversion Factors: SI Units and Many Others. University of Chicago Press, Chicago, IL, USA

Perre P, Dinh AT, Assor C, et al (2013) Stiffness of normal, opposite, and tension poplar wood determined using micro-samples in the three material directions. Wood Sci Technol 47:481–498

Peterson CJ, Claassen V (2013) An evaluation of the stability of *Quercus lobata* and *Populus fremontii* on river levees assessed using static winching tests. Forestry 86:201–209

Petty JA, Swain C (1985) Factors influencing stem breakage of conifers in high winds. Forestry 58:75–84

Pfisterer JA (2003) Towards a better understanding of tree failure: Investigations into bending stresses of branch junctions and reiterates of European filbert (*Corylus avellana* L.) as a model organism. In: Balder H, Strauch K-H, Backhaus GF (eds) Second International Symposium on Plant Health in Urban Horticulture. Federal Biological Research Centre for Agriculture and Forestry, pp 125–131

Pinkard EA, Beadle CL (1998a) Regulation of photosynthesis in *Eucalyptus nitens* (Deane and Maiden) Maiden following green pruning. Trees Struct Funct 12:366–376

Pinkard EA, Beadle CL (1998b) Effects of green pruning on growth and stem shape of *Eucalyptus nitens* (Deane and Maiden) Maiden. New For 15:107–126

Pinkard EA, Beadle CL, Davidson NJ, Battaglia M (1998) Photosynthetic responses of *Eucalyptus nitens* (Deane and Maiden) Maiden to green pruning. Trees Struct Funct 12:119–129

Pinkard EA, Mohammed C, Beadle CL, et al (2004) Growth responses, physiology and decay associated with pruning plantation-grown *Eucalyptus globulus* Labill. and *E. nitens* (Deane and Maiden) Maiden. For Ecol Manag 200:263–277

Pinto JG, Zacharias S, Fink AH, et al (2009) Factors contributing to the development of extreme North Atlantic cyclones and their relationship with the NAO. Clim Dyn 32:711–737

Poulos HM, Camp AE (2010) Decision support for mitigating the risk of tree induced transmission line failure in utility rights-of-way. Environ Manage 45:217–226

Press WH, Rybicki GB (1989) Fast algorithm for spectral analysis of unevenly sampled data. Astrophys J 338:277–280. https://doi.org/10.1086/167197

Proulx OJ, Greene DF (2001) The relationship between ice thickness and northern hardwood tree damage during ice storms. Can J For Res 31:1758–1767

Puijalon S, Bornette G, Sagnes P (2005) Adaptations to increasing hydraulic stress: Morphology, hydrodynamics and fitness of two higher aquatic plant species. J Exp Bot 56:777–786

Puijalon S, Bouma TJ, Douady CJ, et al (2011) Plant resistance to mechanical stress: Evidence of an avoidance-tolerance trade-off. New Phytol 191:1141–1149

Quine CP, Gardiner BA (2007) Understanding how the interaction of wind and trees results in windthrow, stem breakage, and canopy gap formation. In: Johnson EA, Miyanishi K (eds). Academic Press, Inc, Burlington, MA, USA, pp 103–156

Rabe C, Ferner D, Fink S, Schwarze FWMR (2004) Detection of decay in trees with stress waves and interpretation of acoustic tomograms. Arboric J 28:3–19

Ramirez JA, Handa IT, Posada JM, et al (2018) Carbohydrate dynamics in roots, stems, and branches after maintenance pruning in two common urban tree species of North America. Urban For Urban Green 30:24–31

Raupach MR (1989) Stand overstorey processes [and discussion]. Philos Trans R Soc Lond B-Biol Sci 324:175–190

Raupach MR, Finnigan JJ, Brunet Y (1996) Coherent eddies and turbulence in vegetation canopies: The mixing layer analogy. Bound-Layer Meteorol 78:351–382. https://doi.org/10.1007/BF00120941

Raupach MR, Thom AS (1981) Turbulence in and above plant canopies. Annu Rev Fluid Mech 13:97–129

Ray D, Nicoll BC (1998) The effect of soil water-table depth on root-plate development and stability of Sitka spruce. Forestry 71:169–182

Raymond CA, Joe B, Anderson DW, Watt DJ (2008) Effect of thinning on relationships between three measures of wood stiffness in *Pinus radiata*: standing trees vs. logs vs. short clear specimens. Can J For Res 38:2870–2879

Reifsnyder WE (1955) Wind profiles in a small isolated forest stand. For Sci 1:289–297

Reiland M, Kane B, Modarres-Sadeghi Y, Ryan HDP (2015) The effect of cables and leaves on the dynamic properties of red oak (*Quercus rubra*) with co-dominant stems. Urban For Urban Green 14:844–850

Reiterer A, Lichtenegger H, Fratzl P, Stanzl-Tschegg SE (2001) Deformation and energy absorption of wood cell walls with different nanostructure under tensile loading. J Mater Sci 36:4681–4686

Reiterer A, Lichtenegger H, Tschegg S, Fratzl P (1999) Experimental evidence for a mechanical function of the cellulose microfibril angle in wood cell walls. Philos Mag A 79:2173–2184

Reynolds AM (2012) Gusts within plant canopies are extreme value processes. Phys -Stat Mech Its Appl 391:5059–5063

Rodgers M, Casey A, McMenamin C, Hendrick E (1995) An experimental investigation of the effects of dynamic loading on coniferous trees planted on wet mineral soils. In: Coutts MP, Grace J (eds). Cambridge University Press, New York, NY, USA, pp 204–219

Rodriguez M, de Langre E, Moulia B (2008) A scaling law for the effects of architecture and allometry on tree vibration modes suggests a biological tuning to modal compartmentalization. Am J Bot 95:1523–1537

Rodriguez M, Ploquin S, Moulia B, de Langre E (2012) The multimodal dynamics of a walnut tree: Experiments and models. J Appl Mech 79:1–5

Rogers MM, Moser RD (1992) The three-dimensional evolution of a plane mixing layer: the Kelvin-Helmholtz rollup. J Fluid Mech 243:183–226

Roodbaraky HJ, Baker CJ, Dawson AR, Wright CJ (1994) Experimental observations of the aerodynamic characteristics of urban trees. J Wind Eng Ind Aerodyn 52:171–184

Roy S, Byrne J, Pickering C (2012) A systematic quantitative review of urban tree benefits, costs, and assessment methods across cities in different climatic zones. Urban For Urban Green 11:351–363

Rudnicki M, Lieffers VJ, Silins U (2003) Stand structure governs the crown collisions of lodgepole pine. Can J For Res 33:1238–1244

Rudnicki M, Meyer TH, Lieffers VJ, et al (2008) The periodic motion of lodgepole pine trees as affected by collisions with neighbors. Trees Struct Funct 22:475–482

Rudnicki M, Mitchell SJ, Novak MD (2004) Wind tunnel measurements of crown streamlining and drag relationships for three conifer species. Can J For Res 34:666–676

Rudnicki M, Silins U, Lieffers VJ, Josi G (2001) Measure of simultaneous tree sways and estimation of crown interactions among a group of trees. Trees Struct Funct 15:83–90

Ruel JC, Achim A, Herrera RE, Cloutier A (2010) Relating mechanical strength at the stem level to values obtained from defect-free wood samples. Trees Struct Funct 24:1127–1135

Sander H, Polasky S, Haight RG (2010) The value of urban tree cover: A hedonic property price model in Ramsey and Dakota Counties, Minnesota, USA. Ecol Econ 69:1646–1656

Sandi M, Sandi W, Nicolescu VN (2012) Wood discolouration in relation to wound size in northern red oak (*Quercus rubra*) trees subjected to artificial pruning. Span J Rural Dev 3:53–60

Scannell B (1983) Quantifications of the interactive motions of the atmospheric surface layer and a conifer canopy. PhD Thesis

Schelhaas MJ, Nabuurs GJ, Schuck A (2003) Natural disturbances in the European forests in the 19th and 20th centuries. Glob Change Biol 9:1620–1633

Schindler D (2008) Responses of Scots pine trees to dynamic wind loading. Agric For Meteorol 148:1733–1742

Schindler D, Bauhus J, Mayer H (2012a) Wind effects on trees. Eur J For Res 131:159–163

Schindler D, Fugmann H, Mayer H (2013a) Analysis and simulation of dynamic response behavior of Scots pine trees to wind loading. Int J Biometeorol 57:819–833

Schindler D, Fugmann H, Schonborn J, Mayer H (2012b) Coherent response of a group of plantation-grown Scots pine trees to wind loading. Eur J For Res 131:191–202

Schindler D, Jung C, Buchholz A (2016) Using highly resolved maximum gust speed as predictor for forest storm damage caused by the high-impact winter storm Lothar in Southwest Germany. Atmospheric Sci Lett 17:462–469

Schindler D, Mohr M (2019) No resonant response of Scots pine trees to wind excitation. Agric For Meteorol 265:227–244

Schindler D, Mohr M (2018) Non-oscillatory response to wind loading dominates movement of Scots pine trees. Agric For Meteorol 250–251:209–216

Schindler D, Schonborn J, Fugmann H, Mayer H (2013b) Responses of an individual deciduous broadleaved tree to wind excitation. Agric For Meteorol 177:69–82

Schindler D, Vogt R, Fugmann H, et al (2010) Vibration behavior of plantation-grown Scots pine trees in response to wind excitation. Agric For Meteorol 150:984–993

Schmidlin TW (2008) Human fatalities from wind-related tree failures in the United States, 1995-2007. Nat Hazards 50:13–25

Schwarze FWMR, Baum S (2000) Mechanisms of reaction zone penetration by decay fungi in wood of beech (*Fagus sylvatica*). New Phytol 146:129–140

Schwarze FWMR, Ferner D (2003) *Ganoderma* on trees - Differentiation of species and studies of invasiveness. Arboric J 27:1–21

Schwarze FWMR, Fink S (1998) Host and cell type affect the mode of degradation by *Meripilus giganteus*. New Phytol 139:721–731

Sellier D (2004) Analyse numerique du comportement mecanique d'arbres sous sollicitation aerodynamique turbulente. PhD Thesis

Sellier D, Brunet Y, Fourcaud T (2008) A numerical model of tree aerodynamic response to a turbulent airflow. Forestry 81:279–297

Sellier D, Fourcaud T (2005) A mechanical analysis of the relationship between free oscillations of *Pinus pinaster* Ait. saplings and their aerial architecture. J Exp Bot 56:1563–1573

Sellier D, Fourcaud T, Lac P (2006) A finite element model for investigating effects of aerial architecture on tree oscillations. Tree Physiol 26:799–806

Serafimovich A, Thomas C, Foken T (2011) Vertical and horizontal transport of energy and matter by coherent motions in a tall spruce canopy. Bound-Layer Meteorol 140:429–451

Shah DU, Reynolds TPS, Ramage MH (2017) The strength of plants: Theory and experimental methods to measure the mechanical properties of stems. J Exp Bot 86:4497–4516

Shaw RH, McCartney HA (1985) Gust penetration into plant canopies. Atmos Environ 19:827–830

Shaw RH, Tavangar J, Ward DP (1983) Structure of the Reynolds stress in a canopy layer. J Clim Appl Meteorol 22:1922–1931

Shaw RH, Ward DP, Aylor DE (1979) Frequency of occurrence of fast gusts of wind inside a corn canopy. J Appl Meteorol 18:167–171

Shigo AL (1985) How tree branches are attached to trunks. Can J Bot 63:1391–1401

Shigo AL (1990) Tree branch attachment to trunks and branch pruning. HortScience 25:54–59

Shigo AL, Marx HG (1977) Compartmentalization of Decay in Trees, 1st edn. Forest Service, US Department of Agriculture, Washington, DC

Silins U, Lieffers VJ, Bach L (2000) The effect of temperature on mechanical properties of standing lodgepole pine trees. Trees Struct Funct 14:424–428

Sinn G, Wessolly L (1989) A contribution to the proper assessment of the strength and stability of trees. Arboric J 13:45–65

Slater D, Bradley RS, Withers PJ, Ennos AR (2014) The anatomy and grain pattern in forks of hazel (*Corylus avellana* L.) and other tree species. Trees Struct Funct 28:1437–1448

Slater D, Ennos AR (2013) Determining the mechanical properties of hazel forks by testing their component parts. Trees Struct Funct 27:1515–1524

Smiley ET (2003) Does included bark reduce the strength of codominant stems? J Arboric 29:104–106

Smiley ET (2011) Dead-end stop terminated tree support cable systems. Arboric Urban For 37:67–73

Smiley ET (1998) Countersinking for tree bolts. J Arboric 24:245–247

Smiley ET, Greco CM, Williams JG (2000) Brace rods for co-dominant stems: Installation location and breaking strength. J Arboric 26:170–176

Smiley ET, Kane B (2006) The effects of pruning type on wind loading of *Acer rubrum*. Arboric Urban For 32:33–40

Smiley ET, LeBrun E, Gilbert EA (2003) Evaluation of extraction force for wooden guy anchors. J Arboric 29:295–297

Smiley ET, Lilly S (2014) Tree Support Systems: Cabling, Bracing, Guying, and Propping, 3rd edn. International Society of Arboriculture, Champaign, IL, USA

Smiley ET, Matheny N, Lilly S (2017) Tree Risk Assessment, 2nd edn. International Society of Arboriculture, Champaign, IL, USA

Smith RGB, Dingle J, Kearney D, Montagu K (2006) Branch occlusion after pruning in four contrasting sub-tropical eucalypt species. J Trop For Sci 18:117–123

Smith VG, Watts M, James DF (1987) Mechanical stability of black spruce in the clay belt region of northern Ontario. Can J For Res 17:1080–1091

Somerville A (1979) Root anchorage and root morphology of *Pinus radiata* on a range of ripping treatments. N Z J For Sci 9:294–315

Song XP, Tan PY, Edwards P, Richards D (2018) The economic benefits and costs of trees in urban forest stewardship: A systematic review. Urban For Urban Green 29:162–170

Spatz HC, Bruchert F, Pfisterer J (2007) Multiple resonance damping or how do trees escape dangerously large oscillations? Am J Bot 94:1603–1611

Spatz HC, Speck O (2002) Oscillation frequencies of tapered plant stems. Am J Bot 89:1–11

Spatz HC, Theckes B (2013) Oscillation damping in trees. Plant Sci 207:66–71

Speck O, Spatz HC (2004) Damped oscillations of the giant reed *Arundo donax* (Poaceae). Am J Bot 91:789–796

Speck T, Burgert I (2011) Plant stems: Functional design and mechanics. Annu Rev Mater Res 41:169–193

Speck T, Spatz HC, Vogellehner D (1990) Contributions to the biomechanics of plants I. Stabilities of plant stems with strengthening elements of different cross-sections against weight and wind forces. Bot Acta 103:111–122

Sprugel DG (1983) Correcting for bias in log-transformed allometric equations. Ecology 64:209–210

Staszewski WJ (1997) Identification of damping in MDOF systems using time-scale decomposition. J Sound Vib 203:283–305

Stokes A, Fitter AH, Coutts MP (1995) Responses of young trees to wind and shading: Effects on root architecture. J Exp Bot 46:1139–1146

Stull RB (1988) An Introduction to Boundary Layer Meteorology. Kluwer Academic Publishing, Boston, MA

Sugden MJ (1962) Tree sway period - A possible new parameter for crown classification and stand competition. For Chron 38:336–344

Sutton WRJ, Crowe JB (1975) Selective pruning of radiata pine. N Z J For Sci 5:171–195

Tamasi E, Stokes A, Lasserre B, et al (2005) Influence of wind loading on root system development and architecture in oak (*Quercus robur* L.) seedlings. Trees Struct Funct 19:374–384

Taylor AF, Kuo FE, Sullivan WC (2002) Views of nature and self-discipline: Evidence from inner city children. J Environ Psychol 22:49–63

TCIA (2017a) American National Standard for Tree Care Operations - Tree, Shrub, and Other Woody Plant Management - Standard Practices (Tree Risk Assessment a. Tree Failure). Tree Care Industry Association, Inc, Londonderry, NH, USA

TCIA (2017b) American National Standard for Tree Care Operations - Tree, Shrub, and Other Woody Plant Management - Standard Practices (Pruning). Tree Care Industry Association, Inc, Londonderry, NH, USA

Telewski FW (1986) Thigmomorphogenesis: Field and laboratory studies of *Abies fraseri* in response to wind or mechanical perturbation. Physiol Plant 66:211–218

Telewski FW, Pruyn ME (1998) Thigmomorphogenesis: A dose response to flexing in *Ulmus americana* seedlings. Tree Physiol 18:65–68

Theckes B, de Langre E, Boutillon X (2011) Damping by branching: A bioinspiration from trees. Bioinspir Biomim 6:1–11

Thomas C, Mayer J-C, Meixner FX, Foken T (2006) Analysis of low-frequency turbulence above tall vegetation using a Doppler sodar. Bound-Layer Meteorol 1193:563–587

Torrence C, Compo GP (1998) A practical guide to wavelet analysis. Bull Am Meteorol Soc 79:61–78

van Casteren A, Sellers WI, Thorpe SKS, et al (2012) Why don't branches snap? The mechanics of bending failure in three temperate angiosperm trees. Trees Struct Funct 26:789–797

van Casteren A, Sellers WI, Thorpe SKS, et al (2013) Factors affecting the compliance and sway properties of tree branches used by the Sumatran orangutan (*Pongo abelii*). PLoS ONE 8:1–9

Vincent JFV (1990) Structural Biomaterials. Princeton University Press, Princeton, NJ, USA

Vogel S (1984) Drag and flexibility in sessile organisms. Am Zool 24:37–44

Vogel S (2009) Leaves in the lowest and highest winds: Temperature, force and shape. New Phytol 183:13–26

Vogel S (1996) Life in Moving Fluids: The Physical Biology of Flow, 2nd edn. Princeton University Press, Princeton, NJ, USA

Vogel S (1989) Drag and reconfiguration of broad leaves in high winds. J Exp Bot 40:941–948

Vollsinger S, Mitchell SJ, Byrne KE, et al (2005) Wind tunnel measurements of crown streamlining and drag relationships for several hardwood species. Can J For Res 35:1238–1249

Wang X, Wiedenbeck J, Liang S (2009) Acoustic tomography for decay detection in black cherry trees. Wood Fiber Sci 41:127–137

Wang Z, Goonewardene LA (2004) The use of mixed models in the analysis of animal experiments with repeated measures data. Can J Anim Sci 84:1–11

Wardlaw TJ, Neilsen WA (1999) Decay and other defects associated with pruned branches of *Eucalyptus nitens*. Tasforests 11:49–57

Wellpott A (2008) The stability of continuous cover forests. PhD Thesis

White DA, Kile GA (1993) Discolouration and decay from artificial wounds in 20-year-old *Eucalyptus regnans*. For Pathol 23:431–440. https://doi.org/10.1111/j.1439-0329.1993.tb00822.x

Wiseman D, Smethurst P, Pinkard L, et al (2006) Pruning and fertiliser effects on branch size and decay in two *Eucalyptus nitens* plantations. For Ecol Manag 225:123–133

Wood CJ (1995) Understanding wind forces on trees. In: Coutts MP, Grace J (eds). Cambridge University Press, New York, NY, USA, pp 133–165

Xiao X, White EP, Hooten MB, Durham SL (2011) On the use of log-transformation vs. nonlinear regression for analyzing biological power laws. Ecology 92:1887–1894

Yamartino RJ (1984) A comparison of several "single-pass" estimators of the standard deviation of wind direction. J Clim Appl Meteorol 23:1362–1366

Yan W, Kan Q, Kergrene K, et al (2013) A truncated conical beam model for the analysis of the vibration of rat whiskers. J Biomech 46:1987–1995

Yang M, Defossez P, Danjon F, Fourcaud T (2014) Tree stability under wind: Simulating uprooting with root breakage using a finite element method. Ann Bot 114:695–709

Zangvil A (1981) Some aspects of the interpretation of spectra in meteorology. Bound-Layer Meteorol 21:39–46